MICROEMULSIONS FORMATION, STABILITY AND THEIR CHARACTERISATIONS

A thesis submitted for the degree of

Doctor of Philosophy

by

Mahmood Akhtar

Department of Chemistry

Brunel University

(The University of West London)

Uxbridge, Middlesex

UB8 3PH

December 1996

CHAPTER ONE Page

GENERAL INTRODUCTION

1.1 Surfactant Chemistry 1
1.2 Micellisation 3
1.3 Introduction to Microemulsion Systems 6
1.3.1 Microemulsion Stability 7
1.3.2 Phase equilibria in Microemulsion 9
1.3.3 The Optimum Salinity 12
1.4 Applications of Microemulsions 13
1.4.1 Emulsions in the World Energy Context 15
1.4.2 Enhanced Oil Recovery (EOR) 16
1.4.2.1 Introduction and Background 16
1.4.2.2 EOR Economics 17
1.4.2.3 EOR Environment 18
1.4.2.4 Technology 18
1.4.2.5 Adsorption of Surfactants onto Rock Surfaces..20
1.4.3 Microemulsions as Microreactors 20
1.5 Aims of the Research 21
1.6 References 22

CHAPTER TWO

THEORY OF THE FORMATION OF MICROEMULSIONS AND THEIR CHARACTERISATION

2.1 Theories of Microemulsion Formation 26
2.1.1 The Mixed Film (Interfacial) Theory 26
2.1.2 Duplex Film Model 28
2.1.3 Solubilisation Theories 29
2.1.4 Thermodynamic Theories 31
2.1.5 R-Ratio Theory 34
2.2 Characterisation Techniques for Microemulsions 37
2.2.1 UV-Spectroscopy 37
2.2.2 Chromatography 39
2.2.2.1 High Performance Liquid Chromatography..... 39
2.2.2.2 Gas Chromatography 41
2.2.3 Photon Correlation Spectroscopy 42
2.2.4 Viscosity 45
2.2.5 Surface and Interfacial Tensions.....47
2.3 References 50

CHAPTER THREE

MICROEMULSION MATERIALS, METHODS AND EXPERIMENTAL

3.1 Materials 53
3.1.1 Surfactants 53
3.1.2 Solvents 55
3.1.3 Brine 56
3.1.4 Inorganic Salt 57
3.2 Experimental 57
3.2.1 Preparation of Microemulsions 57
3.2.2 The Phase Diagram of a Ternary Mixture 59
3.2.3 Spectrophotometric Measurements 60
3.2.4 Scanning of the Microemulsion Phases 60
3.2.5 Optimum Salinity Scan 61
3.2.6 Electrical Conductivity Measurement 62
3.2.7 Viscosity Measurement 62
3.2.8 Surface Tension Measurement 63
3.2.9 Interfacial Tension Measurement 63
3.2.10 Cloud Point and pH Measurement 64
3.2.11 High Performance Liquid Chromatography 65
3.2.12 Gas Chromatography.....67
3.2.13 Determination of Water.....71
3.2.14 Photon Correlation Spectroscopy (PCS) 72
3.2.15 Summary of Experimental Methods.....74
3.3 References 76

CHAPTER FOUR

CHARACTERISATION OF MICROEMULSION SYSTEMS

4.1 Phase Equilibria in Microemulsions 77
4.1.1 Introduction 77
4.1.2 Effect of Alcohols.....78
4.1.3 Effect of Salinity, pH and Temperature.....78
4.1.4 Results and Discussion 79
4.1.5 Effect of Alcohol 84
4.1.6 Three Phase System on Ternary Diagram 88
4.1.7 Effect of Salinity on the Phase Equilibria 88
4.2 Model Surfactant System for Enhanced Oil Recovery 92
4.2.1 Scanning of the Microemulsion Phases 93
4.2.2 Spectrophotometric Results 96

4.2.3 Optimum Salinity Scan 98
4.2.4 Surface and Interfacial Tension Results 99
4.2.5 High Performance Liquid Chromatography (HPLC) 102
4.2.6 Gas Chromatography (GC) 109
4.2.7 Photon Correlation Spectroscopy (PCS)....113
4.2.8 Cloud Point Determination 118
4.2.9 Viscosity Result 118
4.2.10 Electrical Conductivity Results 120
4.2.11 Summary of Results 123
4.3 References 125

CHAPTER FIVE

ADSORPTION OF SURFACTANTS FROM AQUEOUS AND NONAQUEOUS ENVIRONMENT

5.1 Introduction and Background 128
5.2 Adsorption of Non-ionic Surfactants 129
5.3 Theories of Adsorption 130
5.3.1 Langmuir Adsorption Isotherm 130
5.3.2 Freundlich Adsorption Isotherm 131
5.3.3 Henry's Law: Linear Adsorption Isotherm 132
5.4 Experimental 132
5.4.1 Sample Preparation 132
5.4.2 Ion-Exchange Chromatography (IEC) 133
5.4.3 BET Surface Area Measurement 135
5.4.4 Thermogravimetric Analysis 136
5.4.5 Adsorption From Solutions 136
5.4.6 Summary of Possible Errors in Experimental Methods ...140
5.5 Results and Discussion 140
5.5.1 Ion-Exchange Chromatography (IEC) 140
5.5.2 Thermogravimetric Analysis 143
5.5.3 Adsorption Isotherm 145
5.5.4 Effect of Calcination on Surfactant Adsorption 145
5.5.5 Effect of Temperature on Surfactant Adsorption 147
5.5.6 Effect of Salinity on Surfactant Adsorption 148
5.5.7 Effect of Hydronium Ion Concentration on Adsorption..151
5.5.8 Effect of Ethoxylate Chain Length on the Adsorption ...151
5.5.9 Adsorption From Non-aqueous Solutions 153
5.5.10 Effect of Alcohol on the Adsorption of TX-100....153

5.5.11 Summary of Results 154
5.6 References 158

CHAPTER SIX

APPLICATIONS OF MICROEMULSIONS

(a) COMBUSTION OF MICROEMULSIONS

6.1 Introduction and Review 161
6.2 Mechanisms and Emulsion Characteristics 167
6.3 Experimental 170
6.3.1 Mass Spectrometer.....172
6.4 Results and Discussion 173
6.4.1 Summary of Results.....193

(b) SYNTHESIS OF COLLOIDAL SILICA BY MICROEMULSION METHOD

6.5 Synthesis of Colloidal Silica by Microemulsion Method 193
6.5.1 Introduction and Background 193
6.5.2 Experimental 194
6.5.3 Transmission Electron Microscopy.....195
6.5.4 Results and Discussion 196
6.5.4.1 Particle Characteristics 196
6.5.4.2 Effect of Water/TEOS Molar Ratio (M-ratio) ..198
6.5.4.3 Summary of Results 200
6.6 References 201

CHAPTER SEVEN

CONCLUSIONS AND FURTHER WORK

7.1 Phase Equilibria in Microemulsions 205
7.2 Adsorption of Surfactants onto Rock Surfaces 207
7.3 Microemulsion Droplet Combustion and Synthesis of Colloidal Silica 208
7.4 Further Research 209
7.5 References 210

APPENDIX 211

ACKNOWLEDGEMENTS

I would like to express my sincere appreciation and deep gratitude to my supervisor, Professor PA Sermon for his encouragement and guidance throughout the research programme.

I would also like to thank Dr A Young and Dr J Prosser for their useful discussions during the course of this research, Dr VA Self for her assistance and discussions on combustion experiments and Mr BB Wheals for the use of his HPLC system.

I am grateful to Mr P Szadorski, Mr. D. Herman and Mr FT Coates for their technical assistance, to Dr S Taylor from BP chemicals for the use of tensiometer and Mrs R James for her secretarial work.

Thanks are also extended to my colleague Miss K Holland for her friendship and encouragement during the research programme.

Finally, I would like to acknowledge the financial support I have received from EEC throughout this research project.

ABSTRACT

This thesis is concerned with aspects of the surface and colloid chemistry of various microemulsion systems stabilised by pure nonionic surfactants and alcohol as well as mixtures of nonionic and anionic surfactants. Phase equilibria and interfacial characteristics of the systems are studied with a view to their potential usefulness for enhanced oil recovery, in which salinity and temperature are important parameters. The equilibrium microemulsion phases are scanned at different temperatures and salinities and thus interfacial boundaries can be determined and optimum salinity scans can be performed accurately using a modified spectrophotometer.

Several analytical techniques (e.g. high performance liquid chromatography, gas chromatography, ion-exchange chromatography, mass spectrometry, viscometry, electrical conductivity, photon correlation spectroscopy, UV-spectrophotometry, thermogravimetric analysis, transmission electron microscopy, surface and interfacial tension techniques) have been used to characterise and understand the microchemistry of the microemulsion systems. Ultra-low interfacial tensions (>0.1 μN/m) can be achieved in the microemulsion systems. Surfactant transfer between phases, and phase inversion of microemulsions are shown to occur around the condition which produces minimum interfacial tension.

Adsorption of the surfactants from aqueous and nonaqueous solutions has been investigated and the results show that the extent of adsorption can be reduced significantly in the presence of alcohols (co-solvent). The extent of adsorption increases with increasing temperature and salinity; however, it decreases with an increase in the hydrophilic head group of the surfactant. Adsorption of nonionic surfactants on quartz from the nonaqueous solution (decane) is much greater than from aqueous solution.

In microemulsion applications, droplet combustion of w/o microemulsions is also studied for different surfaces (i.e. silica, oxidised Fecralloy and catalyst coated Fecralloy) in the temperature range of 313-573K. Formaldehyde and acetaldehyde are formed as intermediate combustion products. Thus the microemulsion combustion can lead to new oxygenate products. The w/o microemulsion route is used to synthesize colloidal silica of controlled particle size and morphology. The particle size can be varied by changing the molar ratio of water to TEOS using a water pH of 10.5.

CHAPTER ONE

GENERAL INTRODUCTION

1.1 Surfactant Chemistry

A surfactant is a bi-functional molecule or ion possessing both polar and non-polar regions. Molecules with this type of structure are sometimes referred to as being amphiphilic. The molecular configuration of a surfactant is conveniently represented by a "head and tail" structure where the polar region corresponds to the surfactant head-group and the non-polar region corresponds to the tail-group [1].

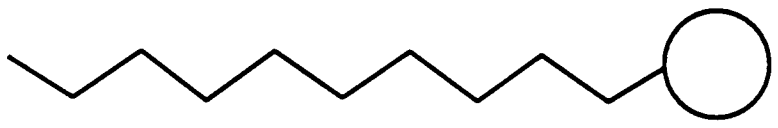

Figure 1.1 Structure of a typical surfactant molecule

The surfactant tail-group usually consists of one or two alkyl chains containing typically between ten and twenty carbon units. The surfactant head-group may be either non-ionic or ionic and surfactants are usually classified according to the type of head-group.

(i) Anionic Surfactants: are those which give *negatively* charged surfactant ions in aqueous solution, Figure 1.2-a, usually originating in sulphonate, sulphate or carboxylate groups. Examples of anionic surfactants include the sodium salts of long-chain n-alkyl sulphates ($C_n H_{2n+1} SO_4^- Na^+$); Sodium dodecyl sulphate, SDS, ($C_{12} H_{25} SO_4^- Na^+$) and n-alkyl benzene sulphonate ($C_nH_{2n+1}C_6H_4 SO_3^- Na^+$). Aerosol-OT (sodium bis (2-ethylhexyl) sulphosuccinate) is an example of double-chain anionic surfactant.

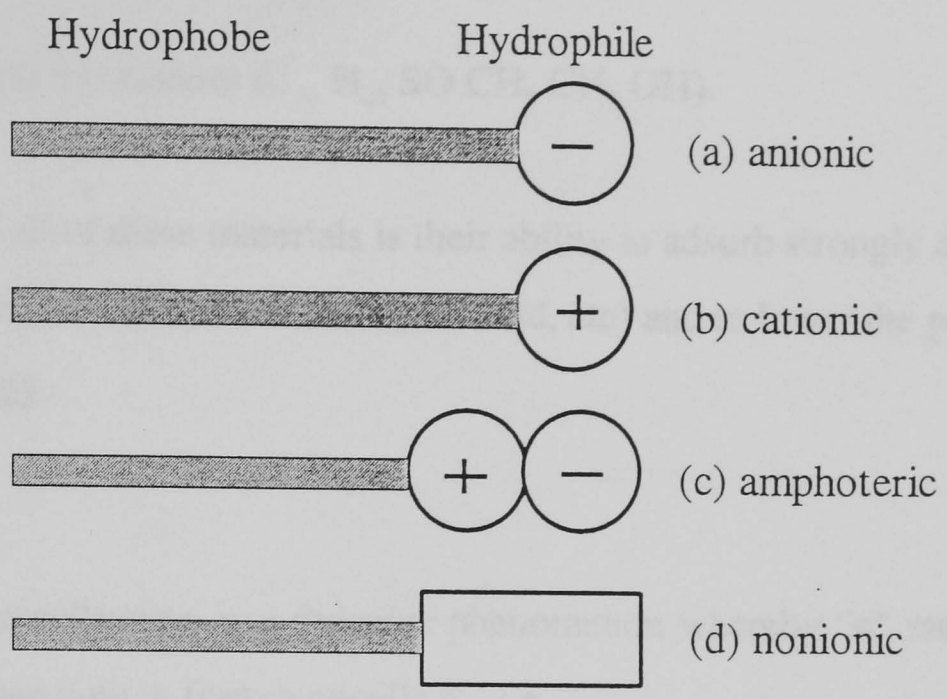

Figure 1.2 Types of surfactants

(ii) Cationic Surfactants: are those which give a *positively* charged surfactant ion in aqueous solution. Figure 1.2-b, examples of cationic surfactants include the long-chain n-alkyl quarternary ammonium salts. These may be single chain e.g. Dodecyl trimethyl ammonium bromide, DTAB, (C_{12} H_{25} N Me_3Br^-) n-alkyl trimethyl ammonium bromides (C_nH_{2n+1} N $(CH_3)_3$ Br^-) or double-chain e.g. di-n-alkyl dimethyl ammonium bromides $(C_nH_{2n+1})_2N(CH_3)_2$ Br^-). As a group these materials usually have good germicidal properties.

(iii) Amphoteric Surfactants: which behave in aqueous solution as anionic *or* cationic surfactants (i.e. give negatively and positively charged surfactant ions (see Figure 1.2-c)). A simple example of this type of material is 3-dimethyl dodecyl amine propane sulphonate (C_{12} H_{25}-N(Me_2)-CH_2-CH_2-SO_3).

(iv) Non-ionic Surfactants: have neutral head-groups, (i.e. do not ionize appreciably in aqueous solution) that are frequently polyoxy ethylene groups (i.e. $(CH_2$ $CH_2O)_n$ where n = 1-20), see Figure 1.2-d. A typical example is alkyl phenol ethoxylate R-C$_6$H$_4$-$O(CH_2CH_2O)_nH$. With this type of compound the head-group is larger than the hydrocarbon chain. However, nonionic surfactants with small head-groups also exist: an

example is dodecyl sulphinyl ethanol (C_{12} H_{25} SO CH_2 CH_2 OH).

The unique property of all of these materials is their ability to adsorb strongly at various interfaces, (e.g. air-water, oil-water, water-solid, oil-solid, etc) and to lower the prevailing interfacial surface energy.

1.2 Micellisation

Micelle formation or micellisation is a dynamic phenomenon whereby "n" monomeric surfactant molecules associate to form a micelle S_n, i.e.

$$nS = S_n \qquad (1.1)$$

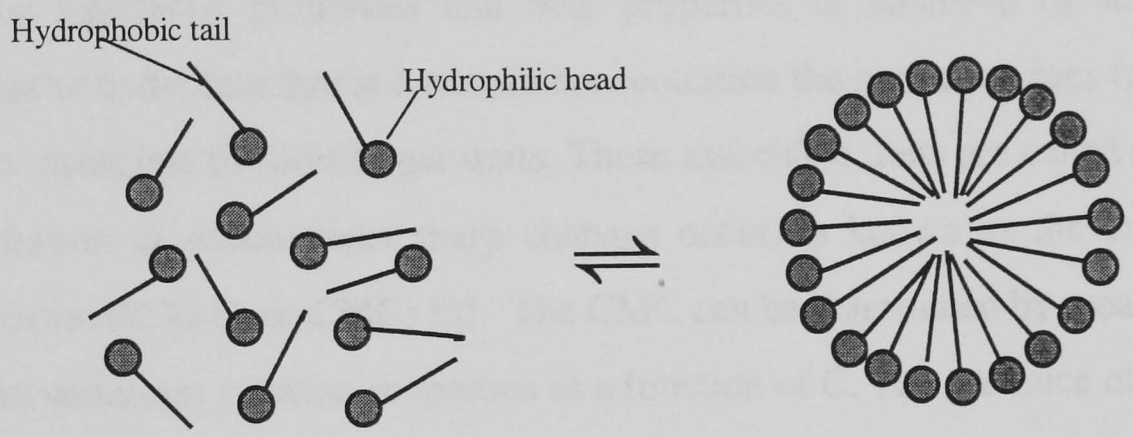

Figure 1.3 Micelles in equilibrium with monomers.

In the dynamic equilibrium, surfactant molecules are constantly leaving the micelle whilst other molecules from solution enter the micelle. The same applies to the counter-ions with ionic surfactants, which can exchange between the *micelle* surface and *bulk* solution.

The properties such as osmotic pressure π, molar conductivity Λ, turbidity τ, surface tension γ, etc. are plotted versus concentration (denoted C) or log concentration as shown in Figure 1.4 for an anionic association colloid (i.e. micelle), as described by Shaw [2].

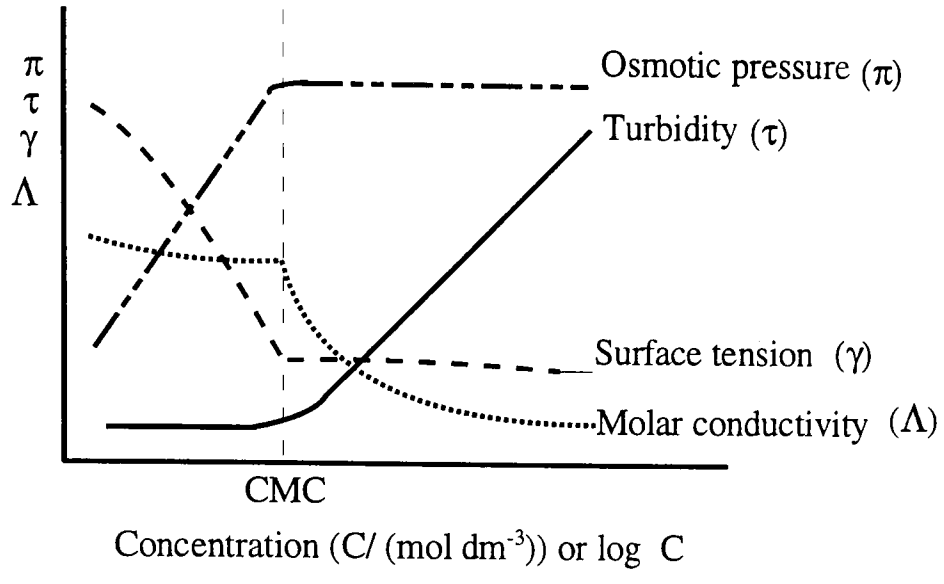

Figure 1.4 Typical variation in the physical properties of an anionic association colloid with concentration

Both the interfacial properties and bulk properties of solutions of surfactants are consistent with the fact that at a certain concentration the surfactant ions (molecules) in solution associate to form larger units. These associated units are called micelles. The concentration at which these sharp changes occur, is known as the critical micelle concentration (C.M.C. or CMC) [3]. The CMC can be determined by measuring any of the above surfactant solution properties as a function of C. The presence of micelles can account for many of the unusual properties of surfactant solutions, e.g. the low osmotic activity and the relatively high conductivity of soap solutions.

In aqueous media, the CMC decreases as the length of the hydrophobic group increases. The decrease in the CMC for nonionic surfactants is greater than for anionics and the decrease becomes less marked as the chain length increases and there is a limiting value (about 18 carbons) above which the CMC remains unchanged due to the coiling of the chains.

The CMC in an aqueous solution also reflects the extent of binding of the counter-ion. The strength of the bond increases with increasing polarisability of the molecule. Small amounts of organic materials (including impurities or by-products from manufacture) can alter the CMC. The CMC decreases in the presence of polar organic compounds which

are incorporated into the micelles. Below the CMC most of the surfactant molecules are unaggregated whereas in the isotropic solutions immediately above the CMC, micelles and monomeric surfactant ions are thought to co-exist; the concentration of the latter changing only slightly as more surfactant is dissolved [3].

The presence of an electrolyte in aqueous solution also decreases the CMC; the effect is more pronounced for anionic surfactants than nonionic ones. In the former, the depression is due to a reduction in the repulsion between the ionic head groups in the micelle. For nonionics, the effect is due to the electrolyte salting out the hydrophilic groups [4].

It is suggested [5] that micelles are spherical in shape containing 10-50 surfactant ions or molecules. The radius of the micelle is approximately equal to the length of the fully extended hydrophobic group [6]. However, Harkins et al [7] proposed micelles of cylinderical shape in which the long chain ions would be aligned parallel to the cylinder's axis with the ionic heads forming the ends (see Figure 1.5).

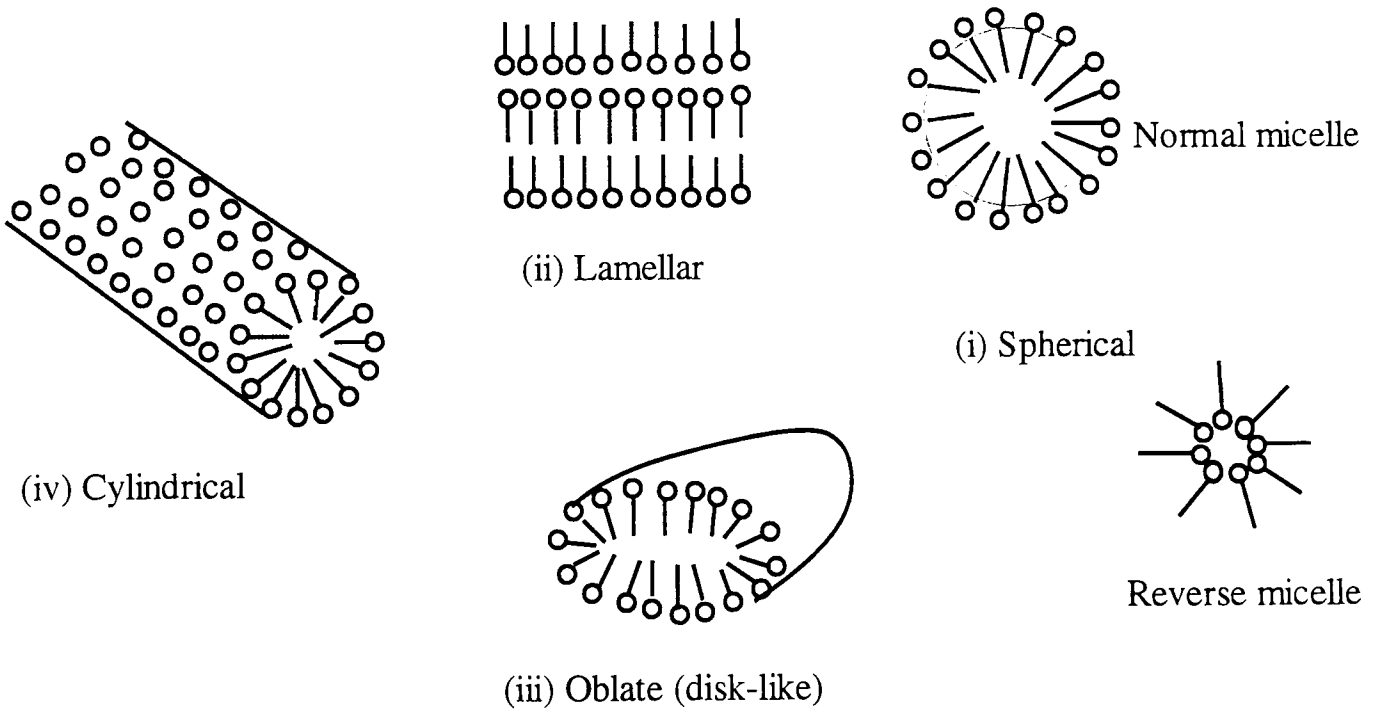

Figure 1.5 Schematic representation of four types of micelles

In a hydrocarbon medium, the structure of the micelle is similar but reversed with the inner region containing the hydrophilic head groups, and the outer region of hydrophobic

groups. Changes in temperature, surfactant concentration and the presence of ions may all cause a change in the micelle size, shape and aggregation number.

1.3 Introduction to Microemulsion Systems

Microemulsions are dispersions of oil in water or of water in oil, stabilized by a surfactant or, more commonly, a surfactant/co-surfactant mixture [8]. These systems were first scientifically reported by Schulman and Hoar in early 1940 [9]. A microemulsion is most generally defined as transparent or translucent stable mixture of oil, electrolyte, and surfactant or combination of surfactants. Microemulsion formation is generally favoured when the volume fraction of the dispersed component is quite low (i.e.<10%). If the oil component in such a system is in excess then a water-in-oil (w/o) microemulsion consisting of surfactant-stabilised water droplets dispersed in an oil-continuous medium is said to be formed.

Microemulsion systems have been studied with varying combination of surfactants, non-polar solvents and water. Probably the most extensively considered systems are those consisting of: ionic surfactant; co-surfactant (usually medium chain length alcohol); hydrocarbon and water [10]. Alcohols are used as an additional ingredient of the surfactant formulation and are often referred to as co-solvent, playing an important role in achieving the desired stability.

Ionic surfactants, such as sodium dodecyl sulphate, are strongly hydrophilic and do not form large micelles [11]. For the preparation of a microemulsion with ionic surfactants, it is necessary to include a more hydrophobic co-surfactant (i.e. the ionic surfactant by itself is not sufficiently hydrophobic to allow for a large enough degree of solubilisation of the oil). Larger chain length ionic surfactants require less co-surfactant than shorter chain lengths [10].

There are two main methods for producing a microemulsion: (a) combination and (b) titration. The combination procedure [12] is the quicker to perform but it produces a two-phase system: a microemulsion layer and excess oil layer. To create a dispersion by this

method the co-surfactant is initially suspended in the oil and then combined with an equal quantity of water or brine solution containing the ionic surfactant. Inverting the vessel and gently shaking causes the surfactant to diffuse out of the oil into the aqueous phase. The surfactant takes up as much oil as possible to form the microemulsion until curvature requirements dictate that it can not take any more oil. The excess oil present then separates out and two phases are present: the lower phase is the o/w microemulsion; the upper phase the excess oil layer. For a system not requiring the addition of a co-surfactant (i.e. many w/o microemulsions) the surfactant is dissolved in the hydrocarbon and then combined with the water or brine constituent.

The titration method [13] involves the dispersing of the surfactant in the oil phase and subsequent mixing of this with a water/brine component. The resulting coarse emulsion is then titrated with co-surfactant until a clear, transparent liquid develops and this is the microemulsion. If using a non co-surfactant system, the surface active agent is initially dissolved in the aqueous phase and into this the oil is subsequently titrated. If the surfactant/aqueous mixture is initially turbid then the system is titrated to clarity with the oil. If, on the other hand, the formative surfactant/aqueous mixture is clear, the system is then titrated with oil from the initial clear state, through turbid, back to a clear one again.

1.3.1 Microemulsion Stability

Microemulsions differ in several important respects from emulsions. Firstly, they are thermodynamically stable [14], as opposed to the kinetic stability of emulsions. The stability arises mainly from the very low interfacial tensions (typically $< 0.01\ \mu Nm^{-1}$), achieved using the co-surfactant/surfactant mixture, between the droplets and the bulk phase. Secondly, they lie in a much smaller size range than emulsions (i.e. radii r are < 50 nm, compared to > 100 nm in emulsions. This very small size also contributes to their stability, owing to the very large entropy of dispersion involved.

Microemulsions have such a low interfacial free energy that it is exceeded by the negative free energy term arising from the entropy of dispersion. The resulting situation is one in which the overall free energy of formation of a microemulsion is negative and is, as such,

thermodynamically stable [8].

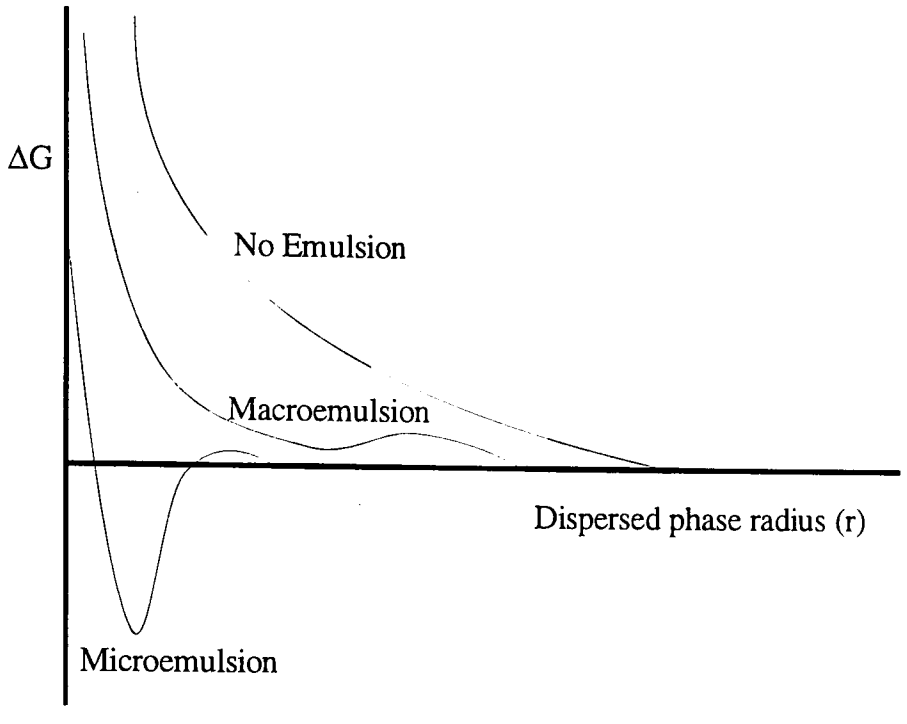

Figure 1.6 Qualitative illustration showing free energy (ΔG) as a function of droplet size.

Schulman et al [15] suggested that microemulsions form when surfactants and co-surfactants in the right proportion produce a mixed adsorbed film that reduces the interfacial tension (γ_i) between the oil and water below zero. They concluded that γ_i must have a metastable negative value, giving a negative free energy variation $-\gamma_i dA$ (where dA is the change in interfacial area) responsible for spontaneous dispersion.

A low interfacial tension is not the only important aspect that controls stability, other factors such as droplet charge and the presence of a steric stabilising layer may lead to repulsion between the droplets and thus a tendency toward stability is attained [16]. Viscosity of the system may also play a part in the stability of the dispersion. A high viscosity of the continuous phase would retard the rate of any creaming tendency and thus improve the shelf-life (long-term stability) of dispersion. It should be noted however that most microemulsions are of a relatively low viscosity and thus this component of stability may be of minor consequence.

Saito and Shinoda [17] studied the stability and interfacial tension of w/o type emulsions

(i.e. cyclohexane-water stabilized with polyoxyethylene nonylphenol ether) as a function of temperature and of the hydrophilic chain length of the emulsifier. Their results show that the interfacial tension of the water and the oil phases changes markedly with temperature and approaches zero near to the phase inversion temperature (PIT).

W/O microemulsions have been studied to determine the effect of various parameters on the size and dynamics of water droplets, inter-droplet attractive interactions, water solubility, and water self-diffusion coefficient in the microemulsion. More recently. the effect of the chain length of the added alcohol on the same w/o microemulsion properties has been investigated [18]. These results show that droplet size and intensity of attractive interactions between droplets increase as the alkyl chain length of the alcohol decreases.

1.3.2 Phase Equilibria in Microemulsions

When a surfactant is added to an oil-water mixture it is preferentially adsorbed at the oil-water interface where it is possible to simultaneously solvate the polar head-groups in water and the non-polar tail-groups in the oil. In some microemulsion water/surfactant/oil systems the lowering of the surface free energy caused by surfactant adsorption at an interface is sufficient to result in the formation of a thermodynamically-stable dispersion [1]. In oil-continuous microemulsion dispersions the formation of surfactant-stabilised water droplets is primarily influenced by specific surfactant head-group interactions such as hydrogen bond or ion-pair dipole interactions. The solvation of surfactant tail-groups by oil solvent molecules is also an important factor in determining the formation of stable oil-continuous microemulsion dispersions.

The various phase domains that are generally found in water/surfactant/oil systems are given schematically in Figure 1.7 in the form of a Gibb's phase triangle, which is a particularly informative method for describing the phase behaviour of three-component mixtures as a function of composition at constant temperature and pressure. In this each corner of the triangle represents one of the components in a ternary mixture. The surfactant-rich corner of the triangle is a liquid crystalline (LC) phase domain which may.

in practice, consist of several ordered phase domains (e.g. bi-layers, hexagonally packed rods, etc.). In the water-rich corner of the triangle an oil-in-water (o/w) microemulsion phase domain is indicated, although in certain cases, liquid crystalline structures may also be favoured in this composition region. At higher surfactant concentrations, and for roughly equal volume fractions of water and oil, the existence of bicontinuous structures is postulated [19-22].

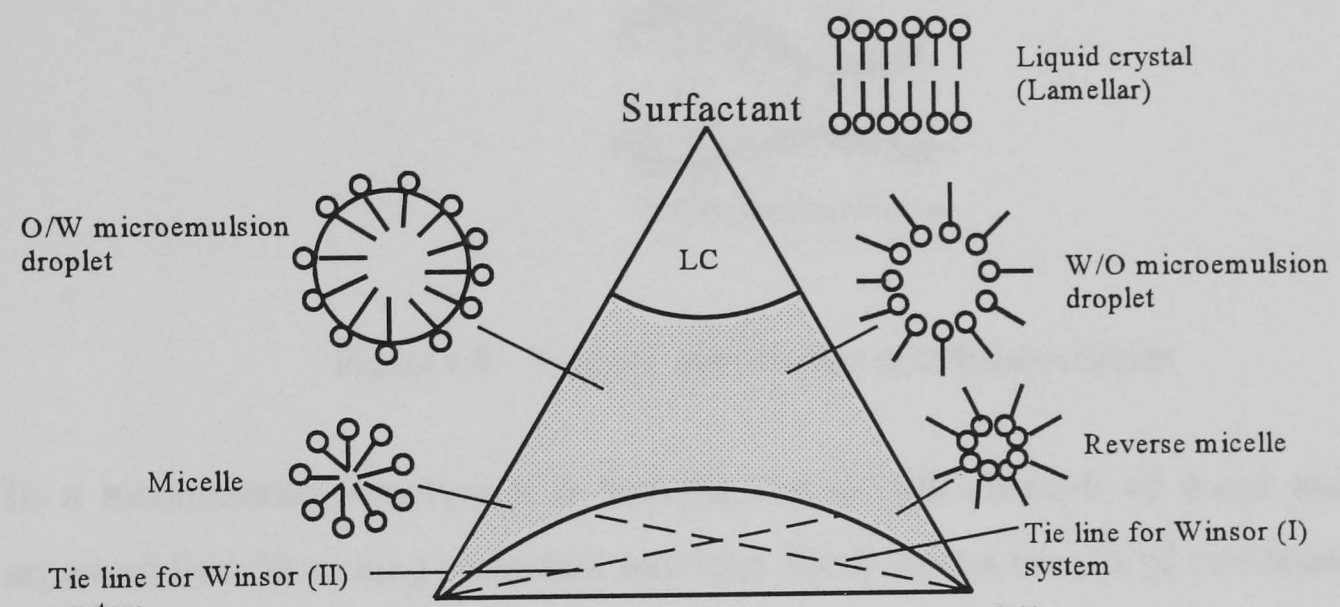

Figure 1.7 An idealised phase diagram at constant temperature and pressure where the shaded area represents the single phase microemulsion

In water/surfactant/oil mixture, the surfactant forms an interfacial region C between bulk water and oil phase as shown in Figure 1.8. On both sides of C, cohesive intermolecular forces (van der Waals, hydrogen bonding, electrostatic) cause solubilization. These interactions are mainly between the oil and the hydrophobic part of the surfactant and between water and the hydrophilic part of the surfactant. Interaction between the same species promote seperation.

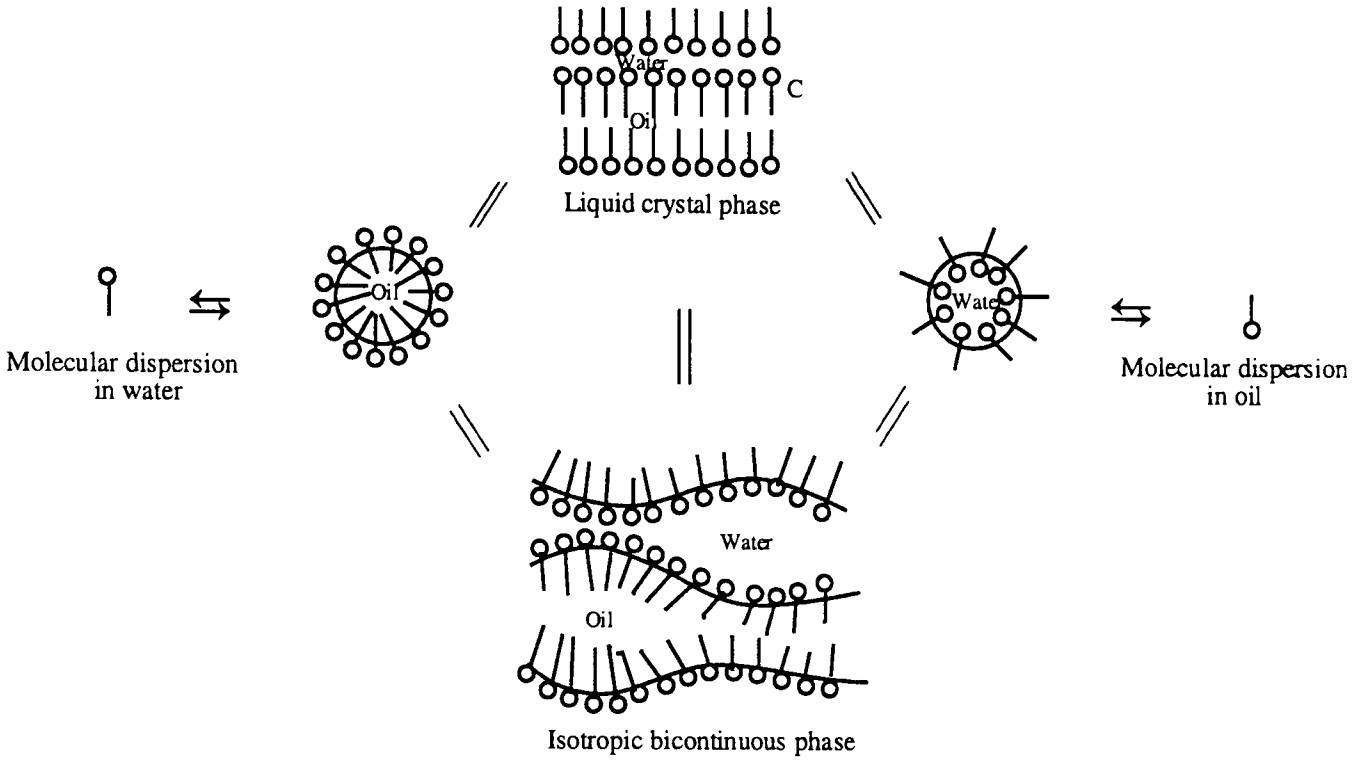

Figure 1.8 Winsor's intermicellar equilibrium concept

In a bicontinuous structure it is thought that flexible channels of water and oil are separated by a fluctuating surfactant interface where the net interfacial curvature is close to zero. Such systems have much higher conductivities than w/o microemulsions. The bicontinuous systems are currently of great interest to the oil industry where the possibility of a continuous single-phase transition from a w/o to o/w microemulsion via an intermediate bicontinuous phase has important implications for enhanced oil recovery.

There is no clear boundary between a micellar and a microemulsion dispersion. One criterion is that a microemulsion droplet is formed when the dimensions of the total aggregate exceed the molecular length of the surfactant. In the case of reverse micellar solutions and w/o microemusions the primary distinction may be the nature of the 'entrapped' water. In a reversed micelle most of the water is involved in the hydration of the surfactant head-groups and is therefore effectively bound to the surfactant molecules. For reversed micelles composed of ionic surfactant molecules the interior of the micelle is also characterised by a high ionic strength due to the presence of surfactant counter-ions. In w/o microemulsions, not all the water is bound to the surfactant head-groups, the 'free' (i.e. non-bound) water is thought to form a fluid water core in the centre of the water droplet which has properties similar to that of bulk water [23, 24].

Healy et al [25] examined the effect of salinity in the multiphase region. When salt is added to a lower-phase microemulsion in equilibrium with excess hydrocarbon, a brine-phase and middle-phase microemulsion eventually appear. Continued addition of salt leads to an upper-phase microemulsion in equilibrium with a brine phase (illustrated in Figure 1.9).

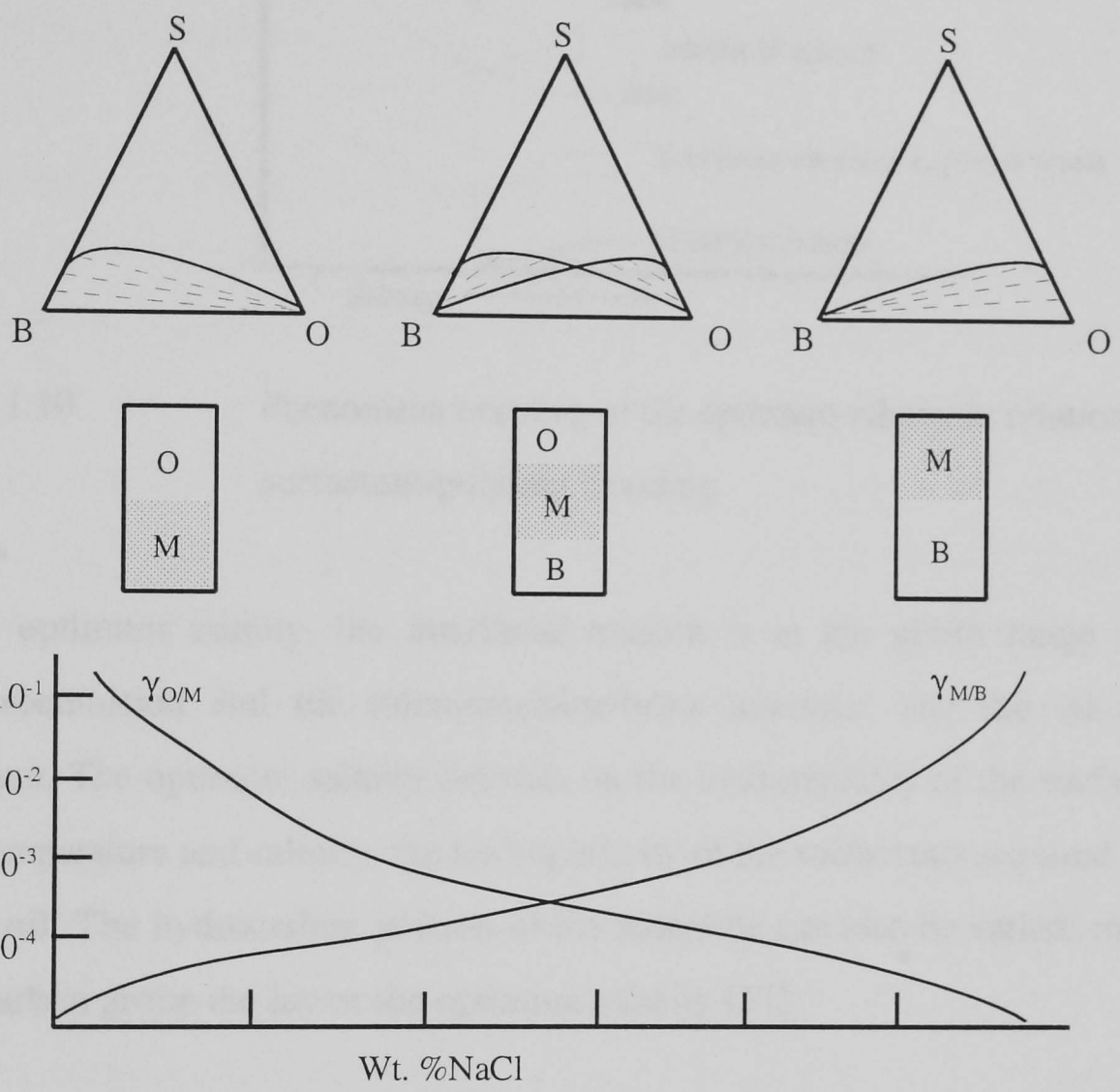

Figure 1.9 Schematic diagram showing the effect of increasing the salt concentration on the phase volumes of multiphase microemulsions.

1.3.3 The Optimum Salinity

A hydrocarbon/brine/surfactant/alcohol system often forms a middle phase microemulsion in an appropriate salinity range. The salinity at which the middle phase microemulsion contains an equal volume of oil and brine is defined as the optimum salinity [26].

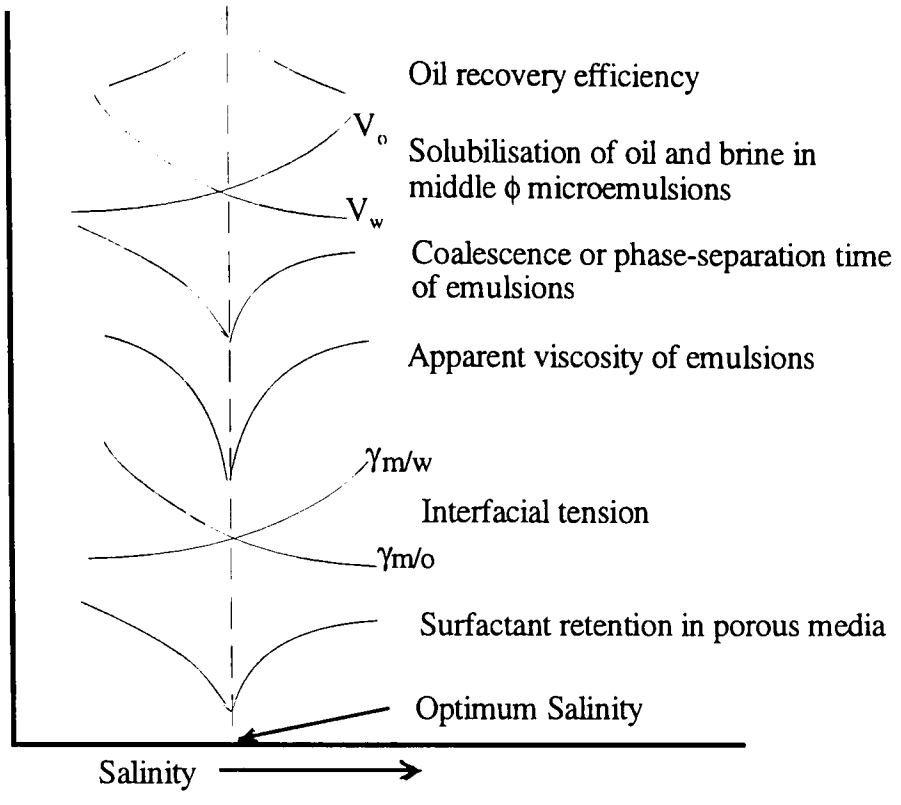

Figure 1.10 Phenomena occuring at the optimum salinity in relation to EOR by surfactant-polymer flooding.

At the optimum salinity, the interfacial tension is in the μN/m range at both the oil/microemulsion and the microemulsion/brine interface, and the oil recovery is maximum. The optimum salinity depends on the hydrophilicity of the surfactant. For a given temperature and salinity, the hydrophilicity of the surfactants required will depend on the oil. The hydrocarbon portion of the molecule can also be varied; the larger the hydrocarbon group the lower the optimum salinity [27].

Healy and co-workers [28] reported that the optimum salinity in a microemulsion system plays an important role in obtaining low interfacial tensions and high oil recoveries. Increasing the salinity causes the microemulsion phase to undergo a transition from lower to middle to upper phases. As the salinity increases, the microemulsion-oil interfacial tension *decreases* and the microemulsion-water interfacial tension *increases*.

1.4 Applications of Microemulsions

Microemulsions have found potential applications in many areas ranging from enhanced oil recovery to their use as novel reaction media for biotechnology applications, e.g. reversed enzyme synthesis [29]. Various uses of microemulsions have been suggested

(including as a low emission diesel fuel [30] and in oil spillage dispersal (e.g. when the Sea Empress was beached off St. Ann's Head (Milford Haven) February 1996) [31]).

The structure of w/o microemulsions has been the focus of much active research in recent years [32, 33]. It is known that some stable gels formed in water-nonionic surfactant-oil systems in the dilute regime (mainly aqueous) [34] have important applications in cosmetics, jet fuels [35] or the formulation of drugs [36].

The process of solubilisate exchange in w/o microemulsions offers an interesting area for carrying out novel reactions [37], providing the rate of reaction between solubilisates is slower than the droplet exchange rate such that the dispersed water component in a w/o microemulsion may be considered as a continuous pseudo-phase. Since w/o microemulsions are chemically compartmentalised systems, consisting of polar and non-polar domains, the reactions may either take place in the aqueous pseudo-phase (if the reactants are hydrophilic) or in the oil medium (if the reactants are hydrophobic). In the case of a mixture of hydrophilic and hydrophobic reactants a reaction may proceed in the droplet interfacial region, particularly if the reactants are surface active.

Microemulsions can be polymerised in order to produce much smaller latex particles than in the case of emulsions. In microemulsion polymerisation, one expects to produce, after polymerisation, a latex having the same characteristics as those of the starting microemulsion (i.e. stability, fluidity and optical transparency). Once the thermodynamic equilibrium is reached, microemulsions are very stable. As changes are likely to occur during polymerisation, it is essential that microemulsions should be carefully formulated in order to use them in polymerisation experiments.

Inverse microlatices (prepared from inverse microemulsions) can be used in the preparation of thickened aqueous solutions in tertiary oil recovery [38-40]. They can also find applications in ground consolidation for oil drilling, manufacture of drilling muds, completion or fracturation fluids and prevention of water inflows into production wells. Water soluble polymers prepared from w/o microemulsions can be used as coagulants to

separate solids suspended in a liquid. In the paper industry, for instance, the addition of microlatices improves water drainage from the paper sheets. Recently, polymer latices have been used in the biomedical field [41-43].

1.4.1 Emulsions in the World Energy Context

Due to the high energy demand, alternative fuels are always welcome to contribute to the supply of energy, as convenient fuels, which can be utilised in an efficient way and burned in a controlled manner. Thus, emulsification represents an alternative method of using bitumens and bottom residuals from refineries [44] as fuels. Extra heavy oils and bitumens represent a large source of hydrocarbons that can be exploited as fuels applying this technique.

Residual oil demand is expected to increase by about 1% per year up to the year 2000. Thus, additional refinery capacity to upgrade heavy oils will be required in the year 2000 because of both higher demand for refined products and the high availability of heavy crude oils produced. Figure 1.11 shows the crude oil production from 1986 to 1990 and shows clearly that the Middle East dominates world oil production.

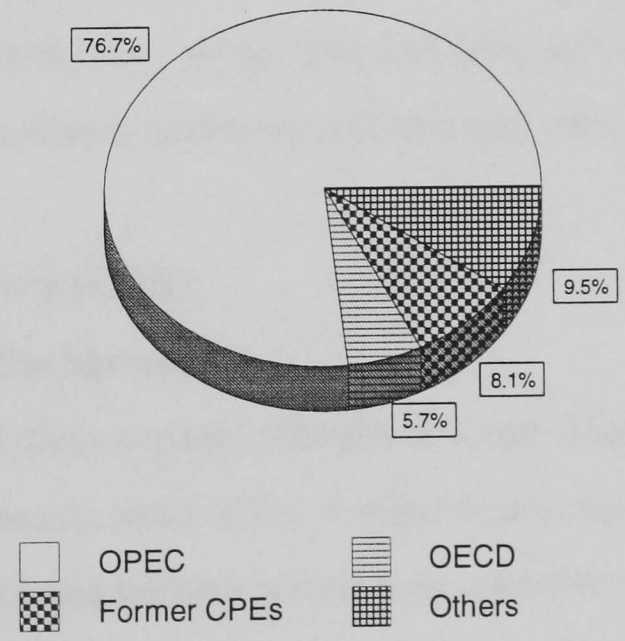

Figure 1.11 Location of the world's crude oil reserves in 1990

In 1990 the oil production was 3,148.9 million tonnes of oil equivalent; 38% of this was OPEC crude oil. In contrast gas production rose to 1,761.6 million tonnes of oil equivalent [45]. Concerning the world crude oil reserves, OPEC has 76.7% of these reserves as shown in Figure 1.11. OECD is referred to as the developed nations member of the Organisation for Economy Cooperation and Development and CPE as Centrally Planned Economy.

Emulsification technique is also useful for the transportation of heavy oils. It reduces the pressure-defined energy requirements and the pipe sizes required for transportation of viscous crude oils in pipelines and eliminates the energy needed to heat the same pipelines. The stability of emulsion is important because in some cases the need is to produce emulsions of long-term stability, whereas in other cases emulsions of controlled but limited stability are required (particularly in multi-stage processes, where it is essential that an initially-stable emulsion eventually breaks). This is the case for transportation of heavy crude oil as emulsions, which later have to be broken down in order to recover the crude oil.

After technical and economic studies testing the different possibilities for the recovery of this oil, emulsification has emerged as the most successful and applicable method available. Conventional methods (e.g. using heat and dilution) were less favourable because of the substantial investment necessary and transportation problems.

1.4.2 Enhanced Oil Recovery (EOR)

1.4.2.1 Introduction and Background

Aerobic bacteria produce oil from organic remains at a rate which depends upon the prevailing temperature and pressure; most of the worlds oil reserves are found at 0.6-1.5 km below the Earth's surface trapped within a porous rock reservoir where it has migrated under the action of gravity [46]. The rocks themselves may be sandstone, limestone, dolomite or clays and may also contain brine and gases. Capillary forces can trap the oil in these reservoirs. In order to mobilise oil ganglia trapped in such water-wet pores, a reduction in the interfacial tension may be helpful, as may emulsification.

Of the world's proven reserves of some 890 billion barrels of light, medium and heavy crudes, more than half of that consist of extra-heavy crudes and bitumens. From these, only one third part is recoverable with present technology. The rest has to be recovered using non-conventional methods. The principle difficulty in the recovery of this type of oil is the high oil viscosity, leading to low oil mobility, which makes displacement by a cheap fluid (e.g. water or gas) inefficient due to the unfavourable mobility ratio (i.e. mobility of the displacing fluid is greater than the mobility of the displaced oil).

World oil demand will it is thought increase from 50 million barrels of oil per day in 1990 to 58 million barrels of oil per day in 2000. In developed nations, demand is expected to increase by 1% per year. Much of this growth will be focused in the transportation sector, especially for refined products such as gasoline and kerosene jet fuel. Gasoline consumption is expected to increase by 1.5 % per year and kerosene jet fuel by 2.5% per year [47].

As the accessible reserves in a particular oil field decrease there may be a movement of operators to new fields or attempts to enhance (EOR) oil recovery from existing fields. Future development of known oil and gas fields depends in part upon enhanced oil recovery (EOR). Chemistry determines whether EOR is technically feasible, but the economic market of course determines whether it will be applied.

For enhanced oil recovery (EOR or improved oil recovery IOR) [48] a chemical engineer's point of view [49] is no more relevant than a physico-chemical evaluation [50]: both can explain viscous fingering [51] or predict phase equilibria [52]. Future growth of known oil and gas fields [53] depends in part upon EOR; hence the importance of this thesis.

1.4.2.2 EOR Economics

The availability and price of oil have a substantial economic and social impact, as seen at the end of 1973 when the price quadrupled. Developed societies are highly dependent on a continuous consumption of energy (which is proportional to their standard of living), although of course the source of that fuel has changed with time. Hence money and

energy are intimately mixed. Indeed many suggest energy analysis or accounting is appropriate as a method of deducing the efficiency of production (in kJ/kg) or a process (in kJ/h) [54]. This has been attempted to estimate and improve the efficiency of industrial processes [55], petroleum processing [56] and oil-field operation where less water injection could be beneficial [57], but might also be applied to planning future fuel usage [58].

1.4.2.3 EOR Environment

There are now environmental concerns over petroleum recovery operations [59] and this may relate to nonyl-phenol species entering water system because of their oestrogenic properties. North Sea reserves are declining [60] and operators are searching beneath Windsor (where 100 million barrels of oil have been predicted in sandstone layers in the Thames Valley 400m under the Castle).

Alkyl phenol ethoxylates have been shown to be major pollutants of water systems by the chemical industry. Their inability to biodegrade aids them in solubilising the vastly increasing amounts of female hormones found in domestic waste. These hormones are then free to enter fish and other animals and so enter our food chain. Natural product molecules could be the answer to these non-biodegradable pollutants from the chemical industry. Naturally occuring phenolic lipids found in the shell of the cashew nut can be converted to friendly surfactant molecules. The "Sturtevant Process" or hot decarboxylation, is used to make "cardanol" which can then be used to obtain biodegradable surfactants.

1.4.2.4 Technology

After primary recovery (which utilises the initially high pressure of the reservoir itself to release oil), secondary recovery with water flooding [61] accelerates oil release (becoming uneconomic as the volumes of water required increase) but may still leave 40% of oil within the reservoir because it is too viscous, etc. Enhanced oil recovery then coming into play includes: thermal methods [62]: steam [63], hot water [64], in-situ combustion [65]; gas flooding: CO_2 [66], inert gas, N_2 ; chemical flooding: surfactants [67], polymers;

alkaline solutions (e.g. NaOH or KOH [68]) or acidising EOR in carbonate reservoirs [69] or solvent EOR [70] and novel methods: microbial [71]. CO_2 EOR [72], which can be thermodynamically modelled [73], may require CO_2 separation from exit gases [74]. Others have used supercritical hydrocarbons [75].

A surfactant to be used in this context must: be soluble in relevant brines (with salinities up to 20% total dissolved solids, where Ca^{2+} and Mg^{2+} may cause sulphonate precipitation) at relevant temperatures (i.e. up to 423K) and pressures (up to 50MPa); be partially soluble in oil; able to form micellar structures and oil/water emulsions; lower oil/water interfacial tensions to <1mN/m; adsorb only weakly on the surface of the rock.

To do this it must be tailored to the precise reservoir conditions. Non-ionic surfactants may adsorb less than anionic or cationic ones [76], but are they resistant to precipitation at relevant p, T and salinity conditions? The chemical wt% composition of crude oils is variable:

	North Sea	South American
light gasoline	5.8	0.1
naphtha	11.0	1.1
kerosene	18.6	4.4
diesel	19.1	9.6
residue	43.5	84.8
Sulphur	0.3	5.5

Low interfacial tension flooding uses low surfactant concentrations in solution, but microemulsion flooding uses higher concentrations. Precipitation by cations [77] and adsorption of surfactants [78] can be important even in foam EOR [79]. The adsorption of anionic surfactants on sand or clay has been followed by FTIR [80]. Factors affecting the critical micelle concentration (CMC) include (i) the hydrophobic group, (ii) the hydrophilic group, (iii) the electrolyte, (iv) organic additives, and (v) temperature. Adsorption is minimal when the adsorbate and the surface have the same charge [81], and of course the latter is pH-dependent.

1.4.2.5 Adsorption of Surfactant onto Rock Surfaces

An understanding of phenomena occurring at the boundary between two phases is often essential for explaining mechanisms of many physical and chemical processes which occur, or are initiated, at that interface. For example: crystallisation, electrode processes, heterogeneous catalysis and adsorption studies. A detailed knowledge of surface phenomena is therefore essential for all those interested in these sciences. Adsorption from solution onto solids is of great practical importance and a large number of papers and text books has been published on this subject.

Adsorption from solution differs from adsorption of individual substances (e.g. gases, vapours and pure liquids) in that the solution contains more than one component and compact layers can form on the surface of the adsorbent. In adsorption at the solid/liquid interface the experimental measurement is the change in concentration of the solution; the isotherm of concentration change is a "composite isotherm" due to the presence of at least two components in the solution. Besides the acknowledgement of the role of the solvent and its competition with the solute for the surface sites, there is also an increasing understanding of the effects of the chemistry of the surface on the adsorption process. The interaction between the surface and adsorbent species can be defined as physical or chemical, as with gas/solid adsorption. Several types of interaction during adsorption may occur simultaneously depending on the chemical structure of both components.

1.4.3 Microemulsions as Microreactors

As previously defined that a microemulsion is a thermodynamically stable, optically isotropic solution of two immiscible liquids (e.g. water and oil) consisting of microdomains of one or both liquids stabilised by an interfacial film of surfactant. The surfactant molecules optimise their interactions by residing at the oil/water interface, thereby considerably reducing the interfacial tension. In w/o microemulsions, the aqueous phase is dispersed as microdroplets surrounded by a monolayer of surfactant molecules in the continuous hydrocarbon phase. The aqueous cores of microemulsions, containing soluble metal salts, are used as microreactors for the synthesis of nanoparticles. Due to the dynamic nature of the microdroplets, an exchange mechanism involves coalescence

and fusion of the droplets upon collision, which then disintegrate into droplets, and this process occurs continuously in the microemulsion [82].

1.5 Aims of the Research

How the molecular configuration and constitution of surfactants and polymers (and their blends with co-surfactants and co-solvents) determine their stability and interfacial characteristics was not well understood. An attempt was to be made here to rationalise this understanding and to optimise enhanced oil recovery with chemicals of optimised stability and interfacial properties under reservoir conditions through thorough understanding of the properties of surfactants and polymers within oil reservoir conditions and thereby to allow these to be tailored to produce the most useful stability and interfacial characteristics to enable the maximum extent of tertiary oil recovery from European reservoirs. In addition, it was anticipated that the fundamental microemulsion science developed would be of value in improving hydrocarbon combustion and materials synthesis. This was also to be tested.

The research work described in this thesis was to be primarily concerned with the formulation and characterisation of a model microemulsion/surfactant system which could in principle be used in the reservoirs to enhance oil recovery. The rate, extent and nature of adsorption of surfactants, from the aqueous and nonaqueous solutions, onto the rock formation were also to be studied at various relevant temperatures and salinities. It was anticipated that the fundamental understanding of the properties, stability and interfacial characteristics of these molecules and the resulting ability to predict the molecular requirements for a chemical flooding of any oil reservoir whose temperature, salinity, permeability, and oil profile were known would be of importance and that the emulsion chemistry developed would be of value in improving the combustion of hydrocarbon fuels with lower pollutant emissions. The combustion characteristics of these microemulsions were to be considered and may represent a new route to high value oxygenates. Finally, the microemulsion route was used to synthesize the colloidal silica of desired particle size and morphology.

References

[1] R.H. Ottewill, unpublished M.Sc. Lecture notes on "Solutions of Surface Active Agents", Bristol University (1990)

[2] D.J. Shaw, in "Introduction to Colloid and Surface Chemistry", 3rd Edn., Butterworths, Kent, England (1980).

[3] J.W. McBain, Trans. Faraday Soc. **9,** 99 (1913)

[4] R. Aveyard, B.P. Binks, S. Clark and P.D.I. Fletcher, J. Chem. Tech. Biotech. **48,** 161 (1990)

[5] G.S. Hartley, B. Collie, and C.S. Smith, Trans. Faraday Soc. **32,** 795 (1936)

[6] J.C. Russel and D.G. Whitten, J. Am. Chem. Soc. **104,** 5937 (1982)

[7] W.D. Harkins,"Physical Chemistry of Surface Films", Reinhold, New York, (1952)

[8] "Interfacial Phenomena" Eds. C.A. Miller and P. Neogi, Marcel Dekker, Inc. New York (1985)

[9] T.P. Hoar and J.H. Schulman, Nature, **152,** (1943)

[10] S. Kumar and H.N. Singh, Colloids and Surfaces **44,** 17 (1990)

[11] S.I. Ahmad, K. Shinoda and S. Friberg, J. Colloid Interface Sci., **47,** 32 (1974)

[12] M.S. El-Aasser, C.D. Lack, J.W. Vanderhoff and F.M. Fowkes, Colloids and Surfaces, **29,** 103, (1988)

[13] H.L. Rosano, T. Lan and A. Weiss, J. Colloid Interface Sci., **72**, 233, (1979)

[14] D.O. Shah, Ed.,"Macro-and Microemulsions Theory and Applications," American Chemical Society, Washington, DC (1985)

[15] J.H. Schulman, W. Stoeckenius and L.M. Prince, J. Phys. Chem. **63,** 1677, (1959)

[16] D.H. Everett,"Basic Principles of Colloid Science" Royal Society of Chemistry Paperbacks, London, (1988)

[17] H. Saito and K. Shinoda, J. Colloid Interface Sci., **32,** 647 (1970)

[18] J. Lang, N. Lalem and R. Zana, J. Phys. Chem., **96,** 4667 (1992)

[19] L.E. Scriven, Nature, **263,** 123 (1976)

[20] L.E. Scriven, in "Micellisation, Solubilisation and Microemulsions", Ed. K. Mittal, Plenum Press, New York , **2**, 877 (1977)

[21] Y. Talmon and S. Prager, J. Chem. Phys., **69,** 2984 (1978)

[22] L. Auvray, J.P. Cotton, R. Ober and C. Taupin, J. Phys. (Paris), **45,** 913, (1984)

[23] P.E. Zinsli, J. Phys. Chem., **83,** 3223 (1979)

[24] M. Wong, J.K. Thomas and M. Gratzel, J. Am. Chem. Soc., **98,** 2391 (1976)

[25] R.N. Healy, R.L. Reed and C.W. Carpenter, Soc. Pet. Eng. J. **15,** 87, (1975)

[26] T.S. Gendy, Y. Barakat and A.I. Mead, Polymer International **24,** 235 (1991)

[27] D.J. Miller, S.P. Van Halasz, M. Schmidt, A. Holst and G. Pusch, J. Pet. Sci. and Eng., **6,** 63 (1991)

[28] R.N. Healy, R.L. Reed and D.G. Stenmark, J. Soc. Pet. Eng., **June,** 147 (1976)

[29] P. Walde, A. Goto, P.A. Monnard, M. Wessicken and P.L. Luisi, J. Am. Chem. Soc., **116**, 7541 (1994)

[30] S.E. Friberg and R.L. Venable in "Encyclopaedia of Emulsion Technology", Ed. P. Becher, Marcel Dekker, **1**, 319 (1983)

[31] T.R. Burridge and M.A. Shir, Marine Pollution Bull. **31**, 446 (1995)

[32] "Microemulsions", Ed. I.D. Robb, Plenum Press, New York (1981)

[33] "Biological and Technological Relevance of Reversed Micelles and Amphiphilic Structures in a Polar Medium", Eds. P.L. Luisi and B. Straub, Plenum Press, New York (1984)

[34] L.S. Schulman, Phys. Rev. **B7**, 1960 (1973)

[35] H. Ishida and A. Iwama, Combus. Sci. Tech., **37**, 79 (1984)

[36] D. Attwood and A.T. Florence, in "Surfactant Systems", Chapman and Hall, New York Chap.11 (1983)

[37] S. Chang, L. Liu and S.A. Asher, J. Am. Chem. Soc., **116**, 6745, (1994)

[38] J.P. Durand, D. Nicolas, N. Kohler, F. Dawans and F. Candau, French Patent 2 565 623 (1987)

[39] J.P. Durand, D. Nicolas, N. Kohler, F. Dawans and F. Candau, French Patent 2565 592 (1987)

[40] J.P. Durand, D. Nicolas and F. Candau, French Patent, 2 567 525 (1987)

[41] T. Suzawa and T. Murakami, J. Colloid Interface Sci. **78,** 266 (1980)

[42] H. Shirahama and T. Suzawa, J. Colloid Interface Sci. **104,** 416 (1985)

[43] H. Shirahama, K. Takeda and T. Suzawa, J. Colloid Interface Sci. **109,** 552 (1986)

[44] K.R. Olen, J.P. Dooher and L.M. Woodworth, International Workshop on Coal-liquid Fuels Technology. Nova Scotia, Canada: Centre for Energy Studies, Technical University of Nova Scotia, (1985)

[45] OPEC. Facts and Figures. A Graphical Analysis of World Energy up to 1990, (1991).

[46] N.J. Clark 'Elements of Petroleum Reservoirs' Soc. Pet. Eng. (AIMMPE) (1969)

[47] Conoco, Pamphlet. World Energy Outlook Through 2000, (1989)

[48] L.W. Lake, 'Enhanced Oil Recovery' (Prentice Hall) New Jersey (1989)

[49] T.J. McMillen, Energy Prog. **4,** 45 (1984)

[50] U.P. Kuvanyshev, Zh.Geol. **11K**, 36, (1990)

[51] F.J. Fayers, M.J. Blunt and M.A. Christie, SPE Reservoir Eng. **7,** 195 (1992)

[52] L.E. Baker, A.C. Pierce and K.D. Luks, J. Soc. Pet. Eng., **22,** 731 (1982)

[53] D.H. Root and R.F. Mast, AAPG Bull. **77,** 479 (1993)

[54] J.A.G. Thomas 'Energy Analysis' Westview Press (1977)

[55] S. Alvarado and J. Iribarne, Energy (Oxford) **15,** 1023 (1990)

[56] B. Olteanu, Rev. Chim. Bucharest **43,** 205 (1992)

[57] A.T. Panarin, Neft. Khoz. **2,** 8 (1992)

[58] T.F. Wall, A.L.Salusinszy, D.B. Ebeling, G.R. Drewe, K.M. Sullivan, P. Beeran and G.B.Smith, Energy Sources, **14**, 253 (1992)

[59] J.C. Harris and L.R. Heinze, Proc. Annu. South West Pet. Short Course **39,** 488 (1992)

[60] The Daily Telegraph 7/12/1994 page 4; Pet. Rev. **Jan** (1995)

[61] M. Kasraie, P.H. Sammon and P.J. Jespersen, J. Pet. Tech. **45,** 888 (1993)

[62] T.B. Reid and P. Colonomos, DOE/BC-93/3/SP

[63] M.S. Jankovic, Transp. Porous Media **13,** 277 (1993); H.K.Van Poolen, 'Fundamentals of Enhanced Oil Recovery' Penwell Books (Tulsa) (1980)

[64] C.G. Bursell and G.M. Pittman J. Pet. Tech. **August,** 997 (1975)

[65] C.F. Gates and I. Sklar, J. Pet. Tech. **August,** 981 (1975)

[66] H.L. Wang, J.L. Duda and C.J. Radke, J. Colloid Interface Sci. **66,** 15 (1978)

[67] US Patent 1823440 (1930); US Patent 3006411 (1958)

[68] K. Liszka, J. Jewulski, J. Stopa and D. Zagrajczuk, Nafta-Gaz **49,** 414 (1993)

[69] J. Tang, J. Satherley and D.J. Schiffrin Chin, J. Chem. Eng. **1,** 223 (1993)

[70] G. Coskuner and R.G. Bentsen, J. Can. Pet.Tech. **26,** 26 (1987)

[71] E.C. Donaldson, Developments in Petroleum Science **31** Elsevier (1991)

[72] K.A.M.Gasem, K.B. Dickson, R.D. Shaver and R.L. Robinson, SPE Reservoir Eng. **8,** 170 (1993); S.L. Kokal and S.G. Sayegh, J. Pet. Sci. Eng. **9,** 289 (1993)

[73] D. Zudkevitch, G.J. Czerwienski and Y.Z. Wang, Proc. Annu. Conv. Gas. Proc. Assoc. 64th 266 (1985)

[74] B.G. Goar, Proc. Annu. Conv. Gas. Proc. Assoc. 64th 330 (1985)

[75] UK Patent 2104132 (1983); German Patent 3144441 (1983)

[76] C.G. Inks and R.I. Lahring, J. Pet. Tech. **11,** 1320 (1968)

[77] R.D. Walker, R.A. Keppel, M.B. Cosper, J.J. Funk and M.J. Meister, Prep. Amer. Chem. Soc. Div. Pet. Chem. **26,** 185 (1981)

[78] D. Kumar, Part. Technol. Surf. Phenom. Miner. Pet., Proc. Fine. Part. Soc. Symp. 235 (1991)

[79] J.T. Patton and S.T. Holbrook, NMRDI-2-75-5231 (1990)

[80] Y. Ju and Y. Zhou, Shiyou Kantan Yu Kaifa **20,** 67 (1993)

[81] B.Tamamushi and K. Tamaki, Trans. Faraday Soc. **55,** 1007 (1959)

[82] H.F. Eicke, J.C.W. Shepherd and A. Steinemann, J. Colloid Interface Sci. **56,** 168 (1976)

CHAPTER TWO

THEORY OF THE FORMATION OF MICROEMULSIONS AND THEIR CHARACTERISATION

2.1 Theories of Microemulsion Formation

The several theories of the mechanism of microemulsion formation can be classified into three main categories: interfacial, solubilisation and thermodynamic.

2.1.1 The Mixed Film (Interfacial) Theory

The first interfacial theory was proposed by Hoar and Schulman [1] who considered that complex formation between surfactant and co-surfactant at the interface between water and oil was responsible for lowering the interfacial tension to very low values leading to a spontaneous increase in the interfacial area that was involved in the formation of the microemulsion.

In 1955, Bowcott and Schulman [2-4] attributed the formation of a microemulsion to the molecular attraction that takes place at the interface and that the interface in equilibrium with both the oil and water phases was described as a third phase. At this interface, it was assumed that this third phase has its own spreading pressure (π).

Schulman et al [5] postulated that the total droplet interfacial tension γ of the microemulsion might be expressed by

$$\gamma = \gamma_{o/w} - \pi \qquad (2.1)$$

where $\gamma_{o/w}$ is the interfacial tension between the oil and the water in the absence of a surface active agent and π is the two-dimensional spreading pressure of the film. According to this equation, if, as a result of the adsorption of surfactant at the interface, π becomes greater than $\gamma_{o/w}$, then energy ($-\gamma dA$) is available to increase the total interfacial area 'A' between two phases until no more energy is available and γ returns to zero. It is also clear from this equation that for γ to become zero or negative, π has to become equal to or greater than $\gamma_{o/w}$. When $\gamma_{o/w}$ is greater than the film pressure π only

a macroemulsion is formed. $\gamma_{o/w}$ is of the order of 30-50 mNm^{-1}, depending upon the type of oil, and in order to reduce the total interfacial tension to zero or become negative, π should take the very high values that would not allow oil molecules to stay in the amphiphilic monolayer.

Prince [6-8] suggested that the presence of a second surfactant (co-surfactant) would reduce $\gamma_{o/w}$ to much lower values and consequently the film pressure would not need to increase to a high value. For this reason, he introduced a subscript 'a' to the interfacial term in equation (2.1) which takes into account any reduction in the value of interfacial tension due to the addition of co-surfactant. The film pressures required to reduce the net interfacial tension to zero or a negative value were much lower and easily attainable. Therefore the equation (2.1) can be written as:

$$\gamma = (\gamma_{o/w})_a - \pi \qquad (2.2)$$

where $(\gamma_{o/w})_a$ is the interfacial tension between oil containing the co-surfactant and water.

The dynamic aspects of the interfacial tension for Schulman-type microemulsions was investigated by Rosano [9]. He observed that strong interactions between surfactant and co-surfactant were *not* necessary for microemulsion formation, and argued that the spherical shape of the droplets (i.e. the shape of minimum surface to volume ratio) implies that the equilibrium surface tension must be positive. Rosano considered that the important factor for microemulsification was the transport of the alcohol (co-surfactant) across the interface, the rate of which was reduced due to the presence of an adsorbed monolayer of surfactant.

It has been suggested [10] that the term "microemulsion" be reserved for systems in which the free energy of formation, ΔG_{form}, is only transiently negative, whilst truly thermodynamically stable systems be termed "micellar solutions", although in practice it may be impossible to distinguish between them.

2.1.2 Duplex Film Model

The concept of a duplex film at the oil/water interface was also introduced [11] and further developed [12] to explain the bending of the interface to form w/o or o/w microemulsions. Thus, the freshly formed flat film will have two different film pressures π'_o and π'_w (i.e. π'_o and π'_w are the film pressures of the flat duplex film at the oil and water side respectively: $\pi'_w = 30\ mNm^{-1}$, $\pi'_o = 10\ mNm^{-1}$). Bending of the interface will then take place to relieve the stress due to the pressure gradients. This expansion continues, to different degrees at each side of the interface, until π drops to $(\gamma_{o/w})_a$.

$$\pi = \pi'_o + \pi'_w \qquad (2.3)$$

Expansion occurs until $\pi'_o = \pi'_w = 0.5(\gamma_{o/w})_a$; the latter equivalence arising from application of equation 2.2. The direction of curvature depends on the relative magnitude of π'_w and π'_o. Figure 2.1 illustrates the mechanism of curvature of a microemulsion film. If initial film pressure π'_o on the oil side is greater than the initial film pressure π'_w on the water side, the duplex film will bend towards the water side to form a w/o microemulsion. On the other hand, if $\pi'_o < \pi'_w$, the film expands on the water side to reduce π'_w until $\pi'_o = \pi'_w$ and as a result of this an o/w microemulsion is formed.

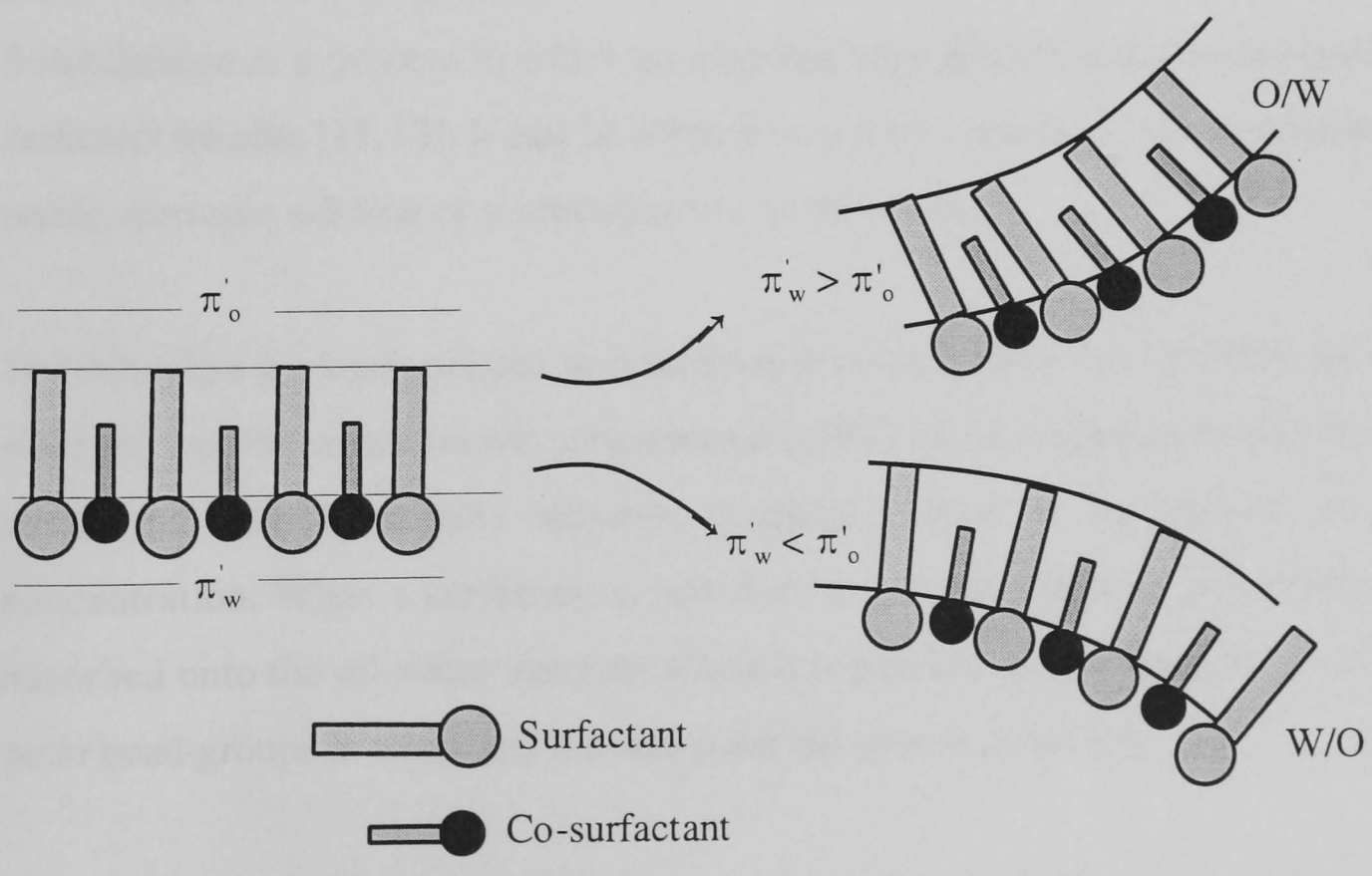

Figure 2.1 Mechanism of curvature of a microemulsion film

Robbins [12] has suggested that a stress gradient is established across the interface arising from the differences in the solvency of the head-groups in water and the surfactant chains in oil. The stress determined the magnitude and sign of the droplet curvature and could be expressed in terms of physically-measurable quantities such as the surfactant molecular volumes (including head and chain volumes), interfacial tensions and compressibilities. Droplet size, interfacial tension, and the number of adsorbed surfactant molecules per droplet were also estimated [12]. Friberg et al [13] investigated water, hexadecane, hexanol and ethoxylate nonionic surfactant systems, and found that predictions based on duplex film theory were in good agreement with the observed phase behaviour.

Prince [7-8] has shown that the correct combination and appropriate concentration of surfactant and co-surfactant are necessary to formulate a microemulsion system. A duplex film with different pressures on each side of the interface is produced [8, 14]. The mixed film concept explains the bending of the interface and thermodynamic stability of microemulsions.

2.1.3 Solubilisation Theories

Solubilisation is a process in which an insoluble substance becomes incorporated into surfactant micelles [15, 17]. It may be referred to as the formation of a thermodynamically stable, isotropic solution of a substance in a given solvent.

Solubilisation is closely related to micellisation since little or no solubility increase is observed until the critical micelle concentration (CMC) of the surfactant is reached, above which the solubility usually increases in direct relation to the increase in micelle concentration. When a surfactant is added to an oil-water mixture it is preferentially adsorbed onto the oil-water interface where it is possible to simultaneously solvate the polar head-groups in water and the non-polar tail-groups in the oil.

Several important factors (such as the structure of the surfactant and solubilisate, the temperature and the addition of electrolytes) affect the solubilisation [15]. Temperature has an effect on the extent of micellar solubilisation which is dependent on the structure

of the solubilisate and of the surfactant. Generally, solubilisation increases with increasing temperature. This is usually due to an increase in solubility of the solubilisate and an increase of the micellar size.

Addition of electrolytes to ionic surfactants usually causes an increase in micelle size and a reduction in the CMC, and hence increases the solubilising power. Non-electrolytes, (e.g., alcohols) which are incorporated in the micelle, lead to an increase in the micelle size and hence lead to an increase in solubilisation.

Chou and Bae [16] also showed that temperature and addition of electrolyte have an effect on the CMC, and that these parameters also affect solubilisation. In general, the two approaches that have been adopted in the description of microemulsion systems have considered them either to be swollen micelles [17, 18] or to involve changes that occur at the oil/water interface [19, 20]. Thus the small microemulsion droplets may be envisaged to be formed in two ways [21]:

(i) by the breakdown of larger droplets on a lowering (if only transiently) of the interfacial surface tension;

(ii) by the swelling of the interior of a micelle by molecular diffusion of the interior phase through the bulk medium.

In surfactant-nonpolar solvent systems, the polar interactions of the head groups not only provide a driving force for the aggregation process, but also provide an opportune location for the solubilization of polar additives. Water is, of course, one of the most important potential polar additives to nonaqueous systems, and it is primarily located in the core. The initial water added likely becomes closely associated with the polar head group of the surfactant, while subsequent additions appear to have the character of free bulk water. The effects of solubilized additives on the micellar properties of nonaqueous surfactant systems vary according to the strucrures of the components.

Surfactant molecules are able to form a diverse range of aggregate structures in water/surfactant/oil systems. The preferred aggregate structure is generally a consequence

of the surfactant molecular geometry, the surfactant concentration, the oil-water volume ratio, the nature of the surfactant counter-ion (in the case of ionic surfactants) and the relative balance of hydrophobic and hydrophilic groups (HLB) on a surfactant molecule [22].

Kumar and Balasubramanian [23, 24] investigated the solubilisation of water and cyclohexane by hexanol and the nonionic surfactant Triton X-100 using different spectroscopic techniques, in particular NMR. At a fixed surfactant/alcohol ratio, in systems of low water concentration (=1%w/w water), the surfactant was molecularly dispersed in the cyclohexane, the water molecules being associated with the ethylene oxide sequence of the surfactant to a limiting value of $1H_2O : 2C_2H_4O$ [24]. At high water concentration (approximately 3% w/w), micelles formed containing both *surfactant-bonded* water molecules and *free* water molecules.

2.1.4 Thermodynamic Theories of Microemulsions

Several thermodynamic theories have been proposed to explain the mechanism of microemulsion formation. Overbeek [12, 25-27] considered the microemulsion system of droplets with uniform size and used the adsorption equation to see the effect of adsorption of surfactant and co-surfactant on interfacial tension. The Gibb's adsorption equation, for multicomponent system, in its general form can be written as:

$$\gamma = \gamma_o - {}_o\int^i \Gamma_i RTd[\ln c_i] \qquad (2.4)$$

where γ_o and γ are the interfacial tensions without and with surfactant and co-surfactant (if any), Γ_i is the amount of adsorption of component i per unit area and c_i is the concentration of ith component. Recently, Overbeek et al [26] related the Gibb's energy of microemulsion at internal equilibrium to the interfacial tension and bending stress as a function of droplet radius and volume fraction. They defined the Gibb's free energy of a microemulsion G^M by the following expression:

$$G^M = F^M + pV^M \qquad (2.5)$$

where F^M is the Helmholtz free energy, V^M is the volume of microemulsion and p is the ambient pressure. They determined the Helmholtz free energy in two steps. *Firstly*, they considered 'n_d' drops within local equilibrium with the surrounding continuous phase. The chemical potentials, λ_i, in drops, in the continuous medium and at the interfaces were assumed to be equal. *Secondly*, the drops were allowed to move freely in the continuous medium creating the free energy of mixing F_{mix}. Under these conditions the Helmholtz free energy can be written as:

$$F^M = \Sigma n_i \lambda_i - pV_m - (p+\Delta p)V_d + \gamma A + F_{mix} \qquad (2.6)$$

where n_i and λ_i are the amount and chemical potential respectively of ith components, V_m is the volume of continuous phase, V_d is the volume of droplets and $(p+\Delta p)$ is the pressure inside the droplets, γ is the interfacial tension between the droplets and the continuous medium depending on the curvature at constant T, p and λ_i , and A is the total interfacial area. The Gibb's free energy of microemulsion G^M can be written as:

$$G^M = F^M + pV^M = \Sigma n_i \lambda_i - \Delta p V_d + \gamma A + G_{mix} \qquad (2.7)$$

where $V^M = V_m + V_d$, $G_{mix} = F_{mix}$ and Δp is the excess pressure inside the droplets. Minimizing G^M in order to find the equilibrium conditions for microemulsions, differentiating the equation (2.7) one obtains:

$$dG^M = \Sigma n_i d\lambda_i + \Sigma \lambda_i dn_i - \Delta p dV_d - V_d d\Delta p + \gamma dA + A d\gamma + dG_{mix} \qquad (2.8)$$

The interfacial tension γ depends not only on all chemical potentials but also on the curvature (2/a) where 'a' is the radius of the curvature and is expressed as follows:

$$A d\gamma = - A \Sigma \Gamma_i \, d\lambda_i + Acd\,(2/a) \qquad (2.9)$$

where Γ_i is amount of the ith component adsorbed per unit area, c is the bending stress coefficient [25-27] and is defined as follows:

$$c = [\frac{\delta\gamma}{\delta(2/a)}]_{T,P,\lambda_i} \qquad (2.10)$$

Ruckenstein and Krishnan [14, 28] assumed that the solubilized molecules as a spherical core and the surfactant is adsorbed at the interface. The Helmholtz free energy per cubic centimeter of microemulsion was determined assuming: a) the surfactant is only soluble in the continuous phase, b) the dispersed globules have a uniform size with a solubilized core radius, and c) the interaction between the neighbouring head groups is negligible. Ruckenstein [29] suggested a new theory based on the assumption that the microemulsion contains uniform size hard globules. The dispersion of globules is in the continuous phase and increase the entropy of the system thereby increases its Helmholtz free energy, Δf, per unit volume of microemulsion. Thus the free energy, f, per unit volume of microemulsion is given by:

$$f = f_o + \Delta f \qquad (2.11)$$

De Gennes and Taupin [30] treated the Helmholtz free energy of a microemulsion in a different way. Because there is no evidence that each surfactant molecule stays at the interface only, the saturated state is never reached and therefore the surfactant molecules may prefer to move into the continuous phase or inside the droplets. In Schulman's description of microemulsion formation, all energies associated with the curvature of the interfaces are ignored. This is perhaps relevant because for many problems involving liquid/liquid interfaces, curvature energies make a very minor contribution and the interfacial energy (γ) becomes dominant. As in microemulsions, the interfacial tension becomes zero or even reaches negative values, the contribution of curvature and entropy change cannot be neglected. De Gennes and Taupin presented the following expression for the curvature-dependent energy contribution per unit area as:

$$F = \gamma - \frac{K}{R_0 R} + \frac{K}{2R^2} \qquad (2.12)$$

where γ is the interfacial tension, 1/R is the curvature of the interface, $1/R_0$ is the spontaneous or natural curvature ($R_0 > 0$ for normal micelles, $R_0 < 0$ for reverse micelles)

and K is the rigidity of the interface. The rigidity constant is defined as the energy required to bend a unit area of the film by a unit amount of curvature average from spontaneous curvature. The above equation holds only if R and R_0 are much larger than the interfacial film thickness.

Robbins [12] ascribed the curvature effects in the phase behaviour of microemulsion of nonionic surfactants. Aveyard et al [31] determined the interfacial tension at the droplet surface as a function of droplet radius for heptane and tetradecane as oil. They concluded that the formation of excess phase occurs when the surfactant monolayer curvature in microemulsion droplet phase is approximately equal to the spontaneous film curvature and gave an approximate equation as:

$$\gamma = \frac{constant}{2R_d^2} \tag{2.13}$$

where R_d is the droplet radius.

Binks et al [33] measured the rigidity constant K with ellipsometric measurements. Their results compare well with theory; the smaller the film rigidity constants, the smaller is the dispersed droplet size and the larger the interfacial tension. The rigidity constant K of a monolayer at the oil/water interface depends on the composition of the interfacial region.

2.1.5 R-Ratio Theory

Bourrel and Schechter [32] related the curvature effects to the R-ratio which defines the relationship between the interaction energies of an amphiphilic interfacial layer C and the oil and water regions which was first developed by Winsor [34, 35]. They divided a single-phase isotropic microemulsion into three distinct regions: an aqueous region W, an oil region O, and an amphiphilic region C [32]. They considered certain cohesive interaction energies that exist within the layer C and are responsible for the stability of this layer. Figure 2.2 shows the different constituents of a microemulsion system and corresponding cohesive interaction energies.

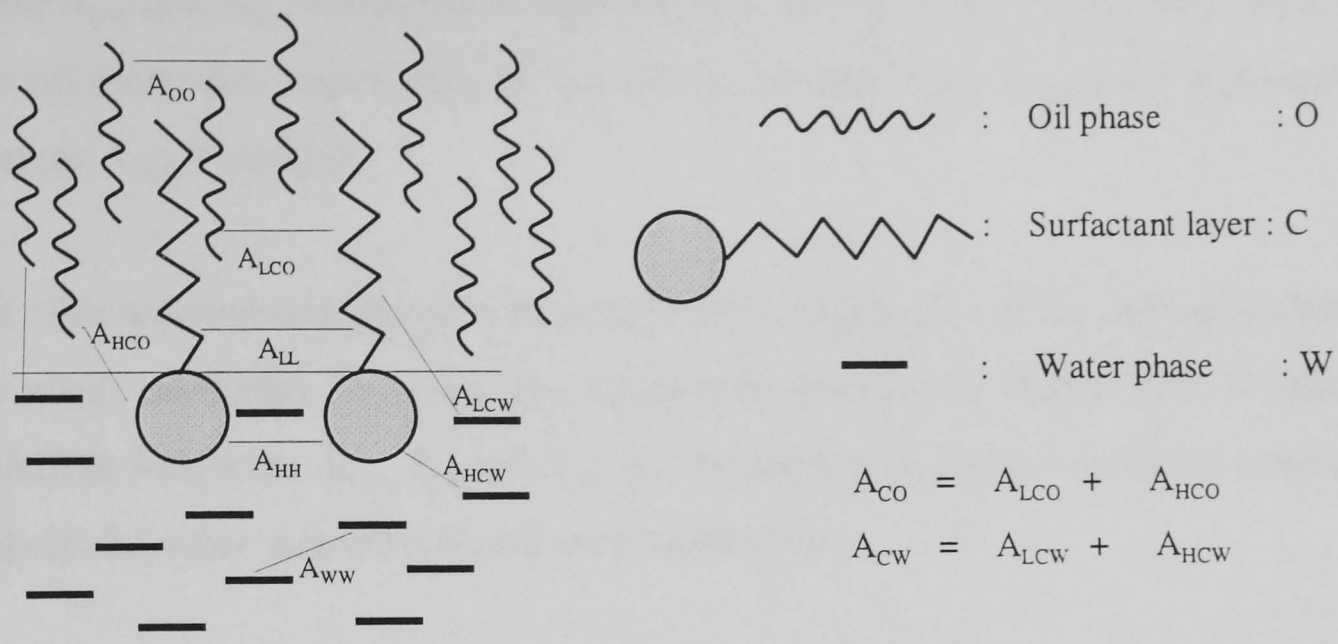

Figure 2.2 Interaction energies in the amphiphilic layer at the water / oil interface

The cohesive interaction energy A_{xy} between two molecules x and y is calculated per unit area within the interfacial layer C and is averaged over the position of molecules x and y. Therefore the cohesive energy as used is positive whenever the interaction forces between the molecules residing within layer C take into account both the lipophilic and hydrophilic interactions. The cohesive energy A_{xy} between molecules x and y is then expressed as:

$$A_{xy} = A_{Lxy} + A_{Hxy} \tag{2.14}$$

where L and H represent lipophilic and hydrophilic respectively. Using this concept, the general definition of R-ratio for system as represented in Figure 2.2 is given as:

$$R = \frac{A_{CO} - A_{OO} - A_{LL}}{A_{CW} - A_{WW} - A_{HH}} \tag{2.15}$$

where A_{oo} is defined as the cohesive energy per unit area between oil molecules residing inside the interfacial layer C, which can further be written as:

$$A_{oo} = A_{Loo} + A_{Hoo} \tag{2.16}$$

where A_{Loo} and A_{Hoo} denote the interaction between the non-polar and polar ends of the two oil molecules respectively. In the case of oil molecules, A_{Loo} is the dominant term whereas A_{Hoo} is ignored.

The other cohesive energies per unit area present in Figure 2.2 are the interaction between the water molecules A_{WW}, and the interaction between the hydrophiles of surfactant molecules with water A_{Hcw}. A_{co} and A_{cw} are the interaction energies between amphiphiles and oil and water respectively and are presented by:

$$A_{CO} = A_{Lco} + A_{Hco} \quad (2.17)$$

$$A_{CW} = A_{Lcw} + A_{Hcw} \quad (2.18)$$

where A_{Hco} and A_{Lco} represent the interaction energies of amphiphiles with the polar and non-polar portions of the oil molecules respectively. Similarly A_{Hcw} and A_{Lcw} denote the interaction of amphiphile molecules with the polar and non-polar character of the water molecules. In many cases A_{Hco} and A_{Lcw} can be neglected and the equation (2.17) and (2.18) can be written as:

$$A_{CO} = A_{Lco} \quad (2.19)$$

$$A_{CW} = A_{Hcw} \quad (2.20)$$

The R-ratio represents the extent of the interface to fluctuate and attain a particular shape depending on the nature of the components of the system, their relative concentration and temperature. If R=1, the mutual solubility of C, W and O reaches a maximum and the interfacial layer C will have no tendency to bend preferentially towards one or the other, oil or water . If $R > 1$ or $R < 1$, the affinity of the layer C is no longer the same for O and W. The stability of interfacial layer C will be maintained at the natural arrangement of molecules in which layer C is convex towards O ($R < 1$) or towards W ($R > 1$).

Bourrel and Schechter [32] used the R-ratio concept to determine the interfacial free energy:

$$\frac{\delta f^s}{\delta r} = -\frac{H}{r^2} \tag{2.21}$$

where f^s is the interfacial free energy per unit of area, r is the radius of spherical interface and H is a key quantity related to R-ratio and approximated by Millar and Neogi [36] as:

$$H = K_r \left(\frac{1}{r} - \frac{1}{R_n}\right) \tag{2.22}$$

where K_r is a constant related to the flexibility of interface and R_n is the natural radius of curvature. The interfacial free energy reaches a maximum at $r = R_n$. The discussion shows that the R-ratio is a real thermodynamic quantity even though no precise relationship of R and H is available.

2.2 CHARACTERISATION TECHNIQUES FOR MICROEMULSIONS

2.2.1 Ultraviolet-Visible Spectroscopy (UV-Vis)

Absorption of ultraviolet and visible radiation provides a convenient means of analysing numerous inorganic and organic species. It involves the absorption of electromagnetic radiation by molecules in the UV-visible region. The absorption of electromagnetic radiation by molecules will lead to electronic transitions between molecular orbitals and therefore the electronic spectra give information about the electronic structures of molecules [37].

The absorption of electromagnetic radiation by some species M can be considered to be an irreversible two-step process, the first step of which can be represented by

$$M + h\nu \rightarrow M^* \tag{2.23}$$

where M^* represents the atomic or molecular particle in the excited state resulting from absorption of the photon $h\nu$. The life time of the excited state is brief (e.g. 1-10 ns), its excitence being terminated by any of several relaxation processes. The most common type

of relaxation involves conversion of the excitation energy to heat; that is

$$M^* \rightarrow M + \text{heat} \tag{2.24}$$

The life time of M^* is so short that its magnitude at any instant is negligible under ordinary conditions. Furthermore, the amount of thermal energy created is usually not detectable. Thus, absorption measurements have the advantage of creating a minimal disturbance of the system under study.

When light is absorbed by a sample, the radiant power of the beam of light is decreased. Light is passed through a monochromator (which may be a prism, grating, or even a filter) to select one wavelength. Light of this wavelength, with radiant power P_o, strikes a sample of length b. The radiant power of the beam emerging from the other side of the sample is P (see below). Some of the light may be absorbed by the sample, so that $P < P_o$.

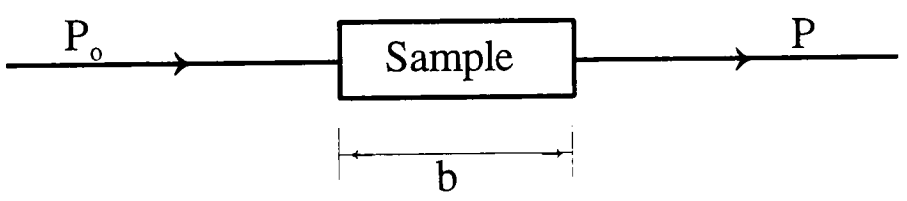

The transmittance, T, is defined as the fraction of the original light that passes through the sample.

$$T = \frac{P}{P_o} \tag{2.25}$$

Therefore, T has the range zero to one. The percent transmittance is simply 100T where $0\% < T < 100\%$.

$$A = \log_{10}\left(\frac{P_o}{P}\right) = -\log T \tag{2.26}$$

Absorbance (A) is important because it is directly proportional to the concentration of light-absorbing species in the sample:

$$A = \varepsilon bc \tag{2.27}$$

This is called the Beer-Lambert law or simply Beer's law. A is dimensionless. The concentration of the sample, c, is usually given in units of moles per dm^3 (M). The path length, b, is commonly expressed in centimetres. The quantity ε is the molar absorptivity and has the units M^{-1} cm^{-1}. In a spectrum A (or ε) is plotted versus wavelength.

2.2.2 Chromatography

The main distinguishing feature between chromatography and other physical and chemical methods of separation is that two mutually-immiscible phases (one stationary and the other mobile) are brought into contact in a column. A sample introduced into the mobile phase undergoes numerous interactions at the interface of the stationary and mobile phases as it is being transported through the column. The interactions exploit differences in the physical and/or chemical properties of the components in the sample. These differences govern the rate of migration of the individual components through the column.

Thus, separated components emerge at the end of the column in the order of increasing interaction with the stationary phase. The mobile phase can be a gas or a liquid, whereas the stationary phase can only be a liquid or a solid. Thus chromatography is divided into two main groups namely liquid chromatography (LC) and gas chromatography (GC) with the mobile phase being liquid and gas respectively.

2.2.2.1 High Performance Liquid Chromatography (HPLC)

In liquid chromatography the sorption mechanisms that cause separation depend on whether a liquid or solid is used as the stationary phase, or what kind of solid is used. There are three main classes of HPLC: liquid-liquid chromatography (LLC), ion-exchange chromatography (IEC) and exclusion chromatography (EC). LLC uses a liquid stationary phase coated on a finely divided inert solid support. Separation in this case is due to differences in the partition coefficient of the solutes between the stationary liquid and the mobile liquid. In normal phase LLC the stationary liquid is relatively polar, whilst reversed phase LLC uses a non-polar stationary liquid and a polar mobile phase. In IEC the stationary phase is an ion exchange resin, and separation is governed by the strength of the interactions between solute ions and the exchange sites on the resin (see Chapter

5). In EC the stationary phase is a wide pore gel that can separate molecules on the basis of their size and shape. Only reversed phase liquid-liquid chromatography was used throughout this work. The stationary phases used today are called microparticulate column packing and are commonly uniformly porous silica particles, with spherical or irregular shape (diameters 10, 5, or 3μm). The different separation mechanisms mentioned above are realized by bonding different chemical groups to the surface of the silica, to produce what are called *bonded phases.*

Bonded phases in which C_{18} alkyl groups are attached to the surface of the silica particles are now frequently used in HPLC; these are called ODS (octadecylsilane) bonded phases. When packed into a column (10-25cm long and 4.6mm internal diameter), the small size of these particles leads to a considerable resistance to flow, so that the mobile phase has to be pumped through the column under high pressure.

In analytical HPLC the mobile phase is normally pumped through the column at 1 - 5cm^3 per minute. If the composition of the mobile phase is constant, the method is termed 'isocratic' elution. Alternatively, the mobile phase composition can be made to change in a pre-determined way during the separation. This is known as 'gradient' elution. Gradient elution is necessary when the range of retention times of solutes on the column is so large that they cannot be eluted in a reasonable time using a single solvent or solvent mixture.

When the separated solutes emerge from the column, they are sensed by an in-line detector. The output of the detector is an electrical signal, the variation of which is displayed on a potentiometric recorder, a computing integrator or a VDU screen. Most of the popular detectors in HPLC are selective devices [38]. This means that they may not respond to all the solutes that are present in a given mixture. UV absorbance detectors are by far the most popular detectors in HPLC and are briefly described here. The principle is that the mobile phase from the column is passed through a small flow cell held in the radiation beam of a UV-visible photospectrometer. These detectors are selective because they will only detect those solutes that absorb UV (or visible) radiation. Such solutes includes alkenes, aromatics, and compounds having multiple bonds between C and O, or

N or S. The mobile phase used must of course absorb little or no radiation. Both fixed and variable wavelength UV-visible detectors are available. The variable types use a deuterium and/or a tungsten filament lamp as the radiation source, and operate between 190 and 700 nm. Fixed wavelength detectors normally operate at 254 or 280 nm, but other wavelengths are possible. The time taken for the solute to pass through the chromatographic system is its retention time. The retention time is a characteristic of the solute for a particular set of chromatographic conditions.

HPLC is a vital tool for the examination of organic pollutants in the environment. It is an excellent technique for the separation of mixtures. The only restriction on the suitability of a sample to be examined by HPLC is its ability to dissolve in a solvent and give a response to a suitable detector. Thus HPLC is suitable for the analysis of all organic compounds, macromolecules, inorganic or other ionic species, labile natural products, pharmaceutical compounds and biochemicals.

2.2.2.2 Gas Chromatography (GC)

In gas chromatography, a gas is used as a mobile phase and either an inert liquid or a solid as the stationary phase. The sample, usually a liquid at room temperature, is rapidly vaporised as it is injected into the injection port, which is maintained at a high temperature (more than boiling point of the sample). The column is enclosed in an oven and kept hot enough to keep the sample in a gaseous state, whilst the sample components are separated by the column. The detector detects the components as they leave the column and gives an electrical out put from which recorder produces a chromatogram.

In analytical gas chromatography the criteria to be considered include:

(i) *resolution*, which depends on the conditions of the separation, i.e. flow rate, temperature, gas type, type of column and choice of stationary phase.

(ii) *sensitivity*, which depends on the type of detector.

(iii) *reproducibility*, which is due to the design of the equipment, i.e. automatic injection and integration is superior to manual techniques.

A gas chromatograph, with a thermal conductivity detector (TCD) is shown in Figure 3.8 (see Chapter 3). It has an injection port which is a heated compartment capped by a septum which is pierced by a syringe needle when the sample (typically $1mm^3$ for a packed column) is injected, and reseals when the needle is withdrawn, a column (packed or capillary) to separate components by their volatility or by their interaction with the stationary phase of the column and a detector (e.g. TCD etc). A polar column will separate two components with similar boiling points, by causing the least polar component to be eluted first, as it has the least interaction with the stationary phase. A similar effect is observed for a low polarity stationary phase, as in 5% SE on diatomite, so that the components would elute in increasing order of boiling points, water (373K), pentan-1-ol (411K), decane (447K) and butylbenzene (490K) in a middle phase (see Section 4.2.6). Increasing the temperature or increasing the flow rate reduces the elution time of the components. The polarity of the column has minimal effect on the separation of the components in this case.

In gas chromatography, the mobile phase is considered to be inert, so that it does not react chemically with the sample or stationary phase. The principle carrier gases are hydrogen, helium, nitrogen and argon. Choosing a particular carrier gas, it is important to consider cost, purity, safety and detector compatibility.

2.2.3 Photon Correlation Spectroscopy (PCS)

In a conventional PCS experiment, the intensity of the light scattered is taken as a time average quantity and no account is taken of the frequency distributions of the scattered light. The technique of dynamic light scattering or photon correlation spectroscopy (PCS) has been used by several workers [39 - 43] to study microemulsion systems. The particles in a suspension can be regarded as forming a three-dimensional diffracting array that, when illuminated with coherent light, produces a random diffraction or "speckle pattern" consisting of small bright spots and dark areas [44 - 47]. As the particles undergo Brownian motion, the speckle pattern will change from one random configuration to another. Thus, if a photomultiplier tube is placed in the scattering field, a fluctuating intensity as that shown in Figure 2.3 can be observed.

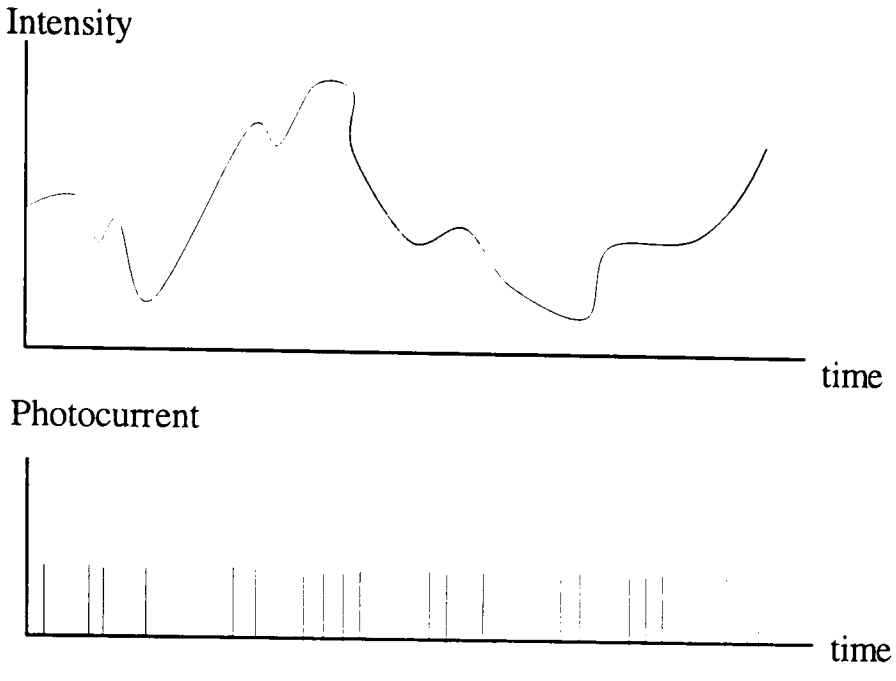

Figure 2.3 Typical fluctuating trace of light intensity at the photomultiplier detector and corresponding standardised output current

The characteristic fluctuation or coherence time T_c of this intensity is approximately the time for a particle to diffuse a wavelength. As a consequence, one can determine the translational diffusion coefficient D. The coherence time may be measured by autocorrelation, using a digital correlator. The correlator measures directly the photocount correlation function of the scattered radiation by detecting individual photoelectron emissions.

The correlation function can be written as follows:

$$g^{(2)}(\tau) = B\,(1 + \gamma^2 |g^{(1)}(\tau)|^2) \qquad (2.28)$$

where τ is the correlation delay time, B is the known background constant to which $g^{(2)}(\tau)$ decays at long delay times. $|g^{(1)}(\tau)|$ is the normalized correlation function of the scattered electric field and γ is a constant of the order of one. PCS measures $\gamma|g^{(1)}(\tau)|$. In the ideal case of a dilute suspension of monodispersed spheres, small compared to the incident wavelength of light λ, the correlation function $|g^{(1)}(\tau)|$ is given by :

$$g^{(1)}(Q, \tau) = \exp(-D\,Q^2\,\tau) \qquad (2.29)$$

where D is the translational diffusion coefficient of a particle, Q is the scattering vector

and τ is the correlation delay time. The diffusion coefficient D is related to the hydrodynamic radius R_H of the particle by the Stokes-Einstein relationship [46 - 47] :

$$D = \frac{kT}{6\pi\eta R_H} \tag{2.30}$$

where k is the Boltzmann's constant, T is the temperature, η is the viscosity of the liquid i.e. the continuous phase in the case of a microemulsion. In this simple case, the measurement of $g^{(1)}(Q,\tau)$ by photon correlation spectroscopy easily provides the fluctuation time $T_c=1/DQ^2$. Since Q, T and η are known, by combining equation (2.29) and (2.30) the hydrodynamic radius R_H can be determined. The above treatment is applied to monodisperse particle dispersions. For a polydisperse system there will be a distribution of diffusion coefficients. The electric field correlation function, then consists of a sum of exponentials:

$$g^{(1)}(Q,\tau) = \frac{\int F(R)I(R,Q)\exp[-D(R)Q^2\tau]dR}{\int F(R)I(R,Q)dR} \tag{2.31}$$

Here F(R) is the distribution function of particle radii, D(R) is given by equation (2.30) in which R_H is set equal to R and I(R,Q) is the intensity of radiation scattered by a suspension of N particles at angle θ.

$$Q = \frac{4\pi}{\lambda} n_2 \sin\theta$$

and I(R,Q) is given by the following relation:

$$I(R,Q) = \frac{16\ \pi^4\ R^6\ N}{r^2\lambda^4}\left[\frac{n_1^2 - n_2^2}{n_1^2 + 2n_2^2}\right]^2 P(Q) \tag{2.32}$$

where P(Q) is the shape (form) factor, n_1 is the refractive index of the particles, n_2 is the refractive index of the continuous medium, λ is the wave-length of the incident light in the

continuous medium, R is the particle radius and r the distance between the scattering sample and the detector.

Dynamic light scattering has been much used to study the droplet radius of the microemulsion systems [48 - 51]. Deviations from a single exponential decay for $g^{(1)}(Q,\tau)$ can be observed in some cases of concentrated microemulsion systems; they are due to interactions between the droplets. In the case of more concentrated systems, estimates of the structure factor S(Q) and of the form factor P(Q) are required. In the case of concentrated dispersions (like microemulsions), the hydrodynamic radius of the particle obtained by PCS may be corrected using the following relationship which gives the collective diffusion coefficient D as a function of its value at infinite dilution D° :

$$D = D^{\circ}(1 + \alpha\phi) \qquad (2.33)$$

where α is a constant equal to 1.5 for hard spheres with repulsive interactions and ϕ is the volume fraction of water [52]. As microemulsions cannot be diluted before being measured, droplet sizing by PCS is limited to dilute systems ($\phi < 0.1$).

2.2.4 Viscosity

All liquids are viscous fluids due to the presence of attractive forces which oppose the relative motion between neighbouring volume elements in the liquid. The viscosity , η_o, is defined as the shearing stress τ exerted across an area when there is unit velocity gradient (du/dy or D) normal to the area [53]:

$$\tau = \eta_o \frac{du}{dy} = \eta_o D \qquad (2.34)$$

for flow in the x direction. In most simple liquids the viscosity is independent of the rate of shearing (or τ is proportional to D) as long as laminar flow takes place. Such systems are termed Newtonian fluids. When a Newtonian fluid is subjected to a sheared force there is a dissipation of energy due to fluid friction. The energy dissipated, J, is given by:

$$J = \eta_o D^2 \tag{2.35}$$

When a dispersion of particles in a fluid is subjected to a shearing force there is an extra contribution to the energy dissipated, resulting from flow perturbations caused by the particles. Thus:

$$J + \Delta J = \eta D^2 \tag{2.36}$$

where η is the viscosity of the dispersion and ΔJ is the extra energy dissipated due to the presence of the particles. Combining these equations gives

$$\frac{\Delta J}{J} = \frac{\eta - \eta_o}{\eta_o} = \eta_{sp} \tag{2.37}$$

where η_{sp} is the specific increase in viscosity, usually called simply the specific viscosity. The quantity η/η_o is called the relative viscosity (η_r) and is given by:

$$\eta_r = \frac{\eta}{\eta_o} = \eta_{sp} + 1 \tag{2.38}$$

For dilute dispersion of spherical, rigid unchanged particles Einstein has derived the relationship between the viscosity of the dispersion and the volume fraction, ϕ and found that:

$$\eta_r = 1 + 2.5\phi \tag{2.39}$$

The particles are assumed to be small compared to the dimensions of the measuring apparatus (so that wall effects can be ignored), but large compared to molecular dimensions, so that the dispersion medium can be considered to be a continuum. The system is also assumed to be at a very low volume concentration so that the inter-particle separation is large and hydrodynamic interactions between particles can be ignored.

Equation (2.39) is a limiting form for the viscosity of a dispersion. It is only strictly valid

at concentrations approaching infinite dilution. If a dispersion does not conform to the above conditions of size, shape, rigidity, concentration and charge then modifications must be made to the equation.

At volume fractions approaching zero the total increase in viscosity due to the particles is the sum of the effects caused by each of the particles. At higher concentrations the viscosity of a dispersion is increased due to the temporary multiplets (doublets, triplets etc.) which increase the rate of energy dissipation. There are very many equations relating the viscosity of concentrated dispersions to the volume fraction of the dispersed phase. Several workers have attempted to modify equation (2.39) by introducing a power series in the volume fraction of the general form:

$$\eta_r = 1 + k_1 \phi + k_2 \phi^2 + k_3 \phi^3 + \text{-----} \qquad (2.40)$$

For dispersion of rigid uncharged spheres equation (2.40) must approach equation (2.39) as ϕ approaches zero. Therefore k_1 must be equal to 2.5.

2.2.5 Surface and Interfacial Tensions

Forces of attraction exist between the molecules of a liquid and indeed the existence of the liquid state is due to these forces. The molecules which are located within the bulk of a liquid are subjected to equal forces of attraction in all directions, whereas those located at a liquid-air interface experience unbalanced attractive forces resulting in a net inward pull. The liquid surface will therefore, tend to contract spontaneously. This is the reason why droplets of liquid and bubbles of gas tend to a spherical shape.

"The surface tension of a liquid is often defined as the force acting at right angles to any line of unit length on the liquid surface" [54]. However, it is more correct to define surface tension and surface free energy as the work required to increase the area of a surface isothermally and reversibly by a unit amount. The surface tension depends directly upon the sum of the intermolecular forces which operate between molecules of the liquid. This is strictly true only for a liquid in equilibrium with its own saturated vapour. Usually the

presence of air in the vapour phase causes an insignificant change because of the very weak dispersion forces which act between vapour phase molecules and liquid.

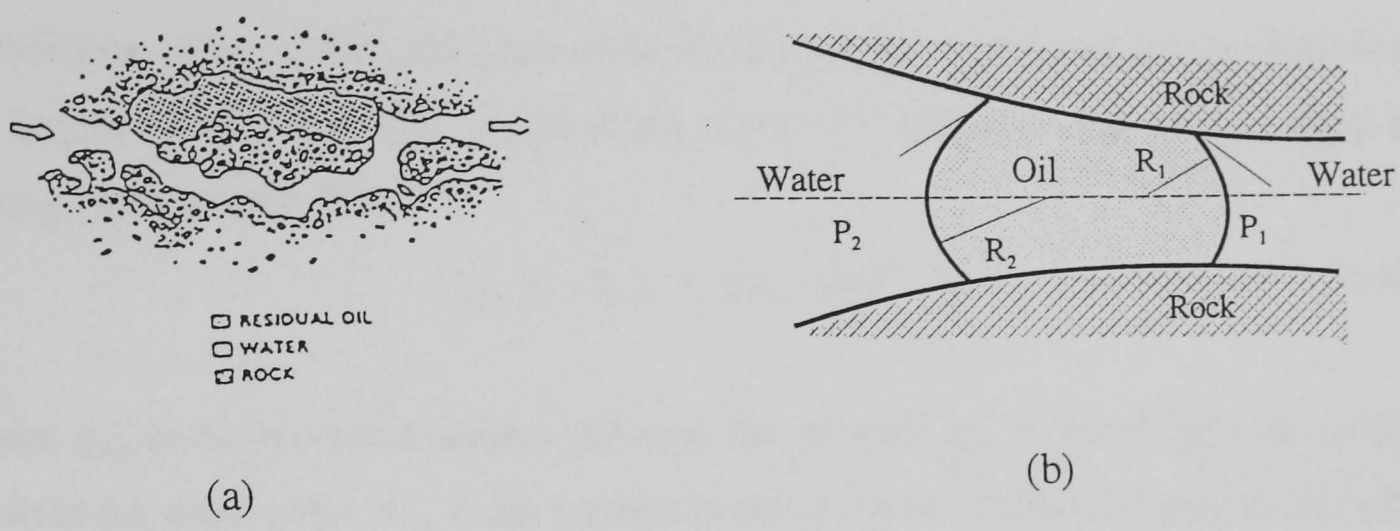

(a) (b)

Figure 2.4 Approximate configuration of residual oil; (a) Real trapped oil ganglion (b) Model of the trapped oil ganglion

In water, for instance, the dipole moment of the molecules give rise to additional polar attractive forces. Hence a large increase in surface tension by comparison with non polar liquids, where only dispersion forces are present. The relatively high value of the surface tension of mercury also reflects the contribution of metallic bonding.

One of the major requirements of a surfactant system for EOR is to generate an ultra-low interfacial tension at the oil-water interface in order to mobilise residue oil. Figure 2.4 shows an oil ganglion trapped by capillary pore constriction. The pressure of the curved interface between the two phases sets up a pressure difference, which obeys the Laplace equation:

$$\Delta \dot{P} = 2\gamma \left| \frac{1}{R_1} - \frac{1}{R_2} \right| \qquad (2.41)$$

where ΔP is the pressure difference across the pore, R_1 and R_2 are the principal radii of curvature for a curved surface and γ is the interfacial tension.

The capillary pressure difference ΔP across the interface is approximated by:

$$\Delta P = \frac{2\gamma}{R} \tag{2.42}$$

Mobilisation of the oil drop will occur when ΔP is exceeded by the pressure gradient over the length of the drop. The interfacial tension is also related to the contact angle by Young's relationship [55]:

$$\gamma_{o/s} = \gamma_{w/s} + \gamma_{o/w} \cos\theta \tag{2.43}$$

where $\gamma_{o/s}$ is the interfacial tension between the oil-solid, $\gamma_{w/s}$ is the interfacial tension between the water-solid, $\gamma_{o/w}$ is the interfacial tension between the oil-water and θ is the angle of contact of the liquid on the solid. The contact angle provides a means of characterising the wetting behaviour of a surface more effectively [56]. The angle which a drop assumes on a solid surface is the result of a balance between the cohesive forces in the liquid and the adhesive forces between solid and liquid.

Several techniques [57 - 59] have been used to measure the surface and interfacial tensions accurately. The dynamic surface tension of a pure liquid is practically identical to static surface tension. However, in solutions of surfactants, the dynamic tension is usually found to be higher than for the static value, because of a finite time required for equilibrium while the surfactant diffuses to the freshly-formed surface. The ring method (Du Nouy) has been adapted to the measurement of dynamic surface tension. By continuously overflowing the vessel with solution from which the ring is pulled, the surface is kept fresh and the pull on the ring measures the *dynamic* surface tension.

References

[1] T.P. Hoar and J.H. Schulman, Nature, **152,** 102 (1943)

[2] J.E. Bowcott and J.H. Schulman, Z. Elektrochem., **59,** 283 (1955)

[3] J.H. Schulman and M.T.S. Roberts, Trans. Faraday Soc., **35,** 716 (1939)

[4] C.E. Cooke and J.H. Schulman, "Surface Chemistry", Munksgaard, Copenhagen, 231 (1955)

[5] J.H. Schulman, W. Stockenhius and L.M. Prince, Kolloid Z, **169,** 170 (1960)

[6] L.M. Prince, J. Soc. Cosmetic Chemists, **21,** 193 (1970)

[7] L.M. Prince, J. Colloid Interface Sci., **29,** 165 (1967)

[8] L.M. Prince, J. Colloid Interface Sci., **29,** 216 (1969)

[9] H.L. Rosano, J. Soc. Cosmetic Chemists, **25,** 609 (1974)

[10] R. Averyard and B. Vincent, Prog. Surf. Sci., **8,** 59 (1977)

[11] L.M. Prince, J. Colloid Interface Sci., **52,** 182 (1975)

[12] M.L. Robbins, "Micellisation, Solubilisation and Microemulsions", Ed. K.L. Mittal, Plenum Press, New York, **2,** 273 (1977)

[13] S. Friberg, I. Lapcynska and G. Gillberg, J. Colloid Interface Sci., **56,** 19 (1975)

[14] E. Ruckenstein and R. Krishnan, J. Colloid Interface Sci., **76,** 201 (1980)

[15] D. Attwood and A.T. Florence, "Surfactant Systems, Their Chemistry, Pharmacy and Biology" Chapman and Hall, London, (1983).

[16] S.I. Chou and J.H. Bae, J. Colloid Interface Sci. **96**, 187 (1983)

[17] K. Shinoda and H. Kunieda, J. Colloid Interface Sci., **42**, 381 (1973)

[18] S.I. Ahmed, K. Shinoda and S. Friberg, J.Colloid Interface Sci., **47**, 32 (1974)

[19] W. Stoeckenius, J.H. Schulman and L.M. Prince, Kolloid Z., **169**, 170 (1960)

[20] L.M. Prince, J. Soc. Cosmet. Chem., **21**, 193 (1970)

[21] B. Vincent and S.S. Davis, "Colloid Science", Ed. D.H. Everett, Specialist Periodical Reports, Chem. Soc., London, **Vol.3** Chapter4, (1979)

[22] W.B. Gogarty and R.W. Olson, US Patent No. 3,254,714

[23] C. Kumar and D.J. Balasubramanian, J. Colloid Interface Sci., **74**, 64 (1980)

[24] C. Kumar and D.J. Balasubramanian, J. Phys. Chem., **84**,1895 (1980)

[25] J.Th.G. Overbeek, Faraday Disc. Chem. Soc., **55,** 76 (1976)

[26] J.Th.G. Overbeek, G.J. Verhoeck, P.L. de-Bruyn and H.N.W. Lekkerker, J.Colloid Interface Sci., **119**, 422 (1987)

[27] J.Th.G. Overbeek, P.L. de-Bruyn and G.J. Verhoeck, in "Surfactants", Ed. Th.F. Tadros, Academic Press, New York, London (1984)

[28] E. Ruckenstein, R. Krishnan, J. Colloid Interface Sci., **71,** 321 (1979)

[29] E. Ruckenstein, J. Colloid Interface Sci., **114,** 173 (1986)

[30] P.G. De Gennes and C. Taupin, J.Phys.Chem., **86**, 2294 (1982)

[31] R. Averyard, B.P. Binks and P.D.I. Fletcher, Langmuir, **5,** 1210 (1989)

[32] M. Bourrel and R.S. Schechter," Microemulsion and Related Systems: Formation, Solvency, and Physical Properties", Marcel Deker, New York, (1988)

[33] B.P. Binks, J. Meunier, O. Abillon and D. Langevin, Langmuir, **5,** 415 (1989)

[34] P.A. Winsor, Trans. Faraday. Soc., **44,** 376 (1948)

[35] P.A. Winsor, Chem., Reviews., **68,** 1 (1968)

[36] C.A. Millar and A.I. Neogi, Chem. J., **26,** 212 (1980)

[37] D.H. Williams and I. Fleming, Eds., "Spectroscopic Methods in Organic Chemistry", McGraw Hill, London, (1989)

[38] S. Lindsay,"High Performance Liquid Chromatography", 2nd Edn., John Wiley & Sons, Chichester (1987).

[39] M. Aoudia, M.A.J. Rodger and W.H. Wade, J. Colloid Interface Sci., **144,** 353 (1991)

[40] S.Q. Zhou and C. Wu, Macromolecules, **28,** 5225 (1995)

[41] P. Baglioni, L. Dei and C.M.C. Gambi, J. Phys. Chem., **99,** 5035 (1995)

[42] A. Shioi, M. Harada and M. Tanabe, J. Phys. Chem., **99,** 4750 (1995)

[43] D.J. Mcclements and S.R. Dungan, Colloids and Surfaces A-Physicochemical and Engineering Aspects, **104,** 127 (1995)

[44] V. Degiorgio, M. Corti, M. Giglio Eds., in "Light Scattering by Liquid and Macromolecular Solutions", Plenum Press, New York, (1980)

[45] P.N. Pusey and R.J.A. Tough, in "Light Scattering and Velocimetry", R. Pecora Ed., Plenum Press, New York, (1965)

[46] B.J. Berne and R. Pecora, in "Dynamic Light Scattering", Plenum Press, New

York, (1975)

[47] D. Senatra and G. Giubilaro, J. Colloid Interface Sci., **67,** 448 (1978)

[48] D.J. Cebula, L.H. Harding, R.H. Ottewill and P.N. Pusey, Colloid Polym. Sci., **258,** 973 (1980)

[49] J.S. Sjoblom, K. Rosenquist and P. Stenius, Colloid Polym. Sci., **260,** 82 (1982)

[50] E.J. Beckman and R.D. Smith, J. Phys. Chem., **94,** 3729 (1990)

[51] A.A. Calje, W.G.M. Agterof and A. Vrij, in "Micellisation, Solubilisation Microemulsions", Plenum Press, New York, (1977)

[52] A.M. Cazabat and D. Langevin, J. Phys. Chem., **74,** 3729 (1981)

[53] J.W. Goodwin, MSc Lectures, Bristol University, (1990)

[54] D.J. Shaw, "Introduction to Colloid and Surface Chemistry" 3rd Edn., Butterworths, London, (1980)

[55] L.R. White, J. Chem. Soc. Fara. Trans. I., **73,** 390 (1977)

[56] R.E. Johnson R.H. Dettre,"Wettability and Contact Angles", Ed. E. Matijevic, Wiley-Interscience New York, **2,** 85 (1969)

[57] H.M. Casel, US Patent No. 2,448,768 (1942)

[58] R.C. Brown and McCormick, H. Phil. Mag. **39,** 420 (1948)

[59] S. Fordham, Proc. Roy. Soc., **A194**, 1, London (1948)

CHAPTER THREE

MICROEMULSION MATERIALS, METHODS AND EXPERIMENTAL

3.1 MATERIALS

3.1.1 Surfactants

(a) Nonionic Surfactants

The work carried out for this thesis is based upon a widely-used commercially-produced family of surfactants (i.e. octyl phenol polyethoxylates) supplied by Rohm and Haas. Their general structure is shown in Figure 3.1 (a). The polyethoxylate head group consists of a Poisson distribution in terms of the number (n) of ethoxylate groups present; the average value of $\bar{n}$ for Triton X-100 being 9-10. Other members of the Triton family include

TX-114	$\bar{n}$ =7
TX-165	$\bar{n}$ =16
TX-305	$\bar{n}$ =30

All are produced by the reaction of p-octylphenol with ethylene oxide.

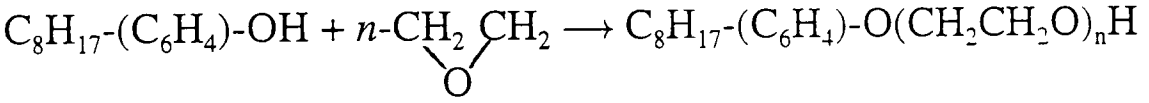

Surfactants are also produced from natural products. For example, phenolic lipids found in the shell of the cashew nut can be converted to readily biodegradable surfactants [1] (i.e. cardanol whose structure is shown in Figure 3.1 (b)). Samples of cardanol were obtained (Johnson Wax, Surrey, England) with $\bar{n}$ equal to13 or 8. Physical properties of the nonionic surfactants are to be found in Table 3.1.

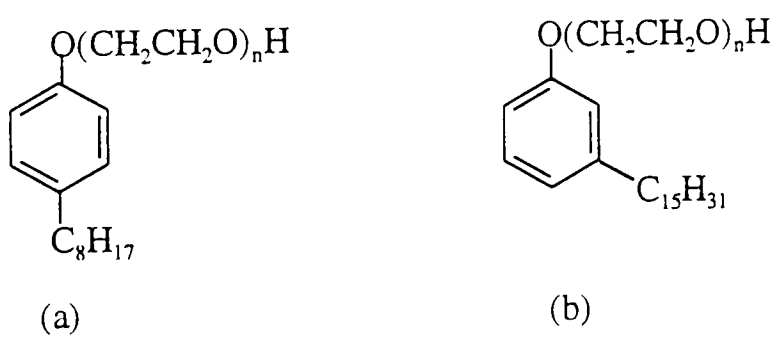

Figure 3.1 The structure of nonionic (a) Tritons with ethoxylates predominantly in a p-position to the alkyl group and (b) Cardanols with ethoxylates predominantly in a m-position to the alkyl group.

Table 3.1 Physical properties of the nonionic surfactants [2]

Surfactant	Av. Molecular mass	% active material	ñ	HLB	CMC (mM)	Cloud point(K) (1%w/v) Solution
TX-114	536	100	7.5	12	0.21	299
TX-100	624	100	9.5	14	0.25	340
TX-165	952	70(30%H_2O)	15	16	0.43	373
TX-305	1526	70(30%H_2O)	30	17	0.75	373
Cardanol	636	98	8	12.6	---	338

(b) Anionic Surfactant

The anionic surfactant Hostapur SAS-60 was obtained from Hoechst UK Limited. This had the general structure:

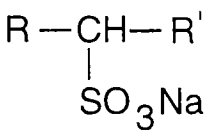

and was therefore a secondary n-alkane sulphonate. R and R' had approximately the following C-chain length distribution:

$< C_{13}$ -n-paraffin maximum	1%
C_{13} - C_{15} -n-paraffin approximate	58%
C_{16} - C_{17} -n-paraffin approximate	39%
$> C_{17}$ -n-paraffin approximate	3%

Sodium dodecyl sulphate (SDS) was also obtained from Aldrich and dodecyl benzene sulphonate (p-dodecyl benzene sulphonate (4DBS)) was provided from Marseille, France. The structure and physical properties of the anionic surfactants are presented in Figure 3.2 and Table 3.2 .

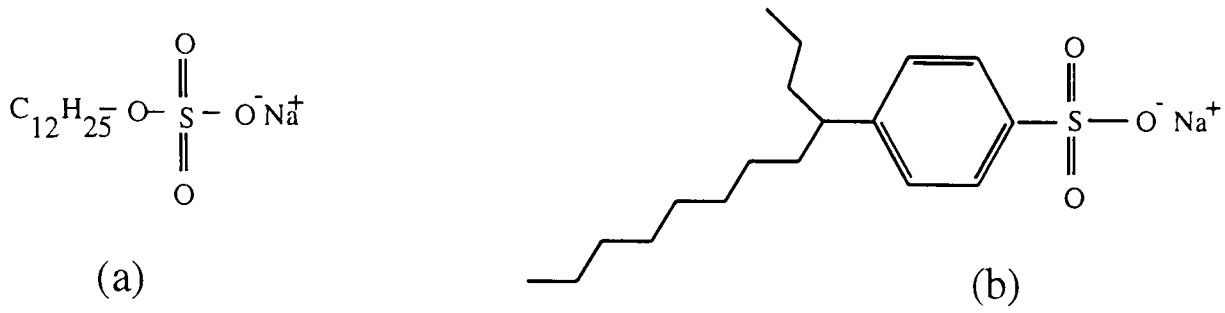

Figure 3.2 The structure of anionic (a) SDS and (b) 4DBS

Table 3.2 Physical properties of the anionic surfactants

Surfactant	Average Molecular mass	Purity (%)	CMC (mM)
SDS	288	99	8.3
4DBS	348	98	1.5
SAS-60	328	96	1.7

3.1.2 Solvents

(a) Hydrocarbons

The organic solvents n-hexane, n-heptane, n-decane, n-hexadecane and butyl benzene were analytical grade (purity >99%) and obtained from Aldrich. All were used without further purification. Their physical properties are given in Table 3.3.

Table 3.3 Properties of hydrocarbons

Hydrocarbon	Boiling point (K)	Density (g/cm^3) at 293K	Dynamic viscosity (cP)* at 293K	Refractive index 294K
n-hexane	342	0.659	0.326	1.374
n-heptane	371	0.684	0.409	1.387
n-decane	447	0.73	0.920	1.412
n-hexadecane	557	0.773	3.34	1.435
butylbenzene	456	0.86	--	1.489

* $cP = 10^{-3}$ kg. m^{-1}. s^{-1}

The other organic solvents, acetonitrile and ethylene glycol were of analytical grade and obtained from Aldrich and used as received.

(b) Alcohols

The alcohol solvents used (i.e. methanol, propan-1-ol, butan-1-ol, pentan-1-ol, hexan-1-ol, heptan-1-ol, octan-1-ol and pentan-1,5-diol) were analytical grade reagents (purity >99%) and were obtained from Fluka Chemical. All were used as received. Their physical properties are given in Table 3.4.

Table 3.4 Physical properties of the alkanols

Alcohol	Boiling point (K)	Density at 293K (g/cm^3)	Refractive index at 293K
Methanol	338	0.7914	1.329
Propan-1-ol	370	0.803	1.385
Butan-1-ol	390	0.8098	1.399
Pentan-1-ol	411	0.812	1.409
Hexan-1-ol	431	0.8136	1.418
Octan-1-ol	469	0.827	1.429
Pentan-1,5-diol	515	0.994	1.449

(c) Water

Water used was deionised doubled-distilled and then further purified by passing it through an ion-exchanger to produce an ultra-pure water solvent of conductivity and surface tension 0.5 μS/cm and 72 ± 0.2 mN/m at 293K respectively. This water was used for all the experiments described here.

3.1.3 Brine

The brine used in the microemulsion experiments was a solution of NaCl (concentration 1-10 g NaCl/100cm^3) in water including divalent ions, 0.5% $MgCl_2$ and 0.4% Na_2SO_4. This is described as synthetic sea water.

3.1.4 Inorganic Salt

Table 3.5 shows the inorganic salts used in the present study as received.

Table 3.5 Properties of salts

Salt	Source	Purity (%)
NaCl	BDH; AnalaR	99.2
Na_2SO_4	Aldrich	99.9
$MgCl_2.6H_2O$	BDH; AnalaR	99.8
$Na_2H_2PO_4.12H_2O$	Acros Chimica	99.6
$CaCl_2.2H_2O$	BDH; AnalaR	99.5

3.2 EXPERIMENTAL

3.2.1 Preparation of Microemulsions

Before preparing microemulsions, all glassware was washed first with an ordinary detergent using hot tap water, and was then exhaustively rinsed with distilled water, and then ethanol before drying in an oven at 313K for 2h.

Microemulsions were produced by mixing known ratios of surfactant, water, co-solvent (alcohol) with a hydrocarbon to make a 100% (w/w) mixture. Each sample was prepared individually and was contained in stoppered $10cm^3$ phase tubes. All the samples were held at a selected temperature to $\pm$ 0.1K in an accurate thermostat (i.e. a water bath). Each sample was vigorously shaken (i.e. by hand) and allowed to equilibrate for 24h. The phase behaviour was determined by visual inspection of samples and also by the modified UV-spectrophotometer (see Section 3.2.4). The time required for phase separation generally depended on the nature of the phase separation and on the viscosity of the separating phases. Single phase microemulsions containing water or oil generally formed clear solutions within a few minutes after shaking. Water/TX-100+pentan-1-ol/n-decane samples usually phase separated within 1h. The compositions of the three phase

microemulsion systems are shown in Table 3.6.

The single-phase microemulsions were prepared for sizing assays with different weight percentages of the disperse phase. These were prepared by mixing the nonionic surfactant TX-100 and pentan-1-ol in 1:1 ratio, and then adding this to decane (continuous phase) and finally by adding water as the disperse phase at 298K. Their compositions are given in Table 3.7

Table 3.6 Composition of three-phase microemulsion systems

Microemulsion System	Composition (wt%)						
	Brine*	TX100	Pentan-1-ol	SAS	SDS	Decane	Butylbenzene
M1	50	10	10	----	----	30	-----
M2	40	4	5	1	----	50	-----
M3	40	4	5	----	1	40	-----
M4	50	10	10	----	----	24	6
	Brine*	TX114	Pentan-1-ol	SAS	SDS	Decane	Butylbenzene
M5	40	5	5	----	----	50	----
M6	40	5	5	----	----	40	10

Brine* represents various concentrations of NaCl (i.e. in the range of 1-10g NaCl/100cm^3)

Table 3.7 Composition of single-phase microemulsions

Composition							
Water		TX-100		Pentan-1-ol		Decane	
wt%	vol%	wt%	vol%	wt%	vol%	wt%	vol%
1.00	0.80	14.00	7.53	14.00	13.80	71.00	77.87
2.00	1.60	14.00	7.55	14.00	13.84	70.00	77.00
3.00	2.42	14.00	7.57	14.00	13.88	69.00	76.12
4.00	3.23	14.00	7.60	14.00	13.92	68.00	75.24
5.00	4.05	14.00	7.62	14.00	13.96	67.00	74.35

3.2.2 The Phase Diagram of a Ternary Mixture

The phase diagram for a ternary mixture was represented on a Gibbs phase triangle at a fixed temperature and pressure (see Figure 3.3), where the sum of the vertical distances from a given point within the triangle to its sides is a constant equal to the height of the triangle. Thus each vertex of the triangle represents 100% of a single component and the opposite side of the triangle represents 0% of that component. The fraction of component W in Figure 3.3 can therefore be indicated by lines parallel to the axis S-O. For example, the mixture denoted 'X' in Figure 3.3 has the composition 40% W, 30% S and 30% O. Each axis of the triangle represents one of the three binary mixtures W-S, W-O and S-O. Any point within the triangle represents a specific composition of a three-component mixture. Composition is usually expressed as mole fraction, weight fraction or volume fraction. Here weight fractions are used.

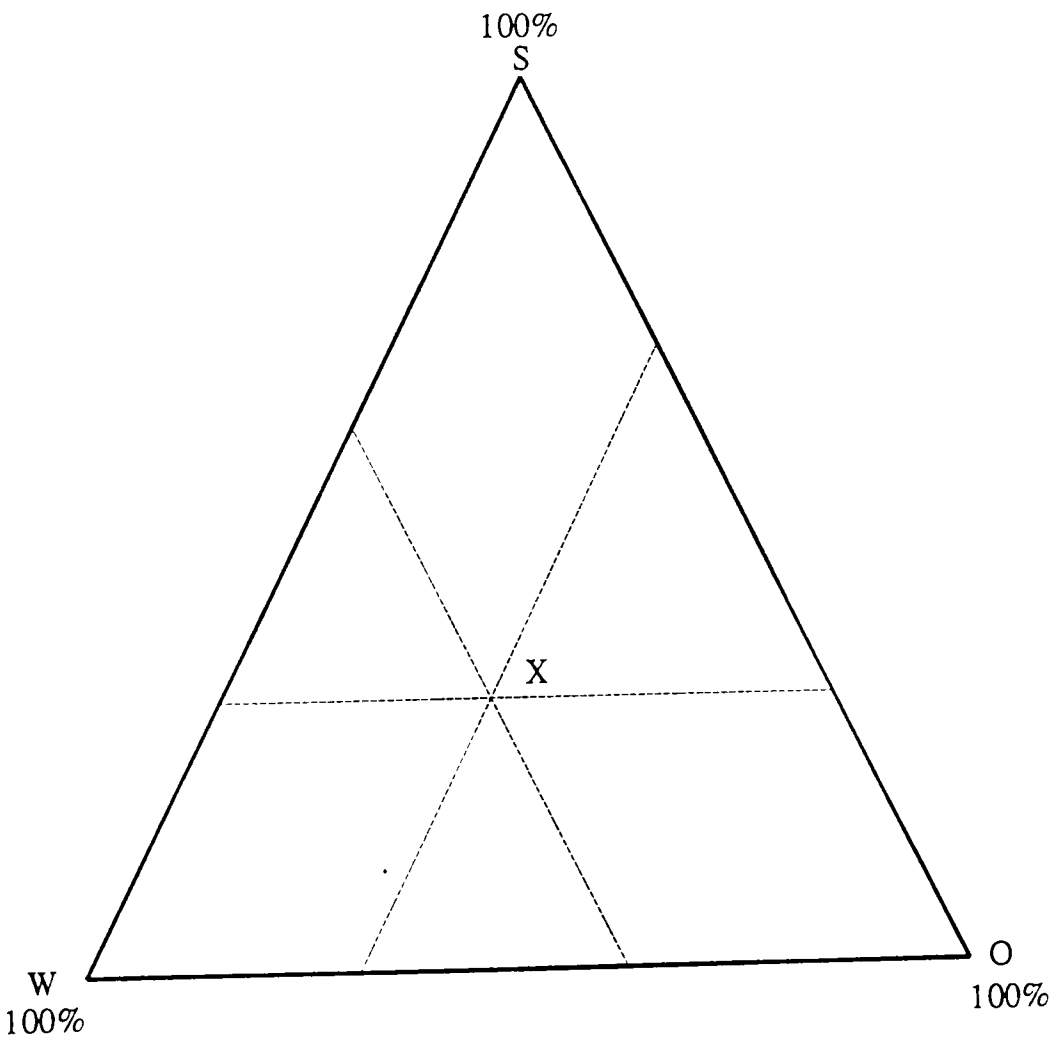

Figure 3.3 The Gibbs phase triangle

3.2.3 Spectrophotometric Measurements

The absorbance of different microemulsion phases was determined using the Perkin Elmer Lambda 9 spectrophotometer. A schematic diagram of the instrument is given in Figure 3.4. The spectrophotometer was calibrated by the standard method [3] prior to the absorbance measurement. The microemulsions were diluted with methanol before their absorbance was measured at 298K. This absorbance was then used to determine the surfactant concentration in each phase of the three-phase microemulsion systems M1 and M5.

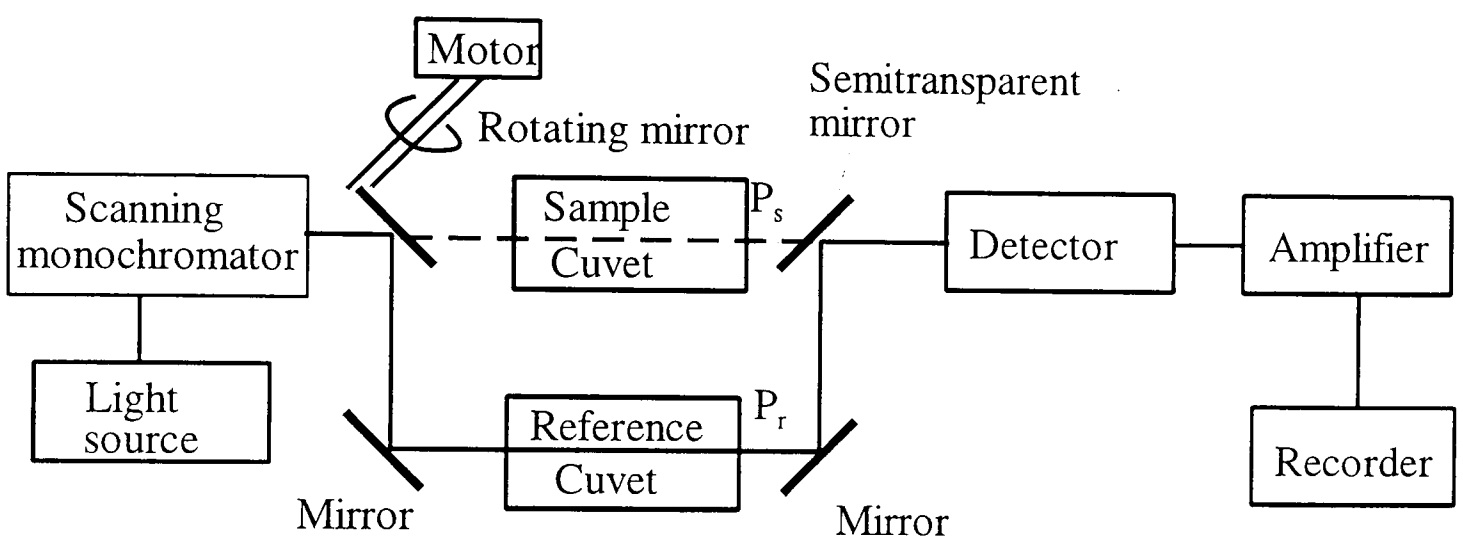

Figure 3.4 Schematic diagram of the spectrophotometer (Lambda 9)

In recording the spectra two quartz cells of 1cm thickness were used: one as the sample cell and the other as the reference cell. The reference cell was filled with the solvent and the sample cell with the solution, so as to compensate for solvent absorption and also for losses by photon scattering and reflection.

3.2.4 Scanning of the Microemulsion Phases by UV-Spectrophotometer

A Pye Unicam SP1800 spectrophotometer was also used to determine the surfactant absorbance (concentration) and the percentage of different microemulsion phases. The apparatus was modified to have a horizontal detector slit, and fitted with a motor driven cell which passes the detector. The apparatus is schematically shown in Figure 3.5.

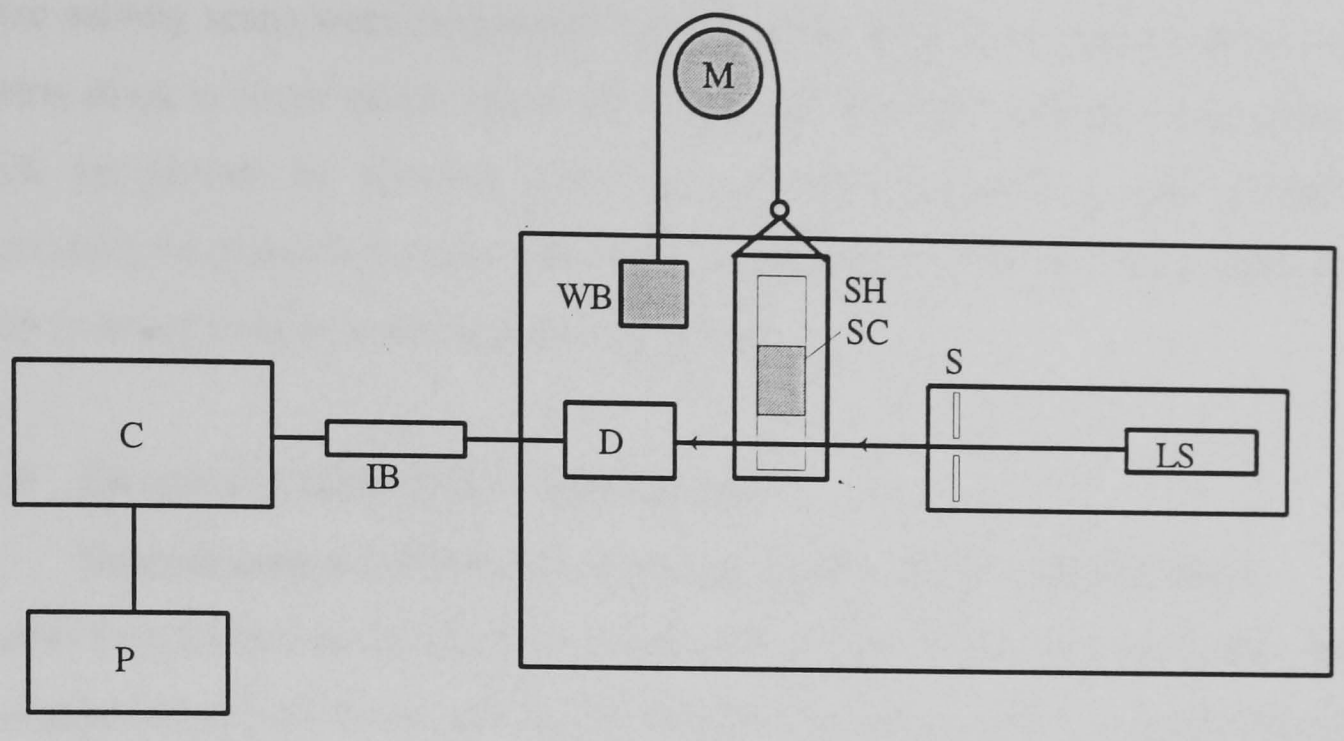

Figure 3.5 Schematic diagram of the modified spectrophotometer, where LS is the light source, S is the slit, SC is the sample cell, SH is the sample holder, M is the motor, WB is the weight balance, D is the detector, IB is the interface box, C is the BBC computer and P is the printer

The microemulsion, which may have two or three phases at equilibrium, was held in a 10 mm quartz cell. The sample cell was accurately thermostatted (to ± 0.5K) during an experimental run by the circulating water. The reference cell contained distilled water or decane. The wavelength used was 275 nm although other wavelengths could have been selected. The instrument output (0 to 1.4 V) was proportional to the absorbance and was accepted into a BBC computer through an interface protecting the computer from excessive voltage fluctuations. The computer programme (see Appendix) was designed to analyse differing absorbances of the microemulsion phases. From this analysis, the volume percentage of each phase and the surfactant concentration could be determined as a function of salinity and temperature.

3.2.5 Optimum Salinity Scans

A salinity scan provides a very rapid indication of the phase behaviour properties of a system and a convenient method for screening potential surfactant systems for oil recovery [4]. Initial phase behaviour experiments involved salinity scans at a constant water : oil weight ratio of 1:1 while scanning the system with respect to brine concentration at a constant surfactant alcohol concentration.

These salinity scans were performed by combining brine, surfactant, pentan-1-ol and decane stock in 10cm^3 phase tubes. After vigorous shaking the phases were allowed to reach equilibrium by standing tubes in a constant temperature bath (298K) and determining the phase boundaries with the modified apparatus described in Section 3.2.4. when constant volume levels had been achieved.

3.2.6 Electrical Conductivity Measurement

(a) Determination of Electrolyte Concentration in the Middle Phase

In order to determine the NaCl concentration in the middle phase microemulsions, initially the conductivity of the brine solution (used to produce three phase microemulsions) was measured at 298 ± 0.1K. The lower aqueous phase was separated from the three-phase system and conductivity was measured using an"alpha 800" conductivity meter. The conductivity cell contained two electrodes, with a cell constant of 1 which was previously determined using KCl solutions. Measurements were performed by completely immersing the electrodes in the electrolyte solutions. The temperature was varied with a thermostat circulating water bath (Grant Instruments) and was determined with an accuracy of ±0.1K.

(b) Phase Inversion in the Microemulsions

In order to observe the transition from one microemulsion type to another, the conductivities of thermodynamically-stable middle-phase microemulsions were measured as a function of salinity at 298K. The electrodes were immersed in the middle phase microemulsion and left to equilibrate for 15min before measurement. A significant conductivity change was noticed at the phase transition.

3.2.7 Viscosity Measurement

Measurement of the viscosity of surfactant solutions was carried out using an Ostwald viscometer (calibrated against water at 298K). The viscosities of the middle-phase microemulsions studied were measured at 298K by timing the flow of a constant volume of each sample in the viscometer (held in a clamp in a water bath maintained at 298 ± 0.1K). A constant volume (8cm^3) was pipetted into the viscometer and it was drawn

above the upper mark of the viscometer slowly (in order to prevent foaming). The average flow time of the samples between the upper and lower marks was measured from at least six experiments.

3.2.8 Surface Tension Measurement

The Du Nouy ring torsion balance (White Electrical Instrument Company Ltd., Malvern) fitted with a platinum ring was used to measure the surface tension of surfactant solutions of varying concentration in distilled water at 298K after being left for 24h to reach equilibrium. The ring (pre-cleaned by flaming carefully in the micro-burner) was lowered until it just touched the surface of the liquid, after which the surface was lowered until the meniscus broke and the ring was free.

3.2.9 Interfacial Tension Measurement

Interfacial tension of the microemulsion phases was measured using the spinning drop interfacial tensiometer (see Figure 3.6) in which rotation of the Pyrex sample tube was driven by an Electrocraft D.C. motor-generator (Model E-650-MG) on a closed-loop control circuit. The Pyrex glass tubes (precision-bore of 0.291cm I.D., 0.73 cm O.D., 2.5 cm long, hemispherical at the closed end) were sealed with a silicone-rubber septum at the loading end and were interchangeably mounted in the slotted brass shaft. A bifilar micrometer microscope (Model M 110A, Gaertner Scientific Corp., Chicago) was used for measuring the drop diameter with an accuracy of ±0.0001 cm, and was mounted in a Gaertner travelling micrometer stage (Model M303) which permitted measurements along the entire observable length of the tube.

The instrument was mounted on a massive cast-iron base with three levelling legs that rest on rubber pads to help dampen vibrations. The drop was illuminated by a stroboscope (General Radio Co., West Concord, Mass.). The temperature of the tube was controlled by flowing air of suitable temperature through coiled tubing located at the pulley nearest the hemispherical end of the tube.

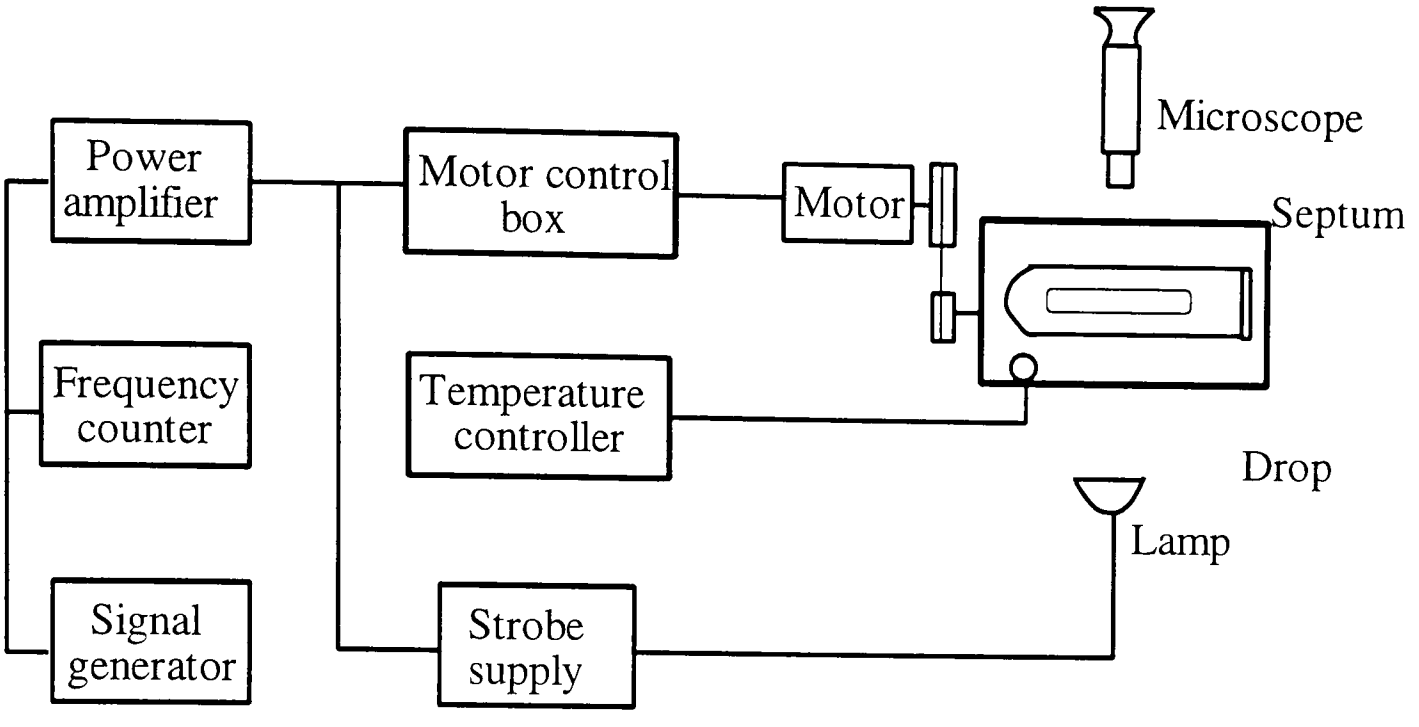

Figure 3.6 Schematic diagram of spinning-drop apparatus

Initially, the tube was filled with the dense phase (with care taken to avoid the formation of air bubbles in the tube) and a drop of the light phase was injected with a $1mm^3$ syringe, after the entire length of the needle had been introduced into the tube. Depending on the tension expected, drop volumes between 0.02 mm^3 (for tensions in the μN/m range) and $10mm^3$ (for tensions of few mN/m and higher) were injected, the criterion being achievement of a length-to-diameter ratio greater than four at the desired rotation speed. Both the droplet length and diameter were measured and the drop volume was calculated. Thus the interfacial tension was determined using the Vonnegut equation [5].

$$\gamma_{12} = \frac{1}{4}\omega^2 r^3 \Delta\rho \qquad (3.1)$$

where γ_{12} is the interfacial tension between liquids 1 and 2, ω is the angular velocity, r is the radius of the droplet and Δρ the density difference of the two phases.

3.2.10 Cloud Point and pH Measurement

Surfactant solutions of 1 % (w/v) with varying concentrations of salinity were heated slowly (at a rate of $1K\ min^{-1}$ near the cloud point) with constant stirring. The temperature

was monitored to within 0.1K until the cloud point was observed. The solution was allowed to cool and the temperature noted when the solution gained its original clarity.

Solution pHs were measured by a PTI-15 Model pH metre pre-calibrated with standard buffers (pH 4.00 and 7.00) at the beginning of the measurements and then after about every 10 readings. The temperature was varied using a water bath thermostat and was accurate to ± 0.5K.

3.2.11 High Performance Liquid Chromatography (HPLC)

A computer-controlled Varian Star HPLC (shown schematically diagram in Figure 3.7) was used in this study. This system has the capability to undertake both isocratic and gradient elution, to generate chromatograms with its detector at 190-367 nm to observe any UV absorbing species. Column blanks of 12.5 cm length and 4.5 mm internal diameter (I.D.) were packed with 5μm diameter Spherisorb silica.

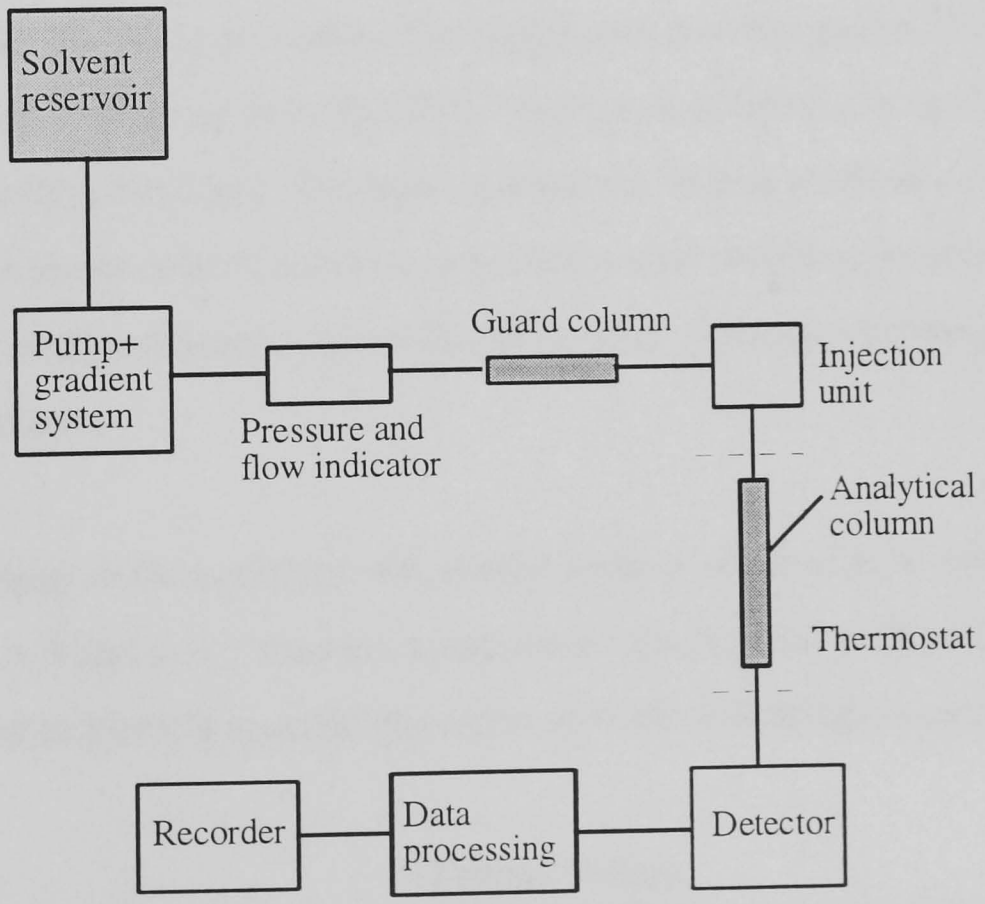

Figure 3.7 Schematic representation of high performance liquid chromatograph used.

The Spherisorb silica has the ability to separate individual oligomers of Triton X-100

when eluted with acetonitrile and pH 3 buffer [6]. The buffer was prepared by dissolving 5.0g of disodiumdihydrogen-phosphate ($Na_2H_2PO_4.12H_2O$) in approximately $1dm^3$ of deionized water, adjusting pH to 3 with orthophosphoric acid, and making up to $1dm^3$ with the water.

The organic modifiers commonly used in HPLC, particularly mixed with water or aqueous buffers, are methanol, acetonitrile, and tetrahydrofuran. These are water-miscible in all proportions and do not absorb in the UV in the common monitoring region above 210 nm. Mixtures of these solvents with pH 3 buffer were prepared and their ability to elute Triton X-100 under isocratic conditions was assessed. The mobile phase was degassed by vacuum filtration before placing it in the reservoir. This was necessary to eliminate air bubbles and particulate matter; the former can cause serious problems in HPLC by reducing the volume of the mobile phase delivered by the pump and so affecting reproducibility.

PTFE tube inserted into the reservoir carried the mobile phase to the pump. The PTFE tube end in the reservoir had a stainless steel filter element push fitted to it to filter the mobile phase before it enters the pump. The pump passed the mobile phase at a constant rate of 1.0 cm^3/min. The guard column removed particulate matter resulting from the wear and tear of the pump, and presaturated the mobile phase with silica thus prolonging the life of the analytical column.

Finally the chromatography of the surfactant was studied under gradient elution conditions and in this context n = 9 and n = 3 markers compounds (synthesized at Brunel by Dr. Peter Payne) were used to identify specific oligomers with the following conditions:

Eluent	Gradient elution A = pH 3 buffer : acetonitrile 80:20 B = pH 3 buffer : acetonitrile 50:50 A to B over 12 min B to A over 5 min A equilibration 3 min
Flow rate	1 cm^3/min

Temperature	Ambient 295K
Pump	Varian 9010
Injector	Valco valve in Varian 9100 auto injection system.
Sample	TritonX-100 1mg/cm^3 in water or methanol +n = 9 and n = 3 as marker compounds.
Detector	Varian 9065 linear diode array UV absorbance detector (wavelength range 190-367 nm) continuously monitored at 274 nm. The chromatogram at 274 nm was usually printed out and used to provide retention data.
Limits of analysis	0.1 ppm

A literature review of that gradient elution HPLC on chemically modified silica is very suitable for both the qualitative and quantitative analysis of oilgomeric mixture. Van Der Maeden [7] has emphasized that sample retention in liquid chromatography depends strongly on the composition of the mobile phase. In many application of liquid chromatography to the separation complex mixture, sometimes containing widely dissimilar components, it is frequently necessary to change the composition of the mobile-phase in order to elute all of the components present in the sample satisfactorily from the column.

Holt and co-workers [8], described a more sensitive and specific method for the analysis of alkyl phenol ethoxylate based on normal-phase HPLC. Allen and Rice [9], reported a relatively simple liquid chromatography method for the isolation of individual oligomers of Triton X-100 and similar polyoxyethylene based surfactant has been developed. The method has been used for the separation of mixtures of oligomers with up to eighteen oxyethylene subunits on silica acid type adsorbent using acetic acid -water-ethyl acetate eluents.

3.2.12 Gas Chromatography (GC)

A Pye Unicam GC system (shown schematically in Figure 3.8, which incorporated a 5% SE on Diatomite column, thermal conductivity detector, (TCD)) was also used and into this 1 mm^3 samples were injected in a He carrier gas. Analyses took 12 min. For the

separation of water, pentan-1-ol, decane and butylbenzene Porapak P and Q columns were found to be incapable of separating water from the sample. A less polar column was required. Consequently a 2 m column of 5% SE on diatomite (80-100 mesh) was chosen. At the optimum injection temperature (523K) four peaks were eluted (water, pentan-1-ol, decane and then butyl benzene) within 12 min when 40 cm^3 He/min was used as carrier gas. The temperature of the detector was 473K and that of the oven was 373K.

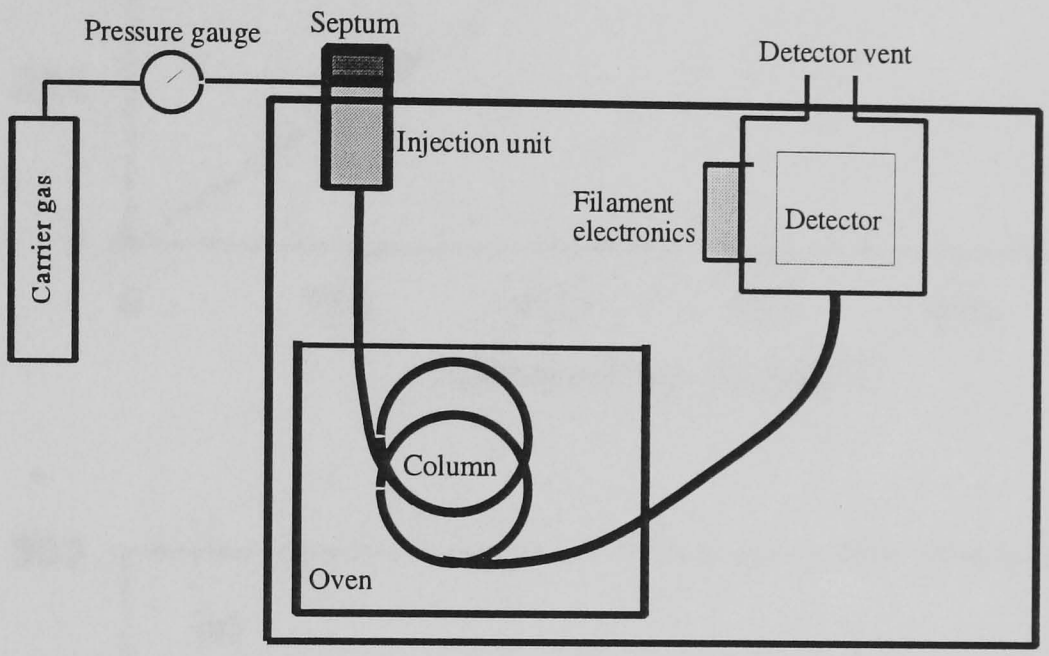

Figure 3.8 Schematic diagram of the gas chromatograph with a thermal conductivity detector

The calibration standards were prepared for each of the four components, as pentan-1-ol, decane and butyl benzene are fully miscible, their calibration standards were prepared as mixtures. Water is immiscible in hydrocarbon, and only partially miscible in pentan-1-ol. Therefore, for the water calibration it was necessary to choose a solvent that was fully miscible with water, and had a retention time different from water. Ethylene glycol was used as the solvent for the water calibration. Each standard was so analysed in triplicate and this produced the four calibration plots (shown in Figures 3.9 and 3.10). The limit of analysis was 0.15ppm.

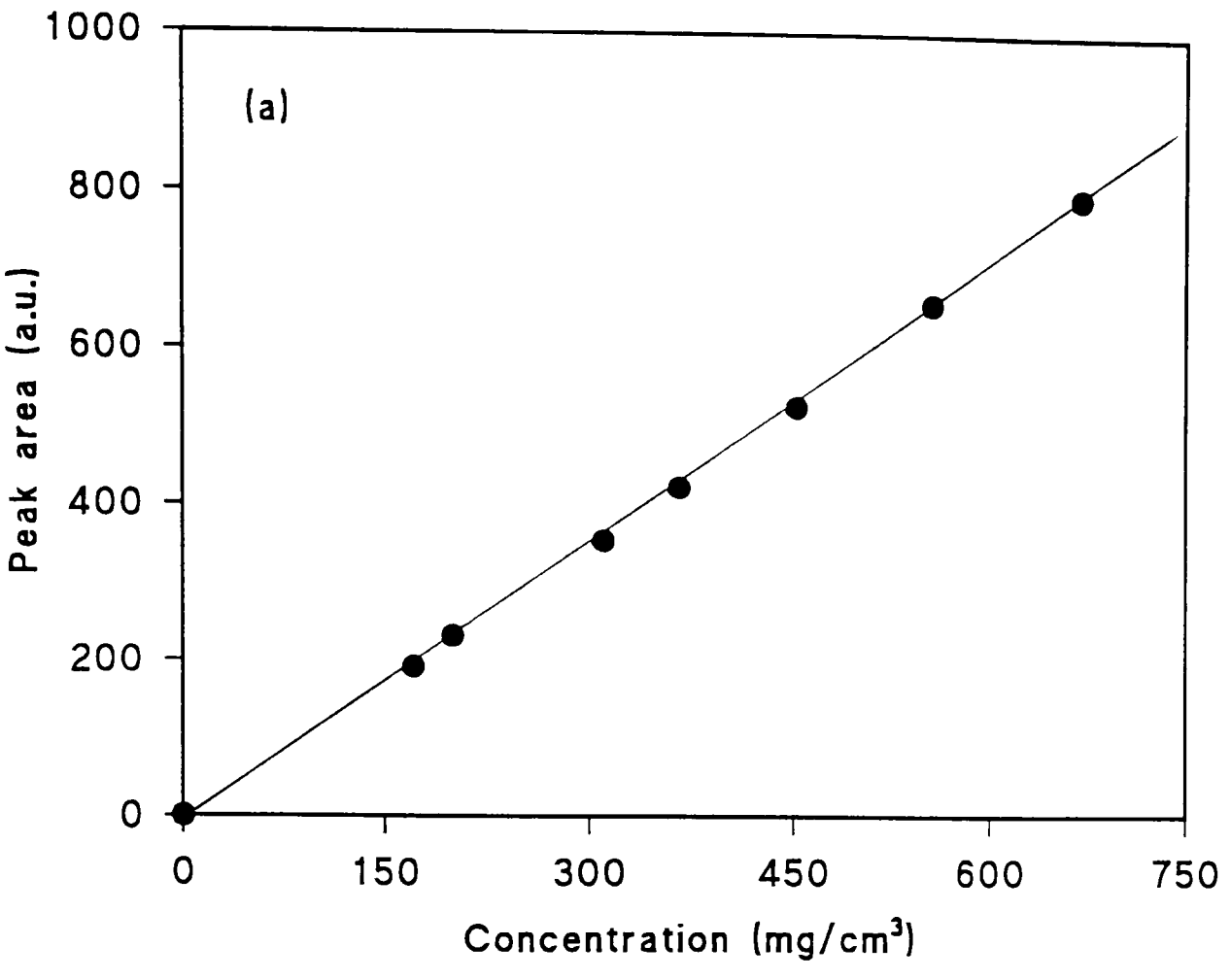

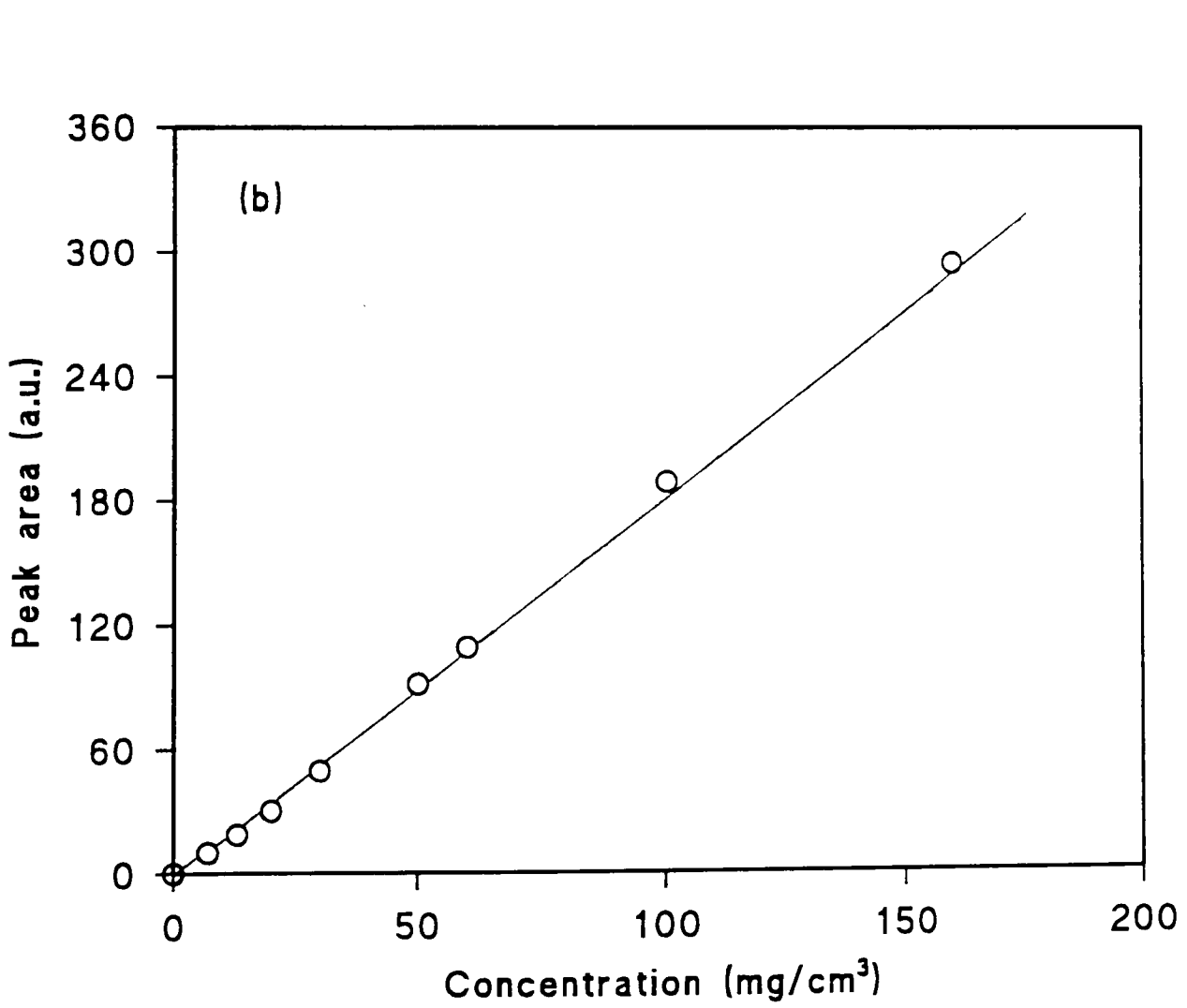

Figure 3.9 GC calibration curves for (a) water (b) pentan-1-ol giving a correlation coefficient 0.9991.

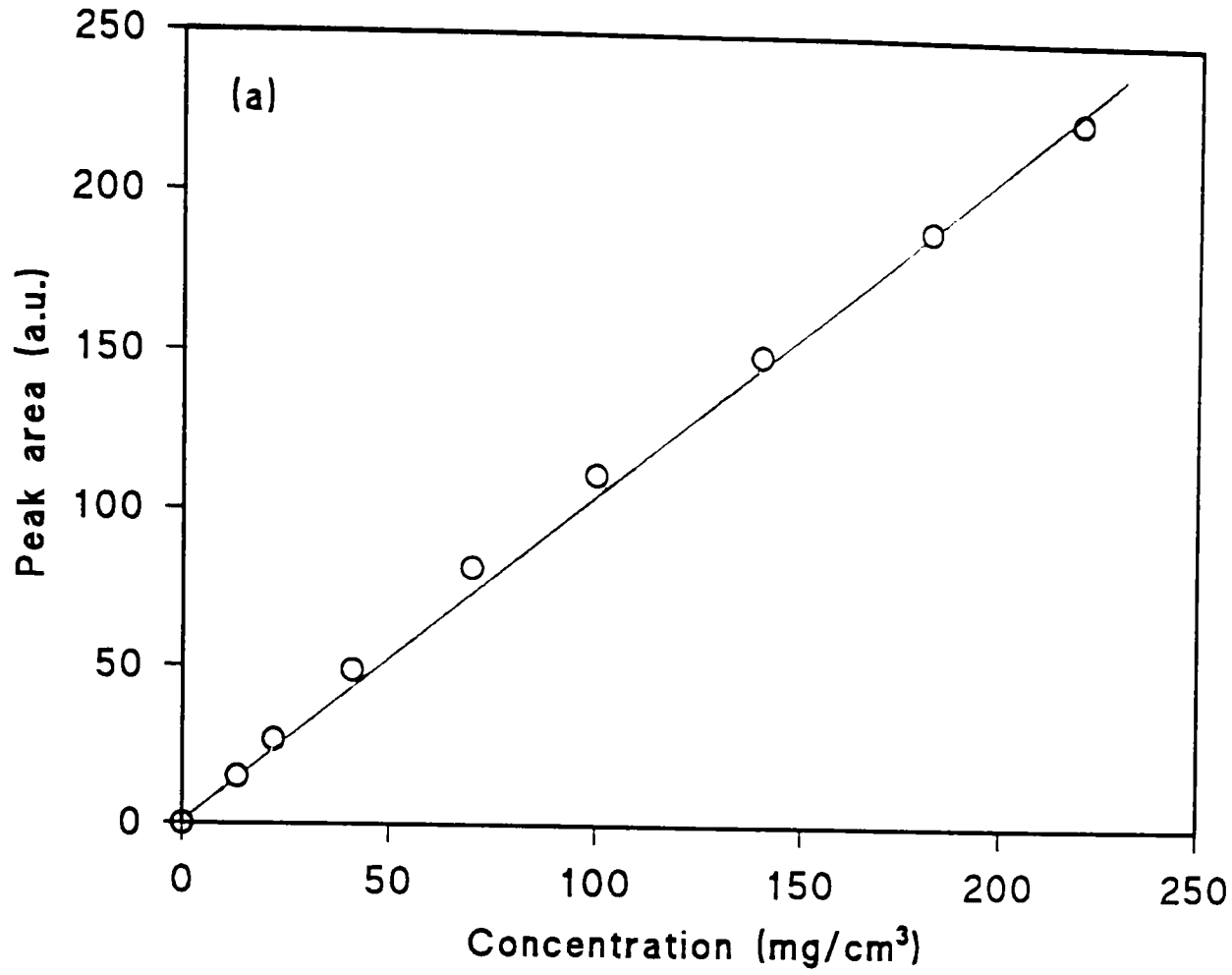

Figure 3.10 GC calibration curves for (a) decane (b) butylbenzene giving correlation coefficients 0.9978 and 0.9986

Quantitative Analysis

For quantitative analysis it is assumed that the height (or the area) of the peak in the chromatogram is proportional to the concentration of the substance that produced the peak. In order to analyse the samples quantitatively it is necessary to calibrate the detector. This is because for equal amounts of each component the detector response is often different. Another reason for calibration is that each component in a sample does not always appear as a separate peak on the chromatogram. Components may co-elute, be retained on the column, or elute without being detected.

The external standard method of calibration was used throughout this work. In this procedure a standard containing the compound or compounds that need to be determined, ideally present at about the same level as in the unknown, is prepared. The chromatograms of the standards and unknown are then compared. From the standard chromatogram, a response factor is calculated for each component of interest as shown in the following equation:

$$Response\ factor = \frac{concentration\ of\ component}{peak\ height\ /\ area\ of\ the\ component\ signal}$$

The response factor represents the concentration of the component that produces a unit detector response. Thus, for the unknown chromatgram, the concentration of each component can be calculated by multiplying the peak height (or area) by the appropriate response factor. The success of this method depends solely on the detector response being linear over the range of concentration being used and also on an identical injection volume of both standard and sample.

3.2.13 Determination of Water

In order to determine the water content in the microemulsions, a Karl Fischer titration apparatus was used (at Thoro System Products, Lakeside, Redditch, Worcs, UK). The apparatus automatically titrated a mixture of sample containing water, diluted in a water-free methanol solvent, with a Karl Fischer Reagent (pyridine-free) containing free iodine

ions in solution. The method, as formulated by Fischer and modified by Smith et al [10], relies on the chemical reaction between iodine, sulphur dioxide and water in the presence of anhydrous methanol and pyridine. It may be represented as:

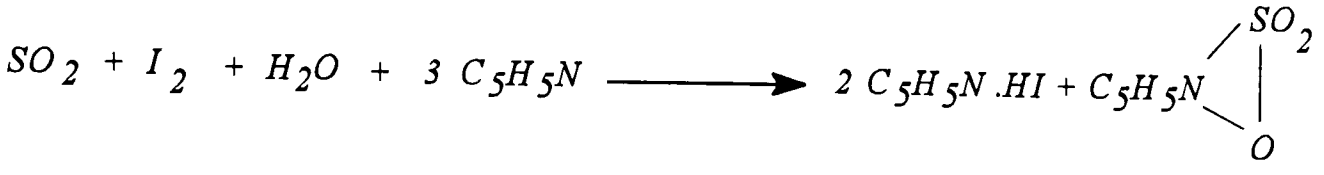

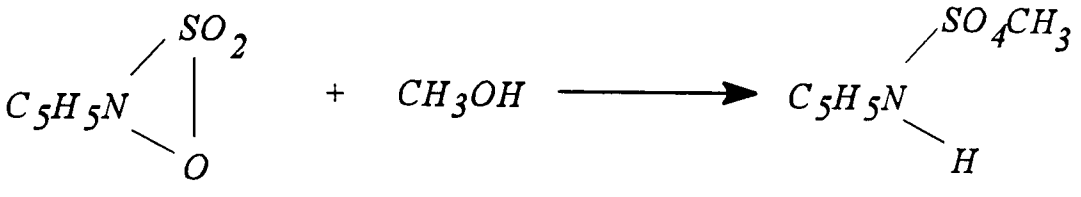

Since each mole of iodine is equivalent to one mole of water, the principle is that the sample is dissolved in a water-free methanol and titrated with standardised Karl Fischer reagent. In the presence of water the free iodine ions form a complex with methanol and the Karl Fischer Reagent which cannot be detected potentiometrically. When all of the water has been complexed, free iodine ions remain in solution producing a sharp rise in the measured potential of the solution; this is automatically detected and corresponds to the end-point of the titration. At least three measurements were made for each sample.

3.2.14 Photon Correlation Spectroscopy (PCS)

Droplet size measurements were performed using a Malvern Zeta Sizer 3 instrument shown schematically in Figure 3.11. The sizing procedure was carried out at 298K on the instrument in its particle sizing mode, with a He-Ne laser (wavelength 633 nm) and "Login" Software package, with the parameter set or assumed as follows:

Refractive Index of Continuous Phase	1.333
Viscosity (cp) of Continuous Phase	0.920
Scattering Angle (θ)	90°
Particle Refractive Index Real	00.00
Particle Refractive Index Image	00.00

Measurement Settings were:

Estimated Size	0.0
Experiment Duration (seconds)	120
Size Analysis Range	0
Number of Repeated Measurements	5

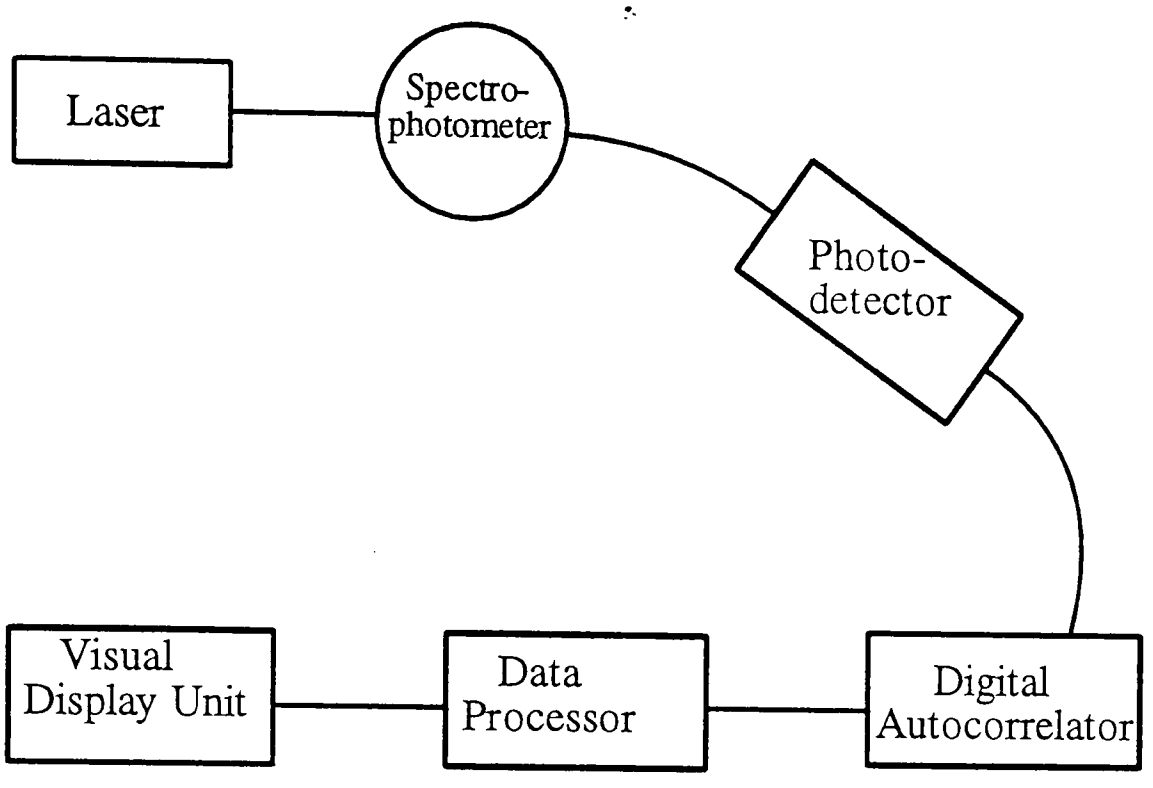

Figure 3.11 Typical sequential arrangement of PCS equipment [11] used

Five runs were performed on each sample and an average of the five measurements was used for both droplet diameter and the polydispersity index (P.I.). The pinhole of the photomultiplier was normally between 100 and 200 μm. All the samples were prepared individually as described in section 3.2.1. Multi-phase samples were pre-equilibrated at room temperature for 24h to allow for any phase separation. A sample of the microemulsion phase (1-3 cm^3) was then extracted from a solution into a separate flask using a Pasteur pipette. The samples were filtered using Millipore filters (pore size 0.2 μm) into glass cylindrical cells, to eliminate any dust particles and left 0.5h to equilibrate and allow any air bubbles to rise. Great care was taken in order to prevent contamination with dust particles that would have interfered with the PCS data.

Prior to a PCS measurement the samples (single phase and multiphase) were requilibrated

at the required temperature for approximately 20 minutes and the cell was then placed into the cell assembly. This procedure was necessary in order to ensure that further phase changes did not occur during an experimental run. The samples were accurately thermostatted (to ± 0.1K) during an experimental run by the circulating water. The composition of the samples prepared are summarised in Tables 3.6 and 3.7.

The hydrodynamic radius R_H and diffusion coefficient D were determined by the PCS experiment using the Stokes-Einstein relationship (as described in Chapter 2):

$$D = \frac{kT}{6\pi\eta R_H} \tag{3.2}$$

where k is the Boltzmann's constant, T is the temperature, η is the viscosity of the continuous phase.

3.2.15 Summary of Experimental Methods

(i) The nonionic surfactants have chromophores which facilitate rapid UV-analysis. Maximum absorbance is at 275nm.

(ii) A phase diagram is a simple and informative method for describing the phase equilibrium behaviour of three or four component mixtures. However, a large number of samples is needed to define a region of interest on the phase diagram.

(iii) The % volumes of the microemulsion phases can be measured at 275nm accurately with the modified spectrophotometer. The measurements are performed when the phases reach equilibrium and constant volume levels are achieved.

(iv) During enhanced oil recovery ultra low interfacial tensions (in the range of 0.01-0.1μN/m) are required for efficient chemical flooding. The spinning drop method is capable of measuring the interfacial tensions at a constant temperature. It is important to achieve a length-to-diameter ratio of four for the accurate measurement of the interfacial tensions.

(v) Viscosity and conductivity provide an indication of the phase inversions in the microemulsion systems. The disadvantages of the viscosity and conductivity experiments are that the use of large volume of the microemulsion phase and

longer time for the equilibrium are required. In the conductivity experiments, it must be ensured that the conductivity cell is completely immersed in the microemulsion phase.

(vi) HPLC is used to characterise and quantify the surfactants as well as the microemulsion phases under the gradient elution. In order to label the peaks, n=9 and n=3 marker compounds should be used to identify specific oligomers.

(vii) Gas chromatography is useful for qualitative and quantitative analysis of volatile components (i.e. hydrocarbons and alcohols) in the microemulsion systems, and particularly with a thermal conductivity detector (TCD) it is possible to detect water in the system.

(viii) Dynamic light scattering is capable of measuring the apparent droplet sizes of the single phase and three phase microemulsions. The main advantage of the light scattering measurement is that only small sample volume is required to complete the analysis. The complication arises in eliminating dust from the sample. Even after careful filtering and protection from airborne particles there will inevitably be contamination and this will have an effect on the apparent particle size.

These techniques were chosen because the alternatives were less convenient and they have the advantage in presenting a comprehensive overview of the phase behaviour of microemulsion systems.

References

[1] I.E. Bruce, A. Long, P.B. Payne and J.H.P. Tyman, J.of Liquid Chromatogr., **13**, 2103, (1990)

[2] Manufacturers specifications: Rohm and Haas Limited, Croydon, England.

[3] A.V. Kiselev and V.I. Lygin "Infrared Spectra of Surface Compounds", Wiley, New York, (1975)

[4] R.N. Healy and R.L. Reed, J. Soc. Pet. Eng. **June,** 147 (1976)

[5] B. Vonnegut, Rev. Sci. Inst. **11,** 6 (1942)

[6] N.A. Ibrahim, PhD Thesis Brunel University (1995)

[7] F.P.B. Van Der Maeden, M.E. Biemond and P.C.G.M. Janssen, J. Chromatogr., **149**, 539, (1986)

[8] M.S. Holt, E.H. McKerrell, J. Perry and R.J. Watkinson, J. Chromatogr., **362**, 419, (1986)

[9] C.F. Allen and L.I. Rice, J. Chromatogr., **110**, 151, (1975)

[10] D.M. Smith, W.M.D. Bryant and J. Mitchell, J. Am. Chem. Soc. **61,** 2407 (1939)

[11] C. Orr, "Encyclopedia of Emulsion Technology", **Vol. 3,** Dekker, New York, (1985)

CHAPTER FOUR

CHARACTERISATION OF MICROEMULSION SYSTEMS

4.1 Phase Equilibria in Microemulsions

4.1.1 Introduction

Surfactants have considerable potential as enhanced oil recovery agents because they are capable of recovering most of the oil contacted in a micellar reservoir flood. For this reason it is necessary to maintain ultra-low interfacial tensions, typically in the range 0.0-0.01μN/m. These conditions can be achieved with an appropriate choice of an optimum surfactant system, where a middle phase microemulsion exists in which equal volumes of oil and water are solubilised. Apart from the surfactant, oil and brine, a co-surfactant, such as an alcohol, is often required to ensure that appropriate optimum conditions exist.

Systems containing water, hydrocarbon and surfactant(s) often consist of two or more phases in contact with each other. The various permutations of the contact between the phases present have been classified by Winsor [1] and designated Winsor (I), (II), (III), and (IV) equilibria.

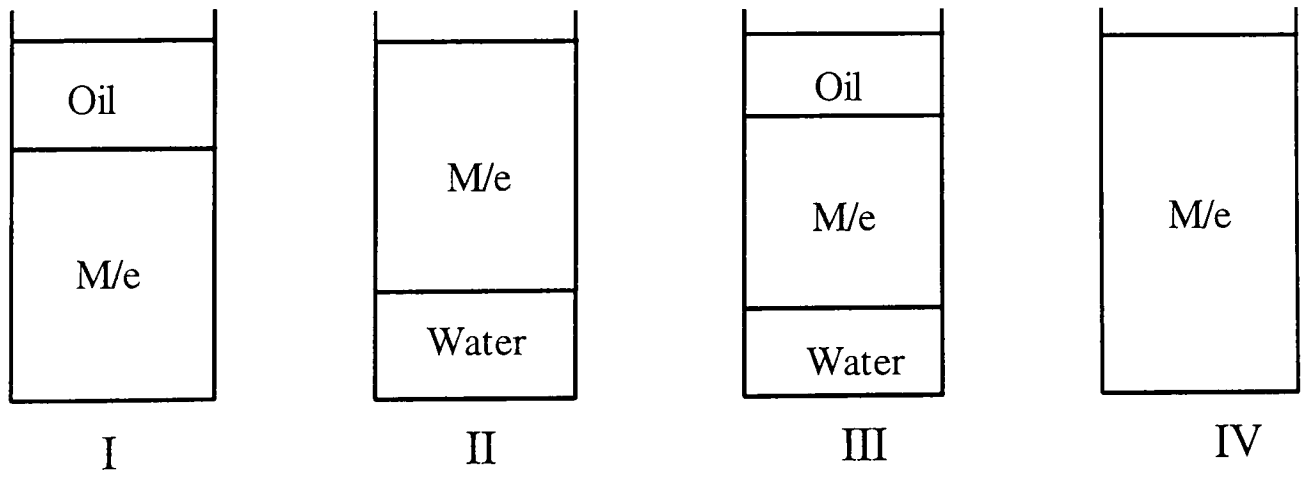

Figure 4.1 Schematic representation of non-order media comprising: surfactant, hydrocarbon and water according to the Winsor classification.

Type (I): systems in which the surfactant is in the aqueous phase and the microemulsion is in equilibrium with excess oil.

Type (II): systems in which the microemulsion is in equilibrium with excess water.

Type (III): systems in which the microemulsion forms a stable middle phase in thermodynamic equilibrium with both excess oil and water.

Type (IV): systems which contain no free aqueous or organic phases and which are macroscopically monophasic fluid media, made of water, hydrocarbon and surfactant, i.e. a microemulsion.

When surfactant (and co-surfactant), water and oil are combined in the correct proportions a single phase microemulsion is formed (type (IV)), which contains discrete droplets as a result of the molecular self-assembly of the system.

4.1.2 Effect of Alcohols (Co-surfactant)

The use of alcohols in making microemulsions has a long tradition. To Schulman and Winsor, the co-surfactant was considered an indispensable ingredient of microemulsions. The presence of alcohols, which are themselves surface-active materials, has profound effects on the phase properties of surfactants-oil-water systems. Alcohols assist the surfactant in enhancing the mutual miscibility of oil and water. In this role alcohols are known as co-surfactants. Mixtures of surfactant, oil and water which usually form turbid macroemulsions can form optically clear or solution-like liquids.

Most commercial surfactants are not balanced with respect to their affinity to water and oil, but can be made so by alcohol addition. Using anionic surfactant, electrostatic interactions have to be screened by salt as a fifth component. The unwanted effects of salt can be compensated by adjusting the alcohol concentration.

4.1.3 Effect of Salinity, pH and Temperature on the Phase Equilibria

The effect of inorganic salts on the phase behaviour of mixtures of water, oil, and ionic surfactant is well known, since 1950, and recently has more interest because of the potential application of micellar systems to enhanced oil recovery [2]. Salt has a marked effect on the phase behaviour of microemulsions prepared with petroleum sulphonates [3,4]. Single phase and multiphase regions on the ternary phase diagram are significantly changed by altering the electrolyte content of the brine phase. Within the single-phase region, physical properties and structure are modified due to changing the preference of

the sulphonates for the oil phase or water phase; decreasing salinity favouring the aqueous phase.

Winsor type (II) systems with anionic or nonionic surfactant NaCl has been found to partition preferentially into the excess aqueous phase in equilibrium with a microemulsion phase [2]. However, the effect is small in the case of nonionic surfactant. An increase in temperature or ethylene oxide units or hydrophilic lipophilic balance (HLB) decreases the effect of most of the surface and thermodynamic properties of the surfactants such as CMC, ΔG_{mic} etc. The only exception is the critical surface tension γ_{CMC} : an increase in temperature has a negligible effect while increasing the number of ethylene oxide units or HLB increases $\gamma_{CMC.}$

4.1.4 RESULTS AND DISCUSSION

Phase behaviour of the nonionic and anionic surfactants was observed using the method as described in section 3.2.2 of Chapter 3. The effects of alcohols (co-solvents), salinity (NaCl) and temperature were extensively investigated and particular emphasis was given to the stability of the three phase microemulsion system. In addition, an apparatus was developed to determine the volume percentage of the different phases formed in the microemulsion systems as a function of salinity and temperature.

The phase equilibrium diagram of water/TX-100+pentan-1-ol/decane system at 298K is shown in Figure 4.2. The solid lines in the figure correspond to experimentally determined phase boundaries. At low surfactant concentrations (<10%), phase separation occured into an opaque and viscous lower emulsion phase. The region of the phase diagram located towards the surfactant corner is structurally very complex and is composed of a variety of lamellar and hexagonal liquid crystalline phases. This region has been studied in some detail by other workers [5] and was not investigated in this work. At high surfactant/co-solvent concentrations (>30%) single phase microemulsions were produced. In this system, large regions of the Winsor types (I) and (II) were also observed. The system has shown a classical phase behaviour.

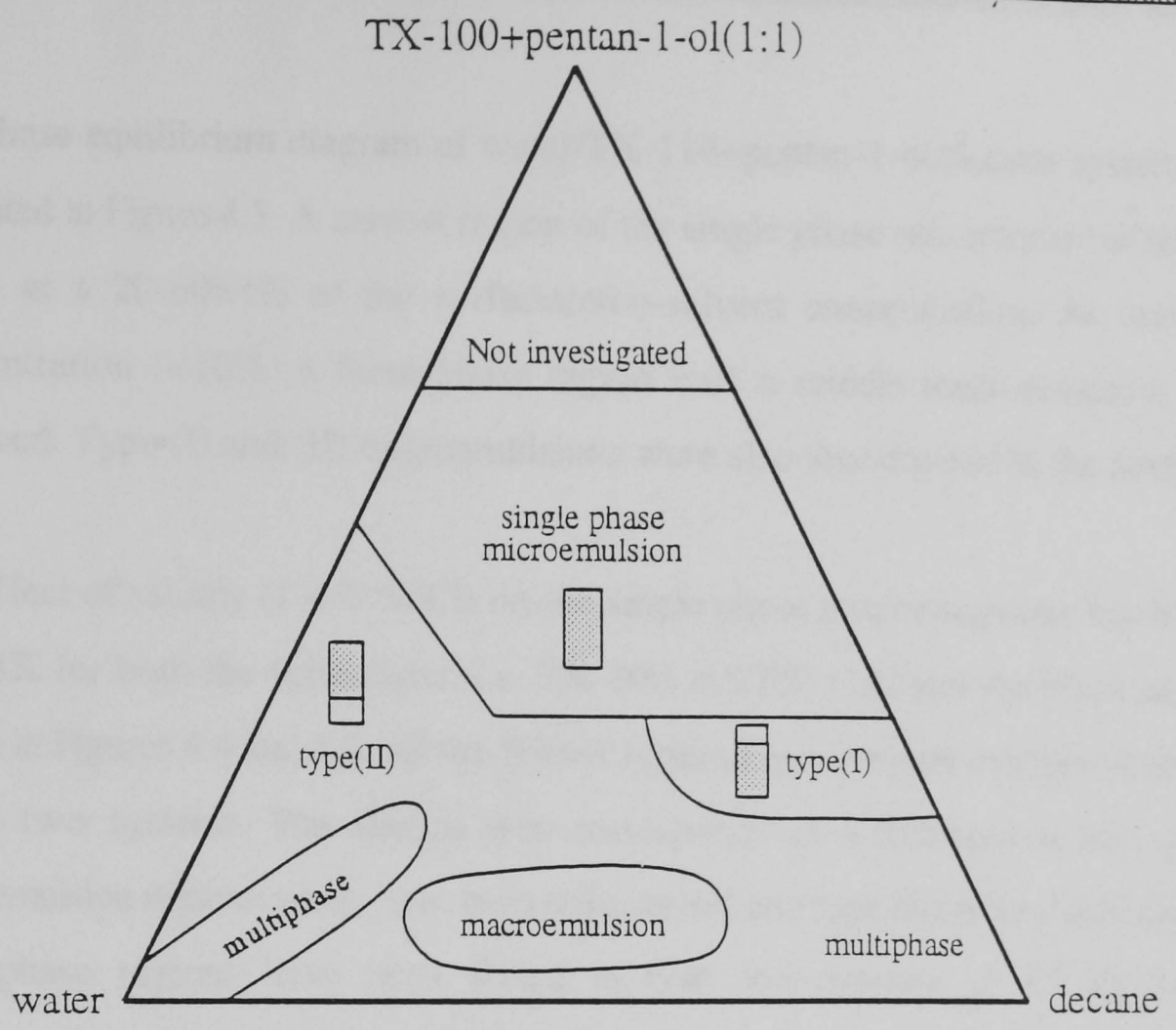

Figure 4.2 Phase equilibrium diagram of water/TX-100+pentan-1-ol/decane system at 298K

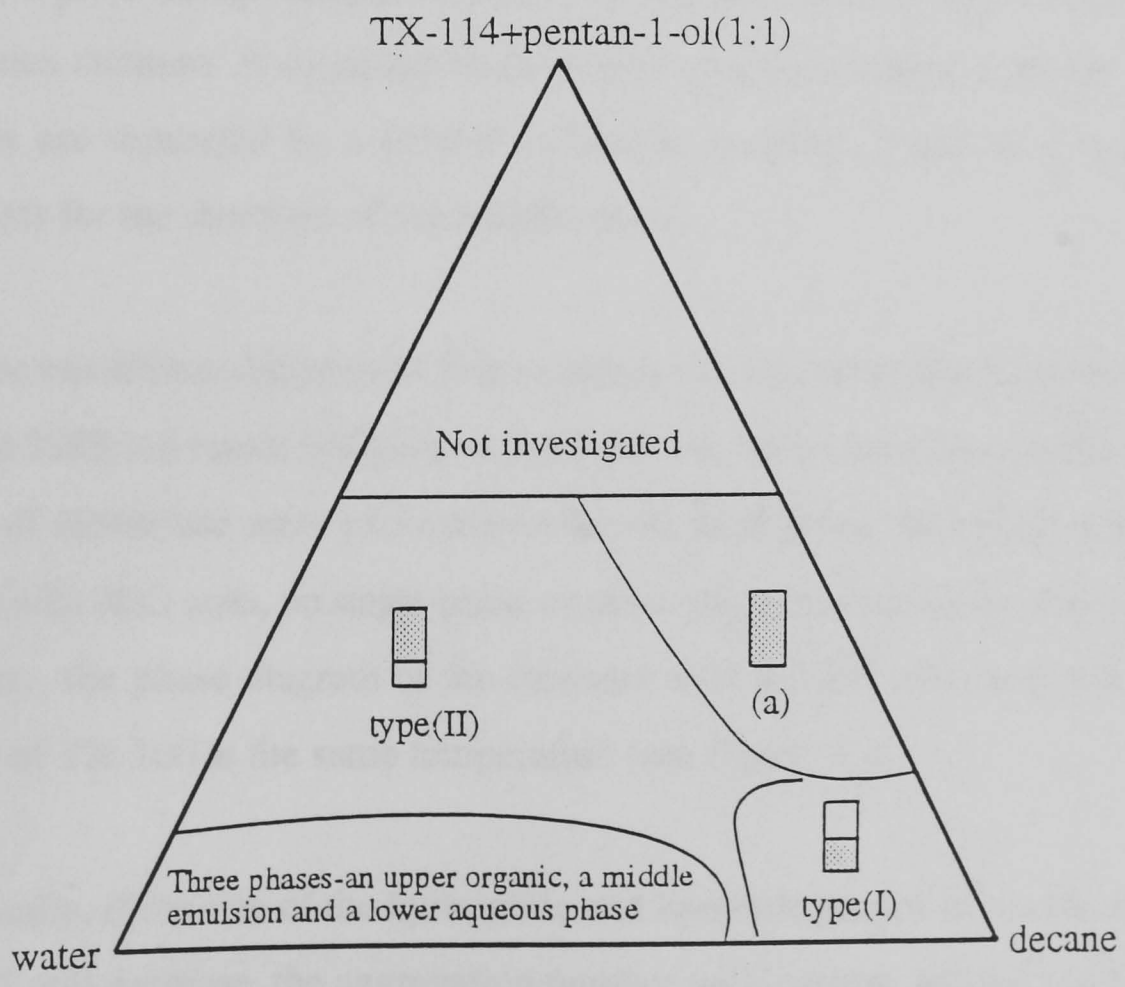

Figure 4.3 Phase equilibrium diagram of brine/TX-114+pentan-1-ol/decane system at 298K, where (a) is single phase microemulsion region.

The phase equilibrium diagram of water/TX-114+pentan-1-ol/decane system at 298K is presented in Figure 4.3. A narrow region of the single phase w/o microemulsion has been found at a 20-60wt% of the surfactant/co-solvent concentration. At low surfactant concentration (<10%) a three phase region with a middle macroemulsion phase was observed. Type (I) and (II) microemulsions were also investigated in the system.

The effect of salinity (1-4% NaCl) on the single phase microemulsions has been studied at 298K for both the surfactants (i.e. TX-100 and TX-114) and the phase diagrams are shown in Figures 4.4 and 4.5. All the Winsor types of microemulsions have been observed in the two systems. The shaded area corresponds to a decrease in the single phase microemulsion regions which have been transformed into type (II) microemulsions. Typical three-phase regions have been found in both the systems at 15-20 wt% of the surfactant/co-solvent concentrations. The middle phase of the three-phase solutions consisted of a transparent viscous liquid. This might suggest that the structure of the middle phase (which contains quite a high proportion of surfactant and water) may not be that of a typical microemulsion consisting of discrete water droplets dispersed in an oil-continuous medium. A so-called bicontinuous structure, where transient oil and water channels are separated by a flexible surfactant interface, might be a more reasonable hypothesis for the structure of the middle phase.

The phase equilibrium diagrams of brine/cardanol (a natural product)+pentan-1-ol/decane system at 298K are traced in Figures 4.6 and 4.7. As can be seen, the cardanol with a large number of ethoxylate units (8.5) shows the classical phase behaviour, whereas, for the cardanol with 3EO units, no single-phase or three-phase microemulsion has been observed. However, the phase diagram of the cardanol with 8.5 EO units is similar to the phase diagram of TX-100 at the same temperature (see Figure 4.4).

Theoretically, if the size of the hydrophile and lipophile groups of a surfactant increases, the CMC will decrease, the aggregation number will increase and the solubilising power will be enhanced. This may be the reason that the brine/TX-100+pentan-1-ol/decane and the brine/ cardanol (8.5EO)+pentan-1-ol/decane systems have shown a better phase

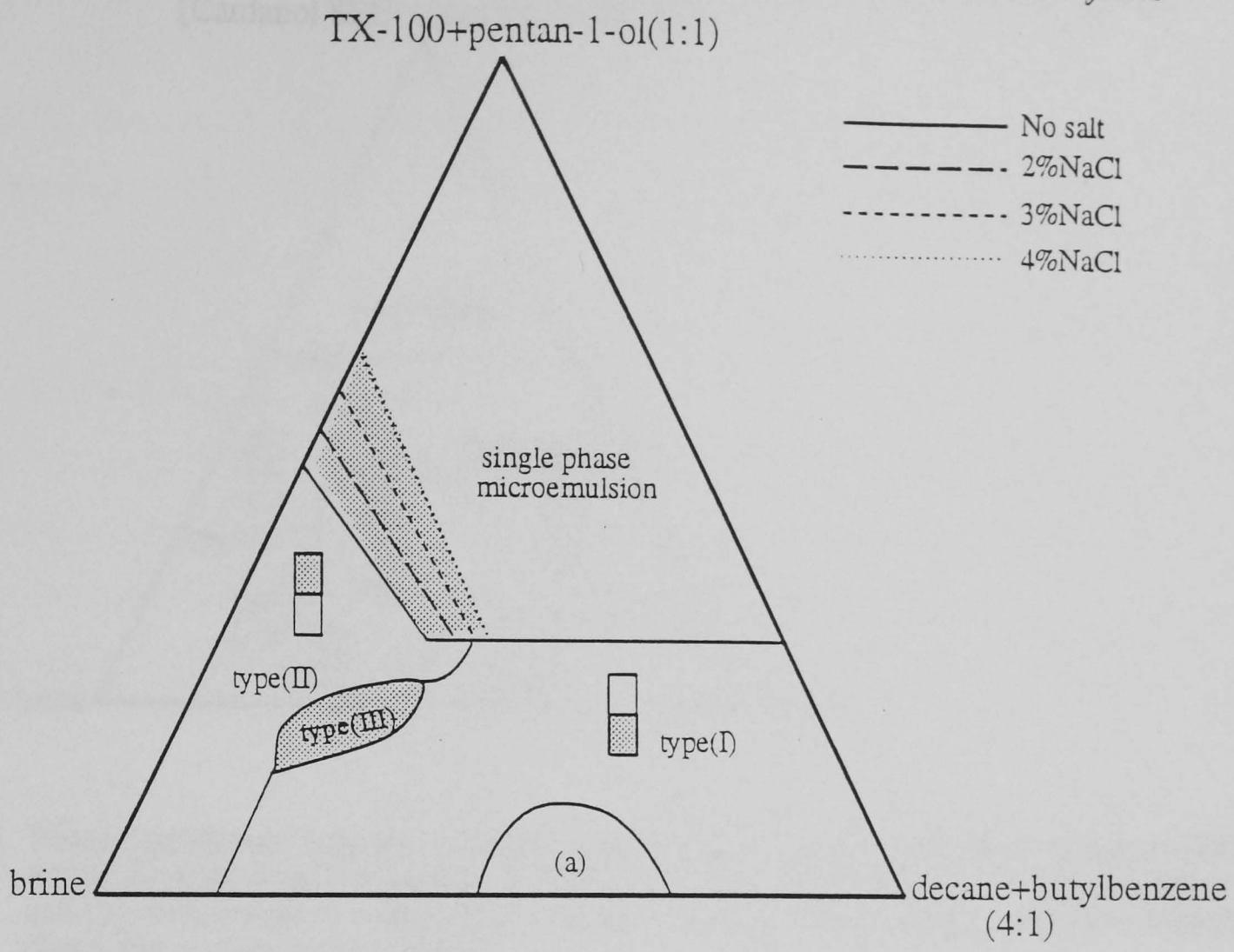

Figure 4.4 Phase equilibrium diagram of brine/TX-100+pentan-1-ol/decane system at 298K Effect of salt on the single phase microemulsion where (a) denotes two phases; an upper emulsion phase and a lower aqueous phase

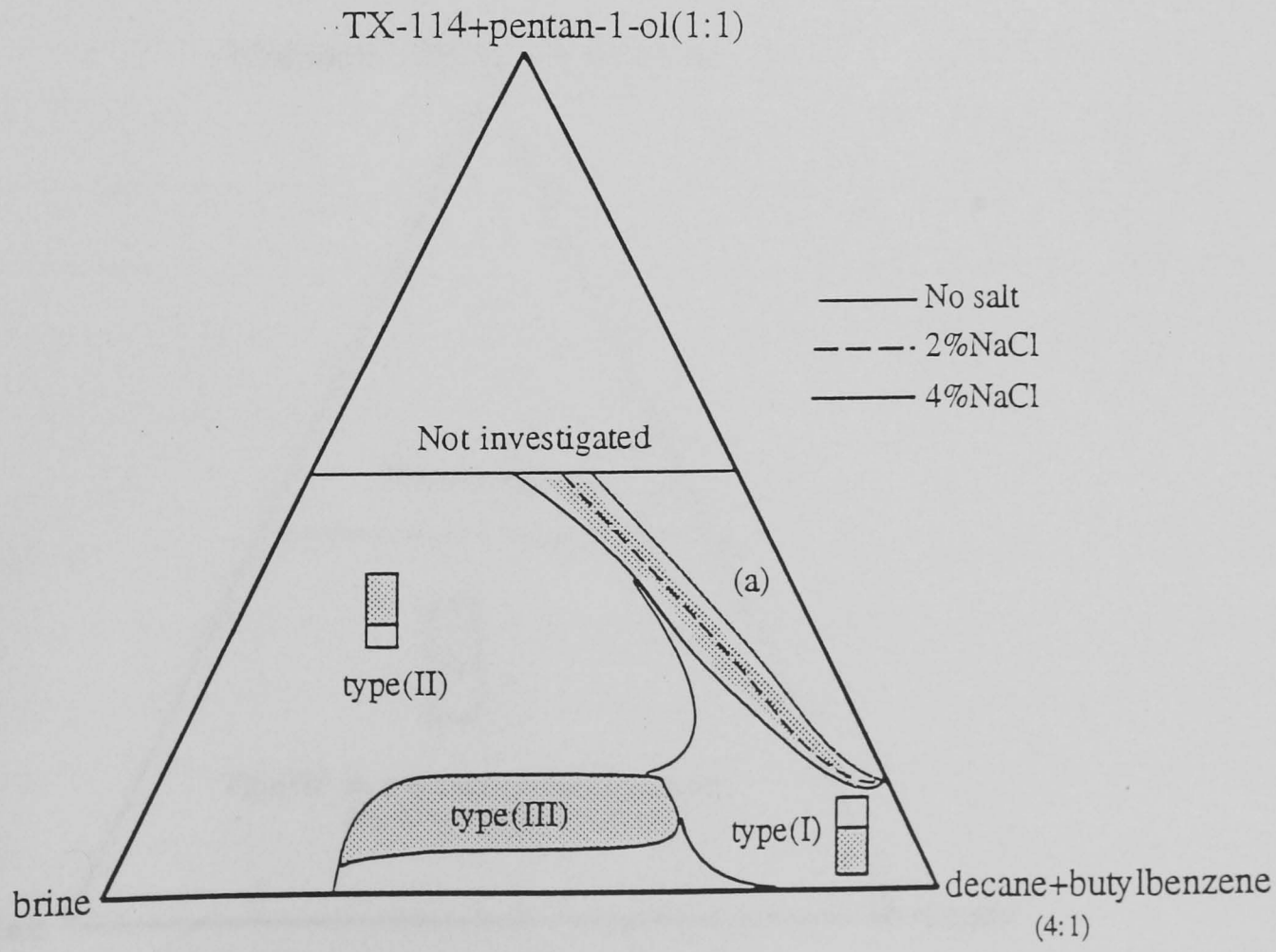

Figure 4.5 Phase equilibrium diagram of brine/TX-114+pentan-1-ol/decane+butylbenzene system at 298K, where (a) is single phase microemulsion region.

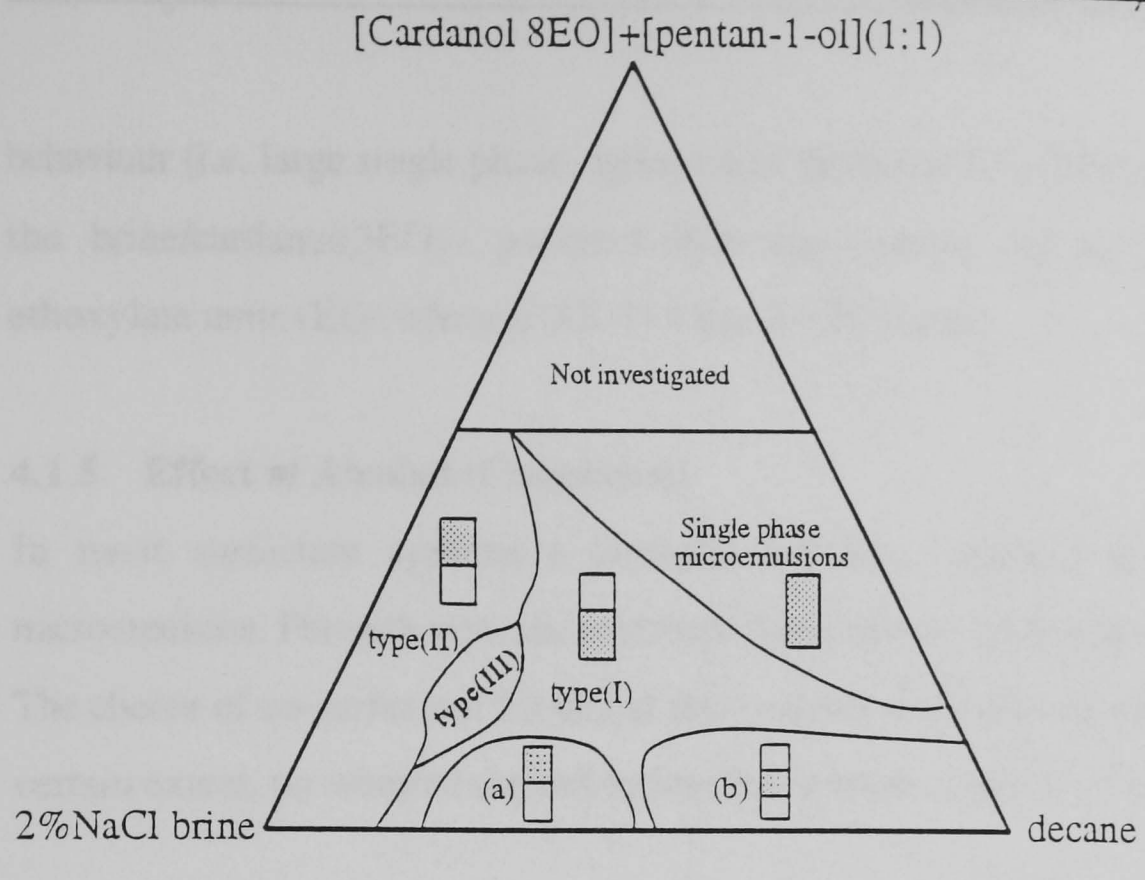

Figure 4.6 Phase equilibrium diagram of brine/cardanol 8EO+pentan-1-ol/decane system at 298K, where (a) represents two phases: an upper emulsion phase and a lower aqueous phase and (b) corresponds to a three phase region: an upper organic phase, a middle emulsion phase and a lower aqueous phase.

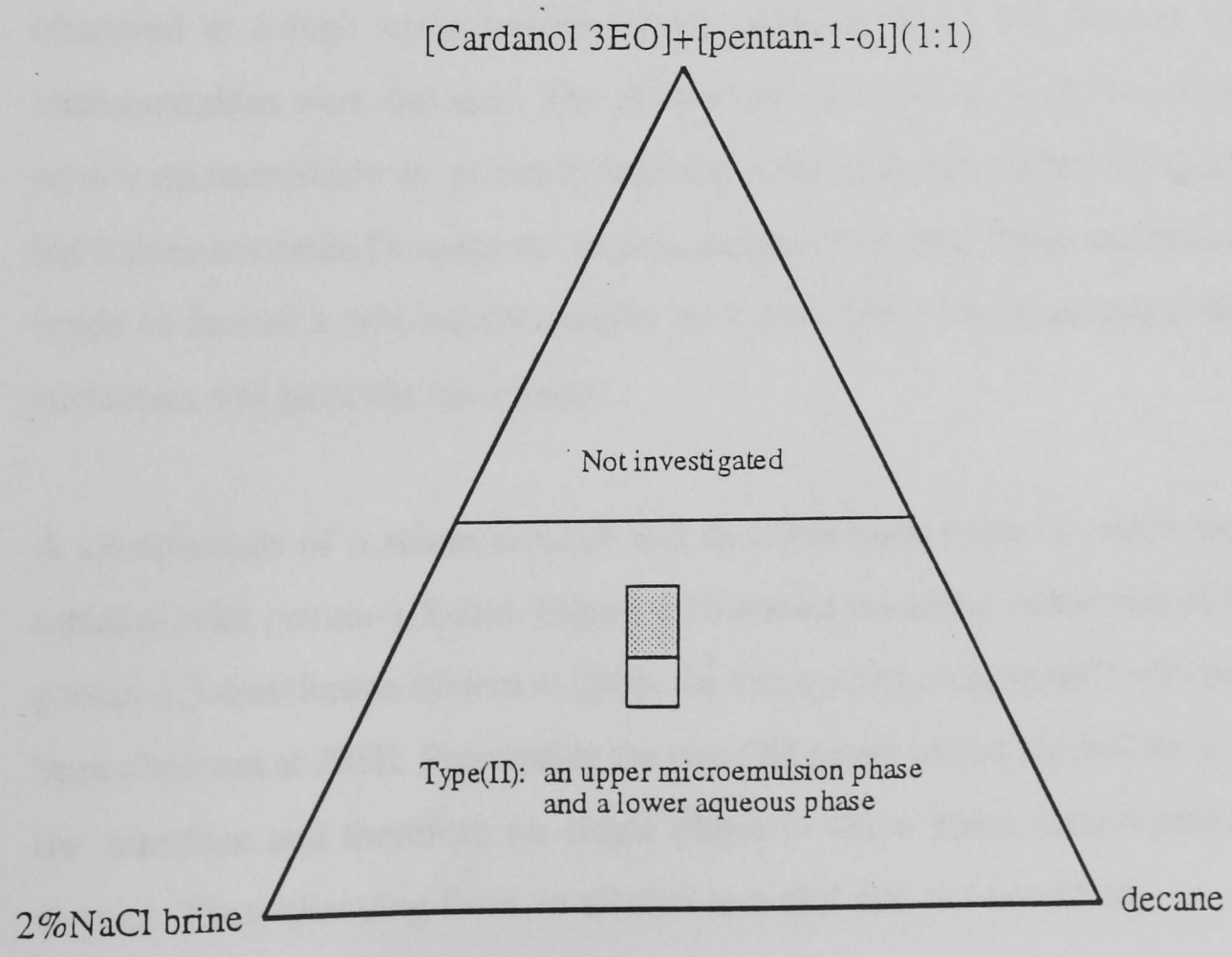

Figure 4.7 Phase equilibrium diagram of brine/cardanol 3EO+pentan-1-ol/decane system at 298K

behaviour (i.e. large single phase region) than the brine/TX-114+pentan-1-ol/decane and the brine/cardanol(3EO)+ pentan-1-ol/decane system. As in TX-100 there are 10 ethoxylate units (EO) whereas TX-114 has 7-8 EO units.

4.1.5 Effect of Alcohol (Co-solvent)

In most surfactant systems a co-surfactant (e.g. alcohol) is required to form a microemulsion. For such systems, selection of the alcohol co-surfactant may be important. The choice of co-surfactant for use in the creation of a microemulsion is dependent, to a certain extent, on whether the desired microemulsion is a w/o or an o/w dispersion.

The effect of different alcohols (including diol) on the phase behaviour of the nonioninc surfactant was investigated at 298K. The phase diagram of water/TX-100+propan-1-ol/ decane system is shown in Figure 4.8. No single-phase or three-phase microemulsions have been observed even at high surfactant/co-solvent concentrations. However, a large region of type (I) microemulsion (i.e. o/w) can be seen. The phase diagram of water/TX-100+ octan-1-ol/decane system is traced in Figure 4.9. Single phase microemulsions have been observed at a high surfactant/co-solvent concentration. The Winsor type(I) and (II) microemulsions were also seen. The short chain alcohol (i.e. propan-1-ol) tends to favour an o/w microemulsion as probably because it can pack the surfactant head group region, but it does not extend into the tail section. Similarly the long chain alcohol (i.e. octan-1-ol) tends to favour a w/o microemulsion as it can screen the head group repulsion of the surfactant and pack the tail region.

A comparison of a mono-alcohol and diol has been made in which pentan-1-ol was replaced with pentan-1,5-diol. Figure 4.10 shows the phase behaviour of brine/TX-100+ pentan-1,5-diol/decane system at 298K. In this system, only type(I) microemulsions have been observed at 298K. Presumably the two OH group on the alcohol molecule destabilise the interface and therefore no single phase or three phase microemulsions have been formed. Thus, changing from an alcohol to a diol was not beneficial.

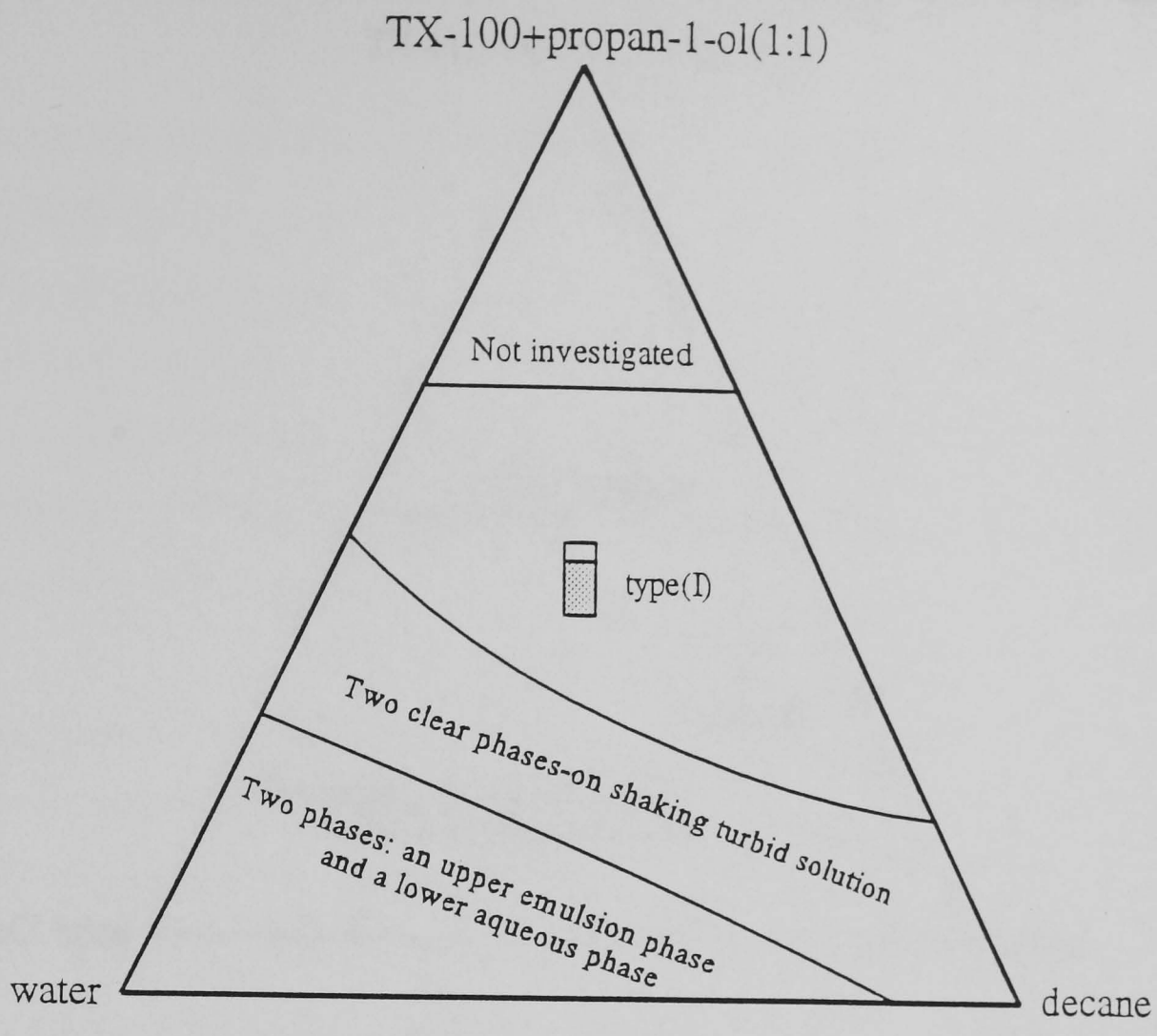

Figure 4.8 Phase equilibrium diagram of water/TX-100+propan-1-ol/decane system at 298K

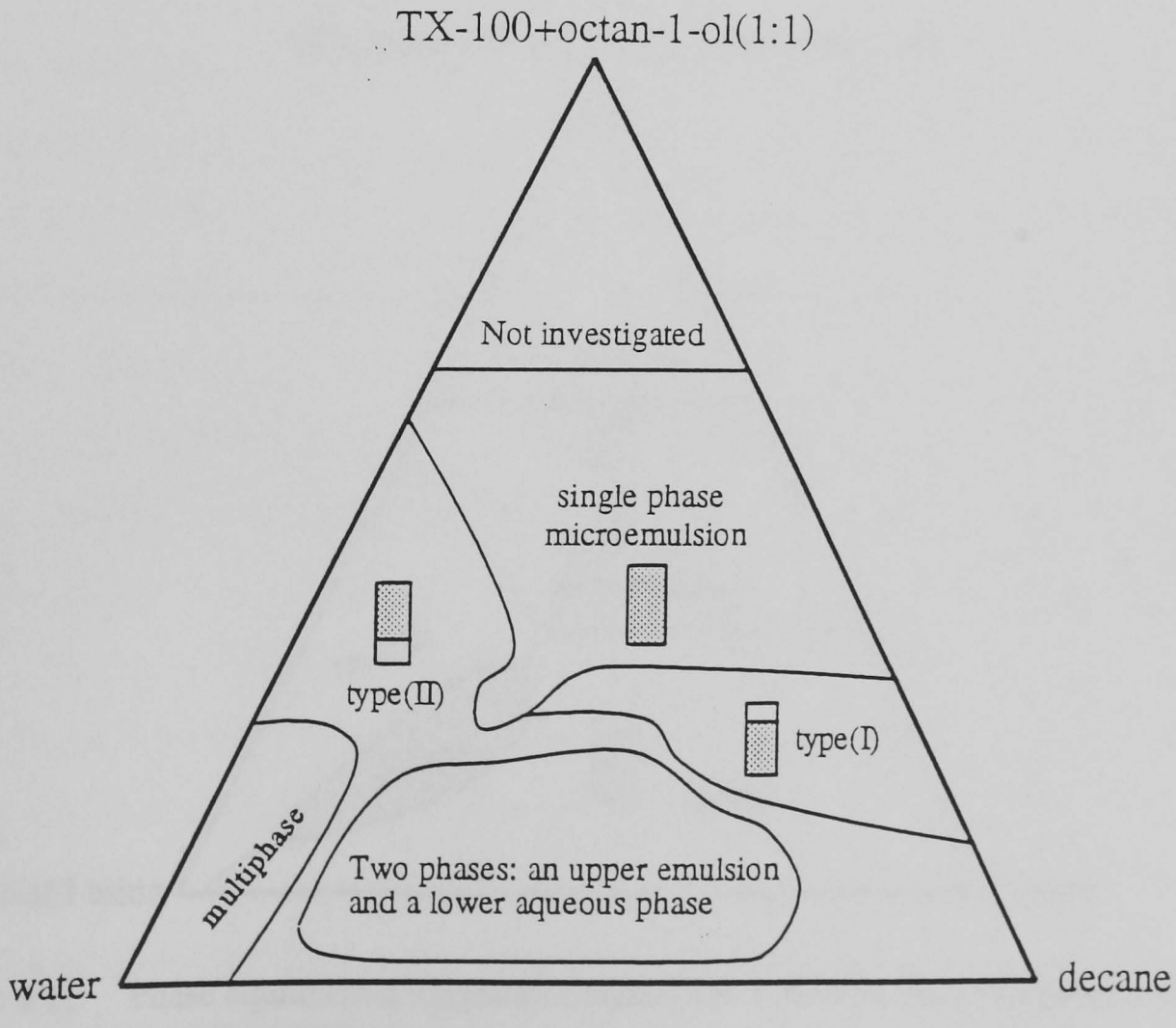

Figure 4.9 Phase equilibrium diagram of water/TX-100+octan-1-ol/decane system at 298K

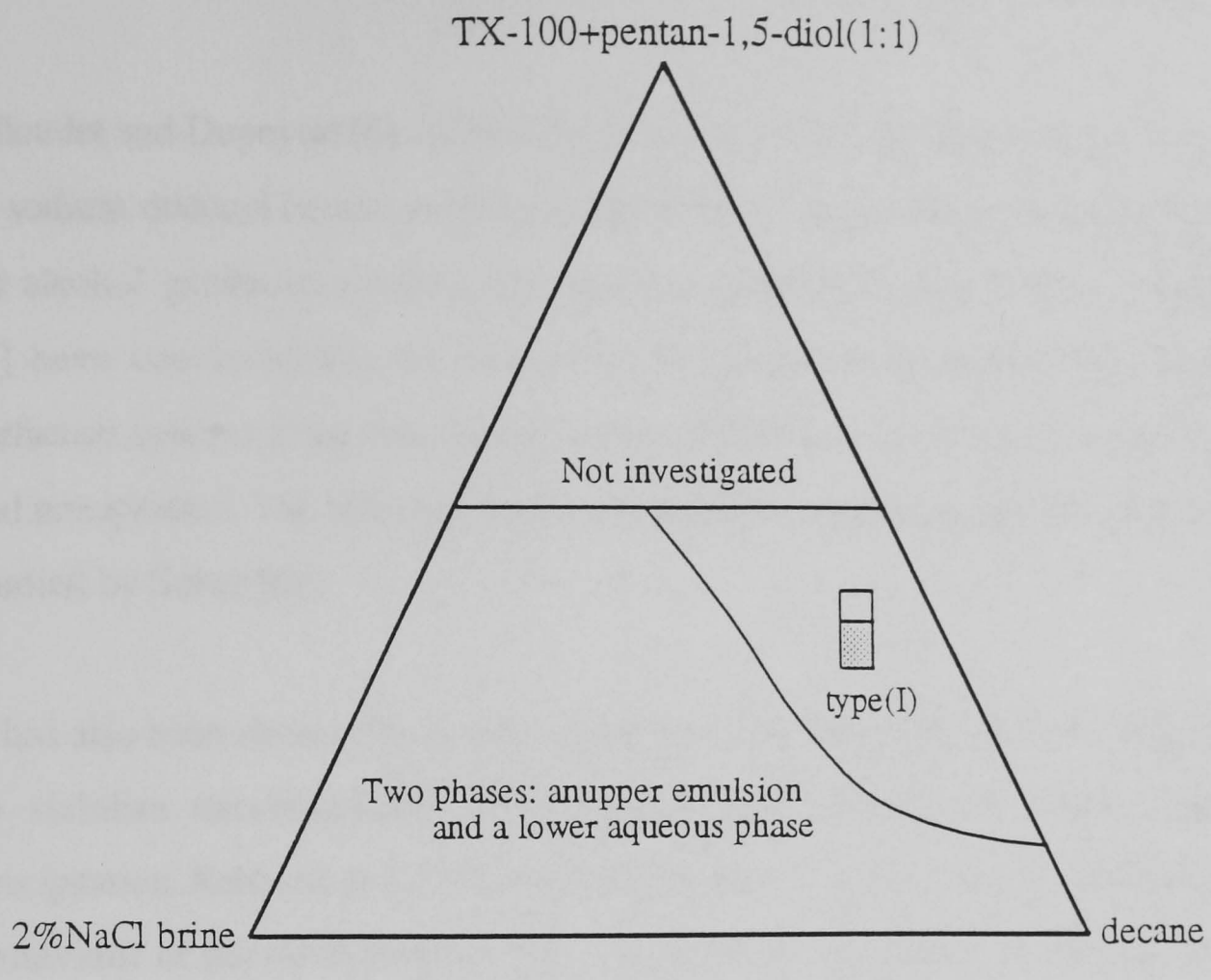

Figure 4.10 Phase equilibrium diagram of brine/TX-100+pentan-1,5-diol/decane system at 298K.

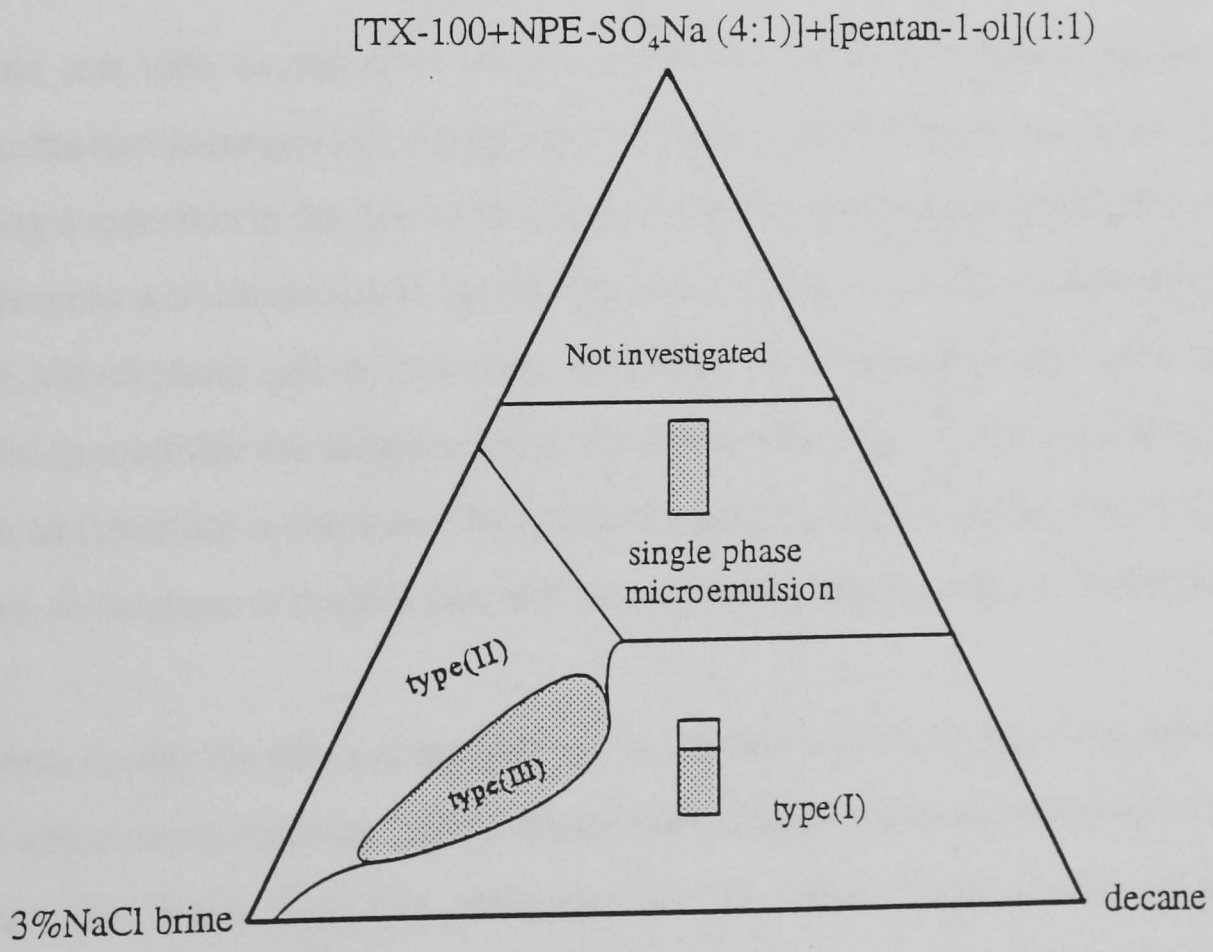

Figure 4.11 Phase equilibrium diagram of brine/[TX-100+NPE-SO_4Na]+[pentan-1-ol]/decane system at 298K

Billoudet and Dupeyrat [6] studied the penetration of short chain alcohols in monolayers of sodium dodecyl bezene sulphate (SDBS) at the decane/brine interface and found that the alcohol produced a substantial reduction in the interfacial tension. Salager and Shah [7] have concluded that the function of alcohols was to increase the solubility of the surfactant systems in the brine and to prevent the formation of viscous gels, liquid crystals and precipitation. The effects of alcohol on different crude oil/surfactant systems were also studied by Salter [8].

It has also been shown [9] that the alcohol acts to modify the surfactant partitioning and to stabilize microemulsions by preventing the formation of liquid crystals, gel or precipitation. Kahlweit et al [10] studied the effect of medium-chain alcohols on the phase behaviour of microemulsions and concluded that referring to alcohols as co-surfactants may obscure their actual significance. It was suggested that they be considered rather as co-solvents that partition between the aqueous domian, the oleic domain, and the amphiphilic film.

Simple test tube experiments on o/w emulsions show that increasing the amount of co-surfactant increases the transparency of the system. This is due to the co-surfactant causing a reduction in the size of the dispersed phase and thus progressively changing the emulsion to a microemulsion. As the alcohol is added, it partitions between the aqueous phase, the oil phase and the interface. This dynamic process provides some of the energy needed to subdivide the dispersed phase [11]. Once the capacity for alcohol of the aqueous phase and interface is exceeded, the excess dissolves in the oil phase. For o/w systems this means an increase in droplet size and an accompanying decrease in transparency [12].

Alcohols modify the effect of surfactants. (a) Water-soluble alcohols solubilize additional brine into a microemulsion. Large amounts of alcohol cause separation of a hydrocarbon phase. (b) Water insoluble alcohols, on the other hand, cause solubilization of hydrocarbon, while decreasing the brine solubility [11]. Hydrocarbon capacity should increase and brine capacity should decrease with increasing alcohol concentration. Excess brine solubility should be zero at the upper limit of stability.

4.1.6 Three Phase System on Ternary Diagram

The particular interest of this thesis is the use of surfactant systems to solubilise oil and water, in oil reservoirs. This is generally accompanied by the formation of a microemulsion [13] and a reduction in interfacial tension [14, 15]. In the literature, it has also been suggested that some systems using nonionic surfactants can be stabilized using a small amount of anionic surfactants [16]. It was therefore decided to add a few percent of the anionic surfactants (SAS or SDS) to enhance the stabilization of microemulsion.

Nonionic surfactants were mixed with the anionic surfactants in different ratios in an attempt to improve their phase behaviour. The anionic surfactants used were secondary alkane sulphonates (SAS), sodium dodecyl sulphate (SDS) and nonylphenol ethoxylate (10EO units) sodium sulphate (NPE-SO_4Na). The phase equilibrium diagrams of brine/TX-100 + NPE-SO_4Na + pentan-1-ol/decane and brine/TX-165 + SAS + pentan-1-ol/decane systems at 298K are shown in Figures 4.11 and 4.12 respectively. In the phase diagrams a wide region of type (III) microemulsion has been observed at low surfactants/ co-solvent concentration (i.e. 15 wt %) near the brine corner. The three phases consist of a small upper hydrocarbon phase, a large middle microemulsion phase and a small lower aqueous phase. Figures 4.13 and 4.14 show the phase behaviour of TX-100+pentan-1-ol with and without SAS and SDS at 298K respectively. A shift in the three phase region towards low surfactant concentration can be seen. In the Figure 4.14 a single phase microemulsion region has also been observed with the addition of SDS. Probably, addition of SAS or SDS changes the HLB of TX-100 and hence the three-phase region is produced at a lower surfactant concentration. The phase equilibria results show that the phase behaviour of the nonionic surfactants can be dramatically improved (i.e. the extent of the three-phase region can be increased) by mixing them with anionic surfactant, SAS or SDS.

4.1.7 Effect of Salinity on the Phase Equilibria

The effect of salinity (2-9%NaCl) on the phase behaviour of the nonionic/anionic mixtures was investigated at 298K. The phase equilibrium diagrams of brine/TX-100+ NPE-SO_4Na +pentan-1-ol/decane and brine/TX-100+SDS+pentan-1-ol/decane systems are presented in Figures 4.15 and 4.16 respectively. It has been observed that the three-phase

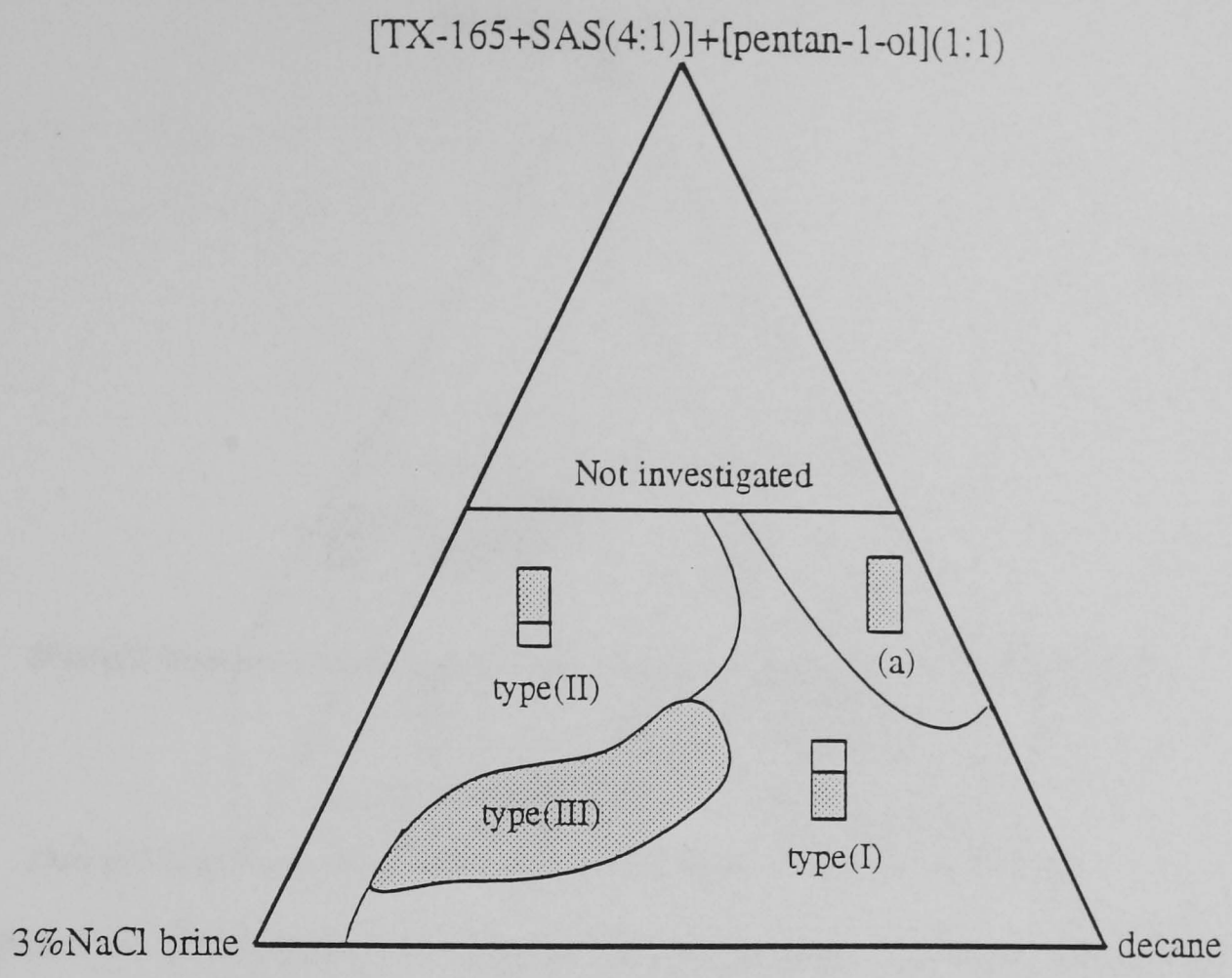

Figure 4.12 Phase equilibrium diagram of brine/TX-165+SAS+pentan-1-ol/decane system at 298K, where (a) represents single phase microemulsion.

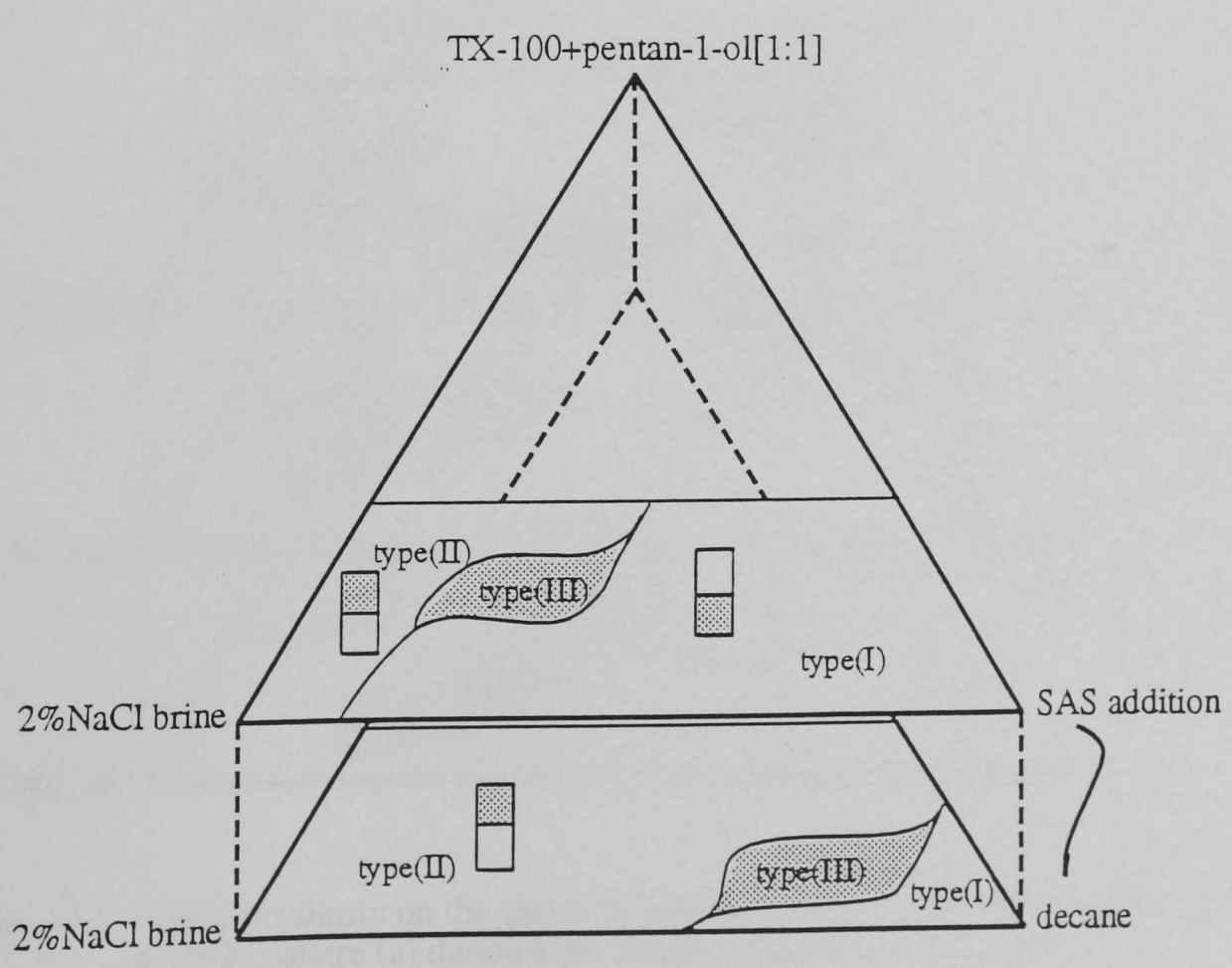

Figure 4.13 Phase equilibria of brine/TX-100+pentan-1-ol/decane with and without SAS at 298K.

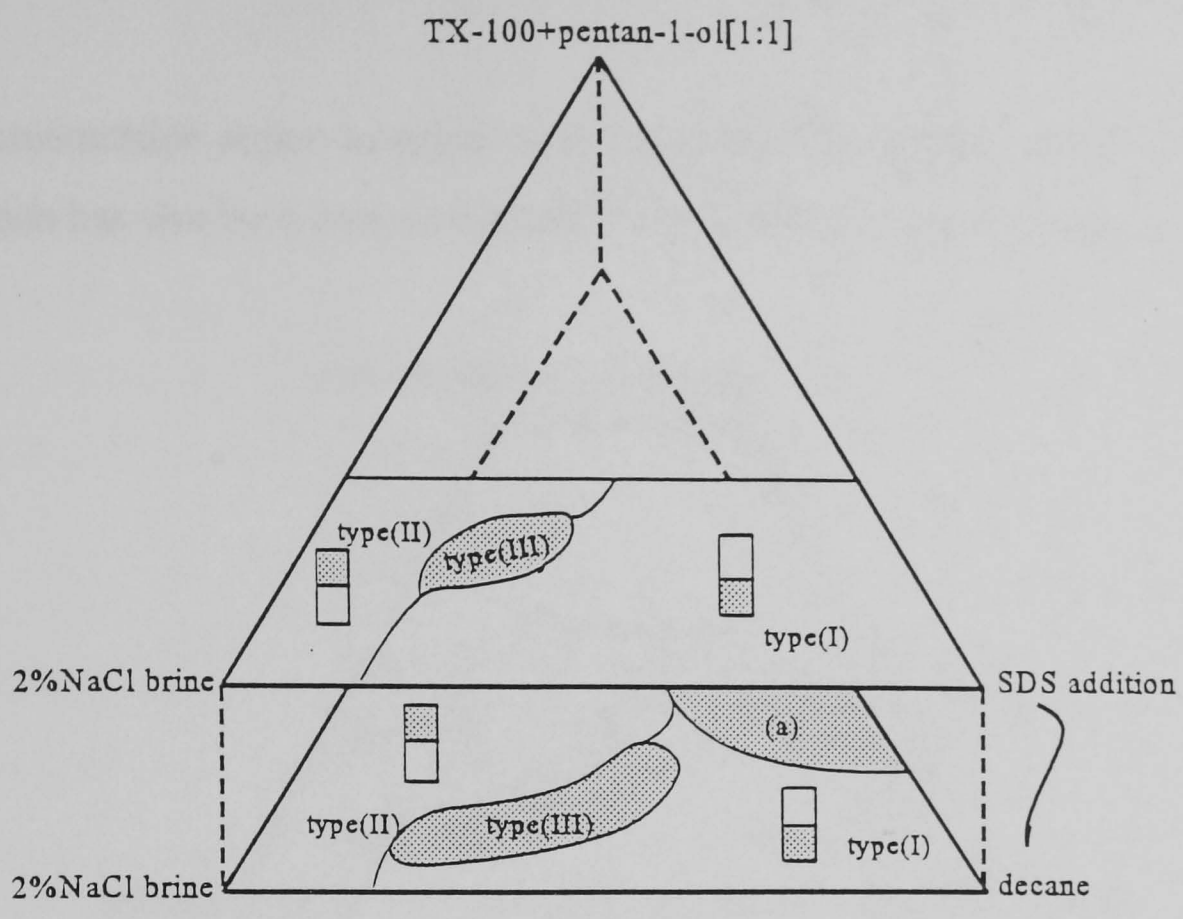

Figure 4.14 Phase equilibria of brine/TX-100+pentan-1-ol/decane with and without SDS at 298K, where (a) corresponds to the single phase microemulsion region.

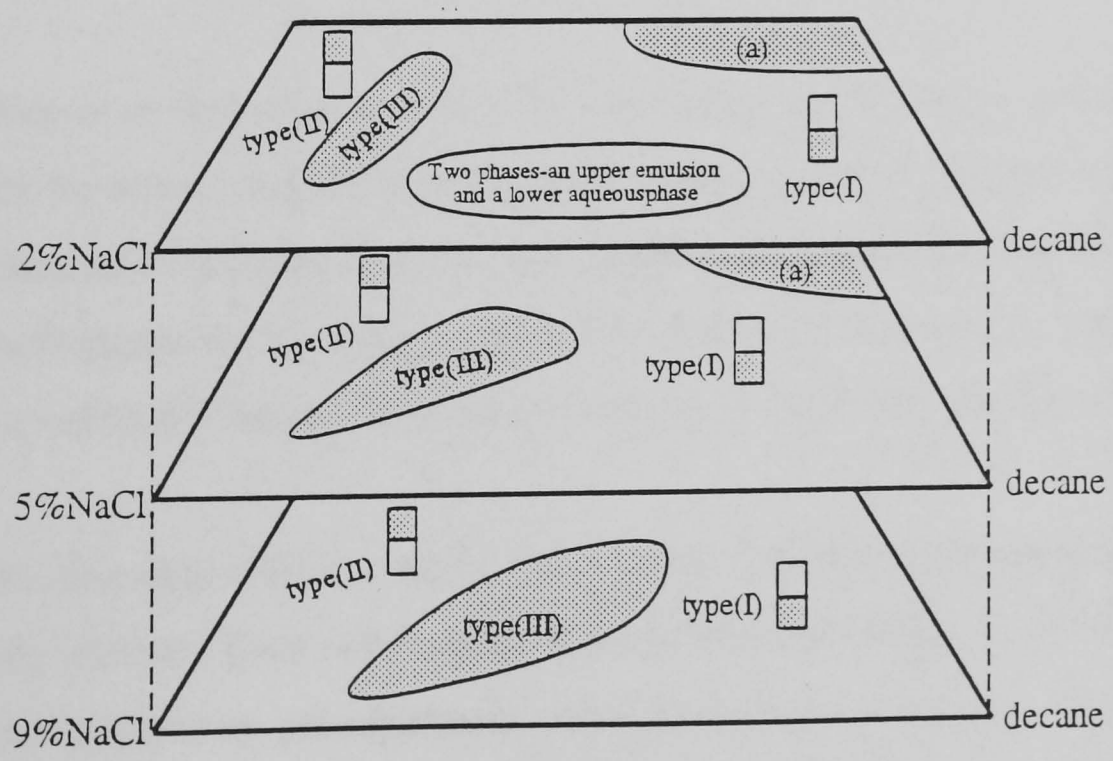

Figure 4.15 Effect of salinity on the phase behaviour of [TX-100+NPE-SO_4Na (4:1)]/decane at 298K, where (a) denotes the single phase microemulsions

microemulsion region increases with increasing the salinity. A shift in the three-phase region has also been noticed towards lower surfactant concentration.

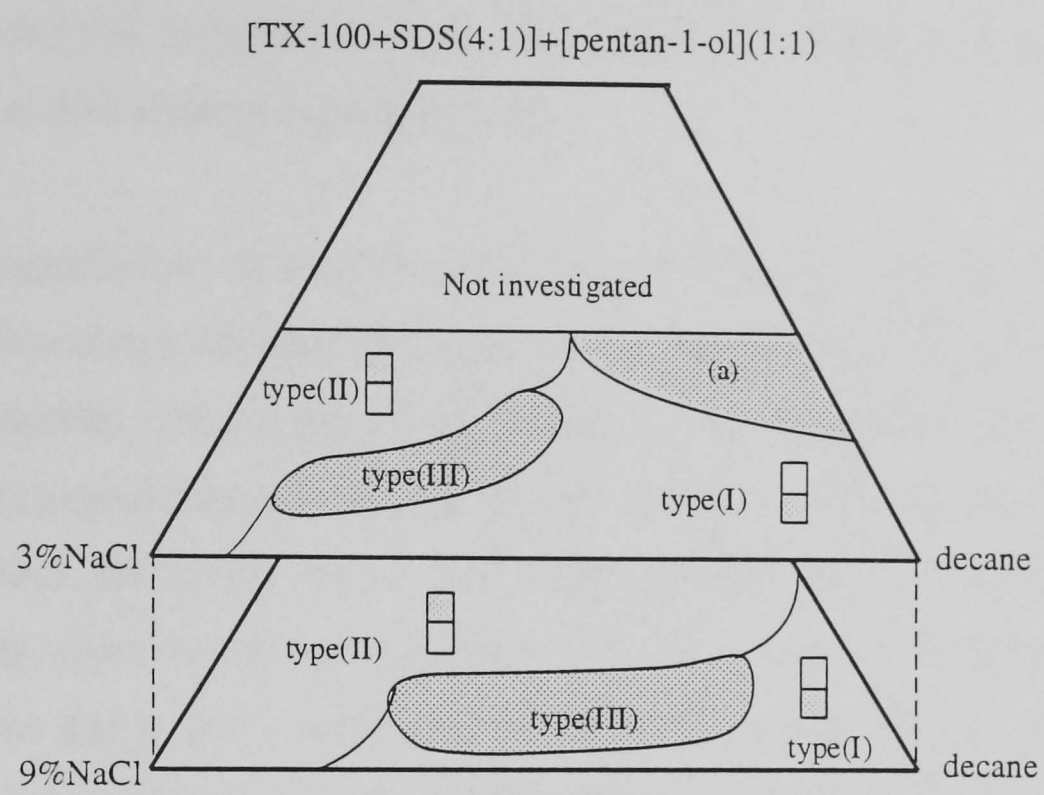

Figure 4.16 Effect of salinity on the phase behaviour of [TX-100+ SDS(4:1)]+ [pentan-1-ol](1:1)/decane at 298K, where (a) denotes the single phase microemulsion region.

Addition of an electrolyte increases the system's affinity for hydrocarbon and decreases its affinity for water. Added electrolyte reduces the amount of alcohol required to solubilize hydrocarbon [17]. Miller et al [18] have studied the phase behaviour of ether sulphonates and have shown that increasing salinity or temperature causes phase separation. However, with a sufficiently long ethylene oxide chain the surfactant is soluble even at high salinity.

Qutubuddin et al [19] have reported the sensitivity of microemulsion phase behaviour to salinity and pH. Their results show that the effect of salinity on phase behaviour can be counter balanced by pH adjustment under appropriate conditions. Addition of electrolyte makes the surfactant system hydrophobic while an increase in pH can make it hydrophilic by ionizing more surfactant.

4.2 Model Surfactant System For Enhanced Oil Recovery (EOR)

The physicochemical aspects of the phase behaviour of microemulsion systems containing commercial petroleum sulphonates as surfactants have been well documented by Healy and Reed [14, 15] and Salter [8]. The commercial surfactants sometimes contained as much as 40% inactive ingredients [20].

Carboxymethylated ethoxylated surfactants were reported on by Olsen and Josephson [21] who showed that they have high tolerance to electrolytes and to temperature and are used in the laundry, cleaning and personal cosmetics industries. These surfactants were studied at high temperatures relevant to North Sea reservoirs and it was found that they required too much ethoxylate content to operate efficiently at the low salinity levels naturally present under North Sea conditions. Sulphated versions of all surfactants were also rejected due to their degradation at elevated temperature [22]. After considering the available literature at the time it appeared that the most suitable choice for a model surfactant would be a mixture of the nonionic and anionic surfactants (i.e. as a co-surfactant). Particularly, when it was considered that the benzene ring in TX-100 provided a chromophore to facilitate rapid UV analysis of surfactant in the microemulsion phases.

The phase behaviour can be influenced by many criteria but the nature of the crude oil is especially important. Crude oils are essentially highly compressed mixtures of aliphatic, aromatic, heteroaromatic, cyclic and heterocyclic hydrocarbons, some of which are gaseous or liquid and remainder solid when isolated under laboratory conditions. The multicomponent nature of crude oils and the varying proportions of these components in crude oils between reservoirs has meant that no complete characterisation of a crude oil has ever been achieved. The initial concept to use pure alkanes as replacements for crude oils was developed by Cayias et al [23, 24] who used binary mixtures of alkanes, alkylbenzene and alkyl cyclohexane.

In conclusion it was proposed that the model surfactant system that would be expected to meet the criteria for EOR and would comprise of decane/TX-100+SAS or SDS+pentan-1-ol/ water/sodium chloride. The microemulsion systems chosen for the characterisation

studies are presented in Table 3.6 in Chapter 3. Full compositional analysis for each phase was achieved by using a variety of analytical techniques. Some of these were developed specifically for use with the model system and were subsequently improved. These analytical techniques are all described in detail in Chapter 3.

4.2.1 Scanning of the Microemulsion Phases

(a) Salinity Scans

The volume percentage of the microemulsion phases and surfactant concentration in each microemulsion phase were determined as a function of salinity and temperature as described in section 3.2.4 of Chapter 3 using the modified apparatus (see Figure 3.5). A plot of absorbance versus distance for the microemulsiom system M2 (sample cell movement) can be seen in Figure 4.17(a). This plot shows a decrease in absorbance, as the sample was moved upward and a constant absorbance can be seen as the light was passed through the oil phase. A sharp increase in absorbance was observed at the o/m (oil/microemulsion) interface because the surfactant adsorbs preferentially at the interface; the absorbance becomes steady as the light was passed through the microemulsion phase. A large decrease in the absorbance was seen as the light passed through the microemulsion/water interface, which was followed by a constant absorbance through the water phase. Maximum absorbance was observed when the light passed through the microemulsion phase which indicated that most of the surfactant was in the microemulsion phase. The local maximum at the oil/microemulsion interface is due to the interface being curved near the quartz walls. One possibility could be that there is reflection of the beam due to this curvature.

Figure 4.17(a) shows that the microemulsion system M2 is composed of three phases: an upper oil phase, a middle microemulsion phase and a lower water phase. The system was scanned as a function of salinity. The volume percentage of these phases is presented in Table 4.1. The absorbance in each phase could also be determined. At this stage absorbance was not taken into account because this was not a true absorbance. The computer programme needed to be modified in order to introduce absorbance calibration versus height. The results could then be calculated as concentration versus height.

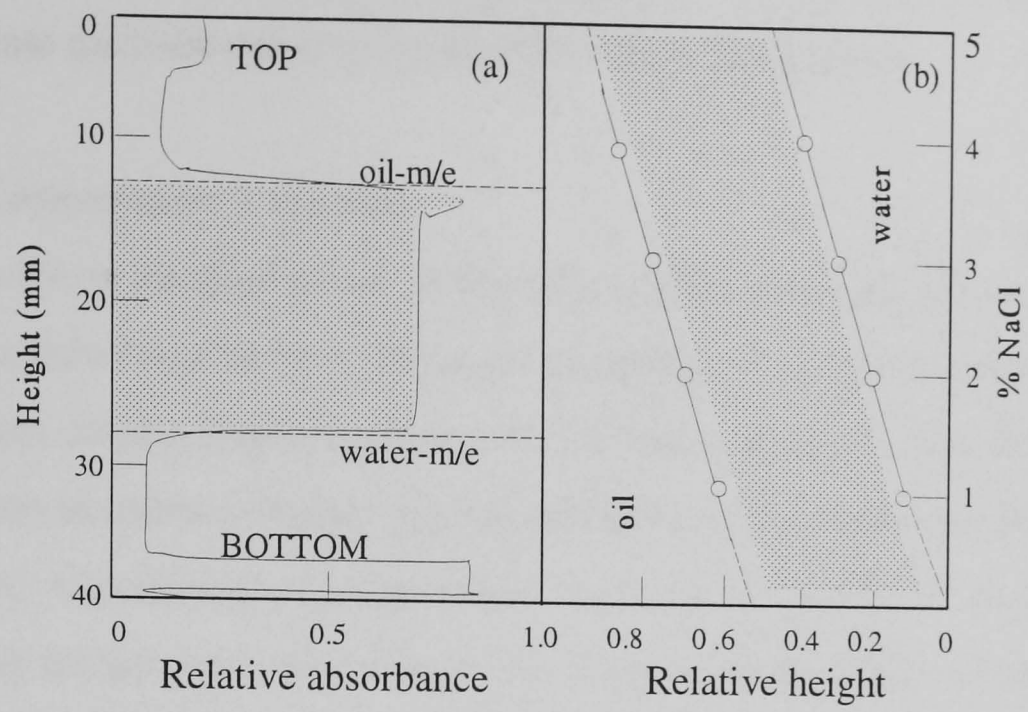

Figure 4.17 (a) Relative absorbance at 275nm versus height in the microemulsion system M2 at 298K where the shaded area is the middle phase microemulsion, with above it a predominantly oil phase and below it a predominantly aqueous phase.
(b) Extent of formation of middle phase at 298K as the salinity of the aqueous phase is increased.

Table 4.1 Phase equilibria data composition (% volume) of the microemulsion phases versus salinity in g NaCl/100cm^3 brine at 298K.

Brine concentration	% volume of microemulsion phases		
(g/100cm^3)	Upper phase	Middle phase	Lower phase
1	37.0	49.7	13.3
2	34.0	48.5	17.5
4	29.6	47.2	23.2
6	25.8	45.4	27.8

Increasing salinity causes the microemulsion phase to undergo transitions from lower to middle to upper. As the salinity increases, microemulsion-oil interfacial tension decreases and microemulsion-water interfacial tension increases. Addition of electrolyte increases the system's affinity for hydrocarbon and decreases its affinity for water. Added electrolyte reduces the amount of alcohol required to solubilize hydrocarbon. When salt is added to a lower-phase microemulsion in equilibrium with excess hydrocarbon, a brine-phase and

a middle phase microemulsion eventually appear. Continued addition of salt leads to an upper-phase microemulsion in equilibrium with a brine phase.

(b) Temperature Variation

The boundary of the three-phases of the microemulsion system M2 was determined over the temperature range 293 to 324K using the method described in section 3.2.4 of Chapter 3. The data composition expressed in % volume is summarised in Table 4.2. Increasing temperature increases a micellar system's affinity for hydrocarbon and decreases its affinity for water. Consequently, requirements for a water-insoluble alcohol increase with increasing temperature. Conversely, the required water-soluble alcohol concentration decreases with increasing temperature [17].

Table 4.2 Phase equilibria data composition (in %volume) of the microemulsion phases over the temperature range of 293 to 324K.

Temperature (K)	% volume of microemulsion phases		
	Hydrocarbon phase	Middle phase	Aqueous phase
293	27.3	44.4	28.2
303	23.0	32.2	44.8
315	20.3	28.2	51.5
324	19.8	26.0	54.2

Increasing temperature favours the migration of surfactant from lower to middle, and eventually from middle to upper phase. As temperature increases, the interfacial tension between microemulsion and oil ($\gamma_{m/o}$) decreases while interfacial tension between microemulsion and water increases [11]. Zhu et al [25] have reported the effects of temperature, water content, and salinity on the aggregation behaviour of Triton X-100 in cyclohexane. "Increasing temperature weakens molecular interactions which results in shifting the monomer-micellar equilibrium toward the monomer." The size of aggregates decreases with increasing temperature. It has also been reported [26] that the effect of increasing the alkane chain length is equivalent to increasing the temperature in

water/AOT/ alkane microemulsions which reflects the reduced solubility of the AOT in increasingly hydrophobic alkane solvents.

4.2.2 Spectrophotometric Results

A Spectrophotometer (Lambda 9) was used to measure the absorbance (as described in section 3.2.3 of Chapter 3) of the surfactant in microemulsion phases and hence, the concentration of surfactant in each phase. Figure 4.18 shows the absorbance spectrum (maximum absorbance at 275nm) and calibration plot (absorbance versus known concentrations) of TX-100 giving a correlation coefficient 0.9996. The microemulsions were diluted with methanol before their absorbance was measured and used to determine the surfactant concentration from the calibration obtained. The microemulsion systems M1 and M5 were chosen for this study. The results are presented in Tables 4.3 and 4.4 which show that most of the surfactant (75%) is in the middle phase. It is also observed that the surfactant concentration is independent of the salinity. However, some monomers are also present in the aqueous and organic phases.

Table 4.3 Spectrophotometric concentration data of three-phases in the microemulsion system M1 in the salinity range of 1-4 g NaCl/100cm^3 at 298K.

Brine concentration (g/100cm^3)	% concentration of TX-100		
	Upper phase	Middle phase	Lower phase
1	13.9	74.5	11.6
2	14.4	72.8	12.8
3	13.9	75.5	10.6
4	15.2	72.1	12.7

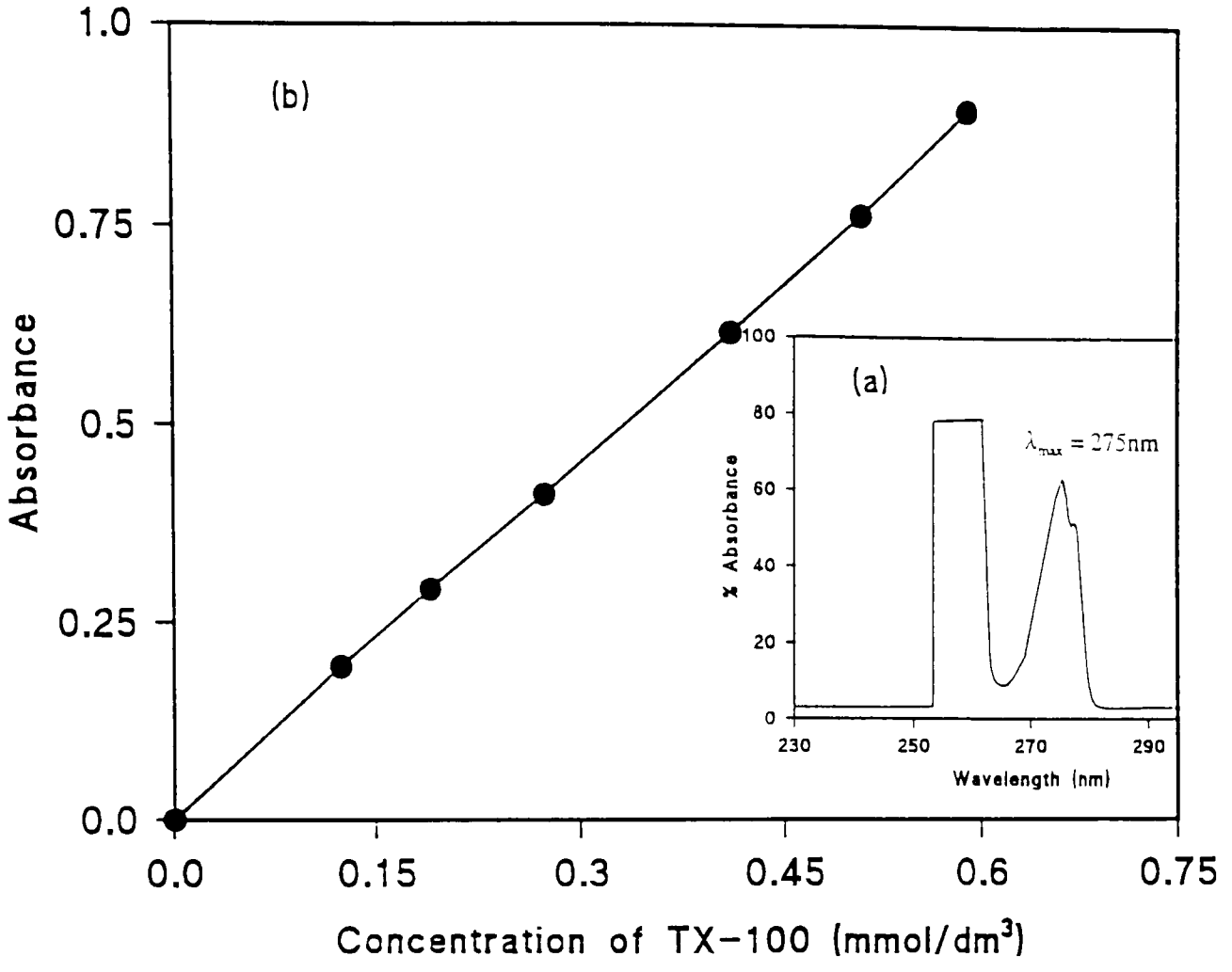

Figure 4.18 Showing; (a) absorbance spectrum (b) calibration curve for TX−100 at 298K giving a correlation coefficient 0.998.

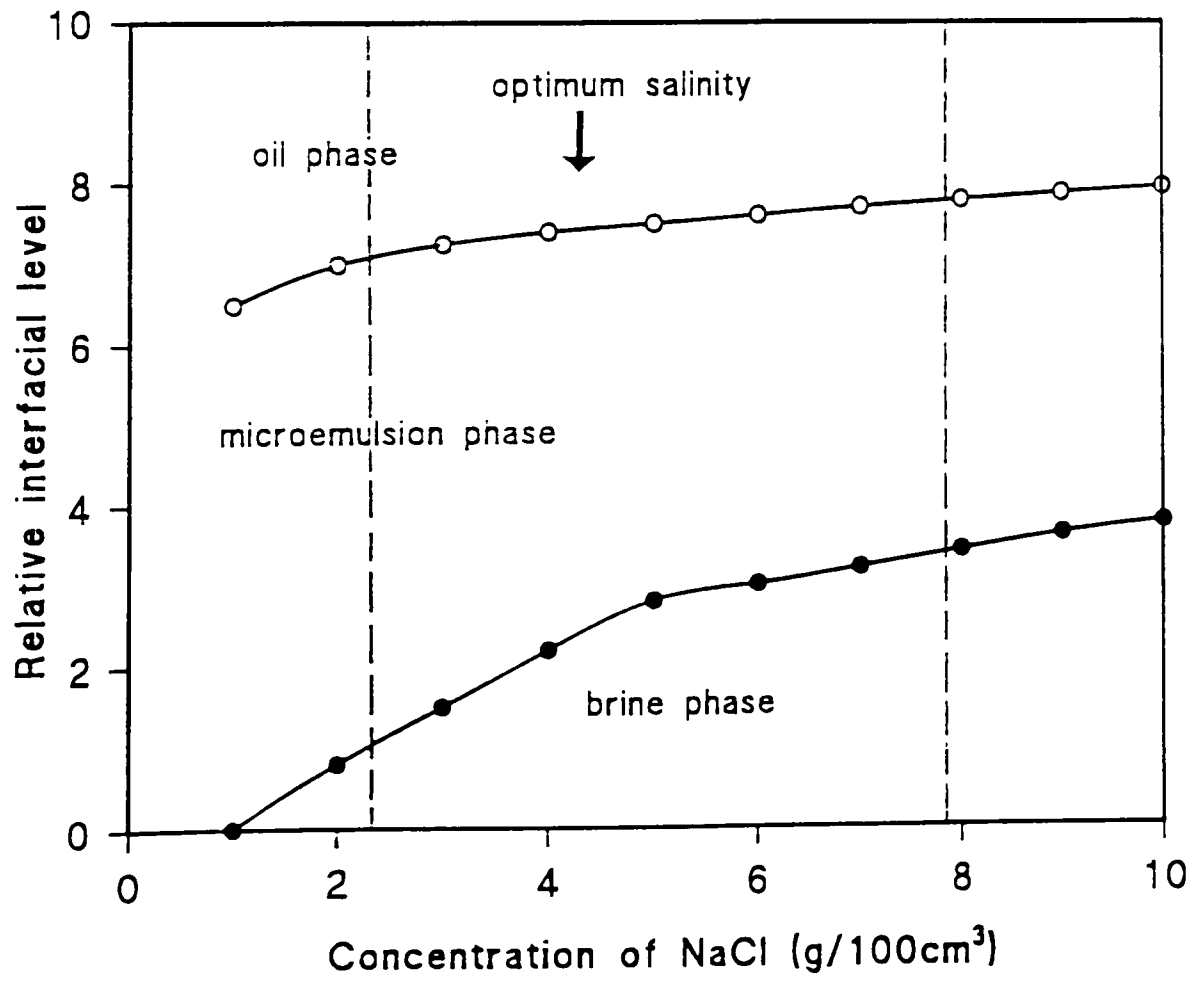

Figure 4.19 Optimum salinity scan for microemulsion system M2 at 298K.

Table 4.4 Spectrophotometric concentration data of three-phases in the microemulsion system M5 in the salinity range of 1-4 g NaCl/100cm^3 at 298K.

Brine concentration (g/100cm^3)	% concentration of TX-114		
	Upper phase	Middle phase	Lower phase
1	12.8	75.3	11.9
2	13.5	76.4	10.1
3	11.7	77.5	9.8
4	12.0	76.6	10.4

4.2.3 Optimum Salinity Scans

The salinity at which the middle phase microemulsion contains an equal volume of oil and brine is defined as the optimum salinity [27]. At the optimum salinity, the interfacial tension is in the μN/m range at both oil-microemulsion and microemulsion-brine interface, and the oil recovery is maximum. The optimum salinity depends on the hydrophilicity of the surfactant.

Healy et al [14] have also reported that optimum salinity with the amounts of oil and water contained in a microemulsion have been shown to play important roles in obtaining low interfacial tensions and high oil recoveries. Nelson [28] called the salinity at which the middle phase microemulsion contains equal amounts of oil and brine as "midpoint salinity". Similarly, Healy and Reed [4] defined the optimum salinity as the intersection point of the interfacial tension curves measured between microemulsion/lower phases and upper/microemulsion phases. Healy et al [15] showed that increasing the salinity in a brine/ surfactant/oil system favours the solubilisation of the surfactant into the oil relative to the brine causing the phase-environment type to shift in the I to III to II direction.

The optimum salinity scan has been performed for brine/[TX-100+SAS(4:1)]+[pentanol] (1:1)/decane system at 298K as described in section 3.2.5 of Chapter 3. The samples were prepared from equal volumes of oil and brine with different brine % concentrations at

constant surfactant concentration. A plot of relative interfacial level as a function of brine concentration is presented in Figure 4.19. The optimum salinity for this system is shown at 4.3 g NaCl/100cm^3 concentration at 298K.

4.2.4 Surface and Interfacial Tension Results

After water flooding, the previously continuous medium of oil in porous rock is replaced by water, while the same oil, referred to as residue oil, becomes trapped as isolated ganglia [15]. To mobilise a ganglion the capillary forces retaining it inside the pore must be reduced. This can be achieved by lowering the oil-water interfacial tension by injecting surfactant into the reservoir [29] and is caused by the surfactant molecules adsorbing at the oil-water interface, producing phase changes, generally accompanied by the formation of a microemulsion [13]. It is these concomitant changes in phase behaviour that are instrumental in producing the required reduction in interfacial tension [14, 15].

Figure 4.20 shows the surface tension curves obtained for TX-100 solutions with varying concentration of NaCl at 298K. The surface tension decreased with increasing the surfactant concentration until a final and constant value was reached. When surfactant is added to an aqueous solution, surfactant monomers adsorb at the air/water interface, thus causing a reduction in surface tension of the water. At very low concentration, the surfactant molecules are lying flat along the surface; as the concentration of surfactant added to the solution increases, the number of monomer molecules adsorbing onto the interface increases too, thereby causing the gradual lowering of the surface tension; the tails of the molecules become entangled with each other but the mutual repulsion of the head-groups prevents a dense surface population being formed. At the CMC, the air/water interface will hold the maximum number of surfactant monomers allowable by the afore-mentioned forces and so the majority of monomer molecules added to the solution will be incorporated into micelles and therefore the suface tension at this point remains constant. The adsorption of surfactant molecules at the interface is a dynamic process. It reaches equilibrium when the numbers of molecules entering and leaving the interface are equal. The CMC decreases with increasing the concentration of NaCl in the aqueous solutions (see Figure 4.20).

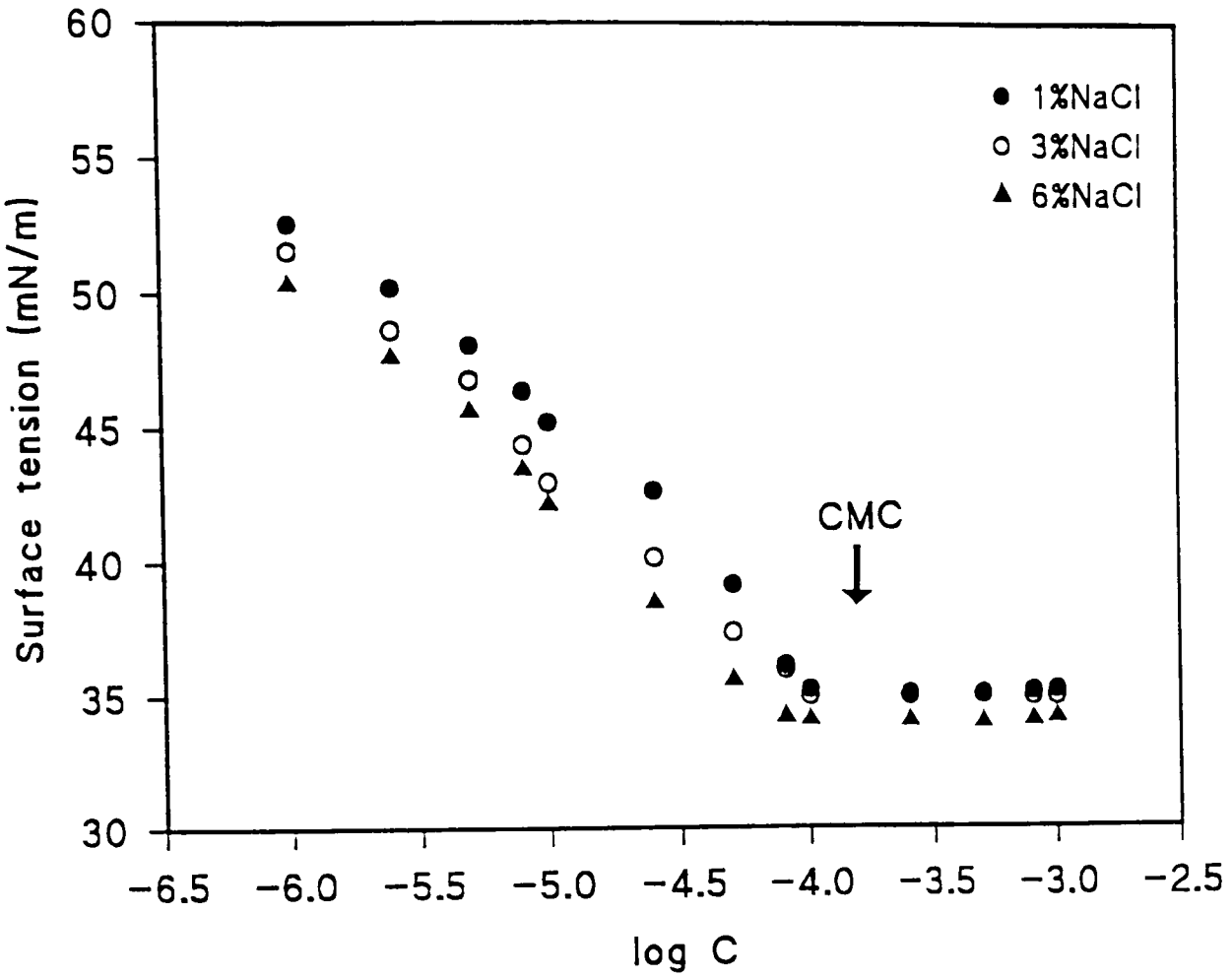

Figure 4.20 Effect of NaCl concentration on the surface tension of TX-100 solution at 298K.

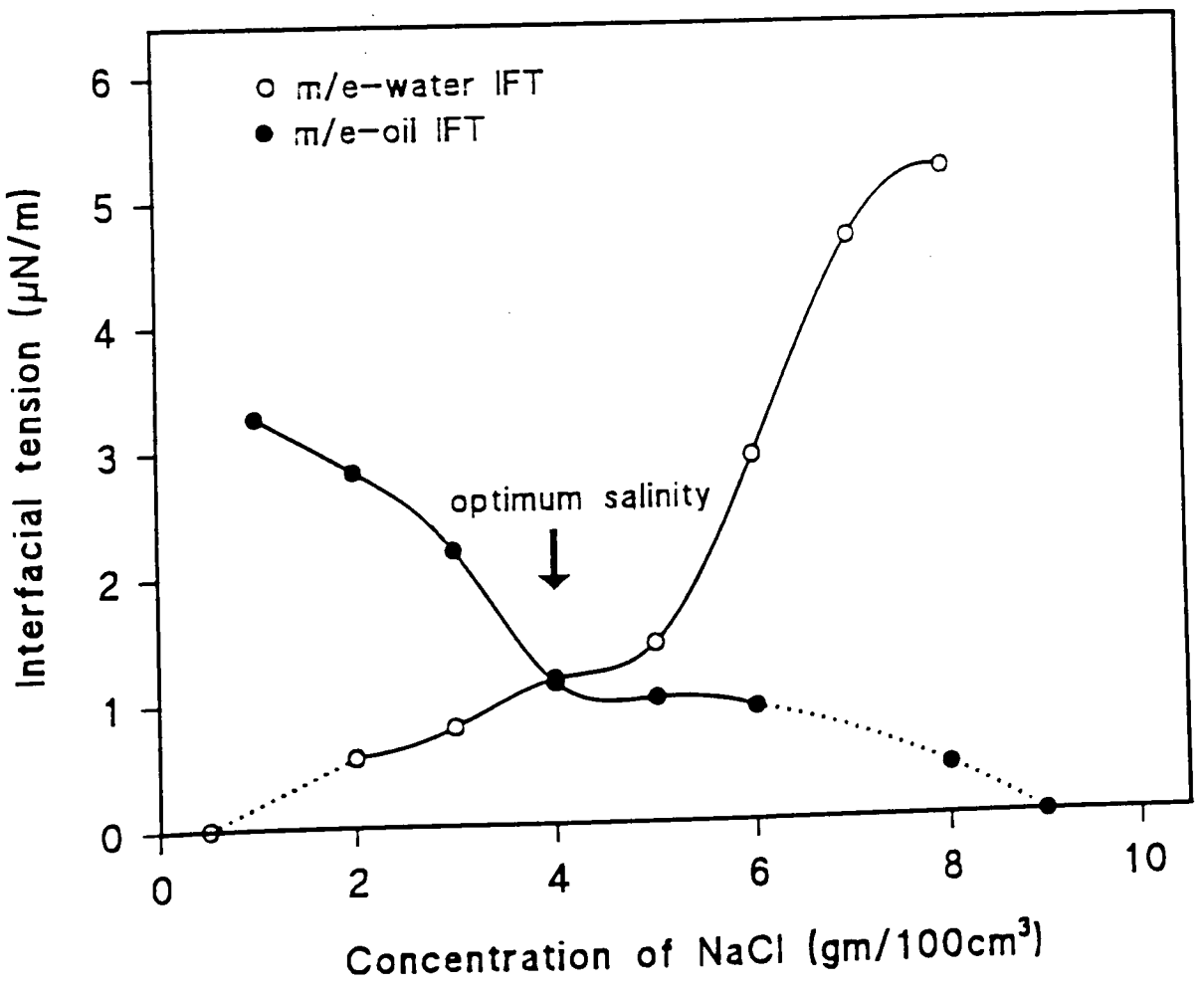

Figure 4.21 Interfacial tension of microemulsion phases (system M3) measured as a function of salinity at 298K.

The interfacial tensions of the microemulsion phases of the system M3 have been measured as a function of salinity (1-10 gNaCl/100cm^3) in both two and three-phase regimes at 298K. The results are shown in the Figure 4.21 which gives the optimum salinity at 4.0g NaCl/100cm^3. The interfacial tension for the system was found to be ultra low (0.5μN/m) at 4.0g NaCl/100cm^3. A reduction in the interfacial tension by three to four orders of magnitude causes significant mobilisation of trapped oil ganglia [30] as the available pressure gradient becomes effective. For good performance it is necessary to achieve optimum phase behaviour between reservoir and injected fluids in which three phases are produced [18, 29]. Interfacial tensions of the systems are found to correlate with the solubilisation parameters for the various multiphase components [31, 32]. As part of this objective a representative model surfactant system containing brine/TX-100+SDS+ pentan-1-ol/decane has been studied.

Phase equilibria and interfacial structures have been inter-related [33], while radio tracer and surface tension measurements have been used [34] to discern surfactants at air/solution interfaces. Similarly, the distributions of oxyethene non-ionic surfactants at cyclohexane/ water interfaces have been probed [35]. Ostwald discussed phase boundaries [36], and as Bronsted reminded 'the boundary between two phases.....is not a sharp one....in the boundary phase between two incompletely miscible liquids the continuous concentration change is due to the unsymmetrical environment of the molecules in the layer' [37]. The quantitative approach to phase equilibria looks rather promising and the method may also allow boundary layers to be investigated.

The monomers of surfactant adsorb at the macroscopic oil-water interface and the micelles or microemulsion droplets in equilibrium with this monolayer are surface inactive. This proposition is given weight by recalling that oil-water interfacial tensions above the CMC are independent of surfactant concentration, even though the concentration of the aggregates is changing.

4.2.5 High Performance Liquid Chromatography (HPLC)

High Performance Liquid Chromatography (HPLC) has been used recently for characterising and quantifying surfactants [38-40], and, for example, is the most suitable analytical procedure for alkyl phenol ethoxylate analysis. However, the sensitivity of the procedure is dependent on the detection method; HPLC of alkyl phenol ethoxylates has usually been coupled to Ultra-Violet (UV) detection [41, 42], and Ahel and Giger [43] have described its application to environmental samples. Kudoh et al [44] have determined trace amounts of alcohol and alkylphenol ethoxylate by reversed-phase HPLC. The ethylene oxide distribution of the determined alcohol and alkylphenol ethoxylate were also obtained by this method.

TX-100 is a p-octyl phenol ethoxylate (see structure in Chapter 3) where n is the number of ethylene oxide units attached to the alkylphenol. The oligomers show a Poisson distribution [45], with $\bar{n}$ an average of about 9.5. By use of HPLC on silica acid adsorbent it has been possible to isolate individual oligomers of Triton X-100 with ($\bar{n}$) up to sixteen or more without the use of large columns and more conveniently than by chromatographic reported methods [53, 54].

Results and Discussion

HPLC analysis of the nonionic surfactant and microemulsion phases has been carried out at 298K using the Varian Star system as described in section 3.2.11 of Chapter 3. Figures 4.22-4.23 show the chromatograms obtained for samples of the Triton family of nonionic surfactants. As can be seen, a narrow distribution is obtained which reflects the distribution of oligomers within the surfactants. The least polar oligomers are eluted first since they have less affinity for the polar column and therefore a lower extent of retention. The larger oligomers are adsorbed onto the column via a series of electrostatic interactions between the column and the ethoxylate chain. As the gradient continues, the polarity of the flushing solvent increases and so the more polar oligomers (i.e. those with a larger number of ethoxylate units present) are eluted until eventually all of the surfactant is driven off the column. Smaller amounts of surfactant were needed for good oligomeric separation, making the gradient favourable for analysis of environmental samples. This gradient works

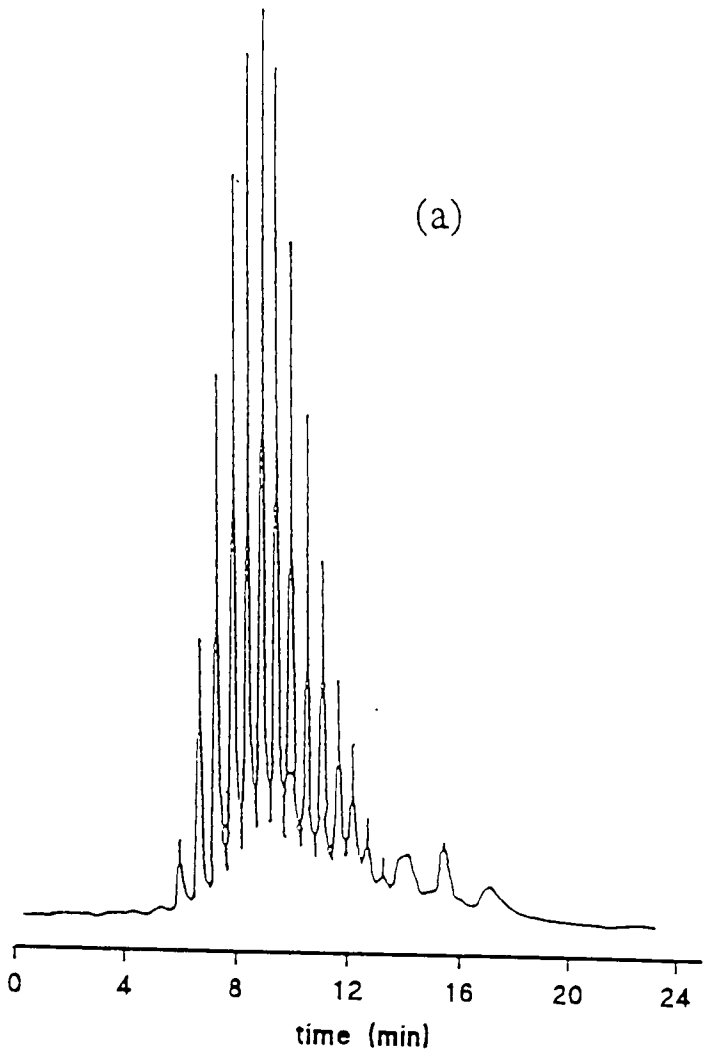

Figure 4.22 HPLC chromatograms showing the distribution of oilgomers: (a) TX-114 and (b) TX-100 at an aqueous concentration 0.022%.

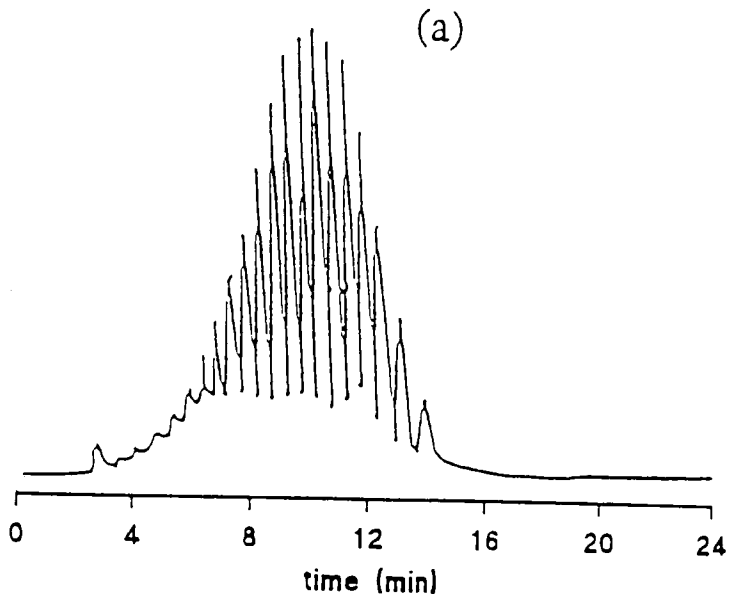

Figure 4.23 HPLC chromatograms showing the distribution of oilgomers: (a) TX-165 (0.028%) and (b) TX-100 (i.e. 0.02%TX-100 + 0.1% n=9 ethoxylate units)

because of the low pH of the buffer which keeps the silanol groups of the silica packing protonated. As the concentration of acetonitrile increases, the silica surface is subtly altered together with the binding force between the surface and the surfactant molecules; the competition between the solvent molecules and the surfactant molecules for the protonated silanol groups of the stationary phase increases. As the pH increases with the gradient, so the larger surfactant oligomers are eluted. It must also be mentioned that good separation of the surfactants was specific to Spherisorb silica only; other silicas with comparable surface areas and pore diameters are apparently not capable of separating the oligomers of alkylphenol polyethoxylate [46].

However, it cannot be assumed that the largest peak on the chromatogram corresponds to the oligomer having, for instance TX-100, ten ethene units since the possibility of drift cannot be ruled out. In order to label the peaks, a sample of polydisperse TX-100 was spiked with a monodisperse sample of known ethoxylate chain length and HPLC was carried out. The chromatogram is shown in Figure 4.23(b). As one can see the n=9 oligomer is clearly visible. The monodisperse oligomer was synthesized via a three stage reaction sequence using chloroethoxy ethane and hexaethylene glycol [46].

HPLC has also been used to analyse the surfactant in the microemulsion phases in the system M1 with varying concentration of NaCl. Since each oligomer is visible on the HPLC trace it is possible to observe distribution of the oligomers in the different microemulsion phases. Apart from dilution, the injected samples required no pre-treatment before injection thus simplifying the analysis. The distribution of TX-100 oligomers observed for the upper-phase, middle-phase and lower-phase in the microemulsion system M1 can be seen in Figure 4.24. Figures 4.25-4.26 show the relative concentration of TX-100 oligomers present in the microemulsion phases present in the system M1 when equilibrated at 298K. Each microemulsion phase shows a Poisson distribution of oligomers. If one superimposes these distributions (see Figure 4.27) we can see a gradual shift in distribution of oligomers; the shorter ethylene oxide chain lengths being present in the organic phase and the longest ethylene oxide chain lengths being present in the aqueous phase as one would expect. Figure 4.28 shows the distribution of TX-100 oligomers

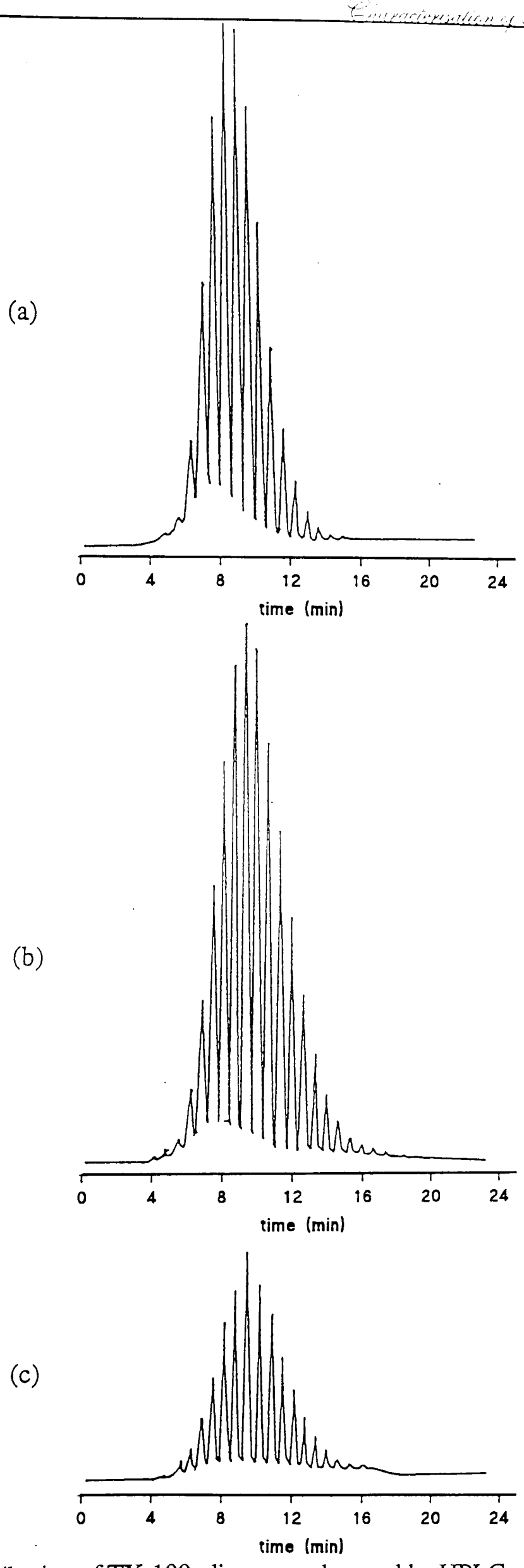

Figure 4.24 Distribution of TX-100 oligomers observed by HPLC analysis of (a) upper-phase (b) middle-phase (c) lower-phase present in the microemulsion system M1 at 298K.

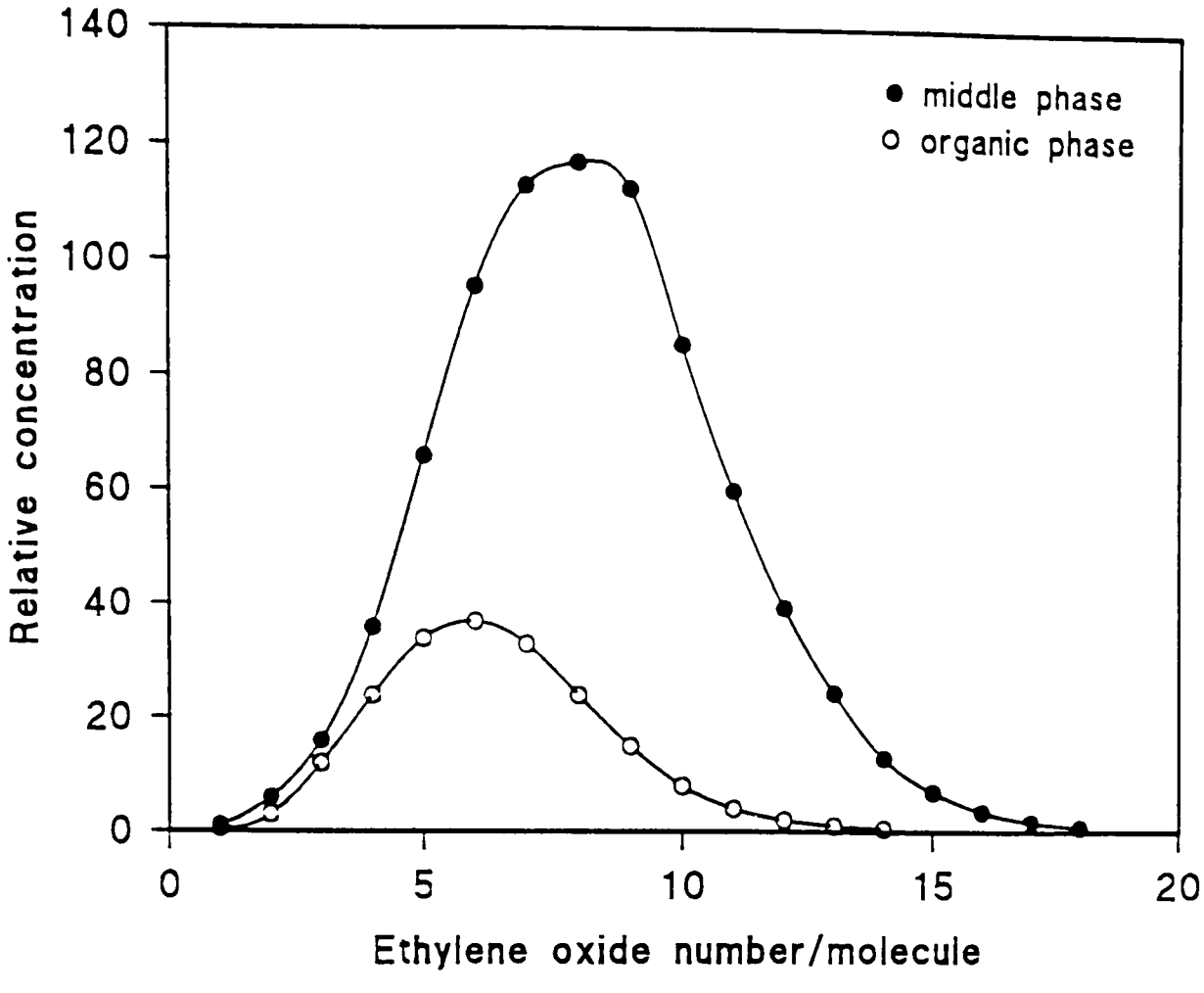

Figure 4.25 Distribution of TX−100 oligomers deduced by HPLC analysis of the middle phase relative to the standard solution of 5μg/dm^3 at 298K.

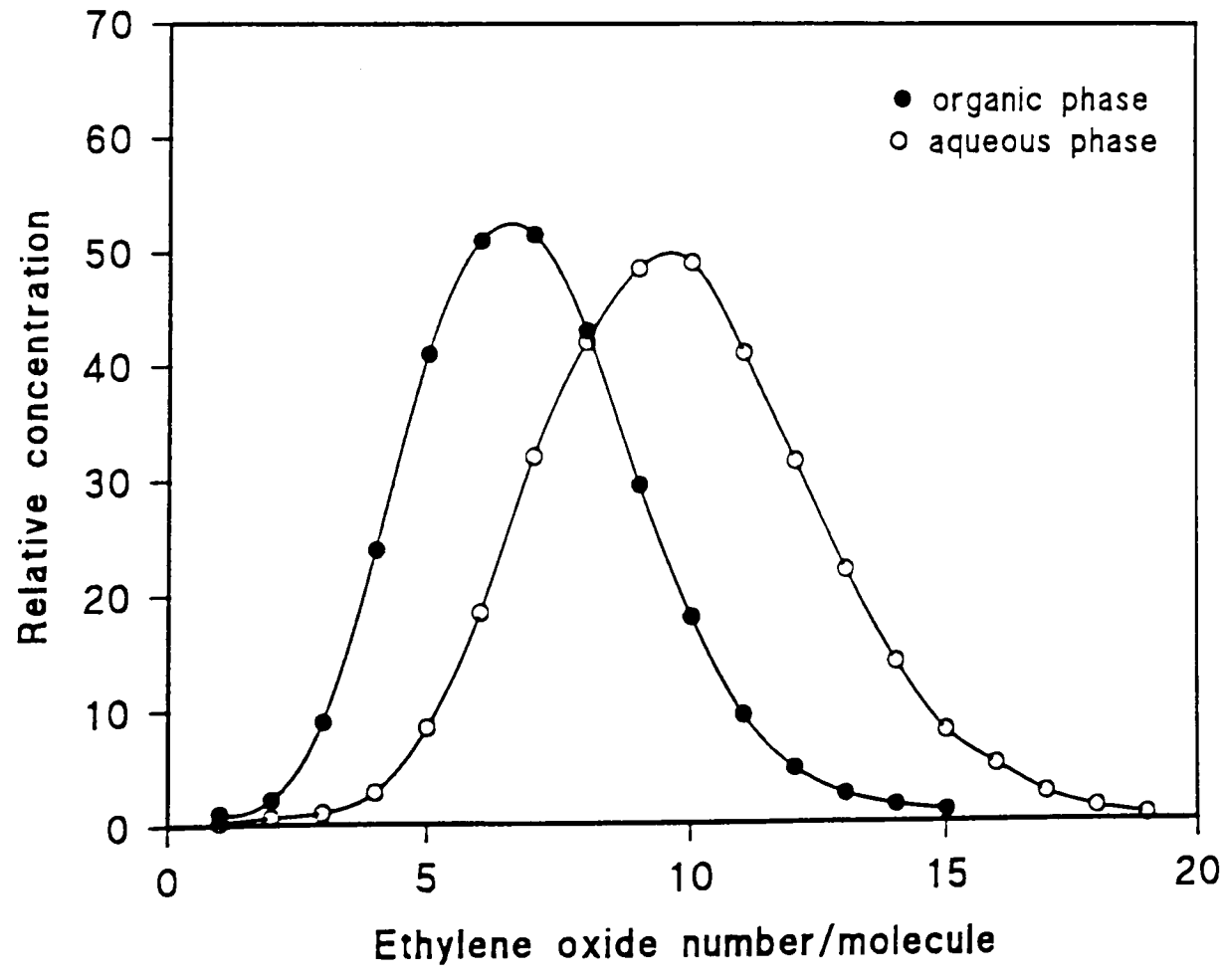

Figure 4.26 Distribution of TX−100 oligomers observed by HPLC analysis of organic and aqueous phases present in the system M1 when equilibrated at 298K.

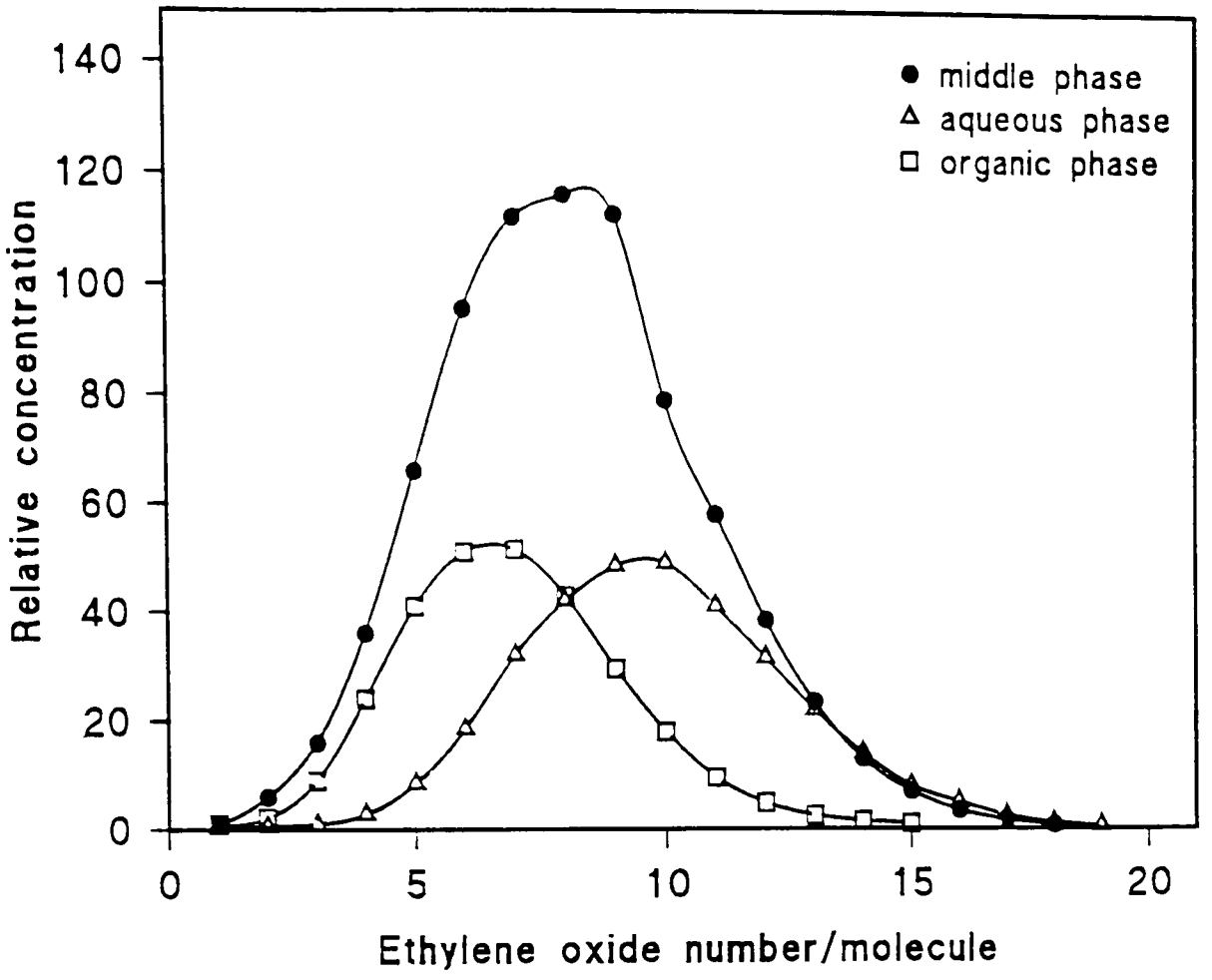

Figure 4.27 Distribution of TX-100 oligomers observed by HPLC for the three microemulsion phases present in the system M1 when equilibrated at 298K.

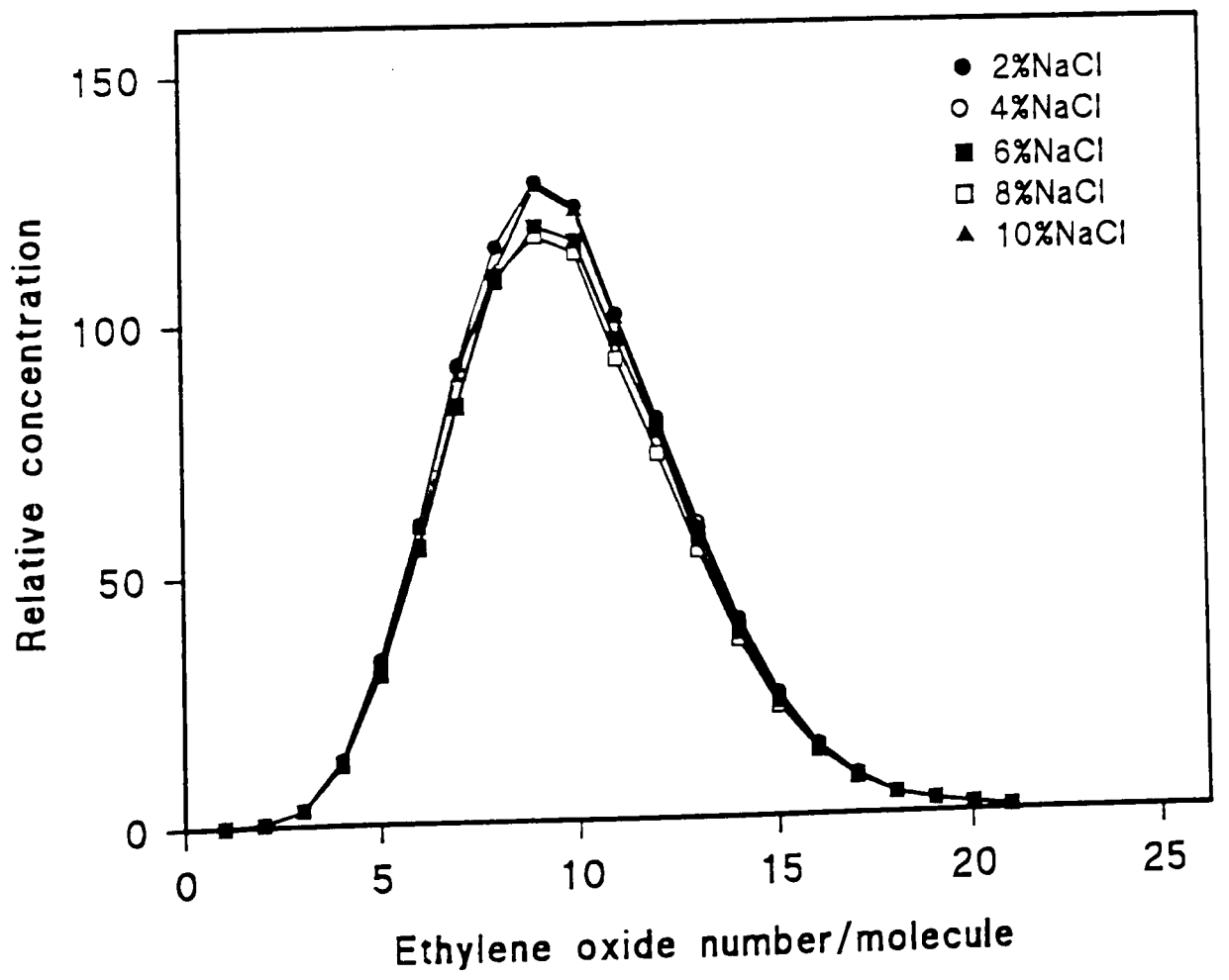

Figure 4.28 Effect of NaCl concentration on the distribution of oligomers in the middle phase microemulsions at 298K.

present in the middle phase at a range of salinity (1-10g NaCl/100cm^3). It is clear that the salinity does not have any effect on shifting the oligomeric distribution of the middle phase at the same experimental conditions.

4.2.6 Gas Chromatography

Gas chromatography has been used to determine the components of the microemulsion phases in the systems M1 and M4 (as described in section 3.2.12 of Chapter 3). In the systems, three-phases were produced at equilibrium and these included a large middle phase. The sample of each phase was analysed by GC separately. Figures 4.29(a), (b) and (c) show the chromatographic profiles for the upper, middle and lower (aqueous) phases of the system M4. Only three peaks (pentan-1-ol, decane and butylbenzene) with retention times of pentan-1-ol 1.7min, decane 5.0min and butylbenzene 6.35min with relative % concentrations of 18%, 66% and 14% were observed. No water peak has been identified in the upper-phase.

The chromatographic profiles for the middle-phase are shown in Figure 4.29(b) in which four peaks can be seen (i.e. water, pentan-1-ol, decane and butylbenzene) with relative concentrations of 57.3% water, 18% pentan-1-ol, 19.9% decane and 4.67% butylbenzene. Similarly, the chromatograms of the lower-phase are traced in Figure 4.29(c). Only two peaks (for water and pentan-1-ol) can be seen on the chromatogram with relative concentrations of 99.5% and 0.5%. The above three-phase analysis shows that the alcohol partitions into both brine and oil but more strongly into the hydrocarbon phase. In the middle phase, a strong association of the alcohol with the surfactant is also clear.

Analyses of the middle-phase microemulsion (i.e. system M1) has been carried out as a function of salinity (1-10g NaCl/100cm^3) under the same experimental conditions. The chromatographic profiles for the components of the middle phase are presented in Figure 4.30 (a) - (f). A decrease in the water peak and increase in the hydrocarbon peak can be observed with increasing salinity. The results of the systems M4 and M5 are summarised in Tables 4.5 and 4.6. It is clear from the data that increasing the NaCl concentration, causes reduction of the water content in the middle phase microemulsion (from 75% to

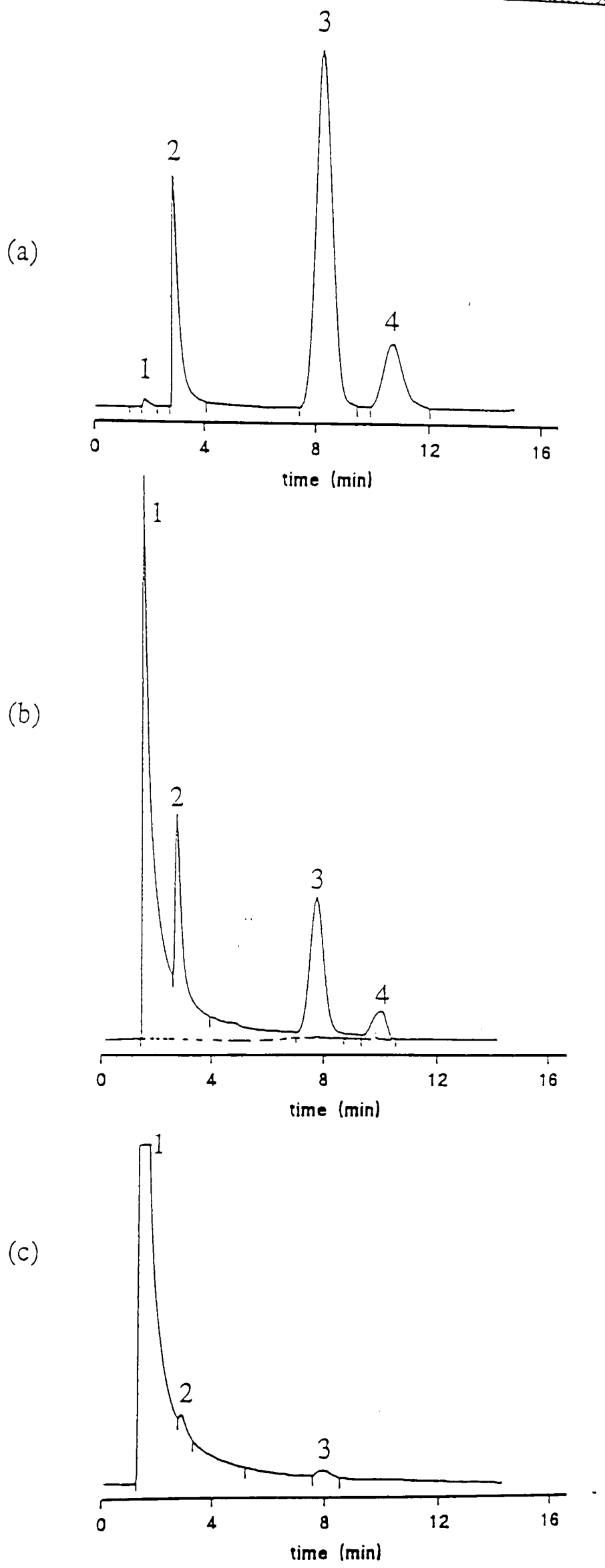

Figure 4.29 GC profiles for (a) upper-phase, (b) middle-phase and (c) lower-phase analysis where peaks 1, 2, 3 and 4 represent water, pentan-1-ol, decane and butylbenzene respectively. 110

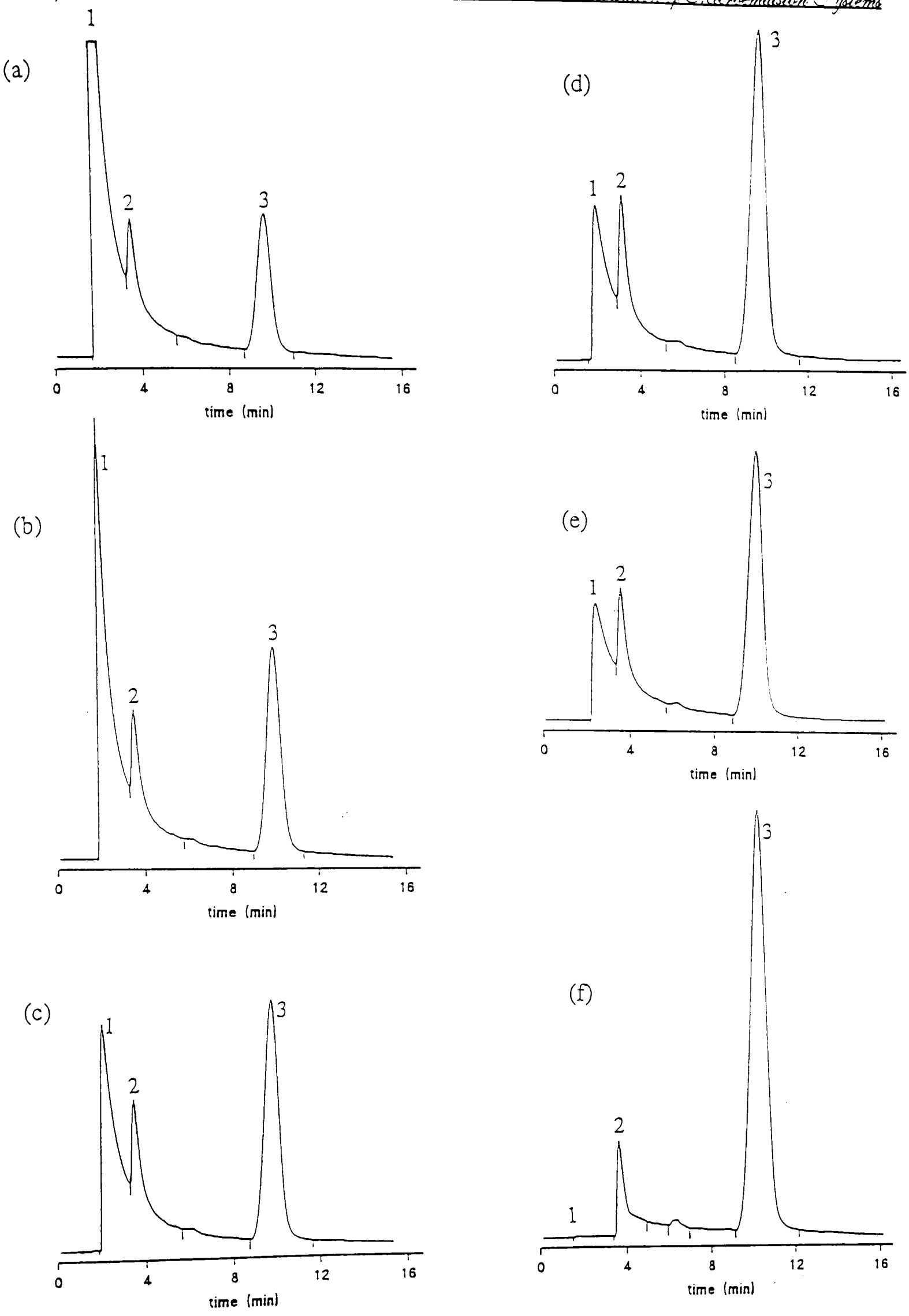

Figure 4.30 GC profiles for the middle-phase microemulsion showing the effect of salinity; (a) 1% NaCl, (b) 2% NaCl, (c) 3% NaCl, (d) 4% NaCl, (e) 6% NaCl and (f) 10% NaCl where peaks 1, 2 and 3 represent water, pentan-1-ol and decane respectively.

52%) and hence increases the hydrocarbon content in the middle-phase microemulsion (from 16% to 34%). These results suggest that at low salt concentration o/w microemulsion are formed, but as the salinity is increased, the o/w microemulsion changes into w/o microemulsion and at the optimum salinity bicontinuous microemulsion is expected. Consequently, at high salinity w/o microemulsions are produced. Addition of electrolyte increases the system's affinity for hydrocarbon and decreases its affinity for water.

Table 4.5 Gas chromatographic data showing the components of the middle-phase in the microemulsion system M4 versus salinity in g NaCl/100cm^3 brine at 298K.

Brine concentration (gNaCl/100cm^3)	% Concentration in the middle phase			
	Water	Pentan-1-ol	Decane	Butylbenzene
1	75.25	8.88	12.55	3.32
2	61.71	12.71	20.26	5.31
3	55.26	13.25	24.87	6.64
4	51.59	14.54	26.72	7.13

Table 4.6 Gas chromatographic data showing the components of the middle-phase in the microemulsion system M5 versus salinity in g NaCl/100cm^3 brine at 298K.

Brine concentration (gNaCl/100cm^3)	% Concentration in the middle phase			
	Water		Pentan-1-ol	Decane
1	82.20	------	5.2	12.57
2	69.86	★70.65	7.4	22.76
4	52.67	★52.10	10.59	36.73
6	40.00	★41.30	12.50	47.50
8	32.83	★34.02	11.94	55.23

where ★ represents the water content in the middle-phase determined by the Karl Fischer titration method.

According to Hwan et al [47] the changes in microstructure can be explained as follows. At low salinity the surfactant forms charged micelles with some solubilized oil in the brine phase. The greater extension of the electrical double layer at low ionic strength prevents these swollen micelles from approaching each other closely. As the salinity is increased, however, the London-van der Waals attractive force becomes more dominant, and at the same time the micelles reduce the free energy of their cores by taking up more hydrocarbon from the excess oil phase. This process continues until, at a sufficiently high salinity, the attractive forces exceed the entropic forces which act to stabilize the lower emulsion phase.

If the volume of solubilized oil in the middle phase is V_o , and the volumes of solubilized water and surfactant are V_w and V_s , the solubilization parameter V_o/V_s or V_w/V_s quantifies the solubilized volume of either oil or water per unit volume of surfactant in the middle phase. When plotted as a function of salt concentration, the two parameters intersect at the optimum salinity.

The volume fraction of oil or brine in the microemulsion phase may be estimated from the observed equilibrium phase volumes and the overall composition, on the assumptions that all the alcohol was in the same phase as the surfactant and that negligible amounts of brine and oil were solubilized by the excess oil and brine phases, respectively. Thus, plots of the volume fraction of brine or oil solubilized in the microemulsion (Figure 4.31) indicate that optimum salinity, as measured by equal volume uptake of oil and brine into the microemulsion, is 4.2g NaCl/100cm^3. Higher salinities will extract more water from the middle phase (salting out), favouring solubilisation of more oil from the upper phase; at the same time, the amount of brine solubilized is decreased

4.2.7 Photon Correlation Spectroscopy (PCS)

Several different techniques have been used to investigate the structural properties of w/o microemulsions including light scattering (static and dynamic) [48-50], small angle neutron and X-ray scattering [51, 52], conductivity [53], and viscometry [54, 55]. The results obtained from these experiments have provided strong evidence in favour of the dispersed

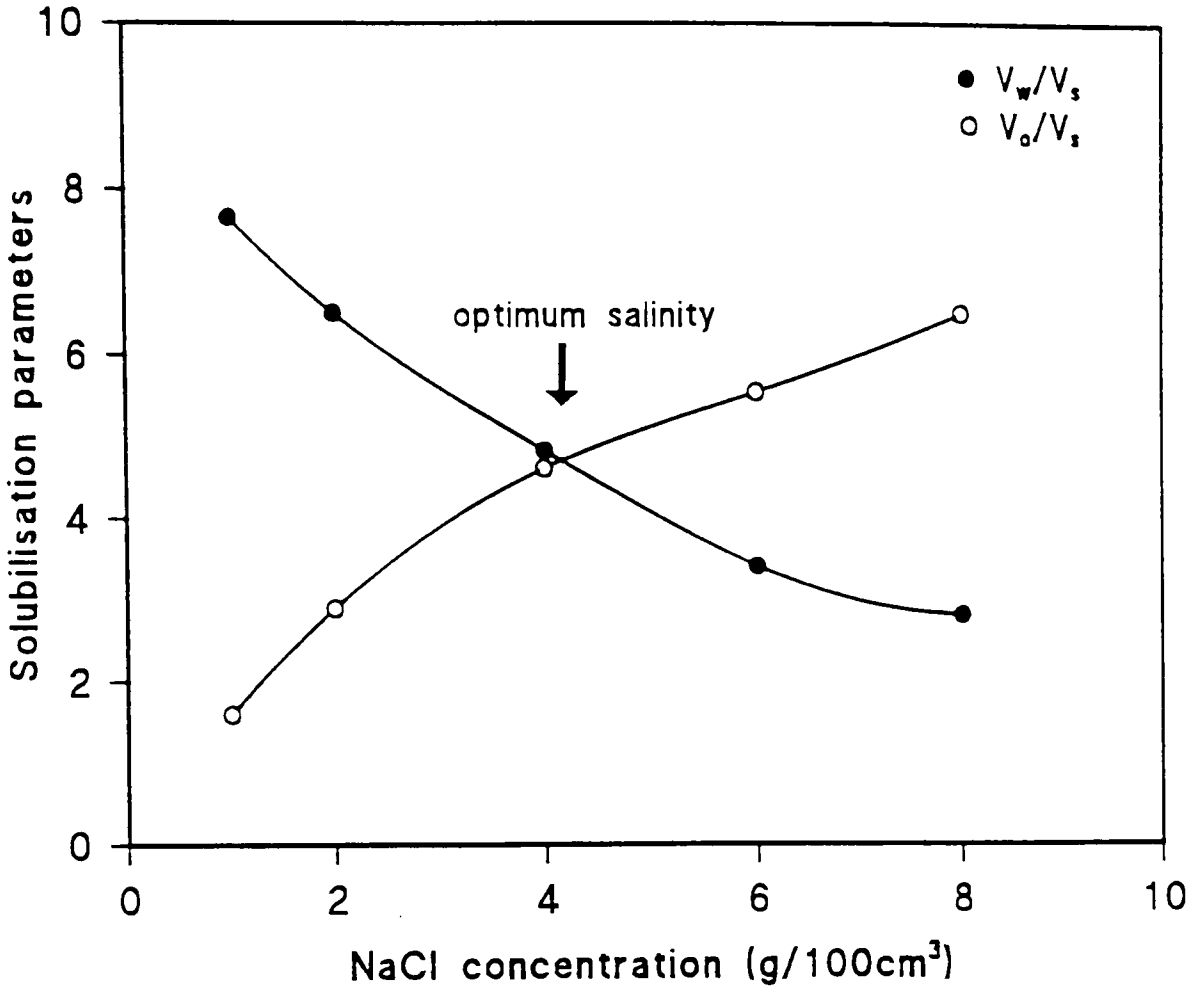

Figure 4.31 Solubilisation parameters derived from the data of Table 4.6.

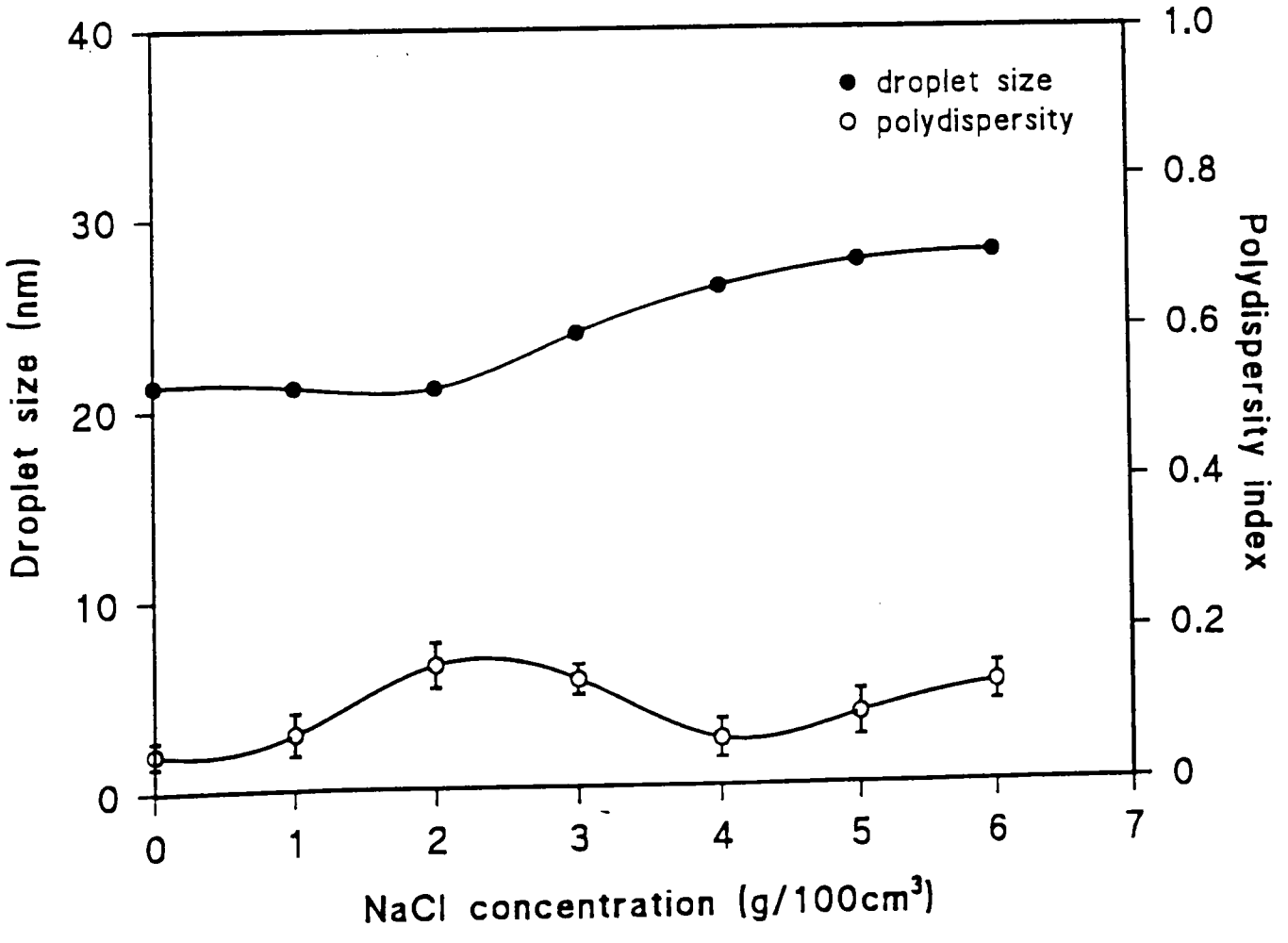

Figure 4.32 Droplet size and polydispersity of the microemulsion phase for system M1 at 298K.

droplet structure proposed for microemulsion systems.

Results and Discussion

The apparent droplet size distribution and the polydispersity index of the resulting single phase microemulsions (of which the composition is given in Table 3.7 in Chapter 3) were determined by PCS as a function of the water content (disperse phase) at 298K. (see Section 3.2.14 in Chapter 3). The droplet diameter, diffusion coefficient and the polydispersity index as a function of the water content for w/o microemulsions are presented in Table 4.7.

Table 4.7 Light scattering evidence of droplet size and polydispersity for the single phase microemulsions at 298K.

% disperse phase (water content)	Droplet size (±0.5nm)	Diffusion coefficient ($x10^{-6}$)	Polydispersity index
1	21.0	0.242	0.120
2	22.2	0.212	0.200
3	23.7	0.197	0.202
4	24.6	-----	0.310

The data clearly show that the samples were well within the microemulsion droplet size range. The diameter of the droplets increased with increase in the water content. This increase was slow and regular. The polydispersity index also increased regularly as the water content was increased. At a low water content, the system is in the stable area of the microemulsion domain. But when the water content is increased to larger values (>15wt%), the system approaches the border of the microemulsion domain and interactions between the droplets increase. If the water content is further increased, the system crosses the border of the microemulsion domain and is no longer a microemulsion.

The size of the droplets dispersed in a w/o microemulsion is found to be a function of the water-to-surfactant mole ratio or R value (where R = [water]/[surfactant]) and is given in

the following equation which is based on the geometry of the systems taking into account that the droplets are spherical.

$$r = \frac{3RV_w}{A_{surf}} + t \qquad (4.1)$$

where r is the mean radius of the droplet water core, V_w is the volume occupied by a water molecule in liquid water ($0.03nm^3$), $A_{surf.}$ is the surfactant head-group area at the droplet interface and t is the length of the surfactant chains. It is assumed that all the surfactant is interfacially bound to the droplets. The phase stability of w/o microemulsion is found to be strongly dependent on the nature of the surfactant stabilizer. In many systems the chain length of the surfactant tail-group is a major factor in determining the stability range of single phase microemulsions as a function of R and temperature.

In order to observe the effect of salt on the droplet size, the microemulsions (system M1) were prepared (as described in Chapter 3) for sizing assays with different percentage of salinity. The resulting middle phase microemulsions were filtered through a 0.2μm Micropore filter and left for 0.5h to equilibrate. Figure 4.32 shows a plot of droplet size and polydispersity as a function of the NaCl concentration at 298K. At low salinity the droplet size decreases and the polydispersity increases. As the salinity increases, the droplet size and polydispersity also increases. At low salinity, the electrolyte dehydrates the hydrophilic head groups and a small decrease in the apparent droplet size is observed. As the data indicate, the effect of an electrolyte at high concentration in the polar core of the reverse micelles is quite complex and not clear at present.

Figure 4.33 shows the droplet size and polydispersity of the system M2 at 298K. Initially, the droplet size decreases and then increases gradually with increase in the electrolyte concentrations. The polydispersity shows a similar trend. The overall apparent droplet size decreases with the addition of SAS in TX-100+pentan-1-ol system. Probably, addition of SAS decreases the CMC of TX-100 and therefore the droplet size is small.

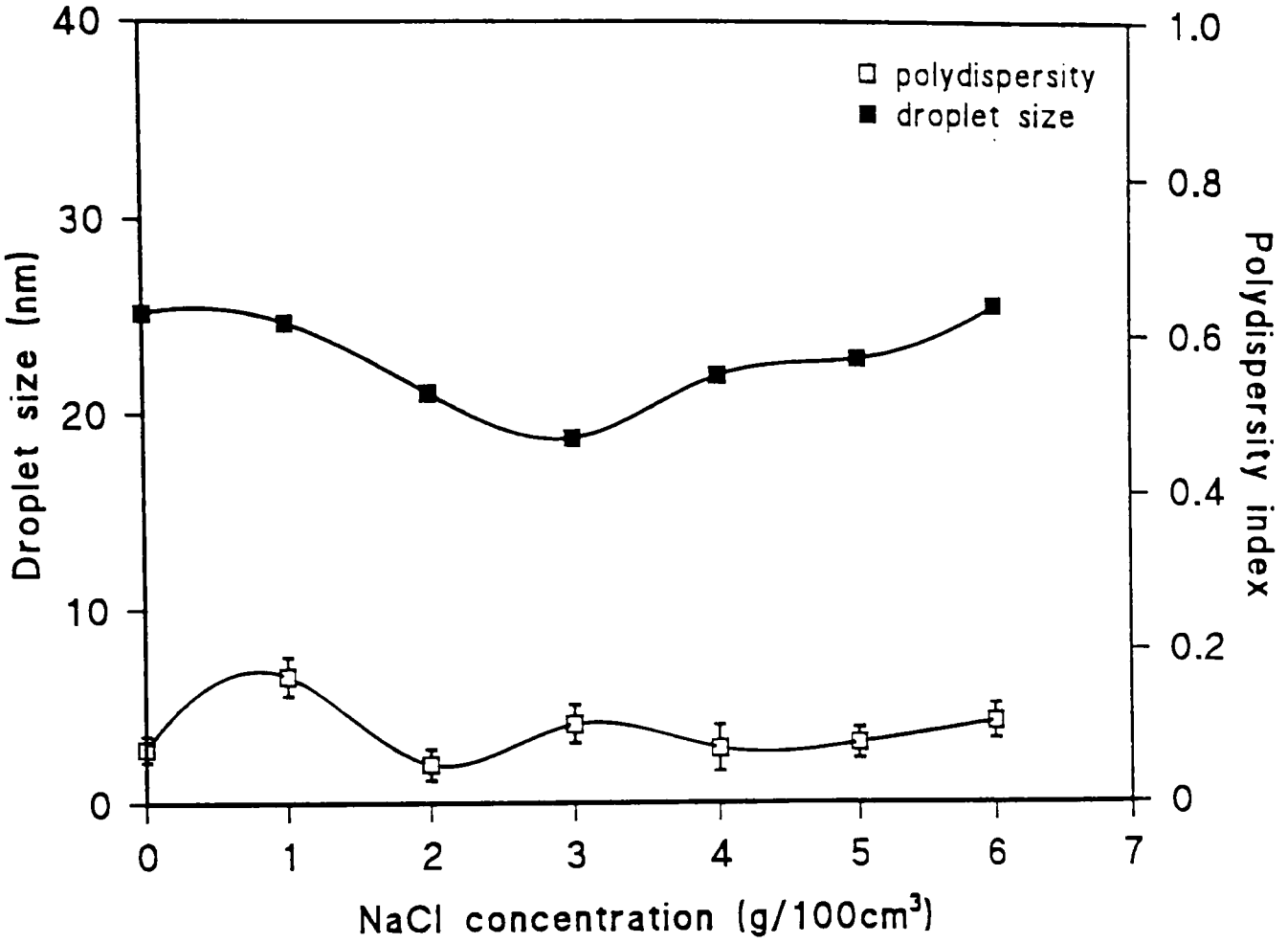

Figure 4.33 Droplet size and polydispersity of the microemulsion phase for system M2 at 298K.

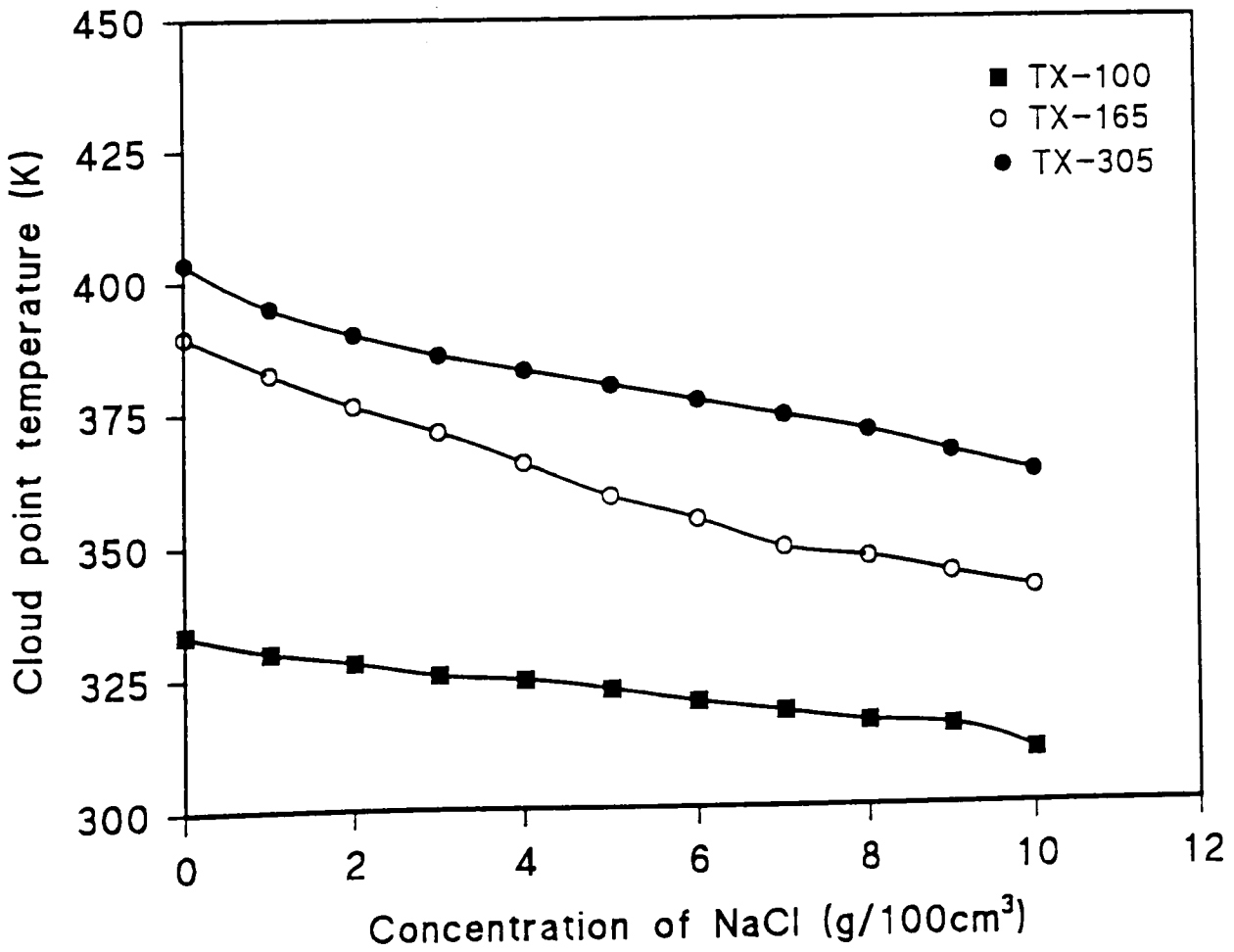

Figure 4.34 Effect of electrolyte on the cloud point temperature of TX-100, TX-165 and TX-305

4.2.8 Cloud Point Determination

As nonionic surfactants are sensitive to temperature, a micellar solution will often turn turbid and precipitate the surfactant out of solution. The temperature at which this occurs is called the cloud point or cloud temperature. It is also the minimum temperature at which a surfactant completely dissolves in a hot solution as it is cooled. The cloud point marks the condition where a surfactant-rich liquid begins to form in equilibrium with the micellar solution. This property is an example of thermotropy, or a phase change caused by a temperature change, and usually reaches a limiting value soon after the CMC.

The cloud point temperatures of 1%(w/v) surfactant solutions with varying concentrations of salinity were determined as described in the experiment in Chapter 3 (see Section 3.2.10). Figure 4.34 shows the effect of NaCl concentration on the cloud points of the Triton series of surfactants. It has been observed that increasing the salt concentration decreases the cloud point of the surfactant. The decrease in the cloud points is larger for the surfactants with fewer ethoxylate units.

As the water solubility and surface activity of surfactants are dependent on the hydrophilic nature of the ether linkages in the ethoxy chain. At room temperature, it is assumed that the ethoxy groups are hydrogen bonded with water, and the water solubility is dependent on the number of hydrated ether linkages. An increase in temperature reduces the forces of hydration and the surfactants begin to form liquid crystal-like phases out of the aqueous solution [56]. As this happens, the surfactant becomes less soluble in water and exhibits a cloud point. Cloud points place a limit on the surfactant type, concentration and temperature which can be used for EOR. Although nonionics can be used above their cloud points, this increases their adsorption onto reservoir rock which is undesirable.

4.2.9 Viscosity Results

The viscosities of the middle-phase microemulsions studied were measured at 298K by timing the flow of a constant volume of each sample in a capillary viscometer as described in the measurement methods of Chapter 3 (see Section 3.2.7). A plot of relative viscosity as a function of salinity for the system M1 is shown in Figure 4.35. The vertical dashed

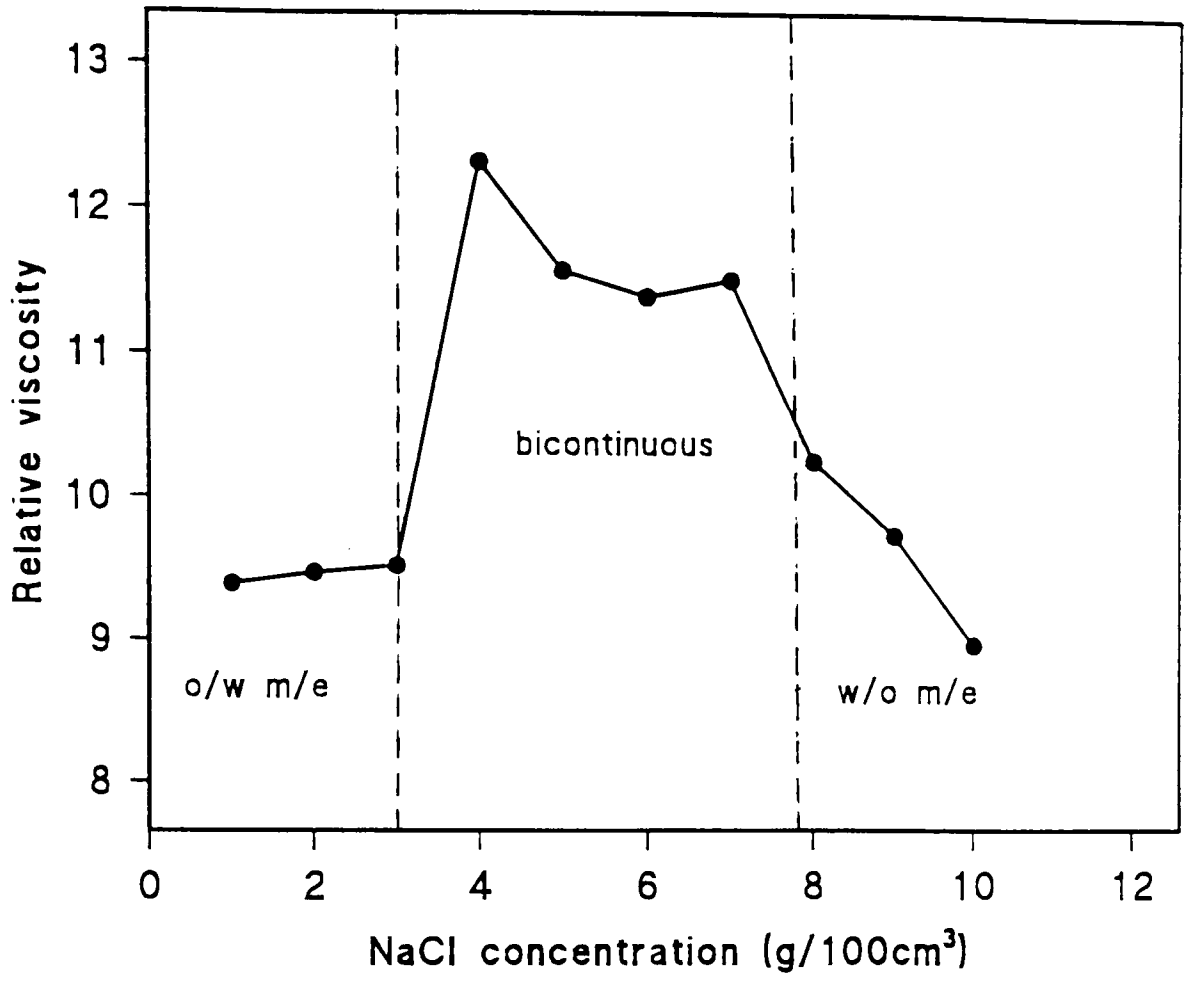

Figure 4.35 Viscosity of the microemulsion system M1 relative to water as a function of NaCl concentration at 298K

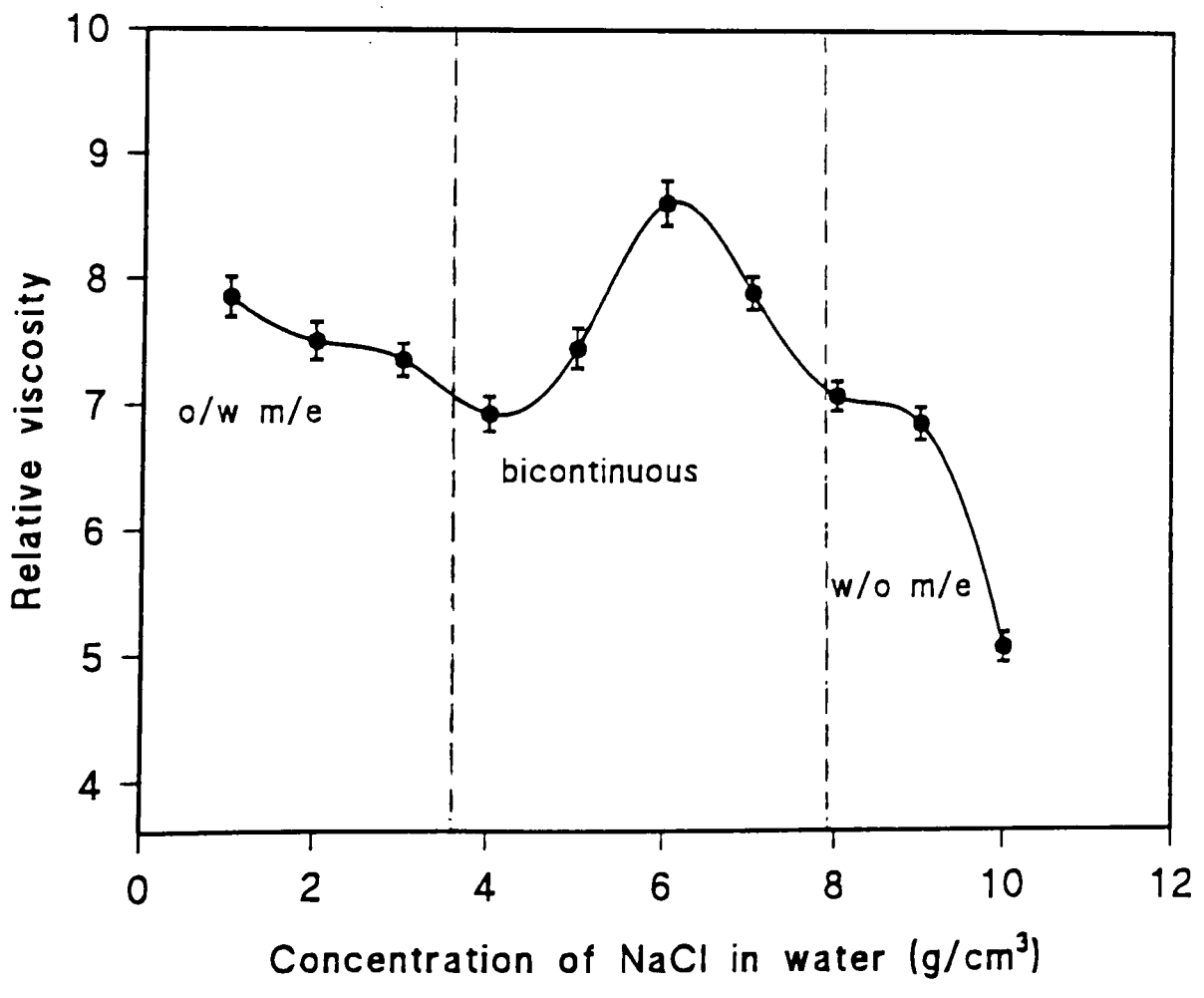

Figure 4.36 Viscosity of the middle phase for the system M2 relative to water as a function of NaCl concentration 298K.

lines mark the salinities for the type (I) → (III) and type (III) → (II) transitions. At low salinity the continuous phase is water so we have o/w microemulsions which show low viscosity. At intermediate salinity, the microemulsions are bicontinuous which show relatively high viscosity. At high salinity w/o microemulsions are formed which show very low viscosity.

Figure 4.36 shows a plot of relative viscosity of the system M2 at 298K. The viscosity of this system is quite high at low salinity which suggests that bicontinuous microemulsions are formed. A sharp drop in the viscosity can be seen at high salinity which indicates that the system is w/o microemulsion. A sharp increase in the viscosity at low salinity is due to maximum solubilisation of oil-in-water. The microstructures in the systems studied here progress with increasing salinity from a solution of swollen micelles to a bicontinuous microstructure rich in water to a bicontinuous microstructure rich in oil to a solution of swollen inverted micelles.

4.2.10 Electrical Conductivity Results

The distribution of surfactant between phases is related to the type of coarse macroemulsion formed by mixing oil/water/surfactant systems. In oil-in-water (o/w) emulsions, surfactant resides in the continuous (water) phase whereas for water-in-oil (w/o) emulsions it resides predominantly in the oil phase. The conversion of one type of emulsion to the other is known as phase inversion and is readily detected by changes in conductivity of the emulsions. The electrical conductivity of the o/w emulsions is high due to the presence of salt in the aqueous phase and it is lower for w/o emulsions. Thus conductivity provides a quick indication of the emulsion type. However, the properties of emulsions are very dependent on the phase volume ratio of oil : water and the surfactant concentration.

In order to determine the NaCl concentration in the middle phase of the three phase microemulsion system, measurements were carried out using an"alpha 800" conductivity meter as described in section 3.2.6. of Chapter 3. The results are presented in Table 4.8. It was seen that the concentration of NaCl increased in the middle phase as the brine

concentration was increased at a constant surfactant concentration.

Table 4.8 Concentration of NaCl in the middle phase of the microemulsion system M1 at 298K.

Brine concentration ($gNaCl/100cm^3$)	Concentration of NaCl after microemulsification left in the lower phase ($gNaCl/100cm^3$)	Concentration of NaCl in the middle phase ($gNaCl/100cm^3$)
1	0.89	0.109
2	1.78	0.218
3	2.55	0.450
4	3.40	0.600

In order to observe the phase inversion in the microemulsion phases, the conductivities of thermodynamically stable middle-phase microemulsions were studied as a function of salinity at 298K. Figure 4.37 shows a plot of the ratio of the electrical conductivity of microemulsion (m/e) to the electrical conductivity of the brine as a function of the NaCl concentration for the microemulsion system M1. The conductivity ratio varies smoothly over the entire scan (i.e. type (I) → (III) → (II)) and does not suggest any of the features of the viscosity data. Reed and Healy [58] also noted this lack of correlation.

However, at low salinity, the system shows type (I) microemulsion, and the conductivity ratio decreases with increase in the brine concentration. The decrease in the conductivity ratio at low salinity is due to; (a) the microemulsions are o/w type i.e. water is the continuous phase and (b) most of the electrolyte is in the aqueous phase. At intermediate salinity, the electrical conductivity decreases with the increase of oil solubility and the system transforms a water continuous medium to a bicontinuous phase. At high salinity, the conductivity is low which indicates that hydrocarbon is the continuous phase. Hence, one can readily distinguish between an oil-in-water microemulsion and a water-in-oil microemulsion.

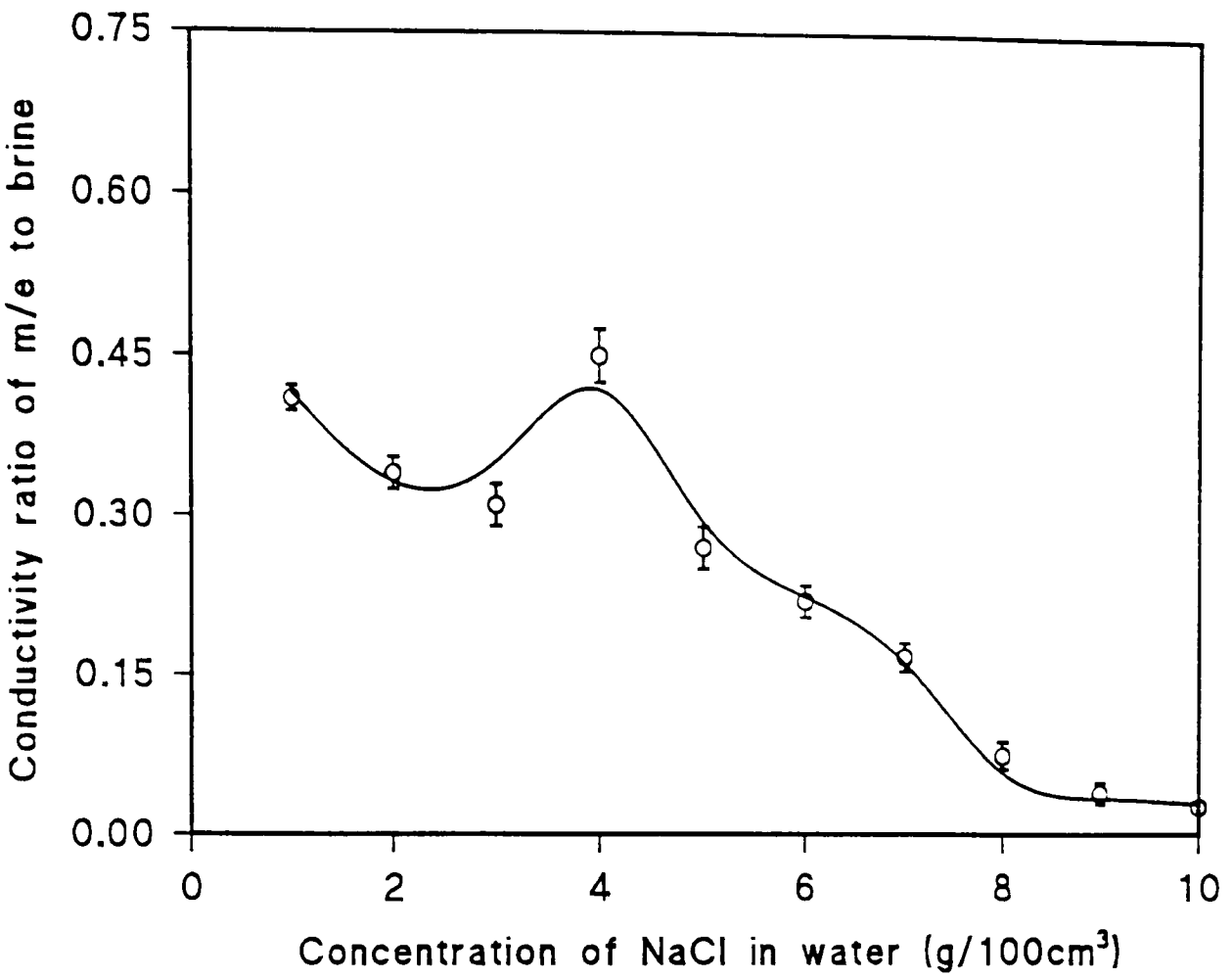

Figure 4.37 Conductance ratio as a function of NaCl Concentration for the microemulsion system M1 at 298K.

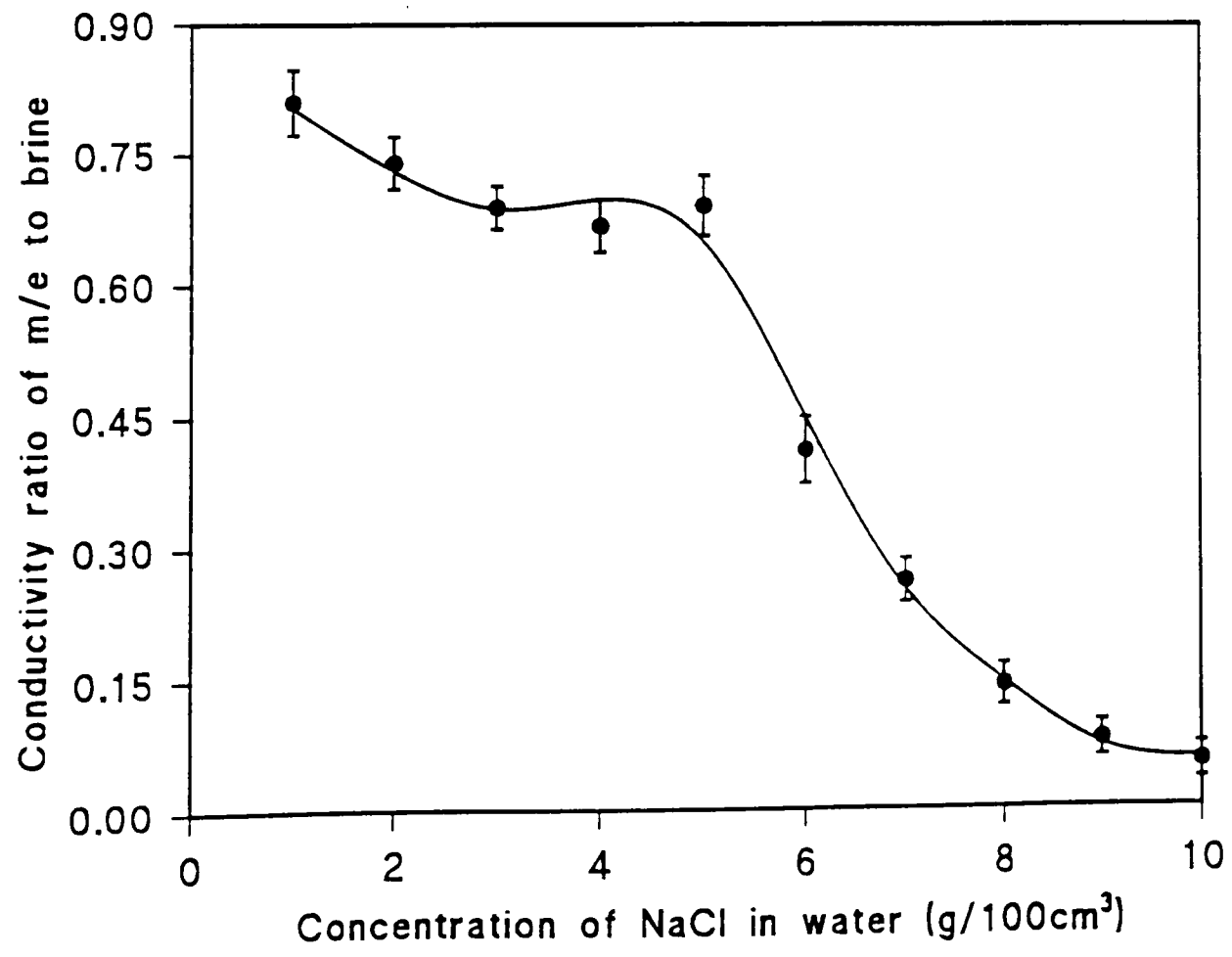

Figure 4.38 Conductivity ratio as a function of NaCl Concentration for the microemulsion system M3 at 298K.

Figure 4.38 shows a plot of the conductivity ratio versus concentration of NaCl for the microemulsion system M3. It can be seen that there is a sharp decrease in the conductivity ratio at low salinity, followed by a gradual decrease in the conductivity as salinity increases. In this system solubilisation of oil increases as the salinity increases. All the microemulsion systems behaved in the same way, showing a sharp decrease in the conductivity ratio in the type (I) microemulsion region, a gradual decrease in conductivity of the middle phase and in type (II) microemulsions electrical conductivity remains quite low. The electro conductive behaviour of all the microemulsion systems has the same general features. The conductivity of w/o microemulsions is also found to increase in the critical region [57].

Phase inversion from o/w to w/o microemulsions occurs as the salt concentration increases, but the salt concentration at which it does so is found to depend on the phase volume ratio. There is not enough evidence to decide about a structure of the microemulsion around inversion on the basis of conductivity results.

Macroscopic properties of microemulsion such as viscosity, interfacial tensions, electrical conductivity and phase behaviour must be related to fluid microstructures. Several structures for microemulsion have been proposed including spherical micelles, inverted micelles, and mixtures thereof [59]; lamellar, tubular and globular structures [59]; and equilibrium bicontinuous structures [60]. It has been suggested [61-62] that the electrical conductivity of microemulsion exhibits percolative behaviour expected of a disordered interspersion capable of bicontinuous structures.

4.2.11 Summary of Results

The information obtained from the phase equilibria and characterisation of microemulsions can be summarised as:

(i) The phase behaviour of nonionic surfactants can be improved by the addition of medium chain alcohols which act as a co-surfactants and enhance the mutual solubility of a brine and oil.

(ii) Mixture of surfactants (i.e. nonionic+anionic) together with a medium

chain alcohol is a model surfactant system in which the middle-phase microemulsion is produced that can be expected to meet the criteria for EOR. The system is stable at a higher salinity and temperature which is the requirement for EOR.

(iii) It is possible with modified spectrophotometer to perform the salinity and temperature scans of the microemulsion phases accurately.

(iv) Several different techniques have been used to characterise the middle-phase microemulsions as a function of salinity and temperature.

The distribution of oligomers in the nonionic surfactants can be traced by HPLC.

Solubilisation of water and oil in the microemulsion, and partitioning of alcohol in the aqueous and organic phases can be determined by GC.

Concentration of the surfactant in the middle-phase by UV-spectrophotometer.

Dynamic light scattering can be used to obtain droplet size and viscometry to determine the phase transition in the microemulsion phases.

(v) Ultra-low interfacial tension can be achieved in the model surfactant system.

References

[1] P.A. Winsor, Trans. Fara. Soc., **44**, 376, (1948)

[2] G.A. Pope and W.H. Wade, ACS Symposium Series, **594**, 142, (1995)

[3] W.B. Gogarty, J. Pet. Tech., **December,** 1407, (1968)

[4] R.N. Healy and R.L. Reed, J. Soc. Pet. Eng. **14,** 491, (1974)

[5] R. Guo, J. of Dispersion Science and Technology, **16**, 373, (1995)

[6] F. Billoudet and M. Dupeyrat, J. de Chimie Physique, **78**, 635, (1981)

[7] J.L. Salager and D.O. Shah, J. Soc. Pet. Eng., **June**, 167, (1978)

[8] S.J. Salter, SPE 6843 Presented at Full Soc. Pet. Eng. Meeting, Denver, October, (1977)

[9] A. Skauge and O. Palmgren, J. Soc. Pet. Eng., 18499 (1989)

[10] M. Kahlweit, R. Strey and G. Busse, J. Phys. Chem. **95,** 5344, (1991)

[11] G.D. Smith, C.E. Donelan and R.E. Barden, J. Colloid Interface Sci., **60,** 488, (1977)

[12] H.L. Rosano, T. Lan and A. Weiss, J. Colloid Interface Sci., **72**, 233, (1979)

[13] P.A. Winsor, "Solvent Properties of Amphipilic Compounds" Butterworths Scientific Publication, London, (1954)

[14] R.N. Healy, R.L. Reed and C.W. Carpenter, J. Soc. Pet. Eng., **February**, 87, (1975)

[15] D.O. Shah, Dev. Pet. Sci., **13**, 41, (1981)

[16] R.N. Healy, R.L. Reed and D.G. Stenmark, J. Soc. Pet. Eng. **June,** 147, (1976)

[17] S.C. Jones and K.D. Dreher, J. Soc. Pet. Eng. **June,** 161, (1976)

[18] D.J. Miller, S.P. Van Halasz, M. Schmidt, A. Holst and G. Pusch, J. Pet. Sci. and Eng., **6,** 63, (1991)

[19] S. Qutubuddin, C.A. Miller and W.J. Benton, ACS Symposium Series, **272,** 223, (1985)

[20] W.J. Benton, J. Natoli, S. Qutubuddin, S. Mukherjee, C.A. Miller and T. Fort, J. Soc. Pet. Eng., **February**, 53, (1982)

[21] D.K. Olsen and C.B. Josephson, Report for US Department of Energy, July, (1987)

[22] T.A.B. Bolsman and G.J. Daane, 3rd European Meeting on EOR, Rome, **April**, (1985).

[23] J.L. Cayias, R.S. Schechter and W.H. Wade, J. Colloid Interface Sci., **59,** 31, (1977)

[24] L. Cash, J.L. Cayias, G. Fournier, D. Macallister, T. Scharres, R.S. Schecter and W.H. Wade, J. Colloid Interface Sci., **59,** 392, (1977)

[25] D.M. Zhu, K.I. Fang and Z.A. Shelly, J. Phys. Chem., **96**, 2382, (1992)

[26] C. Toprakcioglu, J.C. Dore, B.H. Robinson, A. Howe and P. Chieux, J. Chem. Soc., Faraday Trans. I, **80,** 413 (1984)

[27] T.S. Gendy, Y. Barakat and A.I. Mead, Polymer International **24,** 235, (1991)

[28] R.C. Nelson, Soc. Pet. Eng. 8824, First Joint Symposium on Enhanced Oil Recovery, Tulsa, April, (1980)

[29] R.L. Reed and R.N. Healy, "Improved Oil Recovery by Surfactant and Polymer Flooding", Eds., D.O. Shah and R.S. Schechter, Academic Press, New York, 383, (1977)

[30] K.V. Baviere and D.O. Shah, "Micellisation, Solubilisation and Microemulsions", Ed. K. Mittal, Plenum Press, New York, **1**, 87, (1977)

[31] M.L. Robbins, "Micellisation, Solubilisation and Microemulsions", Ed. K. Mittal, Plenum Press, New York, **2**, 273, (1977)

[32] M.C. Puerto and W.W. Gale, J. Soc. Pet. Eng., **June**, 193, (1977)

[33] K.H. Lim, J.S. Reckles and D.H. Smith, J.Colloid Interface Sci., **161**, 465, (1993)

[34] M.S. Aston, Chem. Soc. Rev., **22**, 67, (1993)

[35] Y. Saito,T. Sato and I. Anazawa, Colloids Surfaces, **40**, 107, (1989)

[36] W. Ostwald, Zeit. Phys.Chem.**A158**, 91, (1931)

[37] J.N. Bronsted "Physical Chemistry" W. Heinemann (London)

[38] M.J. Scarlett, J.A. Fisher, H. Zhang and M. Ronan, Water Res., **28**, 2109, (1994)

[39] W.R. Melander, A. Nahum and C. Horvath, J. Chromatogr., **185**, 129, (1979)

[40] P. Jandera, J. Chromatogr., **449**, 361, (1988)

[41] J.F.K. Huber, F.F.M. Kolder and J.M. Miller, Anal. Chem., **44**, 105. (1972)

[42] M. Ahel, J. McEvoy and W.Giger, Environ. Pollution, **79**, 243. (1993)

[43] M. Ahel and W.Giger, Chemosphere, **26**, 1461, (1993); M. Ahel and W.Giger, Anal. Chem., **57**, 1577, (1985)

[44] M. Kudoh, H. Ozawa, S. Fudano and K.Tsuji, J. Chromatogr., **287**, 337, (1984)

[45] C.F. Allen and L.I. Rice, J. Chromatogr., **110**, 151, (1975)

[46] N.A. Ibrahim, PhD Thesis Brunel University (1995)

[47] R.N. Hwan, C.A. Miller and T. Fort, J. Colloid Interface Sci., **68,** 221, (1979)

[48] E.J. Beckmann and R.D. Smith, J. Phys. Chem., **94**, 3729, (1990)

[49] J.S. Sjoblom, K. Rosenquist and P. Stenius, Colloid Polym. **260**, 82, (1982)

[50] D.J. Cebula, L.H. Harding, R.H. Ottewill and P.N. Pusey, Colloid Polym. Sci., **258**, (1980)

[50] A.A. Calje, W.G.M. Agterof and A. Vrij, in "Micellisation, Solubilisation and Microemulsions", Plenum Press, New York, (1977)

[51] S.F. Trevino, R. Joubran, N. Parris and N.F. Berk, J. Langmuir, **10**, 2547, (1994)

[52] G.F. Hall and A.P.F. Turner, J. Electroanalysis, **6**, 217, (1994)

[53] X. Fu, Y. Pan, Z.S. Hu and Z.F. Ma, A: Physicochemical and Engineering Aspects, **110**, 55, (1996)

[54] M.S. Leaver and U. Olsson, Langmuir, **10**, 3449, (1994)

[55] A. Holmberg, L. Piculell and B.Wesslen, J. Phys. Chem. **100**, 462, (1996)

[56] R. Aveyard, B.P. Binks, S. Clark and P.D.I. Fletcher, J. Chem. Tech. Biotechnol., **48**, 161, (1990)

[57] M. Giustini, G. Palazzo, G. Colafemmina, M. Dellamonica and M. Giomini, J. Phys. Chem., **100**, 3190, (1996)

[58] R.L. Reed and R.N. Healy, in "Improved Oil Recovery by Surfactant and Polymer Flooding", Eds. D.O. Shah and R.S. Schechter, Academic Press, New York, 383, (1977)

[59] P.A. Winsor, Chem. Rev., **68**, 1, (1968)

[60] L.E. Scriven, Nature , **263**, 123, (1976)

[61] M. Dvolaitzky, M. Lagues, J.P. Le Pesant, R. Ober, C. Sauterey and C. Taupin, J. Phys. Chem. **84**, 1532, (1980)

[62] M. Lagues, J. Physique Lett., **40**, L331, (1979)

CHAPTER FIVE

ADSORPTION OF SURFACTANTS FROM AQUEOUS AND NONAQUEOUS ENVIRONMENT

5.1 Introduction and Background

When two phases are in contact, there is a region at their interface of which the composition is different from that of the individual bulk phases. The increase in the concentration of a substance at the interface (compared with its bulk concentration) is known as its adsorption. Adsorption may be a physical process (physisorption) which involves intermolecular forces of attraction and repulsion (e.g. van der Waals forces) or hydrogen bonding. Alternatively, it may be due to chemical processes (e.g. the sharing or transferring of electrons between the adsorbed species and surface species to form chemical bonds).

Adsorption from solution onto solids is of great practical importance and many industrial processes involve adsorption at the liquid/solid interface, including detergency [1-3], dyeing [4-8], pollution control [9-11], ion-exchange [12, 13], surface area measurement [14] and chromatographic techniques [15-17], etc. The interest in explaining the behaviour of surfactants at a liquid/solid interface has recently increased due to their widespread use in flotation [18, 19], detergency [20, 21], suspension stabilisation [22], ceramic preparation [23, 24], pharmaceuticals [25-27], cosmetics [28], and enhanced oil recovery [29-32].

Adsorption of a surfactant at a liquid/solid interface is often complex, because of (i) the competitive adsorption of the solute and solvent, (ii) the generally unknown amount of solvent in the adsorbed layer, and (iii) the large number of possible conformations of the long surfactant molecules in that layer. If the liquid is an aqueous solution the situation is made even more complex because ions (coming from the dissociation of solvent water molecules, from the dissolution of the solid, from counter ions of ionic surfactants, or from a salt background) may adsorb at the interface and, change the surface charge. Adsorption isotherms are the most extensively employed method of describing the equilibrium states

of an adsorption system and useful information about adsorption process, and the nature of adsorbate and adsorbent can be obtained from them.

These are a measurement of the amount of solute adsorbed at an interface as a function of its equilibrium concentration. The adsorption capacity of adsorbents or different adsorbates depends on different factors: (i) adsorbate properties (e.g. group functionality, branching geometry, polarity, hydrophobicity, dipole moment, molecular weight and size, and aqueous solubility), (ii) hydronium ion concentration, temperature, adsorbate concentration, ionic strength, and competitive solutes, (iii) the nature of the adsorbent with its surface area, pore size distribution, distribution of functional groups (e.g. the number of OH units/nm^2).

5.2 Adsorption of Non-ionic Surfactants

During the past ten years, many investigations [33-36] have been made on the structure of non-ionic surfactant layers at solid/liquid interfaces, in part under the auspices of enhanced oil recovery projects. In tertiary oil recovery where a surfactant or micellar solution is injected into the rock formation in order to release trapped oil, it is generally assumed that injected solutions should be in contact over a period of months or years. It is, however, quite clear that a concentration gradient is achieved before the solution reaches the oil, since the flow distances are rather long. Any loss of surfactant is partly due to any interactions between the surface active agents and the rock surface (or any solid material occurring in the pores). Adsorption is minimal when the adsorbate and the surface have the same charge [37], and of course the latter is pH-dependent, but for non-ionics the following stages of adsorption may exist as the surfactants concentration is raised:

I: monomer-monomer interactions are minimal and non
-associated molecules adsorb and Henry's Law is obeyed.

II: as the monolayer capacity is reached most of the solvent
molecules will have been displaced from the surface

III: as the CMC is approached the more weakly held end of the
adsorbate will be displaced from the surface

IV: further adsorption may then occur as a result of surfactant-surfactant attraction and aggregation; micelles or hemi-micelles [38] may be produced on the surface.

5.3 Theories of Adsorption

None of the current theories of adsorption is capable of providing a mathematical description of an experimental isotherm over its entire range of concentration because of the complexity of physisorption and chemisorption and the imperfect nature of most solid surfaces. At present, Langmuir, Freundlich and Henry's law are most commonly employed to describe the adsorption equilibria of a particular system.

5.3.1 Langmuir Adsorption Isotherm

Consider a surface that has a fraction θ covered by adsorbed molecules and on which the remaining $(1 - \theta)$ is available for subsequent adsorption. The rate at which adsorption occurs is proportional to the concentration of the solute in solution C and to the extent of free surface, and can be written:

$$\text{Rate of adsorption} = k_{ads.}(1 - \theta).C \qquad (5.1)$$

where $k_{ads.}$ is the adsorption rate constant.

Similarly, the rate of desorption will be proportional to the fraction of covered surface:

$$\text{Rate of desorption} = k_{des.}\theta \qquad (5.2)$$

where $k_{des.}$ is the rate of desorption.

At equilibrium, the rates of desorption and adsorption are equal and so from equation (5.1) and (5.2) one can see that

$$k_{des.}\theta = k_{ads.}(1 - \theta).C \qquad (5.3)$$

$$\theta/(1-\theta) = k_{ads.}/k_{des.}.C = KC \qquad (5.4)$$

where K = equilibrium constant for the adsorption process $(= k_{ads.}/k_{des.})$.

If X is the amount of solute adsorbed at equilibrium concentration C_e and X_m is the amount of solute adsorbed per unit weight of adsorbent required for monolayer coverage of the surface when all the sites are occupied then

$$\theta = \frac{X}{X_m} \tag{5.5}$$

For adsorption from solution by solid adsorbents, the Langmuir adsorption isotherm is expressed as:

$$X = \frac{X_m b C_e}{1 + b C_e} \tag{5.6}$$

where b is a constant related to the heat of adsorption.

As the equilibrium constant, $K = b = k_{ads}/k_{des}$ in the Langmuir equation then

$$b = \exp(-\Delta G/RT)$$

$$b = \exp(-\Delta H/RT + \Delta S/R)$$

and so is related to ΔG and ΔH.

Equation (5.6) indicates that X approaches X_m asymptotically as C_e approaches infinity. In its linear form of the data the equation can be written as:

$$\frac{C_e}{X} = \frac{1}{bX_m} + \frac{C_e}{X_m} \tag{5.7}$$

when C_e/X is plotted as a function of C_e to give a straight line, having a slope $1/X_m$ and an intercept $1/bX_m$ is obtained. Another linear form can be obtained by dividing equation (5.7) by C_e:

$$\frac{1}{X} = \frac{1}{X_m} + \left(\frac{1}{C_e}\right)\left(\frac{1}{bX_m}\right) \tag{5.8}$$

5.3.2 Freundlich Adsorption Isotherm

The Freundlich adsorption equation is perhaps the most widely used mathematical description of adsorption in aqueous system. The Freundlich equation is expressed as [39]:

$$\frac{X}{m} = K C_e^{1/n} \tag{5.9}$$

where X is the amount of solute adsorbed, m is the weight of adsorbent, C_e is the solute equilibrium concentration, and K and 1/n are constants characteristic of the system.

The Freundlich equation is an empirical expression that encompasses the heterogeneity of the surface and the exponential distribution of sites and their energies [40]. For linearization of the data, the Freundlich equation is written in logarithmic form:

$$\log\frac{X}{m} = \log K + \frac{1}{n}\log C_e \qquad (5.10)$$

5.3.3 Henry's Law: Linear Adsorption Isotherm

This represents the simplest isotherm in which the amount adsorbed increases directly with the equilibrium concentration of the solute. It is described by:

$$X = K_h C_e \qquad (5.11)$$

where X = x/m, the amount of solute adsorbed by unit mass of adsorbent; K_h = a constant; C_e = equilibrium concentration. This isotherm is obtained under conditions of low solute concentration. In such a system, the adsorbed layer is extremely dilute and the amount adsorbed is only a fraction of the monolayer capacity. Usually a linear relationship is observed at the lower concentration levels of a total adsorption isotherm. Therefore, the application of Henry's law equation should be restricted to that region of the isotherm. All the adsorption isotherms are reduced to Henry's law *at low concentrations*.

5.4 EXPERIMENTAL

As adsorption of surfactant is a major drawback in a chemical flooding process. Here an attempt has been made to study the adsorption from aqueous and non-aqueous environment at different temperatures and salinities. The effect of alcohols on the adsorption of surfactant has also been investigated. It has been observed that the alcohols reduce the extent of adsorption of surfactant from the aqueous and non-aqueous solutions significantly.

5.4.1 Sample Preparation

A natural quartz adsorbent (C-600 grade, from Sifraco, France) was washed with hydrochloric acid to a pH of 1.5, filtered, washed with doubly distilled water to a pH of 5 to remove anions and cations present at the quartz surface. The quartz sample (Qz) was then dried at 373-378K overnight and cooled in a desiccator. After that, the quartz samples were placed in a Lenton muffle furnace heated at 1273K for different intervals of time, followed by natural cooling to room temperature. The calcined samples are designated Qzx where Qz stands for quartz and x represents the number of calcination hours.

5.4.2 Ion-Exchange Chromatography (IEC)

In order to determine the effect of the acid wash treatment on the quartz sample (i.e. anions and cations), a qualitative analysis was carried out using ion chromatographic analyser (Dionex 2010i) at 298K. A known amount (0.5g) of the quartz sample (i.e. acid treated and untreated) was tumbled with 10cm^3 of distilled water for 24h at 298K. After tumbling, the solutions were centrifuged at 4000rpm for 30min and the supernatant of each sample was analysed using the Dionex analyser (see Figure 5.1) under the following conditions:

For anion analysis		
	HPLC column	AS4A + guard column AG4A
	Eluent	$NaHCO_3$ (0.75mmol), Na_2CO_3 (2.2mmol) and 0.025mol H_2SO_4
	Flow rate	1.2 cm^3/min
	Pressure	6.2 MPa
	Conductivity set at	30μS
For cation analysis		
	HPLC column	CS2 + guard column CG2
	Eluent	5mmol HCl+0.04mol $(CH_3)_4NOH$
	Flow rate	1.5 cm^3/min
	Pressure	6.5 MPa
	Conductivity set at	30μS

Ion-exchange chromatography has been used in the separation of anionic and cationic species. The process concerns an interchange of ions of like sign between the solution and an essentially insoluble solid in contact with the solution. The stationary phase consists of

a polystyrene-based resin cross-linked with divinylbenzene (DVB) and contains fixed charged groups and mobile counter-ions which can be reversibly exchanged for those of a solute carrying a like charge, as the mobile phase travels through the system. The proportion of DVB is 2 to 20% and results in a three dimensional cross-linked structure that is rigid, porous and highly insoluble [41].

For the exchange of cations, the exchange function is usually a sulphonate group; whereas for the analysis of anions, a quaternary ammonium group is commonly employed. The different rates of migration result from variations in the affinity of the stationary phase for different ionic species. The mobile phase contains an ion of low resin affinity, and the separated components collected at the bottom of the column are thus accompanied by a relatively high concentration of this ion. Procedures often adopted in ion-exchange chromatography are 'gradient elution', involving continuous variation in the composition of the eluting agent, 'stepwise elution', in which the composition is altered at specific points during the separation, and 'complexing elution', where a reagent which forms complexes of varying stability with the sample components is included in the solution. Acids, bases and buffers are most widely used as eluting agents.

The Ion-Exchange Chromatograph

The major components of a modern chromatographic instrument, as used in this work and developed by Dionex are illustrated in Figure 5.1. The mobile phase is pumped through the chromatographic system by a double reciprocating pump [42]. The samples are introduced into the system via a loop injector. The two ion-exchange column are coupled in series and form the most important part of the chromatograph. The selection of a suitable stationary phase as well as of the appropriate chromatographic parameters, determined the quality of the analysis. The column bodies are fabricated with inert materials and are generally operated at room temperature. The performance of a detector (which serves to identify and quantify the species being analysed) depends upon (a) linearity, (b) resolution, and (c) noise.

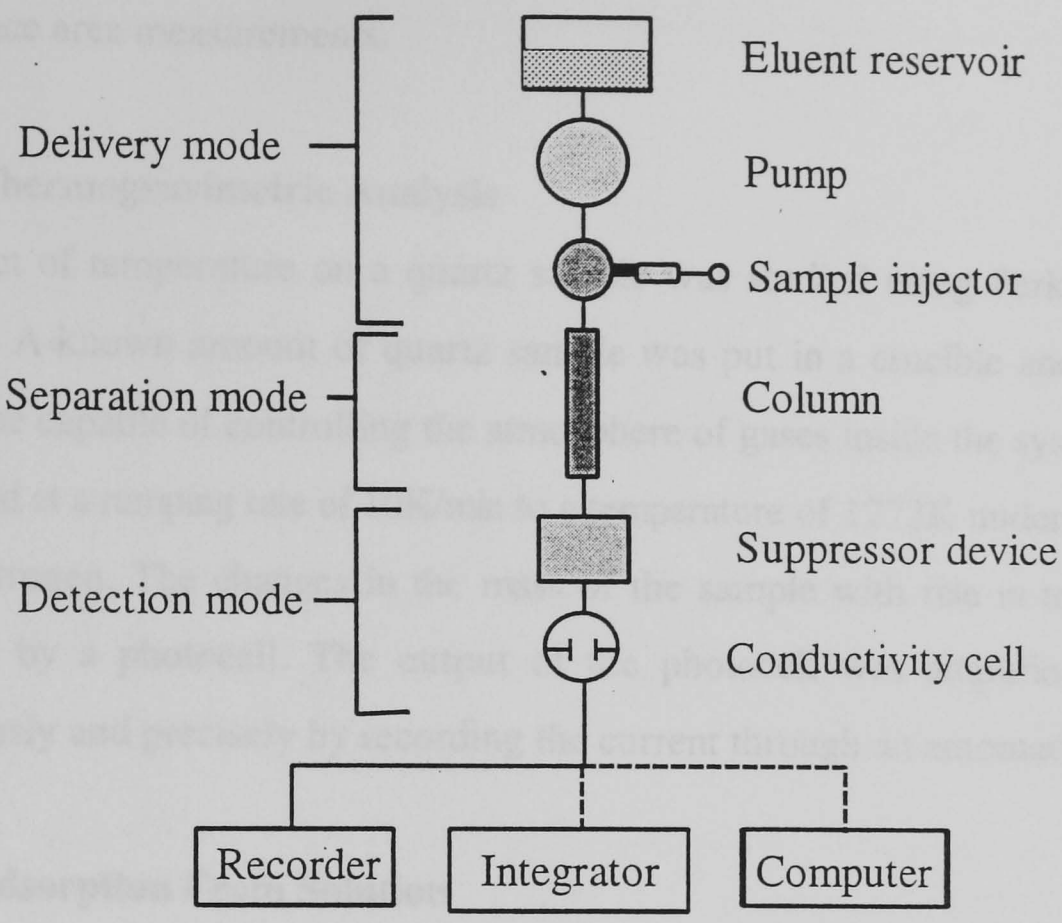

Figure 5.1 A typical Dionex ion chromatograph configuration

5.4.3 BET Surface Area Measurement

The Micromeritics Digisorb 2600 volumetric sorption analyser was used to determine the surface area of quartz samples. Prior to krypton adsorption, all the physisorbed species were removed from the surface of the sample by heating at 393K under a vacuum of 10^{-4} Torr for 16h. The specific surface areas of quartz samples were determined from physical adsorption data of krypton at 77K by applying the BET equation.

$$\frac{p}{V_a(p_o - p)} = \frac{1}{V_m C} + \frac{(C-1)}{V_m C}\cdot\frac{p}{p_o} \qquad (5.12)$$

where p is the adsorption equilibrium pressure, p_o is the saturation pressure of the adsorbate on the sample at 77K, V_a is the volume of a gas adsorbed at relative pressure p/p_o and V_m is the monolayer capacity. The BET equation gives a linear relation between $p/V_a(p_o - p)$ and p/p_o at $0.05 < p/p_o < 0.20$. From the value of monolayer capacity the surface area was calculated from the known molecular cross section of the krypton (i.e. 19.2 A^{o2}/molecule) molecule which is generally considered to be the most suitable adsorbate for

low surface area measurements.

5.4.4 Thermogravimetric Analysis

The effect of temperature on a quartz sample was studied using Perkin Elmar TGS 2 analyser. A known amount of quartz sample was put in a crucible and suspended in a quartz tube capable of controlling the atmosphere of gases inside the system. The sample was heated at a ramping rate of 10K/min to a temperature of 1273K under a constant flow of dry nitrogen. The changes in the mass of the sample with rise in temperature were recorded by a photocell. The output of the photocell was amplified and measured continuously and precisely by recording the current through an automatic recorder.

5.4.5 Adsorption From Solution

(a) Calibration Curve

Initially, a calibration graph for the surfactant under analysis was obtained using solutions of known concentration and measuring their absorbance at 275nm by a UV-spectrophotometer (Lambda 9). The intensity of the sample is then compared to that obtained from the calibration curve of the known standard giving the correct concentration of the surfactant solution. Figure 5.2 shows a calibration plot of TX-100 giving a correlation coefficient 0.9996 at 298K.

(b) Optimum Adsorbate/Adsorbent Ratio

In order to choose an appropriate liquid/solid ratio, the dependence of adsorption on the amount of adsorbent was investigated by tumbling various amounts of quartz with a constant volume (10 cm^3) of 0.7mmol/dm^3 surfactant solution. The adsorbent amount at which maximum adsorption takes place was then used for adsorption experiments. Figure 5.3 shows a plot of amount adsorbed as a function of adsorbent (quartz) weight % at 298K. The maximum amount adsorbed was found at 0.5g of the adsorbent weight (i.e. when the adsorbate : adsorbent ratio of 20).

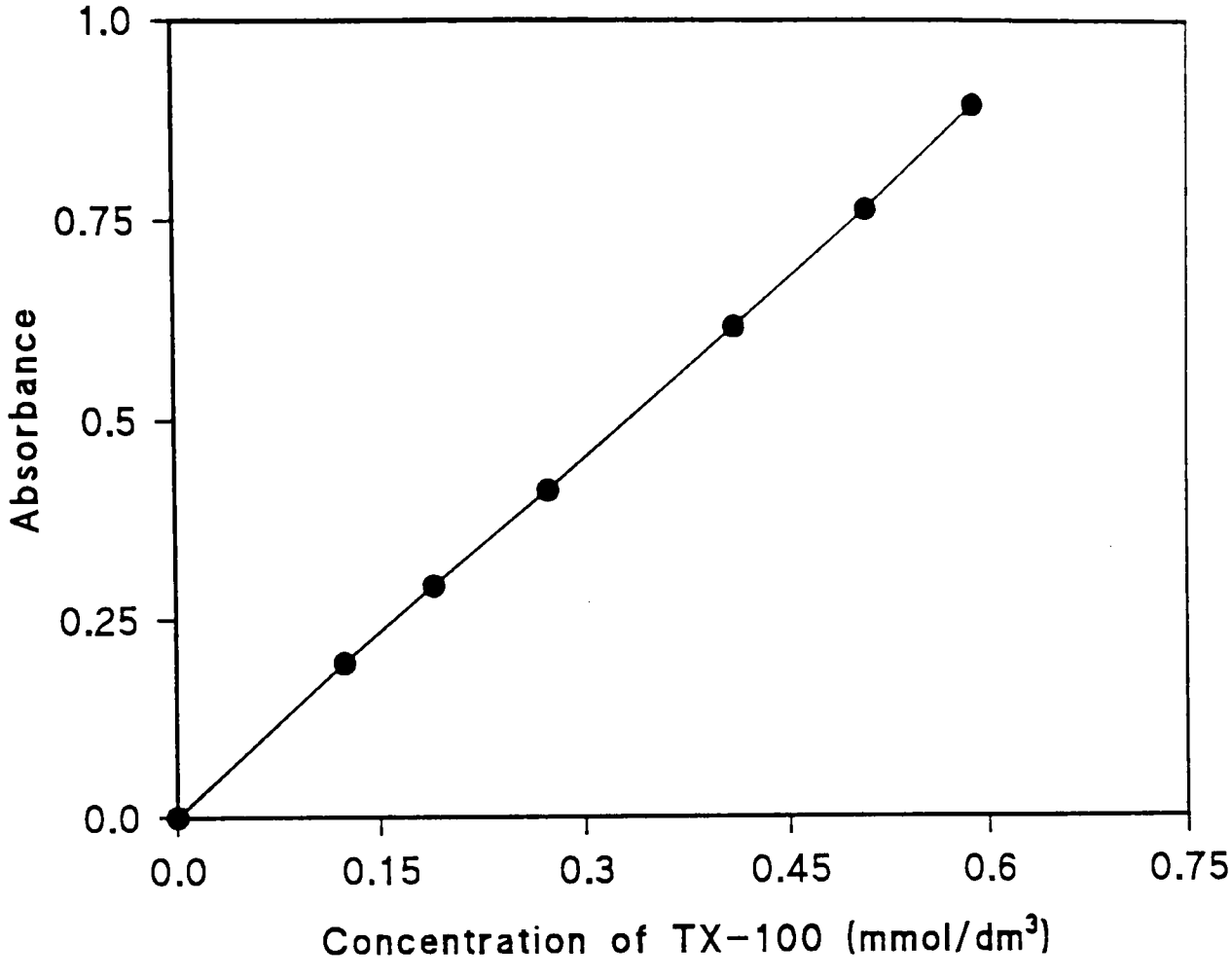

Figure 5.2 Calibration curve for TX−100 giving a correlation coefficient 0.9998 at 298K.

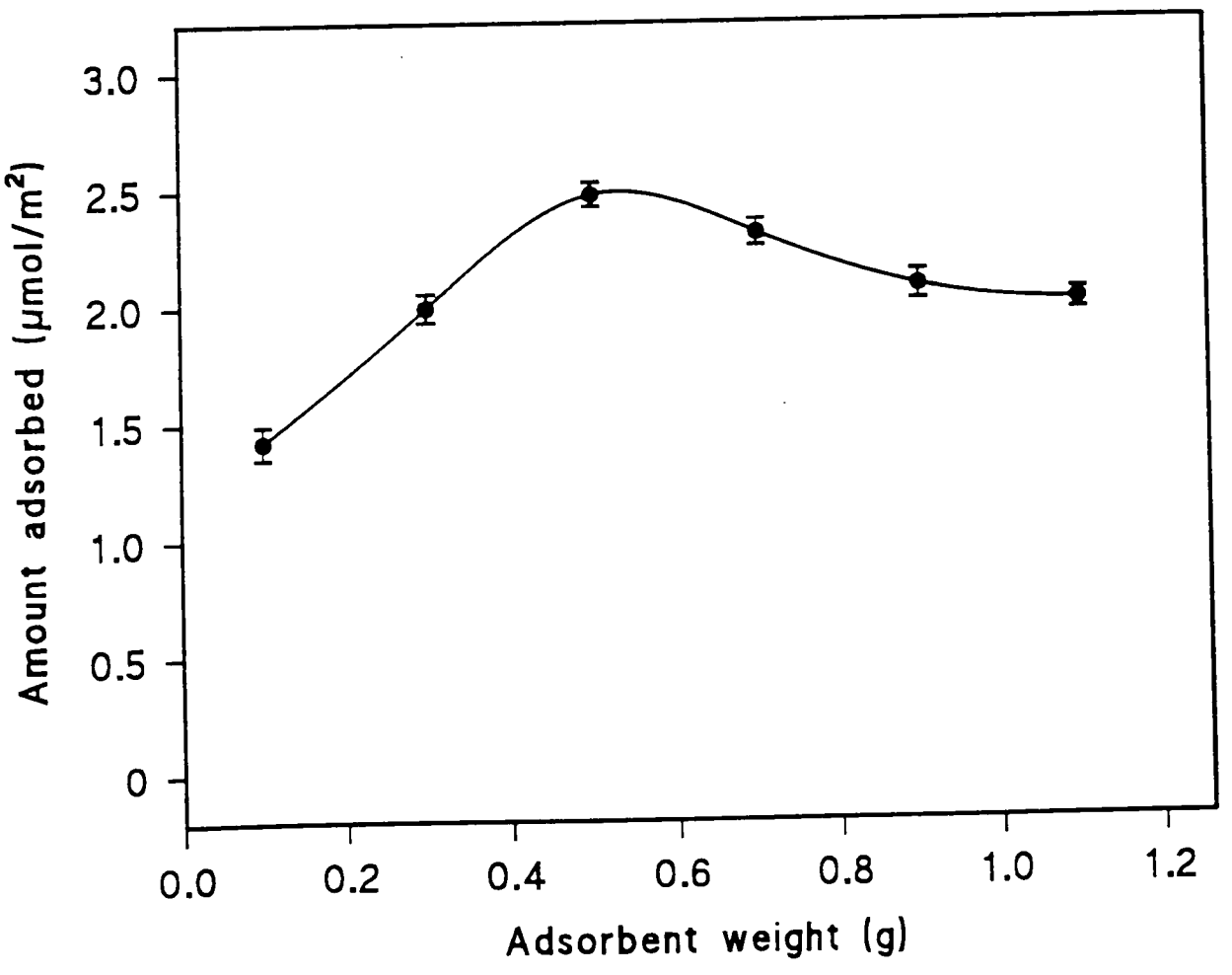

Figure 5.3 Amount of TX−100 adsorbed from 0.7mmol/dm^3 solution as a function of weight of adsorbent at 298K.

(c) Optimum Shaking Time

Prior to the detailed studies of the extent of adsorption of different surfactants from aqueous and non-aqueous media, the time required to ensure an equilibrium between adsorbate and adsorbent was investigated. This was done by shaking 500 mg of quartz with $10cm^3$ of $0.7mmol/dm^3$ solution of surfactant for different interval of times. After shaking, the solutions were centrifuged at 4000rpm for 30min (10min for non-aqueous media to minimize the losses by evaporation which may change the concentration of the liquid) and the aliquot was analysed spectrophotometrically. Figures 5.4(a) and (b) show plots of the amount of TX-100 adsorbed (from aqueous and nonaqueous solutions) as a function of time at 298K. It has been observed that the equilibrium time for adsorption of TX-100 from an aqueous environment is greater (16h) than from nonaqueous solution (i.e. decane) (2h).

(d) Adsorption Isotherm Measurement

The adsorption of surfactant onto quartz samples was then measured spectrophotometrically using a batch technique. Eight solutions ($10cm^3$) of varying surfactant concentration were equilibrated-tumbled with a known amount of quartz. Solutions were then centrifuged at 4000 rpm for phase separation. The initial and equilibrated concentrations of the surfactant solution were measured by spectrophotometer at 275nm. The amount of surfactant adsorbed onto the quartz was calculated as follow:

$$\Gamma = \frac{(C_i - C_f)}{MS_a}.V_s \qquad (5.13)$$

where Γ = amount adsorbed (mol/m^2)

C_i = initial concentration (mol/dm^3)

C_f = final concentration (mol/dm^3)

M = weight of adsorbent (g)

S_a = surface area of the adsorbent (m^2/g)

V_s = volume of solution (dm^3)

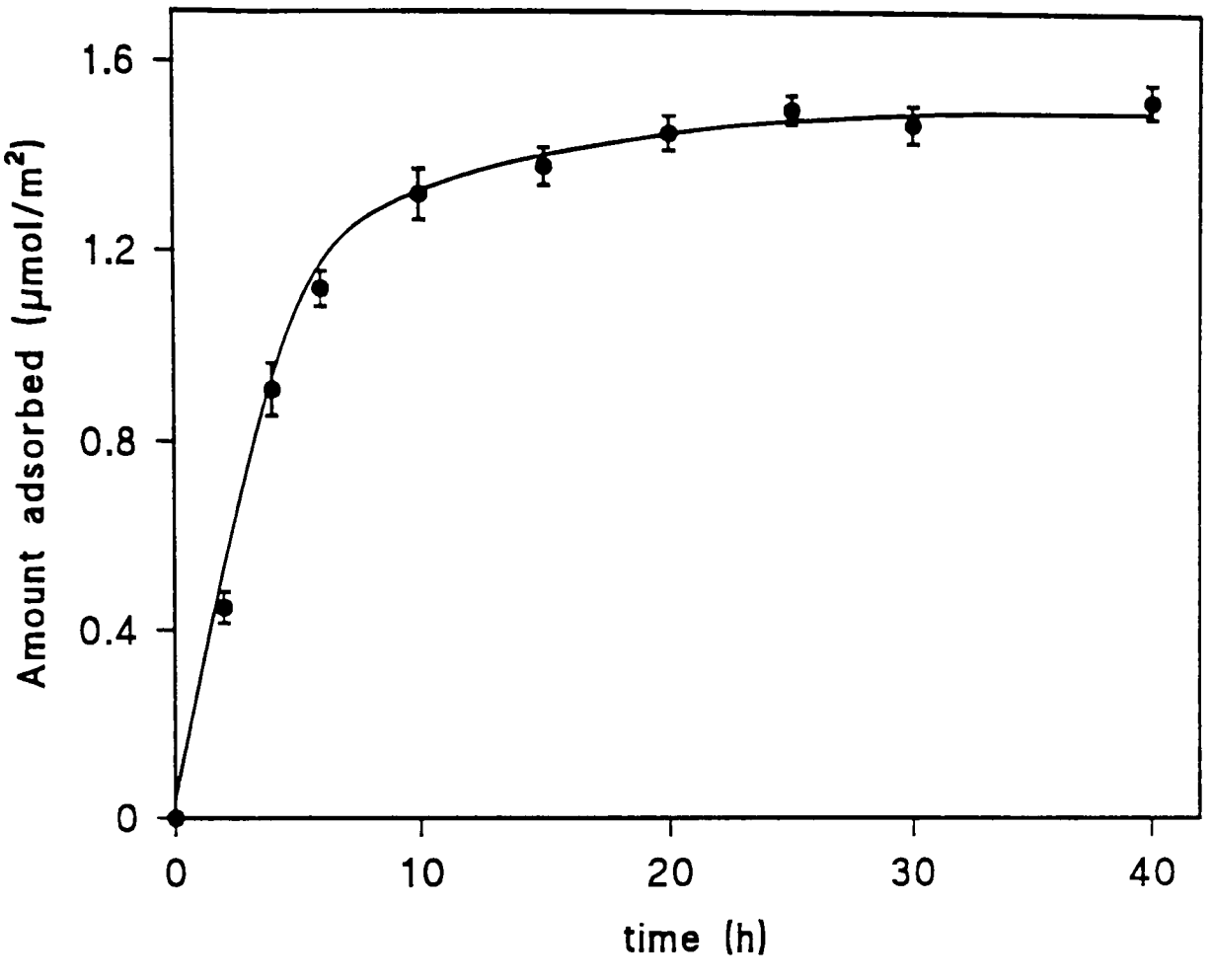

Figure 5.4(a) Time dependency of the extent of adsorption of TX−100 from aqueous solution at 298K.

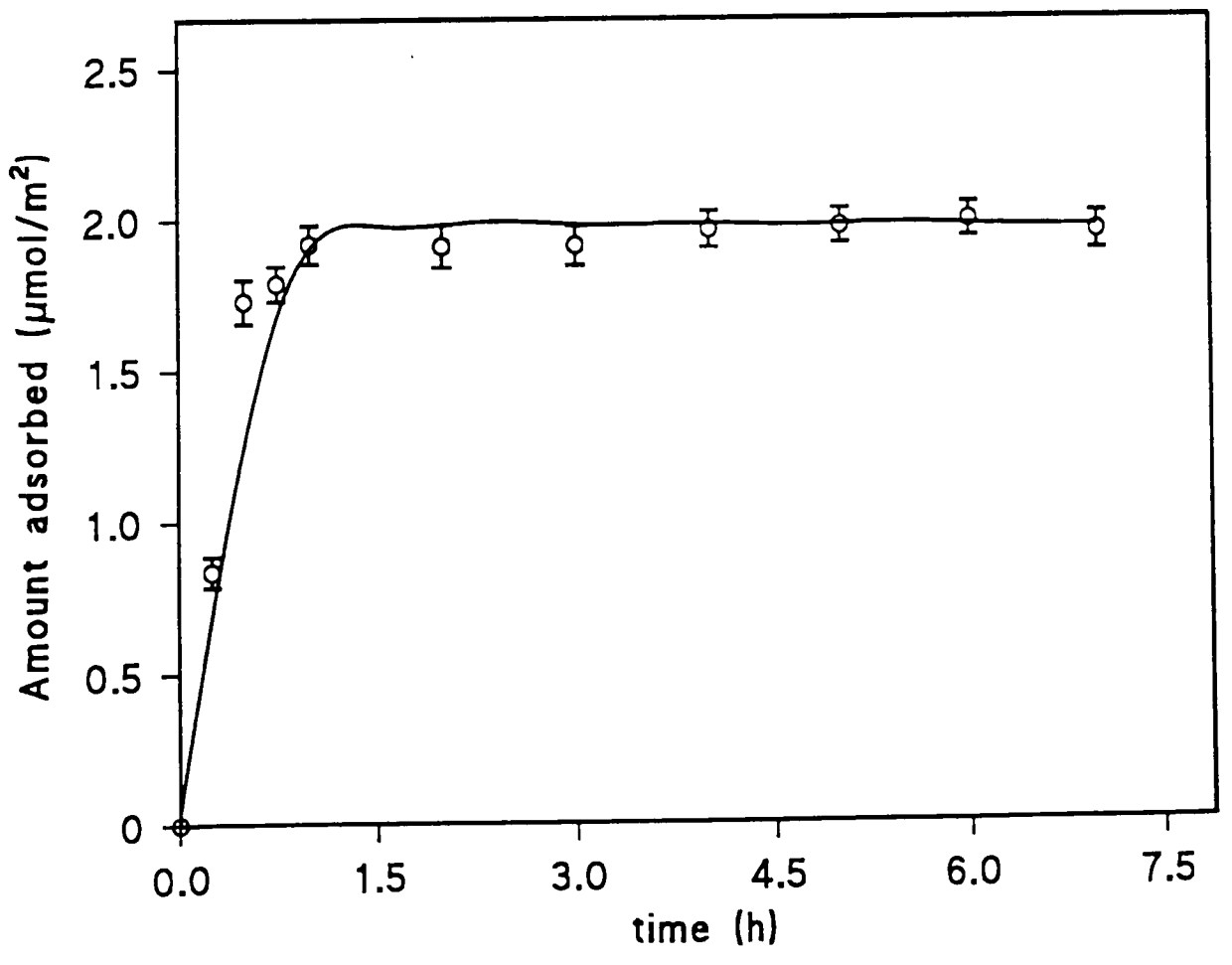

Figure 5.4(b) Time dependency of the extent of adsorption of TX−100 from organic solvent (decane) at 298K.

5.4.6 Summary of Possible Errors in Experimental Methods

(i) The action of solvents on minerals can cause particles from the solid to remain in suspension even after centrifuging. This can result in apparent extra absorption or diffusion of the UV beam, leading to a spuriously large value for the surfactant concentration.

(ii) It is vital to maintain the same solid/liquid ratio at all points in preparing the adsorption isotherm. Variation in this parameter affects the final pH of the solution, which in turn can have an adverse effect on the adsorption equilibrium.

(iii) When the effect of temperature on adsorption from the non-aqueous solutions (i.e. hydrocarbons and alcohols), is studied solvent evaporation can alter the equilibrium surfactant concentration. It can be prevented by using the sealed sample tubes.

(iv) The solvents have an effect on shifting the maximum absorbance of the surfactant. It is important to have the same solvent in the reference cell of the spectrophotometer.

(v) Other errors are those associated with surfactant solution preparation, weighing of the quartz and calculation of equilibrium concentration values from calibration graphs.

5.5 RESULTS AND DISCUSSION

5.5.1 Ion-Exchange Chromatography (IEC)

In order to determine the effect of the acid wash treatment of the quartz sample (i.e. anions and cations) a qualitative ion-exchange chromatographic analysis has been carried out at 298K. The chromatograms of water washed untreated and water washed acid treated quartz for the *anions* are presented in Figure 5.5. It is observed that the acid wash treatment removes the anions (Cl^- and SO_4^{2-}) significantly. However, the chromatographic profiles for water-washed untreated and water-washed acid treated quartz for the cations (Na^+, NH_4^+ and K^+) show that the acid treatment has a smaller effect on the *cations* of the quartz sample (see Figure 5.6).

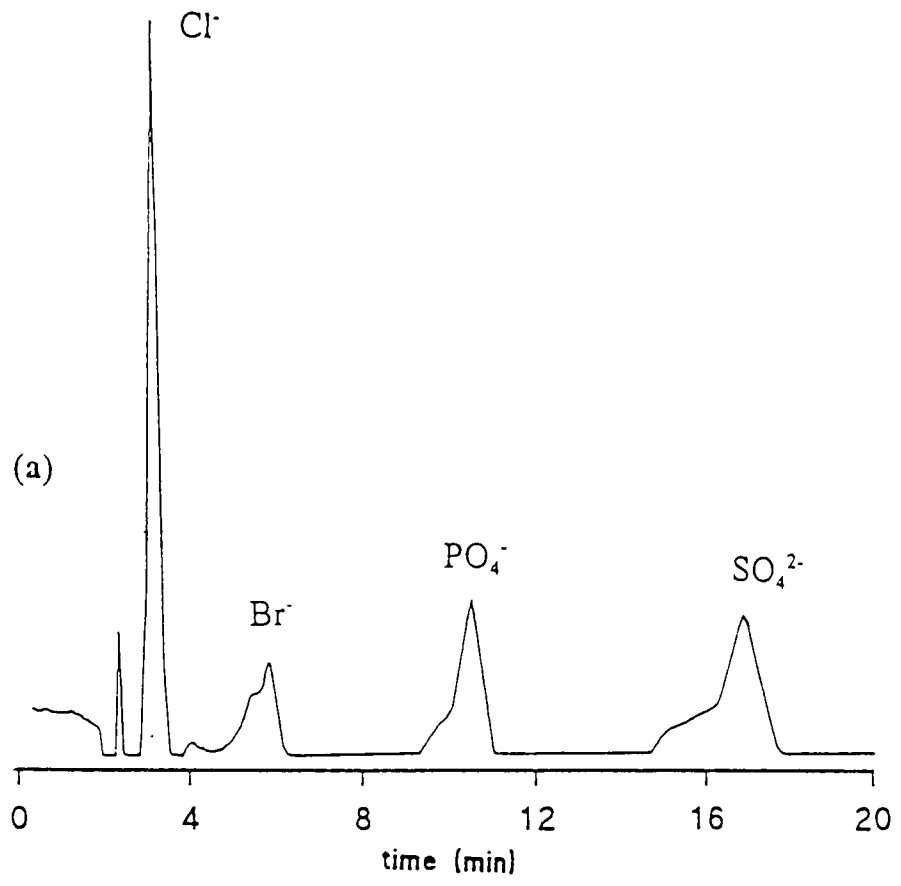

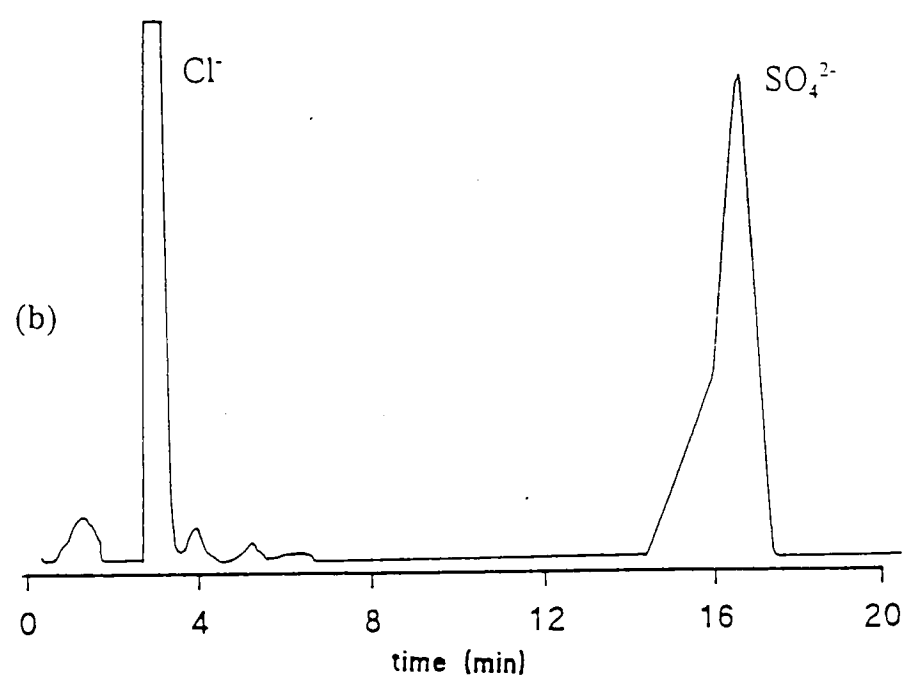

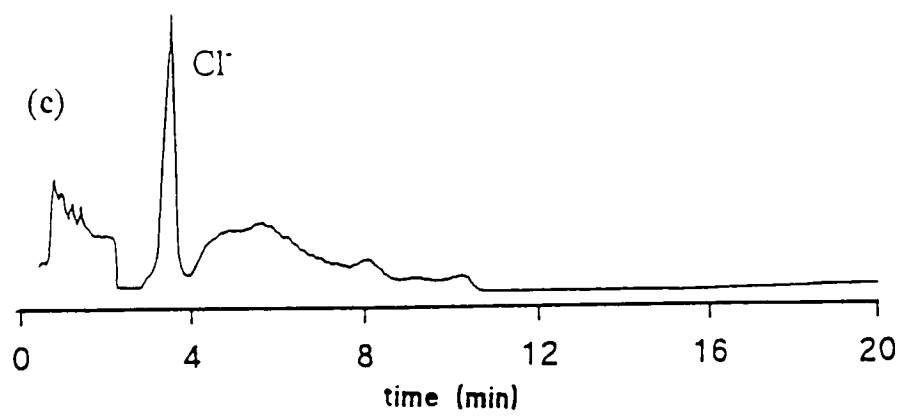

Figure 5.5 Ion-exchange chromatographic profiles for; (a) standard aqueous solution (5ppm) of Cl^-, Br^-, PO_4^- and SO_4^- anions, (b) water washing of untreated quartz and (c) water washing of acid washed quartz.

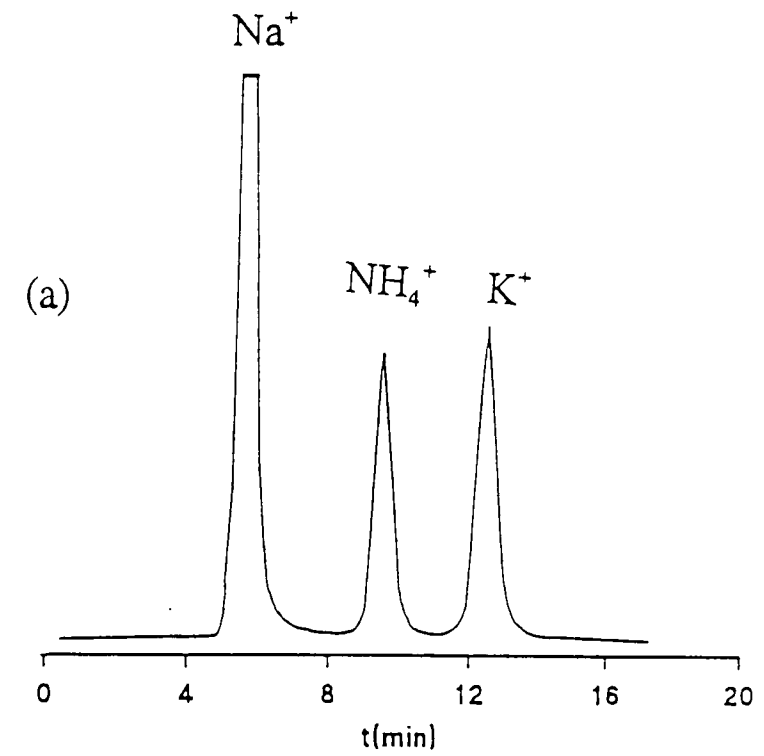

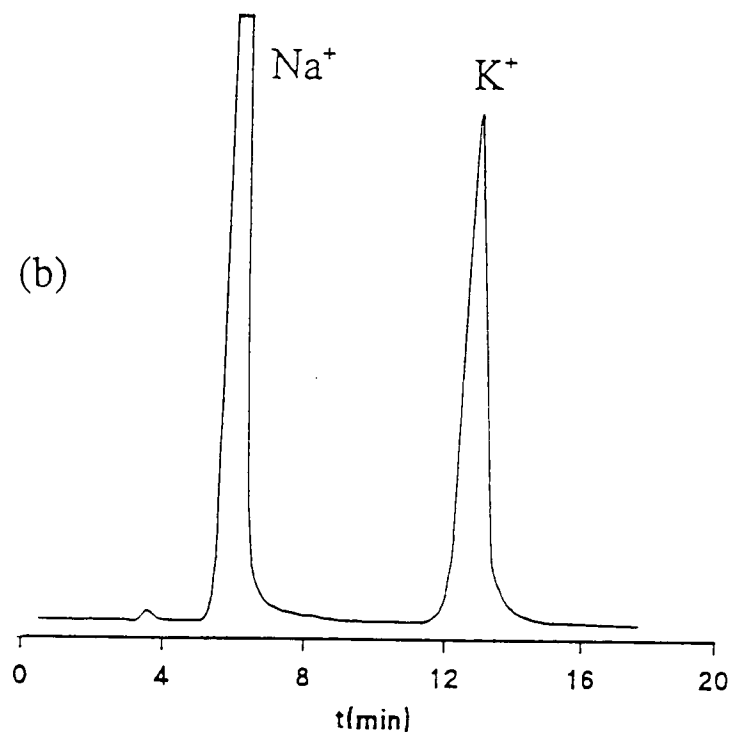

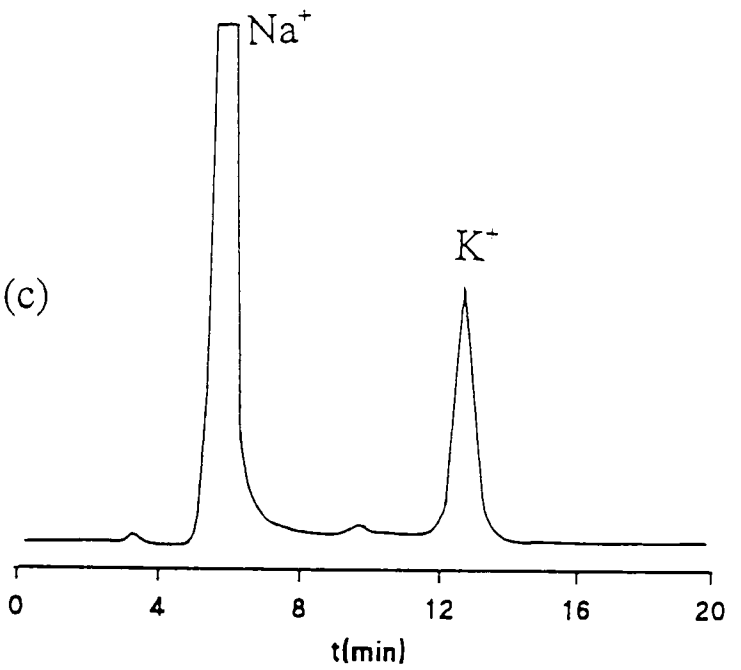

Figure 5.6 Ion-exchange chromatographic profiles for; (a) standard aqueous solution (5ppm) of Na^+, NN_4^+ and K^+ cations, (b) water washing of untreated quartz and (c) water washing of acid washed quartz.

5.5.2 Thermogravimetric Analysis

In order to know the effect of thermal treatment on the hydroxyl contents of the quartz, a thermogravimetric study was carried out under controlled conditions. The thermoanalytical curves for uncalcined and calcined quartz samples are given in Figure 5.7. Thermogravimetric measurements for uncalcined samples show that weight loss is a single step process which is initiated around 560K. Close inspection of the curve reveals, that the process is accelerated at 680-710K and at T>1173K no weight change is observed. The temperature at which weight loss is initiated is quite high indicating that a quartz sample may not have any physisorbed or free water. The TG curve for the calcined quartz sample (Qz1) also exhibits a similar single-step gradual weight loss which started around 540K. The TG curves for quartz sample thermally treated for a prolonged period (Qz10) is completely flat. This suggests that a quartz sample calcined for a prolong period may not have a high hydroxyl content or that the concentration is too low to be detected by our system.

From thermogravimetric data, the concentration of hydroxyl group per nm^2 was determined as follows:

$$OH/nm^2 = \frac{Weight\ loss(g)}{Initial\ weight(g)} \cdot \frac{K}{S} \qquad (5.14)$$

where S = quartz specific surface area (nm^2/g) and K = constant obtained considering the formation of an H_2O molecule from the condensation of two OH groups, and calculated by;

$$K = \frac{2OH}{H_2O.18\ g/mole}.6.023x10^{23}\ molecule/mole$$

The hydroxy contents for different systems determined by the above expression (given in Table 5.1) indicate that the hydroxyl contents are quite large for an uncalcined sample, but when the sample has been calcined for 1h that amount decreases abruptly. A decrease in the surface area of the quartz was observed as the calcination temperature increased. The

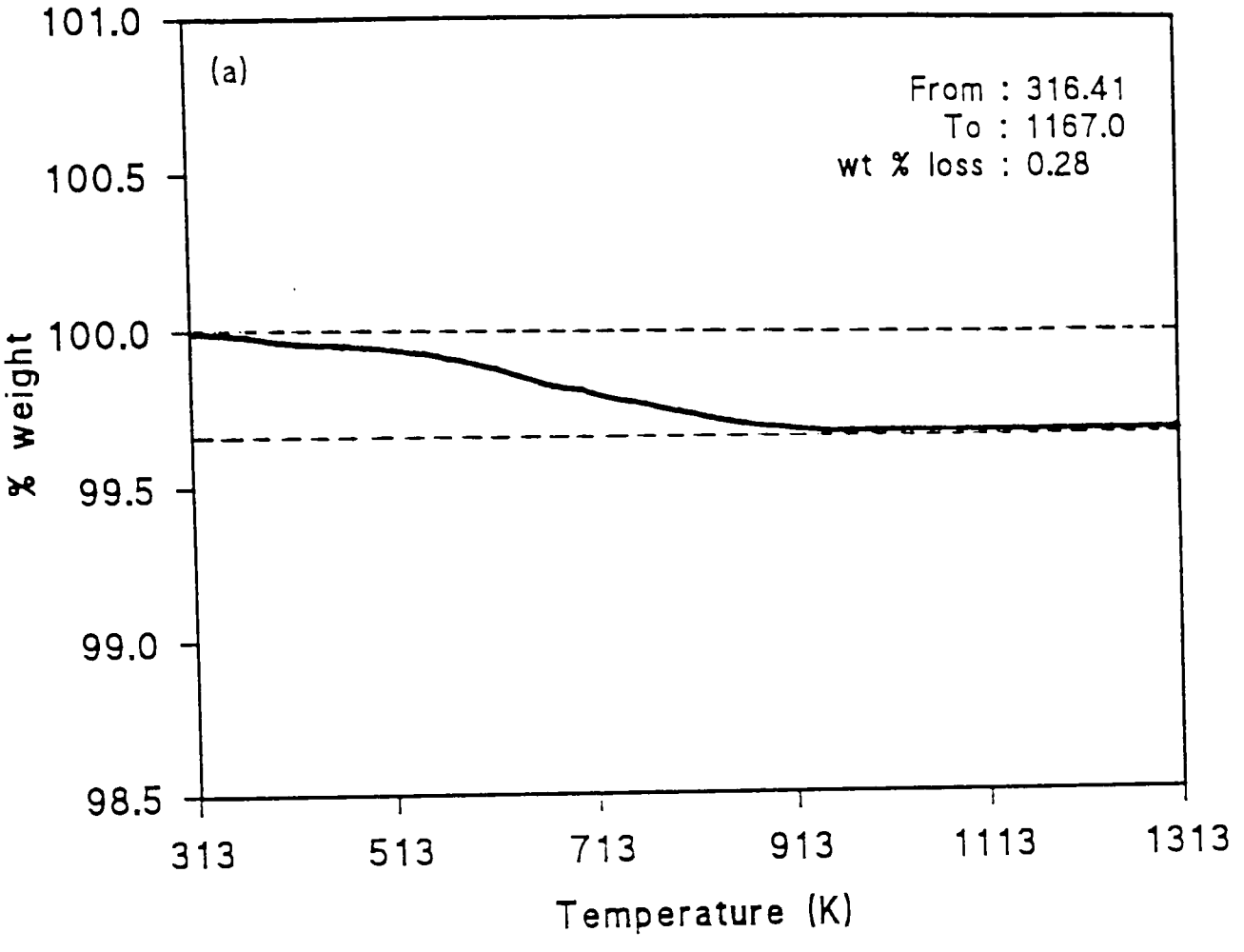

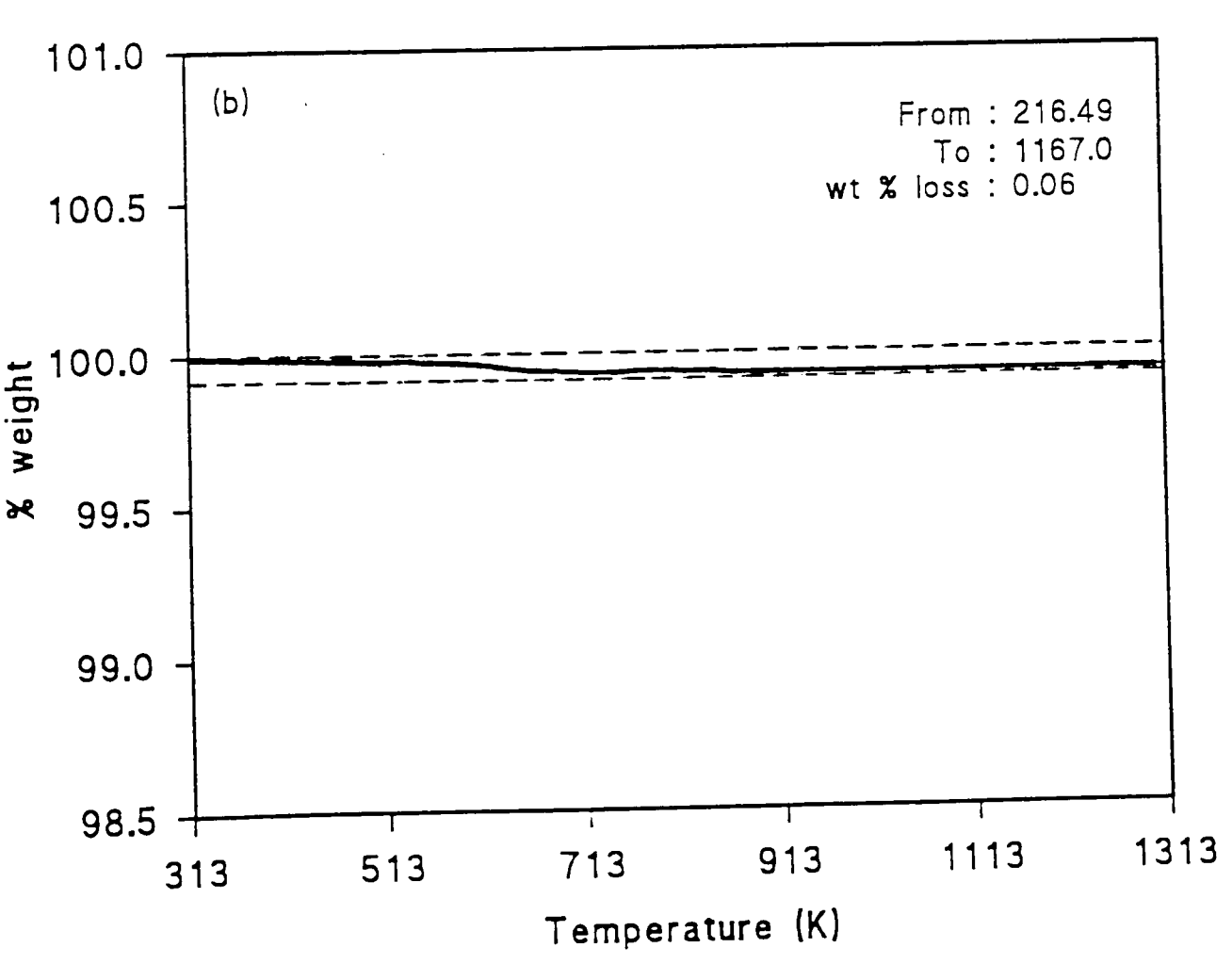

Figure 5.7 Thermogravimetric analysis; (a) uncalcined quartz (Qz) (b) 1h calcined quartz (Qz1).

effect of thermal treatment on the nature and calcination of hydroxyl contents of the quartz samples was also investigated by FTIR [44].

Table 5.1 Thermogravimetric data and BET surface area of the quartz sample

Sample	Total weight loss (%)	OH contents nm^{-2}	Kr BET surface area (m^2/g)
Qz	0.28	44.00	4.22 ± 0.01
Qz1	0.06	9.51	4.01 ± 0.01
Qz10	0.00	0.00	3.77 ± 0.01

5.5.3 Adsorption Isotherm

Adsorption isotherms of TX-100 on uncalcined and calcined quartz samples were collected in the temperature range of 303-333K. All the adsorption isotherms obtained were of S-shape [43], which is an indication of a cooperative mechanism of adsorption. The behaviour is true for all the quartz samples despite the great difference in their surface OH populations. These results are consistent with literature [33] which indicates that initially, isolated molecules are anchored on the surface by H-bonds between the silanol and the oxygen atoms of the oxyethylenic chain. Then there is an aggregation process around these first adsorbed molecules, leading to the formation of surface micelles. This two-step mechanism was also observed by many other authors, who showed by using fluorescence decay, neutron reflection or small-angle neutron scattering that surface aggregates are very similar to bulk micelles.

5.5.4 Effect of Calcination on Surfactant Adsorption

Figure 5.8 shows the adsorption isotherms of uncalcined and calcined silica at 298K. The extent of adsorption or plateau value appeared to be much higher with the calcined quartz than uncalcined one under the same experimental condition. From the characterisation results of the silica (FTIR and TGA), it is clear that heating this at 1273K for 10h removes the OH group from the surface and hence produces more sites for the surfactant adsorption. Calcination at 1173K reduces the surface area of the silica from 4.22 m^2/g to

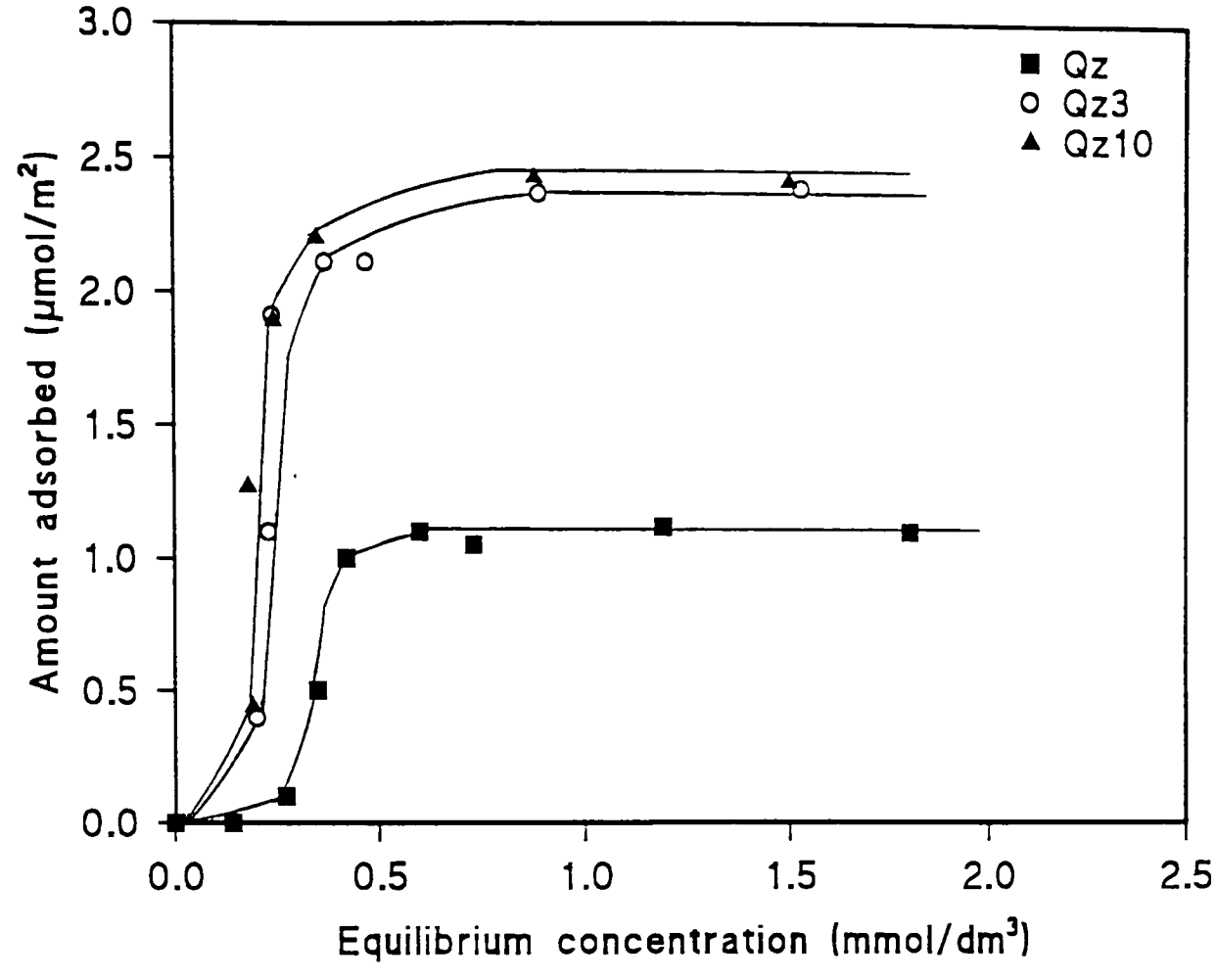

Figure 5.8 Effect of calcination on the extent of adsorption of TX-100 onto quartz from aqueous solution at pH 7 and 298K.

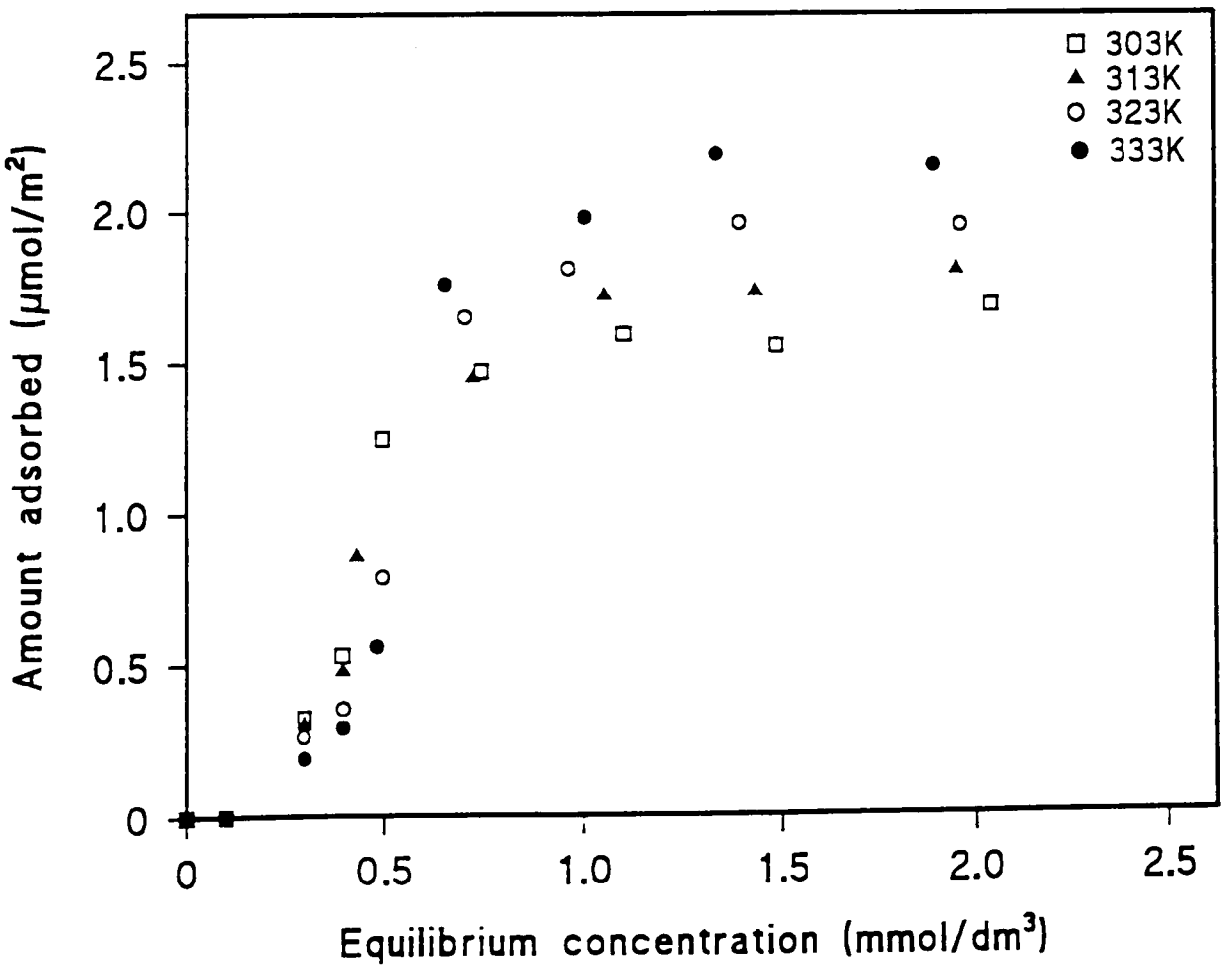

Figure 5.9 Effect of temperature on the extent of adsorption onto quartz (Qz) of TX-100 from aqueous solution at pH 6.8.

3.77 m^2/g (see Table 5.1). Variation in the number of silanol groups can alter the silica adsorption properties; specifically the number of hydroxyl groups can be diminished by heating. Below 400K only the removal of physisorbed water is achieved, silanol groups being eliminated to condense at higher temperatures [44]. It has been proposed [45] that the surface OH group of the silica are responsible for the formation of hydrogen bonds between the silica surface and the surfactant during the adsorption and it must be expected that if the number and nature of the OH groups on SiO_2 samples are changed, then the interactions of the surface produced with Triton during adsorption will also be altered.

The reactivity of quartz is known to depend on the number and nature of the surface hydroxyl groups, via which the surfactant molecules form H-bonds. Varying the numbers of silanol groups therefore can modulate the adsorptive properties of the silica. On heating the quartz the number of OH groups on the surface of the silica decreases; heating at 1273K is known to result in the complete removal of the OH groups from the surface. When an adsorption isotherm is measured using a calcined silica sample, rehydroxylation of the sample cannot be ruled out. The influence of temperature and the duration of hydrothermal treatment on the pore structure of silicas has been investigated [46]. It was found that although the specific surface area of the silicas as reduced upon heat treatment, the mean pore diameters vastly increased. It is possible that the micropores present in the silica samples are changing to mesopores on heat treatment. The BET results (Table 5.1), however, show a decrease in surface area of the adsorbent on calcination. The decrease in area per molecule (i.e. 1.27 to 0.69 nm^2/molecule, Figure 5.8) therefore is not due to increased porosity but is probably due to better packing of the molecules.

5.5.5 Effect of Temperature on Surfactant Adsorption

Figure 5.9 shows the effect of temperature on the extent of adsorption of TX-100 on the quartz sample (Qz) in the temperature range of 303-333K. All the isotherms are S-shape and at low coverage, the amount adsorbed decreased with increasing adsorption temperature. Probably, a higher temperature decreased the number of contact points between the polar chain and the surface, thus decreasing the extent of adsorption of

monomers. This is in general agreement with the literature [47,48]. Also, at this stage in the adsorption process exothermicity is noted and therefore it follows that the amount of adsorbed surfactant will be lower when energy is added to the system. At the position on the isotherm where the process is endothermic (and driven by micellisation rather than individual monomer interactions with the surface), the opposite is true and adsorption is enhanced by the extra energy available. At this stage the adsorption process is driven by the *lateral* interactions between the hydrocarbon tails of the surfactant molecules, and the process is thought to be equivalent to micellisation in solution [49].

An increase in the adsorption temperature shifts the position of the plateau towards the lower concentrations, which is due the decrease in the CMC (the onset of the plateau always happens close to the CMC). The elevation of the adsorption temperature stabilizes aggregates (both micelles and surface aggregates). Denoyel and Rouquerol [50] also observed the same effect and emphasized that at high coverage, the adsorption is governed by interactions between adsorbate segments not in contact with the surface. The amount adsorbed at the plateau as a function of temperature is shown in Table 5.2.

Table 5.2 Effect of temperature on the adsorption of TX-100 at plateau from the aqueous solution of 1.5mmol/dm^3.

Temperature (K)	Amount adsorbed at plateau (μmol/m^2)
303	1.62
313	1.71
323	1.85
333	2.13

5.5.6 Effect of Salinity on Surfactant Adsorption

The effect of introducing a singly charged cation/anion (i.e. NaCl) (in the range of 1-10 g/100cm^3) on the adsorption of TX-100 onto quartz (Qz) at 303K is shown in Figure 5.10. All the adsorption isotherms are S-shape and the extent of adsorption increases with

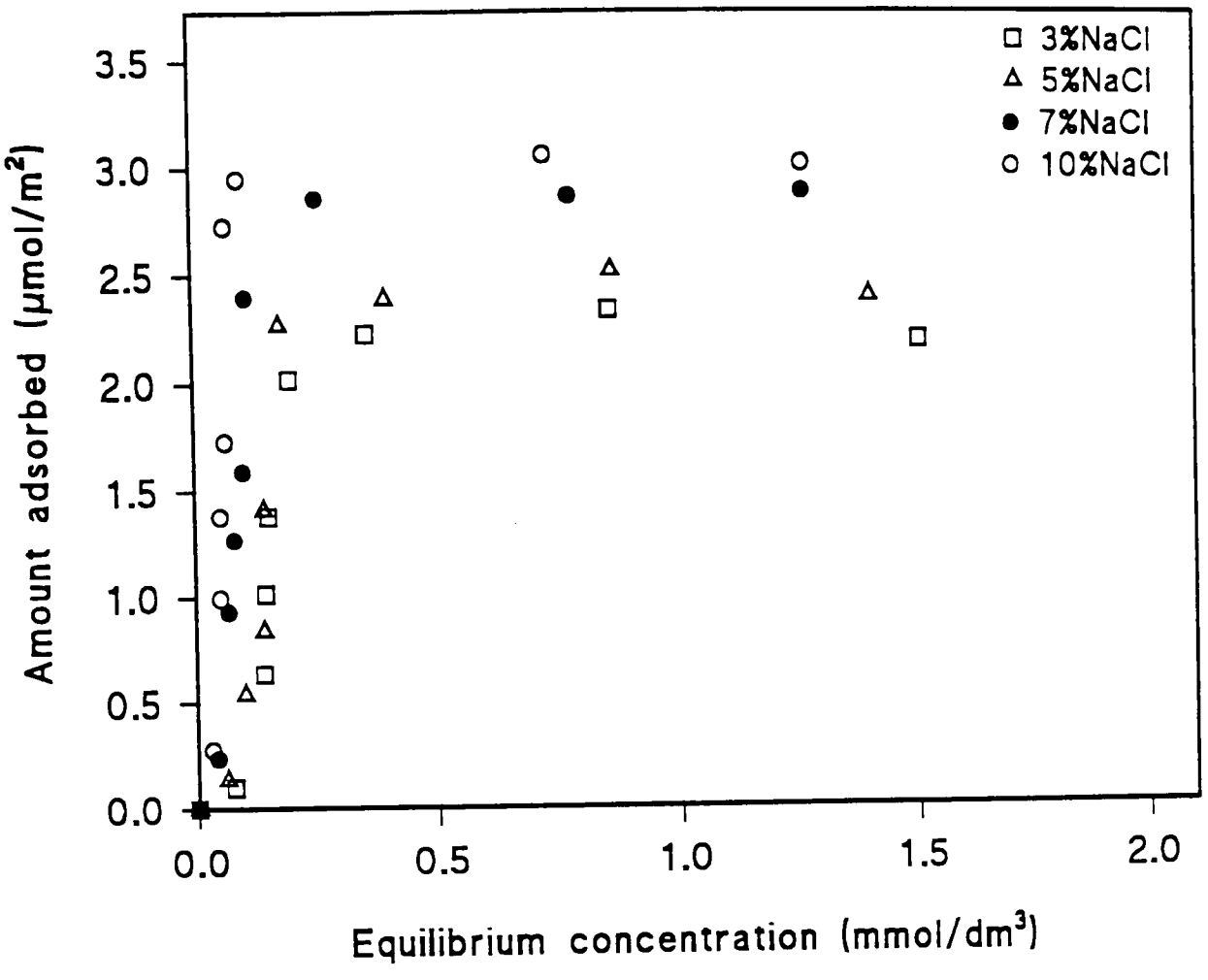

Figure 5.10 Effect of salinity on the extent of adsorption onto quartz (Qz) of TX−100 from aqueous solution at 303K.

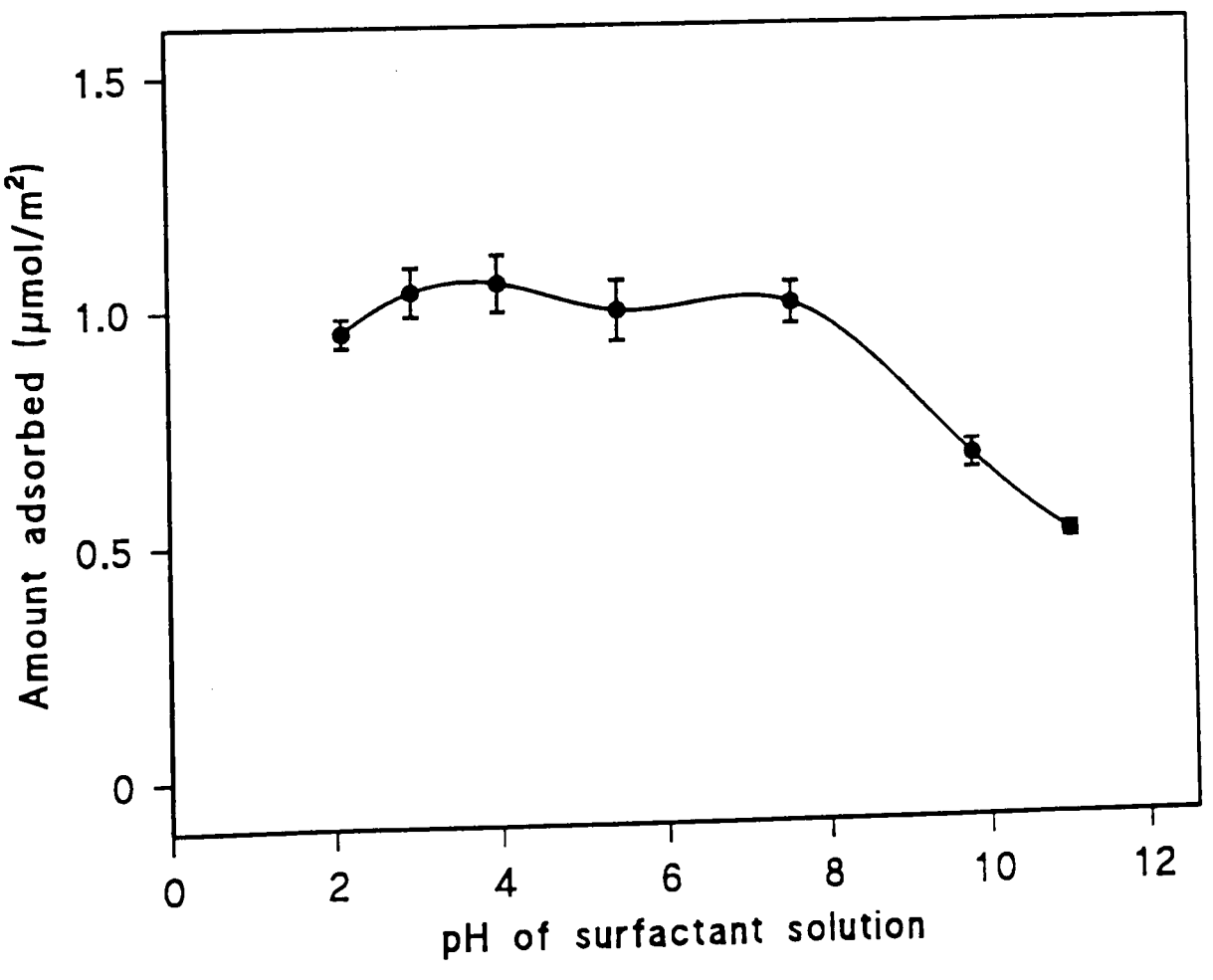

Figure 5.11 Effect of pH on the extent of adsorption onto quartz (Qz) of TX−100 from aqueous solution at 298K and a concentration of 0.5 mmol/dm^3

increasing electrolyte concentration. The isotherms reach a plateau at a concentration which is somewhat above the CMC of the surfactant in the aqueous solution. When an electrolyte is added, it is observed that the plateau value is obtained at even lower surfactant concentrations. The trend in CMC is also the same (i.e. an addition of salt decreases the CMC due to a lowered electrostatic repulsion between the head groups in the presence of the electrolyte [50]).

As the salinity is increased the system becomes more hydrophobic, so that the surfactant molecules have less interaction with the solvent and adsorb more strongly onto the surface of the quartz. The ions in solution may also form a complex with the quartz surface which would increase the surfactant adsorption. In ionic solutions the presence of a diffuse electrical double layer surrounding the surface prevents the coagulation of a mineral oxide [51]. At a pH value of approximately 5, the quartz surface carries a slight negative charge due to the zero point charge of silica being in the region of 2 [50], and so a diffuse layer of positively charged ions may develop about the surface [52]. This layer may not only stabilise the quartz suspension but also attract the electron-rich oxygen atoms of the polyethylene oxide chains of the surfactant molecules towards the surface and thus induce the adsorption process to begin at lower equilibrium concentrations. The amount adsorbed at the plateau as a function of the electrolyte concentration is shown in Table 5.3.

Table 5.3 Effect of salinity on the adsorption of TX-100 at plateau from the aqueous solution of 1.2mmol/dm^3 at 298K.

Concentration of NaCl (g/100cm^3)	Amount adsorbed at plateau (μmol/m^2)
3	2.23
5	2.41
7	2.87
10	3.02

5.5.7 Effect of Hydronium Ion Concentration on the Adsorption of TX-100

The effect of hydronium ion on the adsorption of surfactant was also studied and results are given in Figure 5.11. It was observed that the amount adsorbed onto quartz did not change appreciable in the pH range of 2-8, where as above pH 8, a drastic decrease of amount adsorbed occurred. This indicated that hydrogen bonds are most probable between the polar chain of the non-ionic surfactant and the silanol groups of the surface. At pH 2, the number of uncharged sites is at a maximum, and a greater amount of surfactant can be adsorbed. The surface charge increases with pH, thus decreasing the amount of undissociated silanol groups which are the adsorbing sites for non-ionic surfactants.

5.5.8 Effect of Ethoxylate Chain Length on the Adsorption

In order to study the effect of ethoxylate chain length, adsorption isotherms of Triton series of surfactants were also investigated at 298K from aqueous solutions. Figure 5.12 shows the extent of adsorption of the surfactants under the same experimental conditions. Again, all the adsorption isotherms are S-shape and the extent of adsorption decreases with increasing the EO units of surfactant molecule. Large hydrophilic head groups have more affinity for water and therefore less adsorption. The results show that changing the length of the polar chain is also a way of modifying the direct interaction between the nonionic surfactant and the surface. The main reason being the decrease in solubility at lower chain length and hence a preference for adsorption.

Table 5.4 Effect of ethoxylate chain length on the adsorption of TX-100 at plateau from the aqueous solution of 1.5mmol/dm^3 at 298K.

Surfactant	EO units	Amount adsorbed at plateau (μmol/m^2)
TX-114	7.5	2.55
TX-100	9.5	1.57
TX-165	15	1.03
TX-305	30	0.65

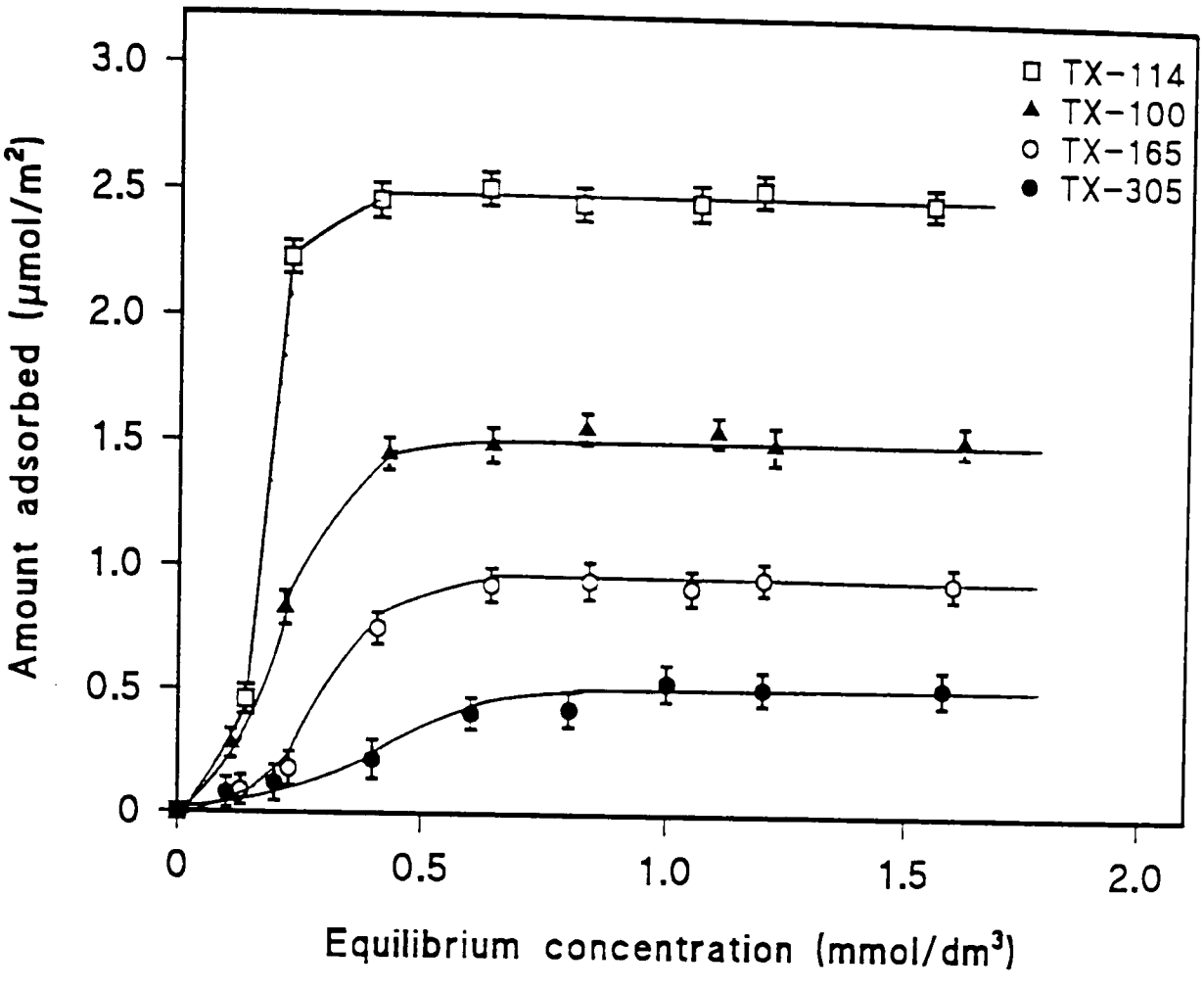

Figure 5.12 Effect of hydrophilic chain length on the extent of adsorption onto quartz (Qz) of TX-100 from aqueous solution at pH 6.8

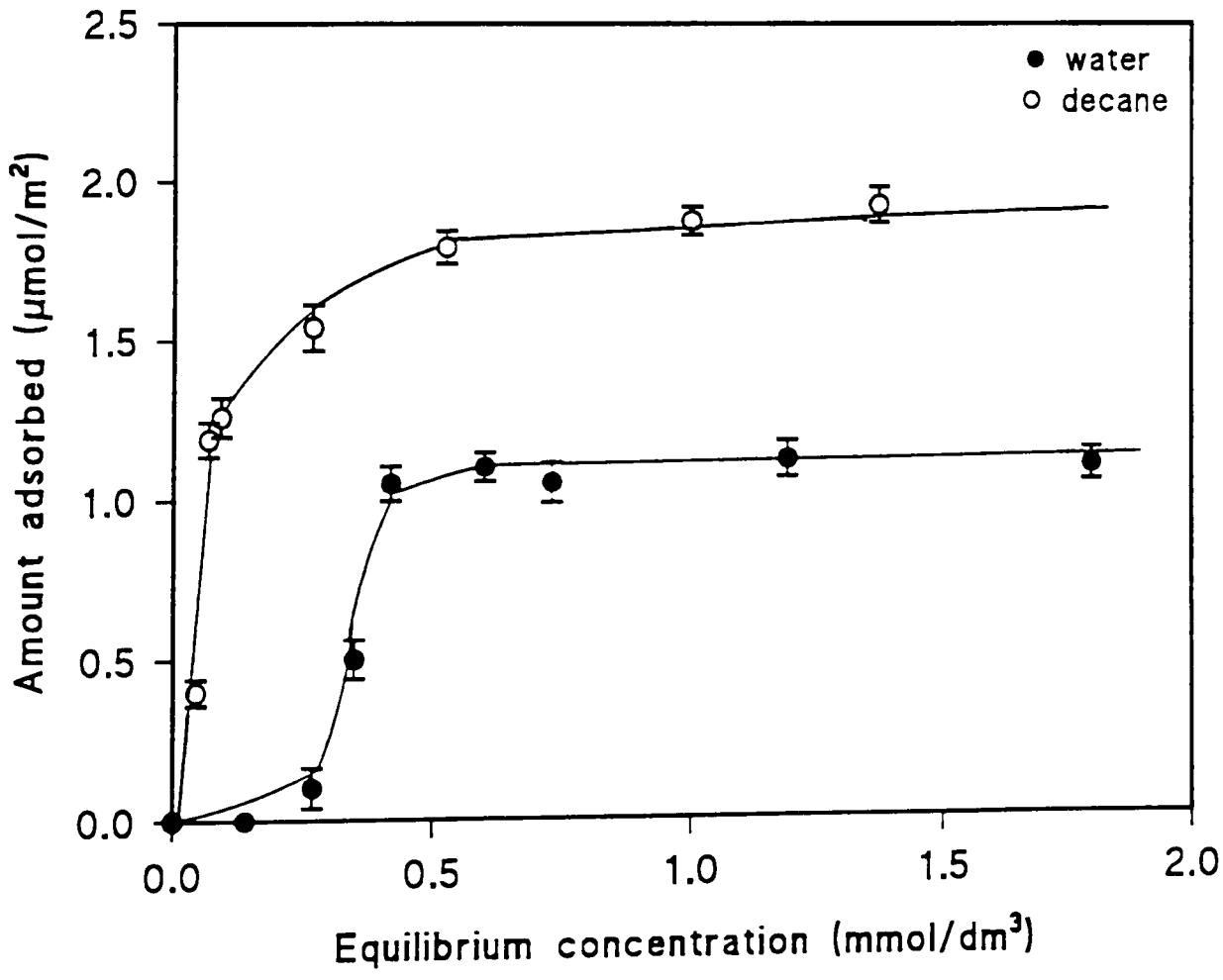

Figure 5.13 Extent of adsorption of TX-00 onto quartz (Qz) from the aqueous and non-aqueous solutions at 298K.

5.5.9 Adsorption From Non-aqueous Solutions

In order to predict the adsorption behaviour of the model surfactant in a real system, it was important to study the adsorption from hydrocarbons. The adsorption isotherm from the organic solution (decane) at 298K is shown in Figure 5.13. The isotherm from the nonaqueous solvent is L-shape which is different from the adsorption isotherm from aqueous solution, S-shape . The extent of adsorption of the surfactant is much higher in the hydrocarbon environment than the aqueous solutions (i.e. the plateau value is 1.2μmol/m^2 from the aqueous solution and 1.8 μmol/m^2 from the organic solvent for the TX-100). This can be explained by considering the interactions between the solvent and the adsorbate (surfactant). As the surfactant molecule has large hydrophilic head group, therefore in the organic environment, it has less affinity for the solvent than the adsorbent. On the other hand, in the aqueous media the surfactant has great affinity for the solvent and there is competition between the solvent and the adsorbate for the adsorption sites on the silica surface.

5.5.10 Effect of Alcohol on the Adsorption of TX-100

The importance of knowing the adsorption behaviour of a surfactant from an alcohol solution is correlated to the use of microemulsion as flooding systems in enhanced oil recovery. As defined previously, a microemulsion is a homogeneous mixture of water, surfactant, co-solvent and oil which is thermodynamically stable and it possesses the properties of oil as well as water [53-55]. This feature makes the solution very valuable for the proposed technological application. In the middle-phase microemulsion one has a comparable amount of water and oil (bicontinuous structure). The results of the gas chromatography (see Chapter 4) show that the co-solvent (normally a short or medium chain alcohol e.g. pentan-1-ol) and surfactant partitioned in the organic phase as well as the aqueous phase.

(i) Effect of Alcohol on the Adsorption of TX-100 from Non-aqueous Solutions

The adsorption of TX-100 from decane was studied as a function of alcohol concentration (0-20% alcohol) at a constant temperature (298K) and the surfactant concentration

(1.9mmol/dm^3). The effect of alcohol chain length (propan-1-ol, pentan-1-ol, octan-1-ol and decan-1-ol) was investigated at a constant temperature (298K). Figure 5.14(a) shows that the extent of adsorption decreases as the alcohol concentration is increased at a constant temperature and concentration. A significant decrease in the adsorption of TX-100 is observed at the low concentration of alcohol. The effect of alcohol at low surfactant concentration (0.8 mmol/dm^3) is presented in Figure 5.14(b) which shows similar trend as at the high concentration of surfactant. The short chain alcohols seem to decrease the adsorption to almost zero at 15-20% of their concentrations. On the other hand, the long chain alcohols do not appear to decrease the adsorption to a zero value even at their high % concentration. The short chain alcohols are hydrophilic, therefore they have high affinity for the surfactants and prevent the adsorption.

(ii) Effect of Alcohol on the Adsorption of TX-100 from Aqueous Solutions

The effect of short chain alcohols (methanol, ethanol, propan-1-ol and butan-1-ol) on the adsorption on quartz of TX-100 from an aqueous solution (i.e. concentration 0.7mmol/dm^3 and 1.8mmol/dm^3) was also studied at 298K. Figures 5.15(a) and (b) also show that the extent of adsorption decreases as the alcohol concentration is increased at a constant surfactant concentration. The results show that the short chain alcohols also reduce the adsorption of TX-100 from an aqueous solution significantly. It is evident from the characterisation and adsorption results that a detailed knowledge of the mineralogy of the rock formation together with model adsorption studies can predict the behaviour of the injected surfactant solution (or microemulsion) in the real system.

5.5.11 Summary of Results

The information obtained from the adsorption studies can be summarised as follows:

(i) The acid-wash treatment of the quartz removes the anions and cations, however, the effect is larger for the anions.

(ii) The thermal treatment reduces the number of hydroxyl groups on the quartz surface.

(iii) The temperature affects the solubility of the adsorbate on adsorbent. Generally, an

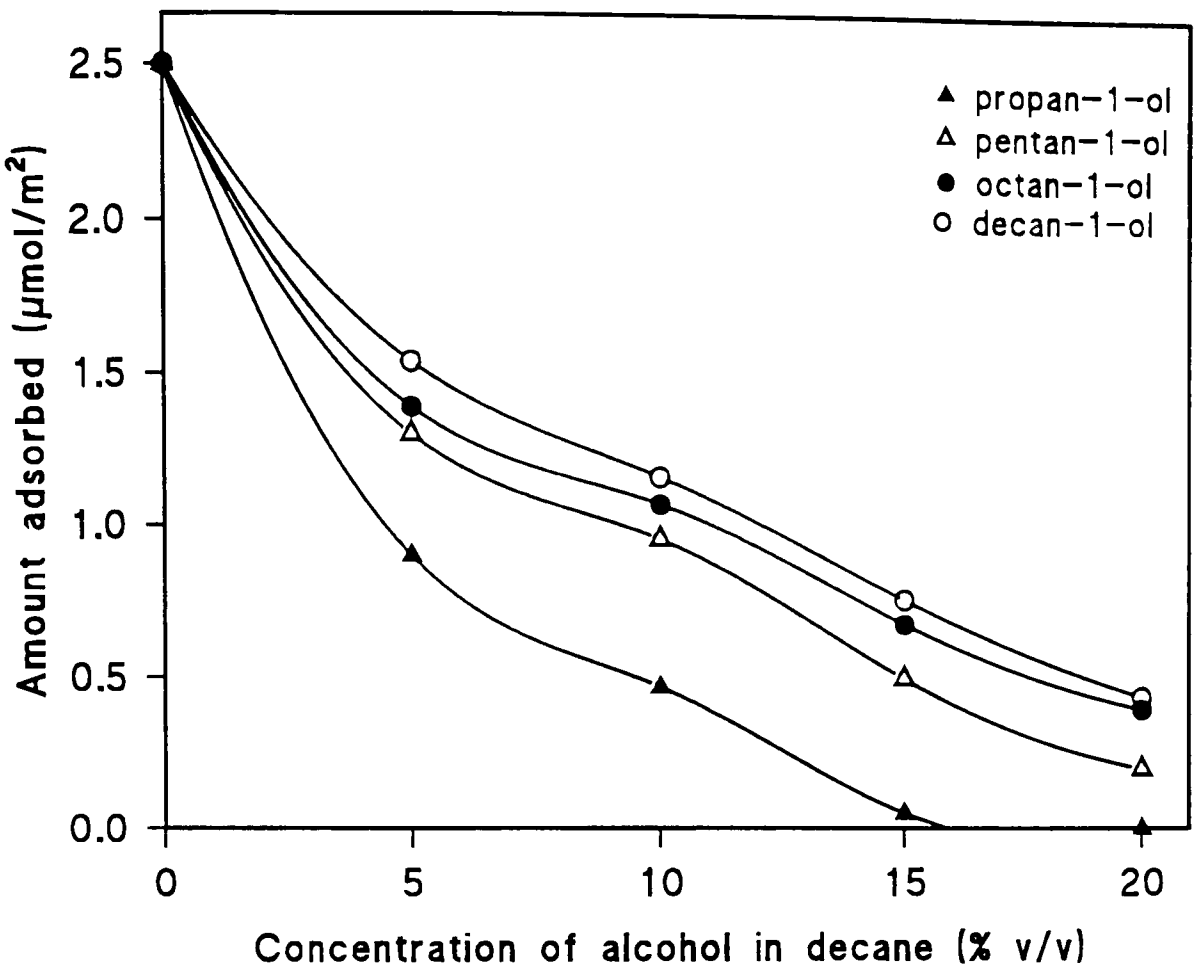

Figure 5.14(a) The effect of various concentrations of different alcohols present in a concentration 1.9mmol/dm^3 on the adsorption on quartz (Qz) of TX-100 in decane solution at 298K.

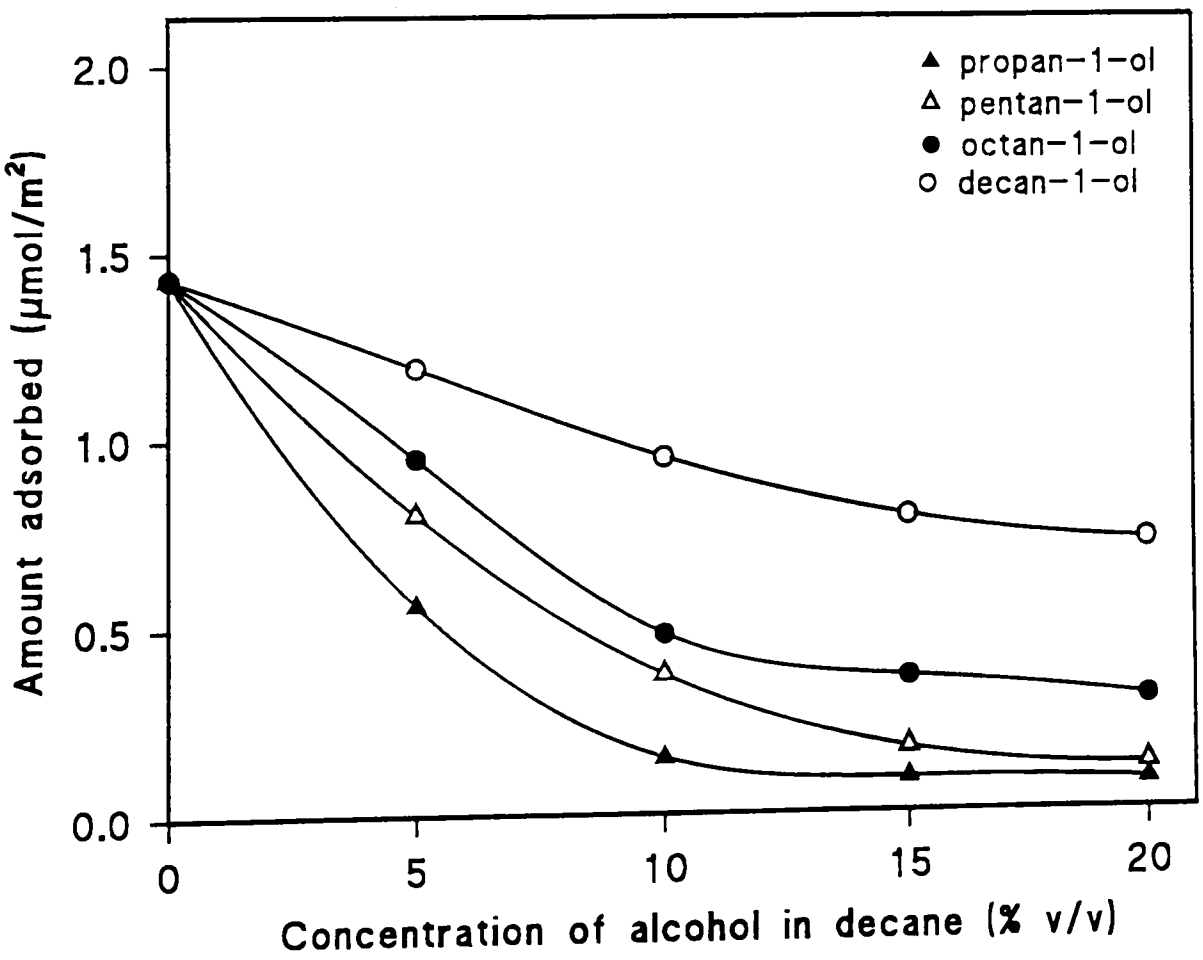

Figure 5.14(b) The effect of various concentrations of different alcohols present in a concentration of 0.84 mmol/dm^3 on the adsorption on quartz (Qz) of TX-100 in decane solution at 298K.

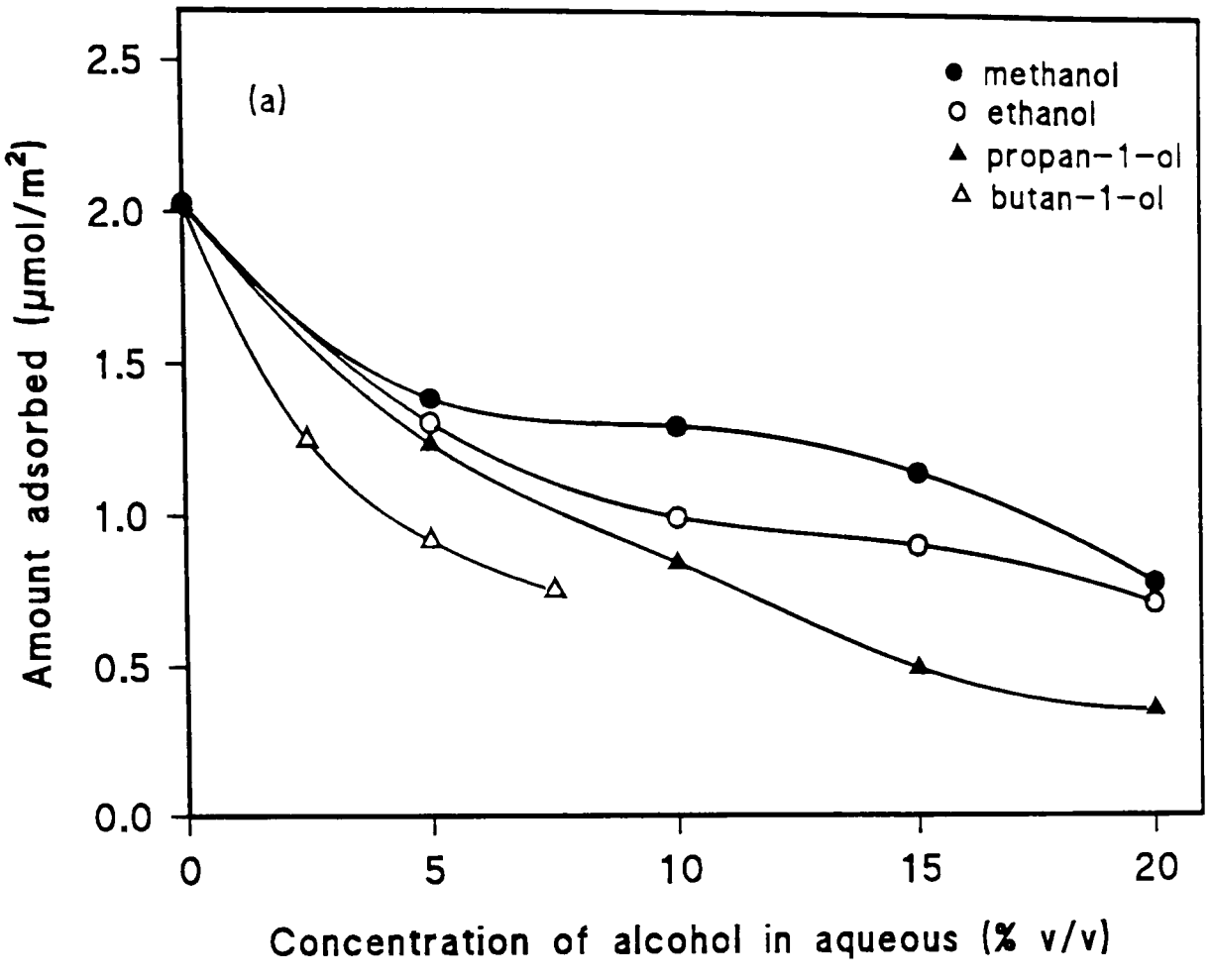

Figure 5.15(a) The effect of various concentrations of different alcohols present in a concentration 1.95 mmol/dm^3 on the adsorption on quartz (Qz) of TX-100 in aqueous solution at 298K.

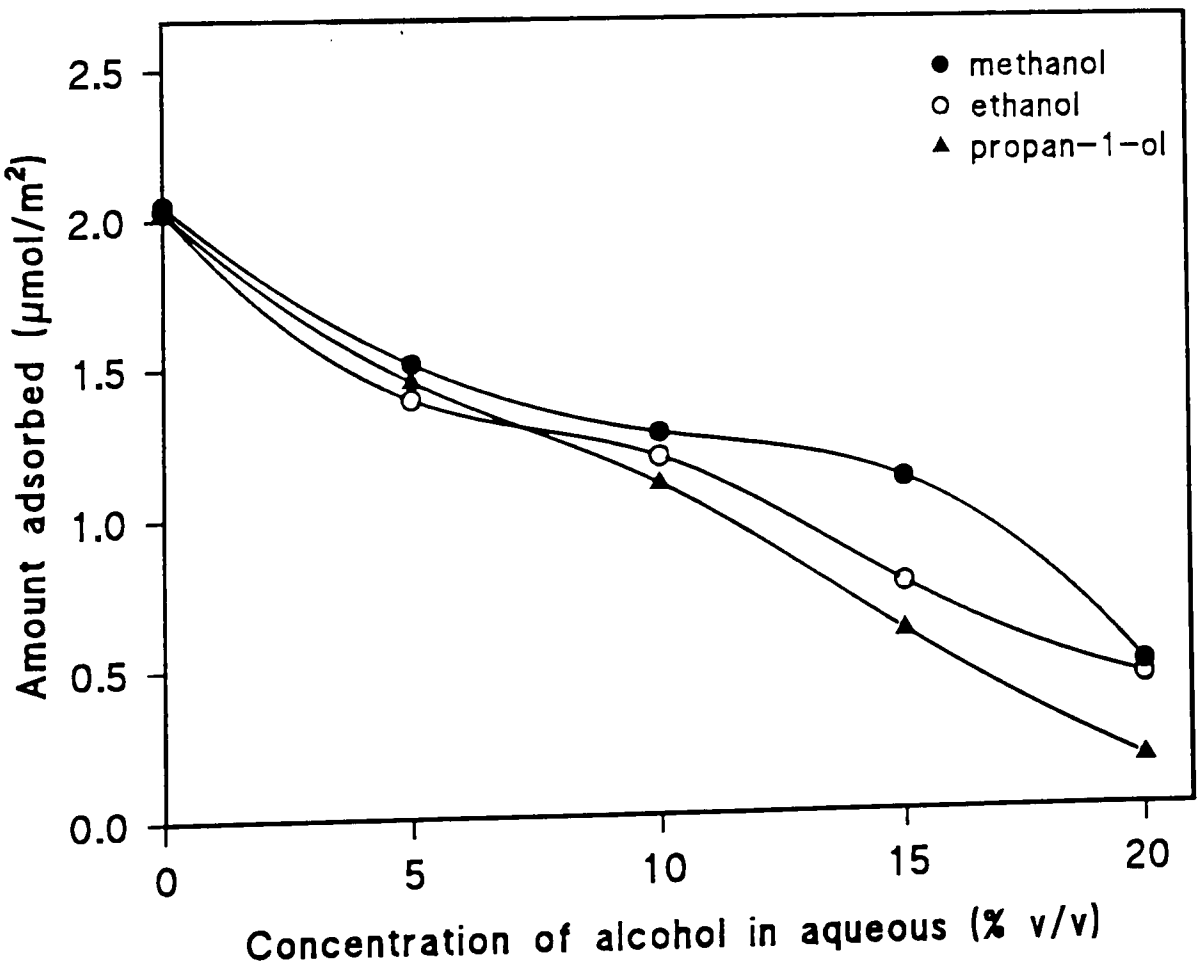

Figure 5.15(b) The effect of various concentrations of different alcohols present in a concentration 0.85mmol/dm^3 on the adsorption on quartz (Qz) of TX-100 in aqueous solution at 298K.

increase in temperature increases the solubility and thus adsorption is reduced. However, the reverse is true for surfactants at, or nearing, their cloud point.

(iv) The extent of adsorption of surfactant decreases with increasing ethoxylate chain length of surfactant.

(v) The extent of adsorption of surfactant is much higher in the hydrocarbon environment than the aqueous solutions.

(vi) The presence of alcohol reduces the extent of adsorption of surfactants by increasing their solubility in aqueous and non-aqueous solutions.

(vii) The amount of adsorption of surfactant increases with increasing electrolyte concentrations.

References

[1] L. Thompson, J. Colloid Interface Sci.. **163**, 61 (1994)

[2] N. Azemar, I. Carrera, and C. Solans. J. Disp. Sci. Tech., **14**, 645 (1993)

[3] G.Y. Drachev, I.V. Semiletova, N.Y. Kovarski, Colloid Journal, **56**, 34 (1994)

[4] T.H. Davies and P.D. Cottingham, J. Water Science Technology, **29,** 227 (1994)

[5] A. Delamaza and J.L. Parra, Textile Research Journal, **64,** 255 (1994)

[6] A. Delamaza and J.L. Parra, J. Soc. Dyers Colouristic, **110**, 64 (1994)

[7] A. I. Zouboulis, J. Minerals Engineering, **8,** 1477 (1995)

[8] C.A. Lucy and R.S. Underhill, J. Analytical Chem. **68,** 300 (1996)

[9] R. Sadler, H. Olszowy, G. Shaw, R. Biltoft and D. Connell, J. Water Air Soil Pollution, **78,** 189 (1994)

[10] N.A. Katsanos and F. Roubanikalantzopoulou, J. Chromatography A, **710**, 191 (1995)

[11] J.C. Means, J. Marine Chemistry, **51,** 1 (1995)

[12] F. Esmadi and J. Simm, Colloids and Surfaces A: Physicochemical and Engineering Aspects, **104,** 265 (1993)

[13] P. Janvion, S. Motellier and H. Pitsch. J. Chromatography A, **715**,105 (1995)

[14] B.L. Sorensen and R.J. Wakeman, J. Water Research, **30,** 115 (1996)

[15] A. Marcomini and M. Zanette, J. Chromatography A, **733,** 193 (1996)

[16] A.T. Kiewiet and P. Devoogt, J. Chromatography A, **733**,185 (1996)

[17] T. Cserhati and E. Forgacs, J. Chromatography A, **722**,33 (1996)

[18] D.B. Gupta and M.L. Gulrajani, J. Soc. Dyers Colouristic, **110,** 112 (1994)

[19] A. Delamaza and J.L. Parra, J. Soc. Dyers Colouristic, **110**, 64 (1994)

[20] L. Cohen, R. Vergara, A. Moreno and J.L. Berna, J. Am. Oil Chemists Soc., **70,** 725 (1993)

[21] S.G. Oh and D.O. Shah, J. Am. Oil Chemists Soc., **70,** 673 (1993)

[22] C.A. Miller and K.H. Raney, Colloids and Surfaces A: Physicochemical and Engineering Aspects, **74,** 169 (1993)

[23] R.C. Chiu and M.J. Cima, J. Am. Ceramic. Soc., **76,** 2769 (1993)

[24] T. Itoh, S. Masuda and F. Gomi, J. Electrostatics, **17,** 911 (1994)

[25] Y.C. Chiu and H.J. Hwang, Colloids and Surfaces A: Physicochemical and Engineering Aspects, **90,** 155 (1994)

[26] M. Korman, J. Vindevogel and P. Sandra, J. Electrophoresis, **15,** 1304 (1994)

[27] M.J. Lawrence, J. Chem. Soc. Rev. **23,** 417 (1994)

[28] I.V. Gorlov, V. Kim and Y.G. Frolov, Colloid Journal, **57,** 283 (1995)

[29] R. Denoyel, and J. Rouquerol, J. Colloid Interface Sci., **143,** 555 (1991)

[30] P. Levitz, H. Van Damme and D. Keravis, J. Phys. Chem., **88,** 2228 (1984)

[31] B. Tamamushi and K.Tamaki, Trans. Far. Soc. **55**, 1007, (1959)

[32] N.A. Klimenko, Koll. Zh. **42**,561,(1980)

[33] F. Giordano, R. Denoyel and J. Rouquerol, Colloid and Surfaces A: Physicochemical and Engineering Aspects, **71,** 293 (1993)

[34] M.W. Rutland and T.J. Senden, Langmuir, **9,** 412 (1993)

[35] K. Steinby, R. Silveston and B. Kronberg, J. Colloid Interface Sci., **155,** 70 (1993)

[36] J.X. Zhao and W. Brown, J. Colloid Interface Sci., **179,** 281 (1996)

[37] B. Tamamushi and K. Tamaki, Trans. Fara. Soc., **55**,1007 (1959)

[38] N.A. Klimenko, Kolloidn. Zh., **42**, 561 (1980)

[39] S.D. Faust and O.M. Aly, Eds., "Adsorption Processes for Water Treatment", Butterworth, London (1987)

[40] D.M. Young and A.D. Crowel, Eds., "Physical Adsorption of Gases", Butterworth, London (1962)

[41] F.W. Fifield and D. Kealey, Eds., "Analytical Chemistry", International Textbook Co., Ltd., London, (1983).

[42] J. Weiss, Ed., "Handbook of Ion Chromatography", Calif., (1986)

[43] C.H. Giles, D. Smith and A. Huitson, J. Colloid Interface Sci., **47,** 755 (1974a)

[44] D.M. Nevskaia, M.L.R. Cervantes, A.G. Ruiz and J.D.L. Gonzalez, J. Chem. Tech. Biotechnol., **63**, 249 (1995)

[45] F. Giordano, R. Denoyel and J. Rouquerol, J. Colloid Interface Sci., **165,** 82 (1994)

[46] A.V. Kiselev, V.M. Lukyanovich, Y.S. Nikitin, E.B. Oganesyan and A.J. Sarakhov, Kolloidn. Zh., **3**, 388 (1969)

[47] Th. Van den Boomgard, Th.F. Tadros and J. Lyklema, J. Colloid Interface Sci.. **116,** 8 (1993)

[48] P. Levitz and H.Van Damme, J. Phys. Chem., **90**, 1302 (1986)

[49] M. Lindheimer, E. Keh, S. Zaini and S. Pertyka, J. Colloid Interface Sci.. **138,** 83 (1989)

[50] R. Denoyel and J. Rouquerol, J. Colloid Interface Sci., **143,** 555 (1991)

[51] G.A. Parkes and W. Stummed, Adv. Chem. Ser. **67**, 121 (1966)

[52] R.L. Rea and G.A. Parkes, Acs. Symp. Ser.. **416**, 260 (1990)

[53] K.L. Mittal, Ed., "Micellization, Solubilization and Microemulsions", Plenum Press. New York, (1977)

[54] K.L. Mittal and E.J. Fendler, Eds.. "Solution Behaviour of Surfactants", Plenum Press, New York, (1982)

[55] K.L. Mittal and B. Lindman, Eds., "Surfactants in Solution", Plenum Press, New York, (1984)

CHAPTER SIX

COMBUSTION OF MICROEMULSIONS

6.1 Introduction and Review

Depletion in hydrocarbon fuel stocks has lead to a search for a means of enhanced oil recovery. Microemulsion systems have been found successful in the recovery of oil fragments which can subsequently be used as alternative fuel supplies. The combustion of such water/oil microemulsions have also been found beneficial from an economical and emissions point of view where they have been found to produce reduced levels of emissions of NO_x and particulates. Microemulsions offer benefits over macroemulsion systems due to the spontaneous emulsification, increased stability and ultralow interfacial tension.

Studies have been carried out on single phase microemulsion systems (5μl droplets in O_2 or He flows) comprising TX-100 + SDS + pentan-1-ol + decane with water concentrations in the range 1-10 wt %. These have average microscopic particle sizes in the range of 22-26 nm (measured with Photon Correlation Spectroscopy as described in section 3.2.14 of Chapter 3). The oxidation/vapourisation characteristics have been studied between room temperature and 573K over silica, oxidised and catalyst-coated alloy materials. The evaporation rate was found to depend strongly on water concentration. At 573K, very low levels of CO were produced and no NO_x was determined via residual gas analysis (RGA) or chemiluminescence. The production of formaldehyde and acetaldehyde as intermediate oxidation products was suspected and is of fundamental importance in fuel economy. The extent and circumstances of their formation have been investigated here with a view to its utilisation in combustion processes.

Bitumen is the heavy hydrocarbon component of oil extracted from geological reservoirs. It is black, sticky and extremely viscous. Bitumen is found in large amounts in the tar sands of Canada and in the Orinoco belt in Venezuela. One way to convert bitumen to a consistency which is easier to handle, is to heat it. In 1981, the Venezuelan oil company, Petroleos De Venezuela, solved the bitumen problem by devising a process which would

disperse the natural bitumen in fresh water. The process has two main stages:

1) the bitumen is mixed with 26% to 30% fresh water by a series of dynamic and static mixture to produce a water-in-oil emulsion.

2) a small amount (2%) of non-ionic nonyl phenol surfactant is then added which stabilises the medium; although only below 353K - 303K this is not the case.

The effect of this emulsification gives an emulsion the consistency of black ink, rendering it easy to handle and transport at 293K - 303K. When tried as a fuel (known as Orimulsion), the presence of water reduced the buring efficiency by about 2%, but in comparison with other fuels there were some advantages. Table 6.1 shows some typical characteristics of Orimulsion. The presence of sulphur means that on burning, levels of sulphur dioxide can be traced. However the company maintains that low levels only are produced which can be easily removed using standard technologies. There are low levels of NO_X emissions when compared with coal, due to lower temperature of the flame. The ash content of this fuel is lower than that produced by coal and consists of over 98% V or Ni compounds. In some countries these are removed from the ash and have their own value. Very small amounts of soot are produced since the hydrocarbons burn out completely.

After technical and economic studies were performed to test the different possibilities for the recovery of extra-heavy oils, the emulsification method emerged as the most successful and applicable. The other conventional methods such as the use of heat dilutants were not favoured because of the substantial investment necessary and transportation problems. Thus, Orimulsion appears to be the most economical medium for producing and transporting heavy crude oils.

In the last few years, work has been done on the mechanism of combustion of bitumen-water slurries and comparisons made with this and other established fuels. Williams and Pourkashanian [1] studied the combustion of bitumen-water mixtures. They compared ignition temperatures, burning time and droplet size with those for coal - water slurries and oil. It has been found that droplet size is inversely proportional to the efficiency of a fuel

to ignite [2]. Orimulsion is a useful fuel although much energy is needed to convert the oil-water mixture into a dispersion. By considering the spontaneously formed microemulsions, the droplet size effects and the cleanliness of emissions of these microemulsions on burning, for ideal systems.

Table 6.1 Characteristics of Orimulsions [4]

	Typical values	Typical range
Water content, % w/w	29.3	(27 - 30)
Medium droplet size, μm	10	(8 - 15)
% droplets>100μm	0.7	(0.5 -1.5)
Density (288K), kgm^{-3}	1,010	(990 - 1,020)
Vanadium, ppm	300	(270 - 340)
Sodium, ppm	30	(15 - 50)
Magnesium, ppm	350	(300 - 450)
Flash point, (K)	393	
Ash, % w/w	0.2	
	Elemental analysis, %w/w	
Carbon	60.0	
Hydrogen (from bitumen)	7.3	
Sulphur	2.7	
Nitrogen	0.5	
Oxygen (from bitumen)	0.2	

The vapourisation and combustion behaviour of water-in-oil microemulsion systems of kerosene and diesel fuel have been found to be dependent on hydrocarbon chain length [3]. Two different modes of fuel burning were investigated. With a wick flame there was reduction in soot and progressive lowering of the mass burning rate with increasing water content. In spray burning a considerable decrease was found in NO_x emitted as well as CO in excess O_2 environments. The microemulsions were found to allow a unique structure

for water which must undergo vapourisation before mixing with the oxidising gas. Within this structure water droplets of 10-50nm were possible by comparison with 0.2-50μm in macroemulsions. Single phases were completely miscible and with increasing hydrocarbon chain length the volatility of water decreased. The extent of endothermic or exothermic process was measured by TGA where endotherms represent vapourisation or vapourisation/degradation processes. Vapourisation was found to occur at 553K and 623K for diesel and 483, 503 and 533-543K for kerosene.

Fuel microemulsions have also been studied with regard to jet engine smoke reduction [5]. Water/oil microemulsions are formed spontaneously by simple mixing with particle sizes of 0.01-0.2μm. JP4 and JP8 having 10 and 20% dispersed phase have been tested in reduction of exhaust smoke. The reduction by water and alcohols appears to be determined by the degree of increase in hydrogen/carbon ratio of the fuel blend. Increased OH radical concentration enhanced the rate of free carbon oxidation. Combustion efficiency was greater for water/fuel than ethanol/fuel solutions. At low power, differences in fuel atomisation and vapourisation rates existed and combustion was controlled by fuel vapourisation. Combustion and droplet vapourisation was controlled by viscosity and boiling point distribution. The temperature of vapourisation was found to be approximately the boiling point of the most volatile component. Since droplet temperature was depressed by ethanol presence, decreased combustion was found in ethanol/fuel blends. Until water had evaporated, fuel droplet ignition did not occur. Ethanol blends were found to reduce the production of nitrogen oxides (i.e. NO_x) while water-in-oil microemulsions increased production.

The effects of surfactant on evaporation and shell formation have been studied [6]. The evaporation of slurry droplets was found to be slower than for pure JP10 and suppression was increased for higher loadings (droplet diameter 130 ± 50μm). For a fixed solid loading suppression of evaporation was increased with increasing surfactant concentration until reaching a critical concentration (0.01 to 0.02) above which the suppression was constant. The intensity and tendency towards disruption was enhanced by pyrolysed surfactant bound particles in a tightly packed shell. Surfactant pyrolysis also promoted the formation

of an impermeable shell although an alternative disruption mechanism may also exist. Shell character and disruption behaviour was investigated with respect to different surfactant concentrations and particle sizes. At different surfactant concentrations disruption intensity increased. Shells on slurrey droplets with smaller particles were more compact and plastic. Because of the high energy content of slurry fuels they are applicable to boiler, diesel and turbine applications. The high energy density is good for volume limited propulsion systems. After the loss of liquid fuel, slow burnout of the solid agglomerates occurs which may cause a problem. However, this may be rectified by microexplosion occurring for particular slurry formations. This invokes shattering of particles into smaller droplets which helps burning to be faster and more complete. In this case shell formation plays an essential role. Higher molecular weight surfactants tended to disperse particles and promote the formation of packed shell structures. Droplets shrink via a d^2 route until microexplosion occurs. Decomposed surfactants link solid particles to form an impermeable shell for the highest loadings (66 wt%) or impermeable for more dilute loadings (10-40 wt%). However microexplosion times are independent of solid loading. Differences in shell character and disruptive behaviour were seen for different particle sizes. All droplets had a d^2 evaporation period (d^2-d_o^2 = kt) where k was the evaporation constant. Al and B were found to have different shell characters due to particle size differences.

Evaporation and ignition of fuel droplets was also studied on a hot surface [7]. The ignition of droplets and delay was found to be of prime importance in designing and development of fuels for diesel engines and alternative fuels. Average droplet temperatures reach saturation temperature just before the droplet disappears.

Vapourisation and micro-explosion of emulsion fuel droplets on a hot surface has been investigated [8]. Dynamic evaporation characteristics need consideration in production of microexplosion as well as thermodynamic criteria. For w/o microemulsions if the oil boiling point is sufficiently high then superheating occurs as a result of suppression of vaporisation of the surrounding oil. When the temperature exceeds a critical point then microexplosion occurs. For low water contents water vapourises first. For high water content (above 22%) in n-octane then n-octane vapourises first leaving a water residue.

n-octane, n-decane, n-dodecane and n-hexadecane were tested. For n-octane water vapourises first for less than 22% water and n-octane first for more than 22% water. Early depletion of water may be due to the lower boiling point and higher density of water with respect to n-octane. For o/w emulsions boiling point and density have no influence and oil droplets vapourise first. The oil component decreases more slowly in o/w than w/o emulsions. For n-decane w/o emulsions the boiling point of decane is higher than octane and overall vapourisation characteristics are similar. For w/o vapourisation histories show two distinct regions in droplet squared versus time plots with initial slopes larger than final.

The effect of pressure on micro-explosion in w/o emulsion droplets over a hot plate [9] was found to inhibit disruption by suppression of vapour bubble expansion dynamics. The dynamic instability of the microexplosion at atmospheric pressure was suppressed at high pressure. Unsteady combustion and vapourisation of fuel droplets [10] has been witnessed for spherical fuel droplets where the named distance to diameter ratio of the droplet was used in place of the group combustion number to characterise the behaviour of such sytems. The combustion of fuel oil sprays in oxygen [11] with jet-mixing burners has shown that for heavy oil (not gas oil) the low value of burning rate and combustion intensity was due to excessive cracking and slow-burnout of carbon.

For the combustion of microemulsion sprays [12] the burning characteristics of air-assisted atomised sprays of Jet-A fuel and its microemulsion with 5 - 10% water solutions are still transparent but with 15 and 20% the appearance is milky. A higher water content lowers stability. The presence of water prolongs ignition delay and reduces vapourisation rate. Emissions of NO and CO were found to decrease when the microemulsion was used in place of pure fuel. The microexplosion of emulsified fuels was determined by measuring the flashing temperature of superheated water [13]. Kerosene, diesel fuel and tetradecane were used as fuels and methanol and ethanol as dispersed phase. The flashing temperature was found to decrease with increasing surface area per unit volume of sample and was dependent on both continuous and dispersed phases.

The effect of water addition on combustion processes in natural gas flames has been

investigated by Jordan et al [14]. The effect of water vapour adddition on flames is well documented. High concentrations of water vapour present in a flame zone will enhance hydrogenation recombination thus releasing heat slightly more rapidly. Cunningham and Gliddon [15] studied water as an additive for the combustion of extra-heavy fuel oil, and concluded that substantial reductions in unburnt carbon are possible with modest (<10% by wt) water additions. The alcohol as fuel [16] has shown advantages of finer atomization, more rapid vaporization, greater ignitability and flame stability, with low production of NO_x, together with disadvantages of greater fire hazard, toxicity and water solubility and high production of CO.

6.2 Mechanisms and Emulsion Characteristics

The addition of water may have both physical and chemical kinetic effects on combustion phenomena, the magnitudes of which will depend on how water is introduced to the combustion environment.

(a) Chemical Kinetic Effects of Water Addition

The catalytic effect of water-vapour on carbon monoxide combustion has been well documented to occur from an enhanced production of hydroxyl radicals [17], primarily through

$$H_2O + H^{\bullet} \rightarrow H_2 + OH^{\bullet}$$
$$H_2O + O^{\bullet} \rightarrow OH^{\bullet} + OH^{\bullet}$$
$$H_2 + O^{\bullet} \rightarrow OH^{\bullet} + H^{\bullet}$$

resulting in an increased reaction rate for

$$CO + OH^{\bullet} \rightarrow CO_2 + H^{\bullet}$$

In fuel-rich combustion, it is very probable that changes in radical concentrations by water vapour addition may produce inhibition of gas phase soot formation. It has been suggested that hydroxyl radicals are very effective in oxidising soot precursor species, thus reducing polymerization and carbon nucleation rates [18].

(b) Physical Effects of Water Addition

The addition of water to the oil in the presence of surfactant, leads to the formation of a microemulsion in which the water is dispersed in the oil as droplets of the order of 25-30 nm in diameter. Despite the fact that water-oil emulsions have been used for a long time as a way to improve the combustion performance in sprays, it has not been until recently that researchers started to work on its basic mechanism.The primary mechanism for the reduction of carbon emissions that ensues is almost certainly enhanced atomization. Once the emulsion is sprayed into a combustion chamber heat is rapidly absorbed by the dispersed water phase droplets producing steam and results in an abrupt volume increase which explosively disrupts the oil droplet in so-called micro-explosions [20].This phenomenon observed during the buring or vaporization of either emulsified or multicomponent fuel droplets is the result of the formation, growth and bursting of vapour bubbles within the superheated droplet interior.

As a result of the complex interactions experienced in conventional spray combustion, single droplet combustion experiments represent the simplest starting point. Jacques and co-worker [21] made an experimental investigation of the combustion of water-in-oil emulsions. The results show that the addition of water in the form of an emulsion has very little effect on the rate constant k_p but resulted in a substantial increase in the mass loss prior to ignition due to the massive disruption which takes place during this period. Consequently, the suspended droplet experiments show that water addition results in micro-explosion which affects the ignition characteristics.

For water-in-oil emulsions, since the water is dispersed and isolated in the emulsion as relatively immobile microdroplets, evaporation from the surface of the droplet is primarily from the continuous oil phase. As this can sustain a very high temperature during combustion, water can be easily heated beyond its boiling point and may even approach its limit of superheat. At this temperature, for a given pressure, water nucleates and subsequently the drop disintegrates spontaneously, shattered by the internal formation of vapour bubbles and the consequent rapid vaporization of superheated water.

This process is so disruptive as to shatter the primary emulsion droplet into many fragments, which in spray combustion is considered as a secondary atomization process with all the advantages that this phenomenon could create on the combustion performance. The recent interest in water-in-oil emulsions [22-24] is primarily associated with the exploitation of this phenomenon. Combustion studies of emulsion droplets [25] show that the emulsified fuels burn faster than anhydrous ones, water improves the combustion process due to the breaking of the droplets, to the increase in evaporation surface area of the droplets and to a better mixing of the buring species in air.

Kinetic [26] and hydrodynamic [27] calculations suggest that steam bubble growth is dependent upon the dispersed phase size distribution. Other factors include the possibility that the steam produced could result in increased swelling of the fuel droplets that would then be more easily oxidized [28]. Enhanced radiation heat transfer into droplets containing water has been discussed by Jordan and Williams [29]. It is possible that the resulting increase in droplet heating rates could result in better cracking of fuel molecules. The effect of surfactants on aggregation behaviour of coal - water slurry particles have been investigated during the early stages of combustion [30]. Slurries containing no surfactant disaggregate, producing significantly higher number densities of small particles (0.4 - 10 μm) than the slurry containing surfactant.

Because of the importance of micro-explosions as a mechanism that improve the combustion performance in emulsions, it is necessary to consider certain parameters which can provoke the onset of micro-explosions and yet increase the violence of them. The intensity of the micro-explosion phenomena is a function of properties such as degree of initial superheat necessary to produce the phase transition, physical properties of the dispersed and continuous phases and size of the droplets.

A necessary condition for micro-explosion of an emulsified fuel droplet is that the limit of superheat of the emulsion be less than the boiling point of the fuel. Thus, it is necessary to understand the process by which vapour bubbles nucleate in superheated emulsions. Bubble nucleation in a liquid which is not in contact with a gas phase and has a zero

contact angle with all surfaces, will produce bubbles completely within the liquid. Such nucleation is termed homogeneous nucleation and is to be contrasted with heterogeneous nucleation, or nucleation at an interface between the volatile liquid and another phase it contacts. Heterogeneous nucleation can occur only if the contact angle of the volatile found is greater than zero. The problem of superheating, vaporization and nucleation of internal phase droplets of an emulsion is more complex than the one for a pure substance. This is because of the multiplicity of potential nucleation sites introduced by the interface between phases.

6.3 EXPERIMENTAL

Three single phase microemulsion systems were tested (denoted SM1, SM2 and SM3) comprising TX-100 + SDS + pentan-1-ol + decane with varying water content (in the range 1-10%), in vapourisation/oxidation experiments. These were prepared by mixing the nonionic surfactant TX-100 and anionic surfactant SDS in a ratio of 4:1. Pentan-1-ol was used as a co-solvent and the surfactant mixture was combined with this in the ratio 1:1. By mixing with decane (continuous phase) and finally by adding water as the dispersed phase at 298K, microemulsions were prepared of the composition shown in Table 6.2.

Table 6.2 Composition of the single-phase microemulsion systems.

Sample Identification	Composition (wt%)				
	Water	TX-100	SDS	Pentan-1-ol	Decane
SM1	2.0	10.0	2.5	12.5	73.0
SM2	4.0	10.0	2.5	12.5	71.0
SM3	6.0	10.0	2.5	12.5	69.0

5mm^3 droplets of pure decane and the above microemulsions were studied at temperatures in the range 313-573K within the combustion cell shown in Figure 6.1. The cell was located within a projector system such that the droplet could be magnified for ease of the macroscopic particle size measurement. At 313K evaporation of the droplets was studied in 6%O_2 and He flows (100cm^3/min) via a Residual Gas Analyser (RGA) and through

measurements of the droplet diameter with time in the flow. Estimates of diameter^2 versus time and d^2-d_0^2 versus time were used to determine the kinetics (initial and final) of the reaction.

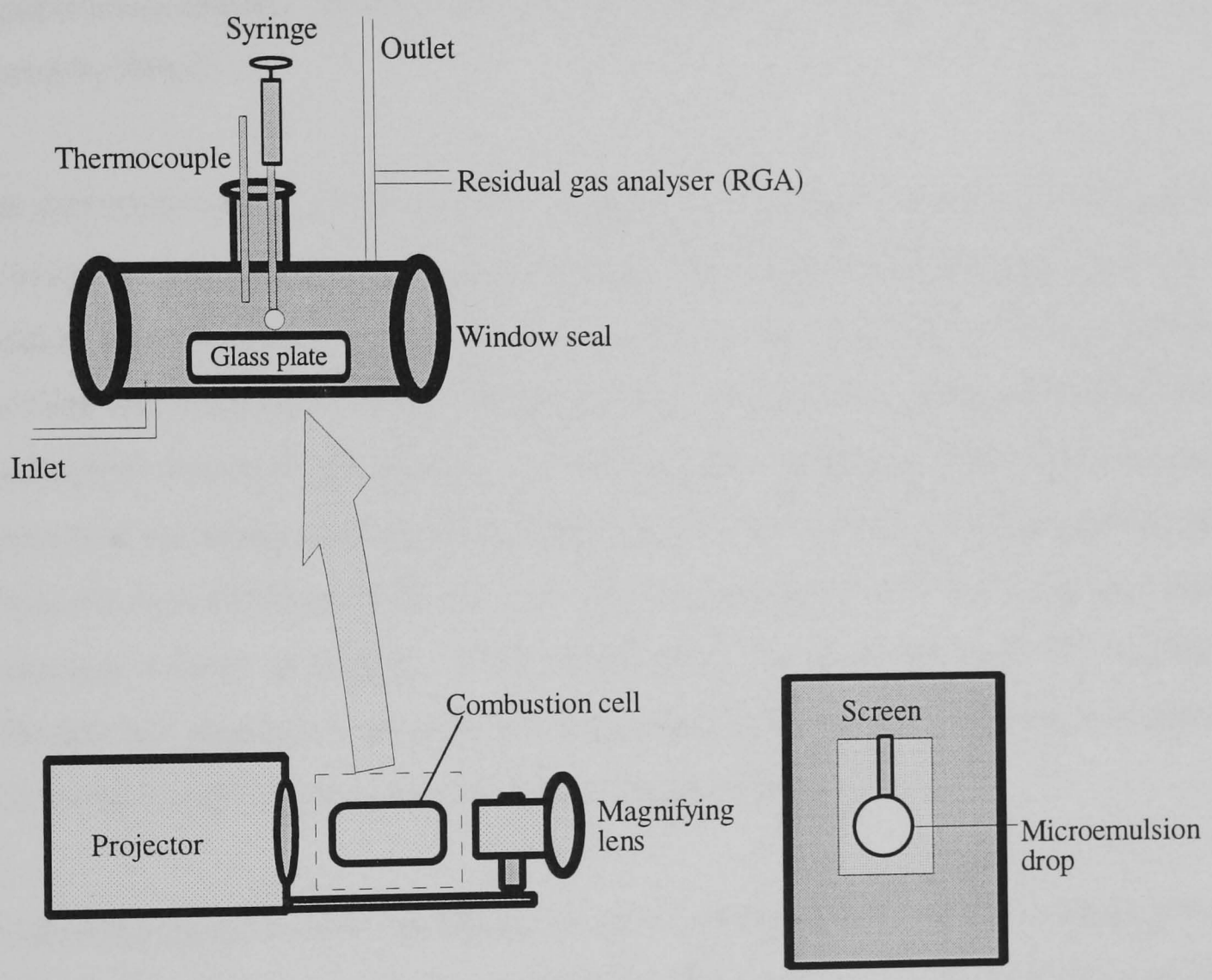

Figure 6.1 Schematic diagram of the combustion reactor

Oxidation studies were carried out over silica, oxidised and catalyst-coated Fecralloy at 423 and 573K in the 6%O_2 stream. Vapourisation was instantaneous at these temperatures (presumably due to the small particle size) and hence particle size determination proved impossible within the current experimental setup. RGA analysis was obtained with time for all systems. Accurate determination of temperature was achieved by means of a thermocouple probe inserted into the system at the same point as the droplet injection.

The presence or otherwise of formaldehyde and acetaldehyde formation within the reaction was determined using calibration cartridges (Supelco). The low pressure drop DNPH cartridge is an air sampling device designed for sampling carbonyls (e.g. formaldehyde) in ambient indoor, and industrial atmospheres. Carbonyls are trapped on a high purity silica adsorbent coated with 2,4-dinitrophenylhydrazine (DNPH), where they are converted to the hydrazone derivatves. The derivatives are eluted from the cartridge in acetonitrile and analyzed by HPLC.

Blank determinations (5 min in the 6%O_2 stream over oxidised Fecralloy at 573K) and equivalent determinations for microemulsions SM1 and SM3 were obtained. The cartridges were flushed using 5cm^3 of acetonitrile to elute the dinitrophenylhydrazone equivalent and analysed by HPLC using a zorbax ODS (silica treated with octadecyl silane:Dupont) column of particle size 7μm. The column length was 12.5cm with internal diameter 0.45 cm having reversed phase separation. The solvent used was acetonitrile and water in the ratio 50:50 at a flow rate of 1cm^3/min. A pressure of 4.1MPa was used and an injection volume of 20mm^3. The detector used was a Spectroflow 757 variable wavelength UV absorbance detector at a wavelength of 360 nm. Absorbance sensitivity was 0.1 with a chart speed of 10 mm/min and range, 10mV.

Pure dinitrophenylhydrazone equivalent crystals of formaldehyde and acetaldehyde were also prepared for confirmation and concentration determination. These were prepared by dissolving 0.25g of DNPH in 5cm^3 of methanol and then subsequently adding 0.4-0.5cm^3 of concentrated H_2SO_4 slowly. The warm solution was filtered and then 0.1-0.2g of the carbonyl compound (formaldehyde or acetaldehyde) in a small volume of methanol was added. Solid crystals were produced and these were recrystallised.

6.3.1 Mass Spectrometer (MS)

The exit stream from the reactor was analysed using a VG Quadruples VG300D Sensorlab mass spectrometer controlled by a PC (Viglen Genie II, 80286). The inlet to the mass spectrometer was a fused silica glass capillary which was heated to 373K. The inlet pressure range for operation of the instrument is 50 to 202 kPa [31]. The VG300D was

a quadrupole mass spectrometer (QMS) with radio frequency mass selection [32]. The QMS used an enclosed, electron impact ion source with two thoriated, iridium filaments which were current monitored from one filament to the other at 120 μA at an accelerator voltage of 70 eV. The VG300D had two detectors a Faraday cup and a Secondary Electron Multiplier. The detector used was of the Faraday cup type which could be left in operation continuously and was robust [33]; but which is relatively slow in operation and is insensitive compared to the secondary electron multiplier (i.e. the Faraday cup detector had a detection limit for nitrogen of 100ppm compared to a detection limit for nitrogen for the secondary electron multiplier of 5ppm). The secondary electron multiplier was used for experiments where it was necessary to collect data rapidly or where greater sensitivity was required. This detector relied on an accelerator voltage for its operation which had to be set each time it was used. It required 1- 2 h of operation before a stable response was produced and it was also unable to operate above a flow rate of 25 cm^3 min^{-1} or a pressure of 101kPa. Two analytical modes were used to study the combustion products [34]. The first was a logarithmic histogram mode, where each mass was represented by a separate peak and which showed all the decade ranges selected. The second analytical mode was multiple ion monitoring [31] in which up to sixteen m/e values could be studied simultaneously and their values displayed in real time. Although only a limited number of fragments could be scanned in this mode it allowed data to be collected at a much higher rate than in the logarithmic histogram mode so that any fine detail could be resolved.

6.4 RESULTS AND DISCUSSION

The room temperature evaporation results for decane, microemulsions SM1-SM3 in both He and 6%O_2 are shown in Figures 6.2-6.8, the rate and extent of decane vapourisation was reduced in the 6%O_2 stream. Decane droplets were found to decrease in size faster in the He stream presumably due to its inertness, hence the time of evaporation was shorter in He. The microemulsions show that more decane is released in He than in 6%O_2 (see Figures 6.2-6.8) and that microemulsion SM1 releases decane more quickly i.e. after 1min with microemulsions SM2 and SM3 having maxima after 5 min.

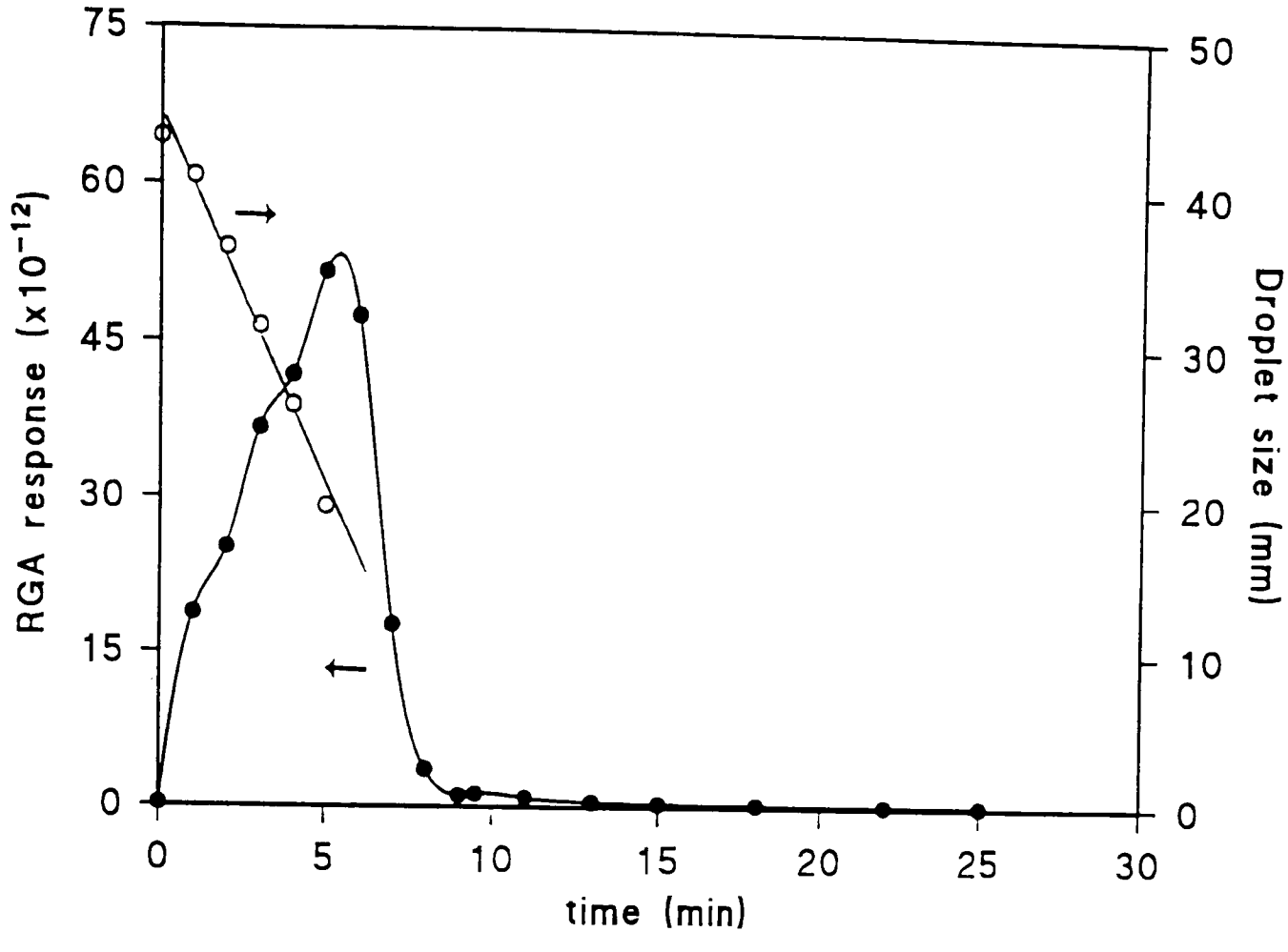

Figure 6.2 Evaporation of decane droplet in He as a function of time at 313K.

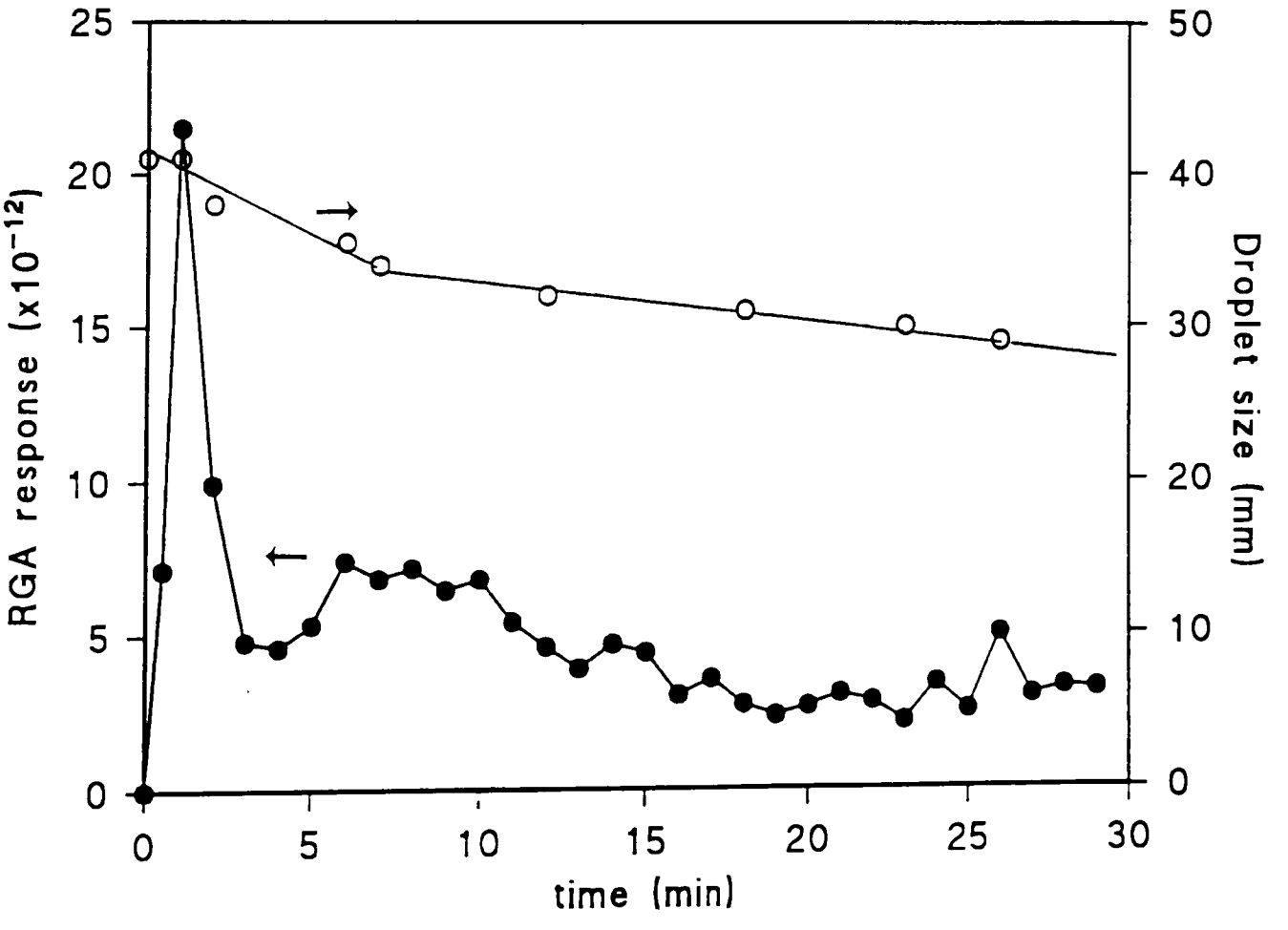

Figure 6.3 Evaporation of decane from microemulsion SM1 in He stream as a function of time at 313K.

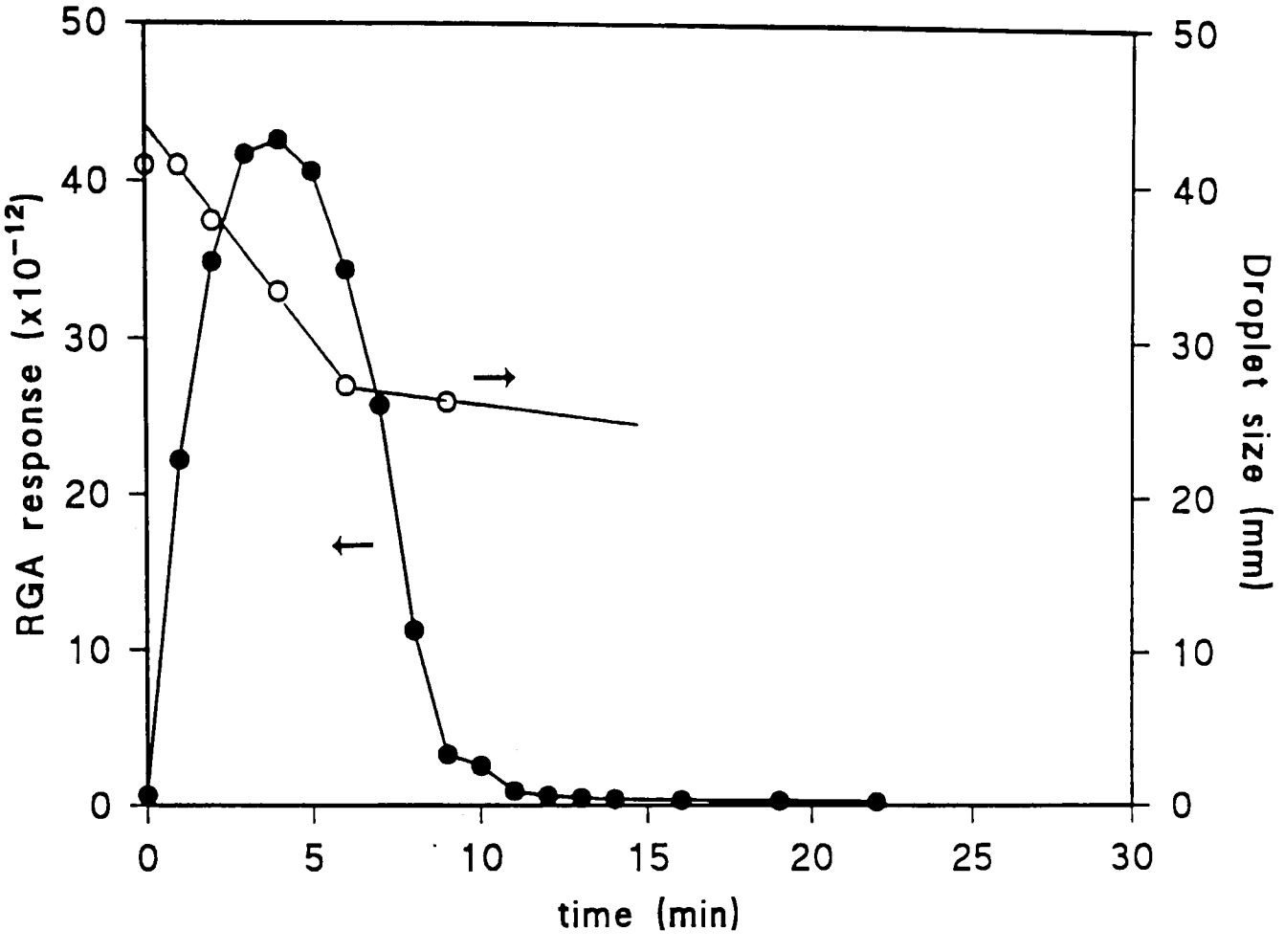

Figure 6.4 Evaporation of decane from microemulsion SM2 in He stream as a function of time at 313K.

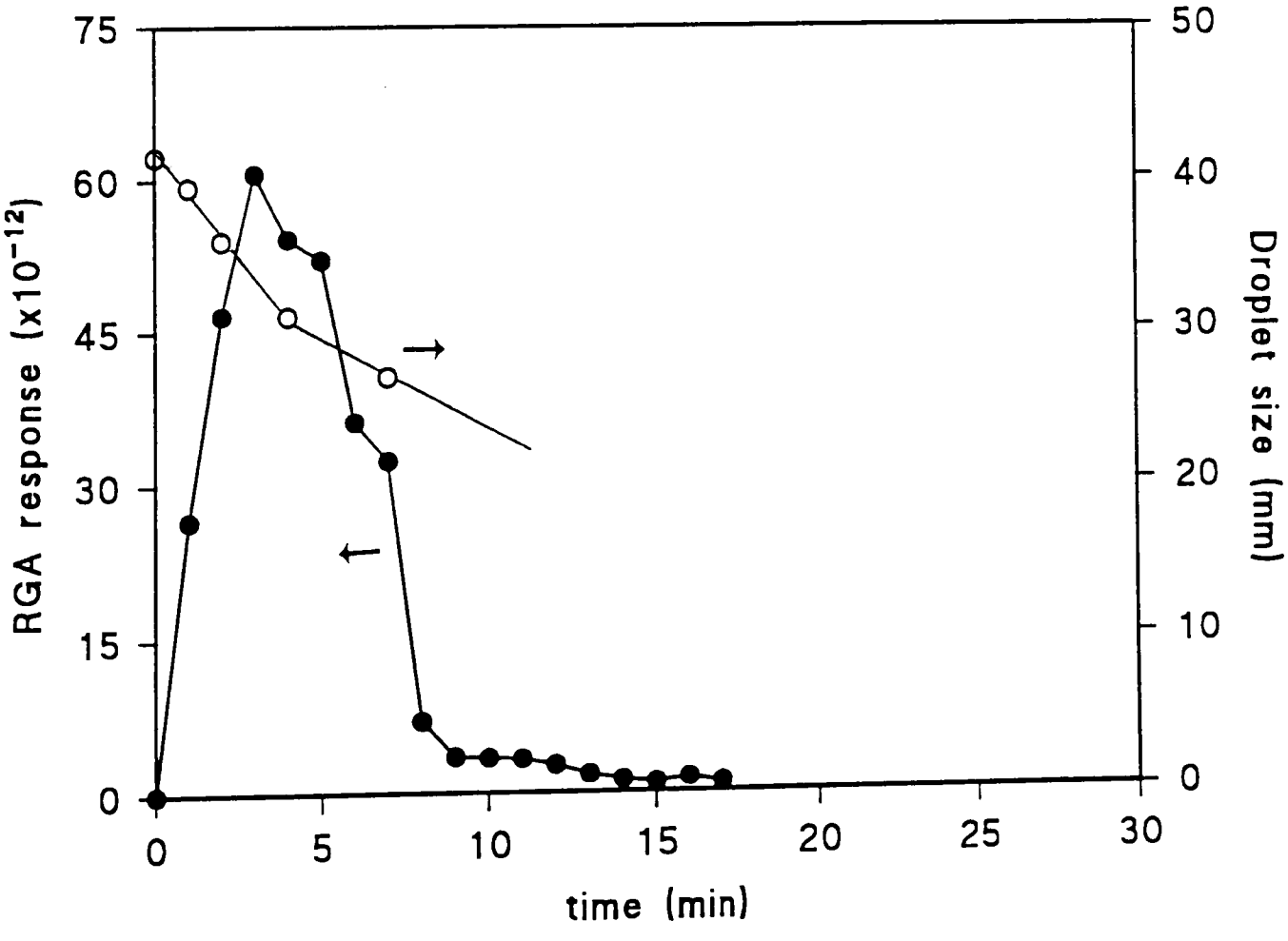

Figure 6.5 Evaporation of decane from microemulsion SM3 in He stream as a function of time at 313K.

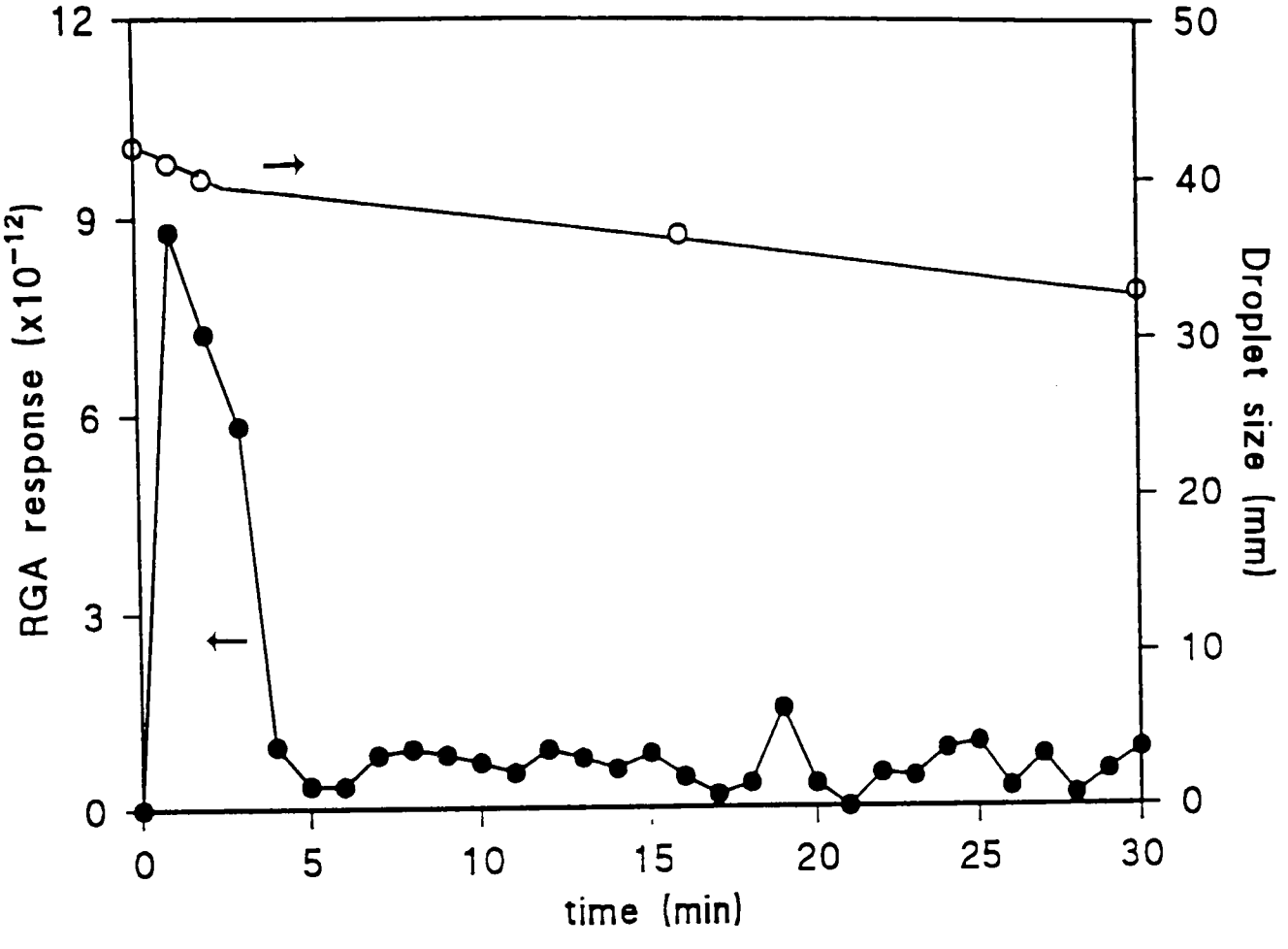

Figure 6.6 Evaporation of decane from microemulsion SM1 in 6%O_2 stream as a function of time at 313K.

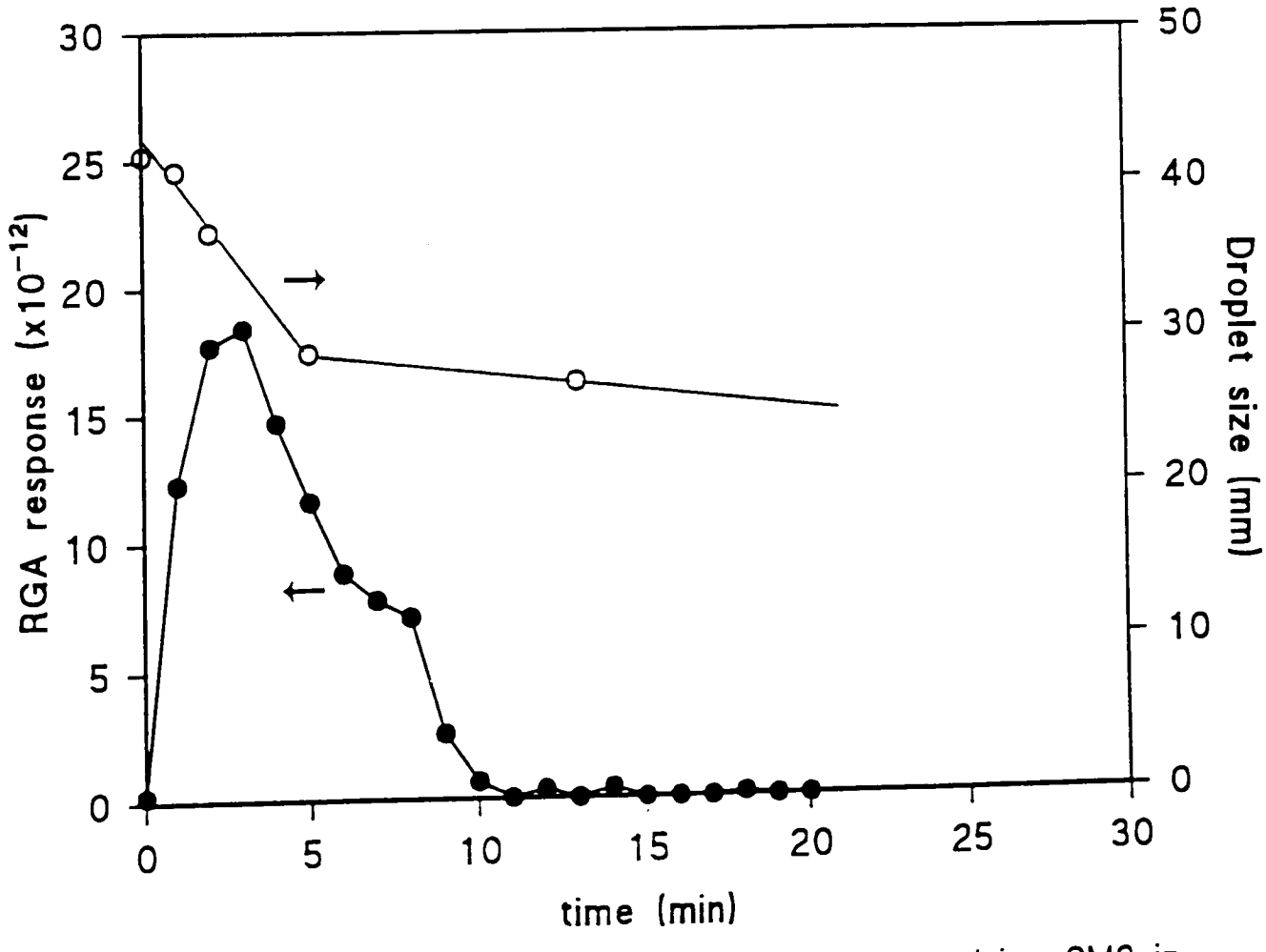

Figure 6.7 Evaporation of decane from microemulsion SM2 in 6%O_2 stream as a function of time at 313K.

Since in the microemulsions, the surfactant molecules form a thin monolayer on the droplet surface, the controlling evaporation mechanism becomes the diffusion of liquid through the surfactant layer. Consequently the evaporation rate can be some what reduced [35].

The droplet size was smallest for microemulsion SM1 (determined from particle size measurement (Malvern Instruments Zetasizer)), having a particle size of 22nm compared with 24 and 26nm for microemulsions SM2 and SM3 (see Chapter 4). The droplet size was found to diminish more slowly in microemulsion SM1 than in SM2 and SM3 i.e. over 30min for SM1 and 10-12 min for SM2 and SM3. The characteristics of microemulsion SM1 vaporisation appeared very different from those of SM2 and SM3.

The plots of droplet size (mm) versus time showed the vapourisation histories of the emulsion droplets (see Figures 6.3-6.8). For all microemulsions the initial slope was larger in both He and 6%O_2 than that of the final as expected for w/o microemulsion systems [8]. The initial slope was found to be smaller with smaller water contents which is also evident here (e.g. for the system SM1, the slope is 0.063 and for the system SM3 the slope is 0.307).

Plots of d^2-d_o^2 versus time allow calculation of the evaporation rate constant (slope of the line) [6] and evaporation suppression factor via k/k_o where k and k_o are the evaporation-rate constants for emulsion droplets and pure decane droplets respectively (see Figures 6.9 and 6.10). Calculated values of the evaporation suppression factor for the initial and final rate constants are presented in Table 6.3. It is clear from the table that the evaporation suppression for the initial slope (k_1) increased considerably with increasing the disperse phase of the micreoemulsions (i.e. the evaporation suppression for SM1=0.205 and SM3=0.545). Again the plots for microemulsion SM1 showed more enhanced differences than for emulsions SM2 and SM3.

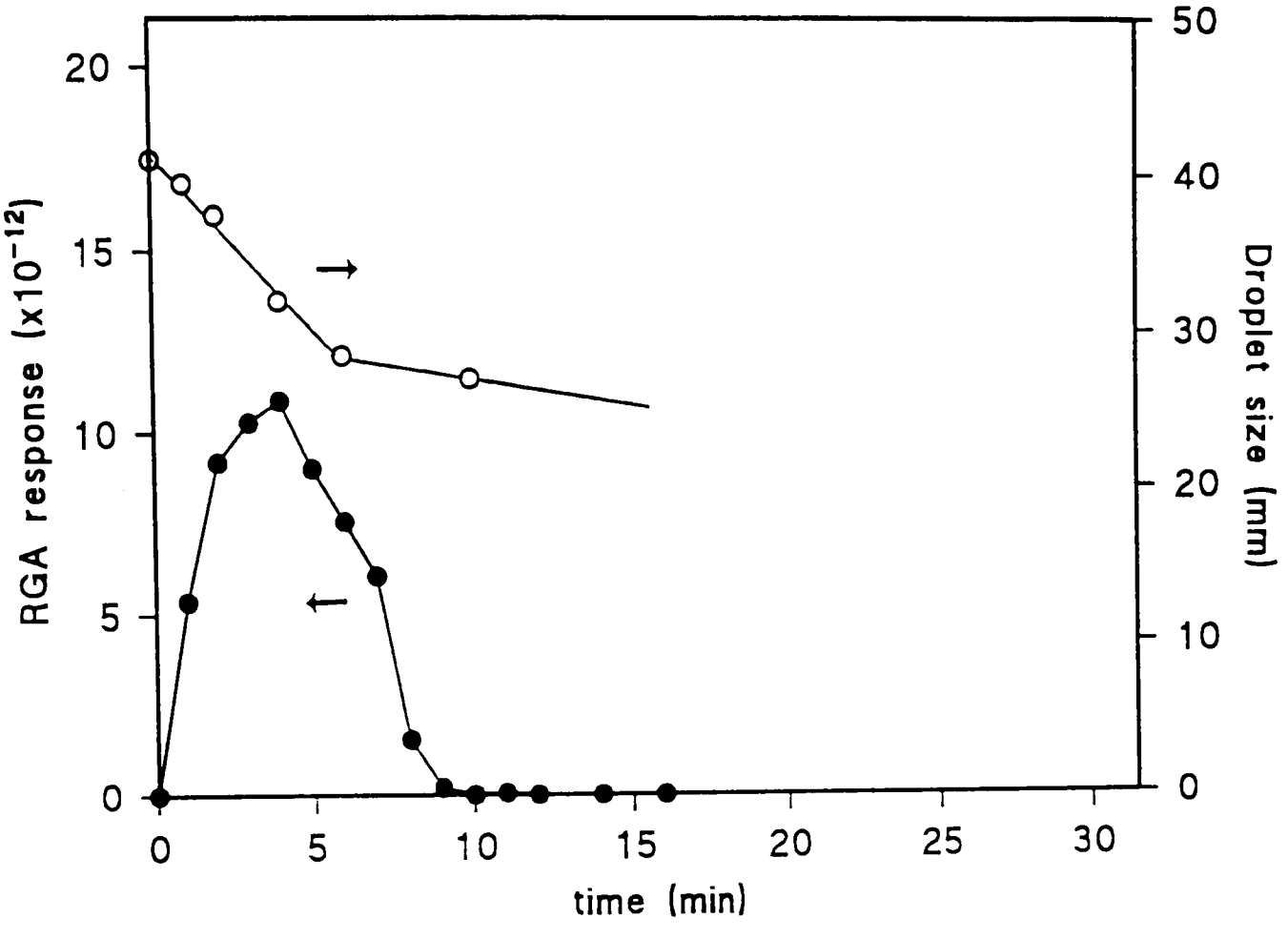

Figure 6.8 Evaporation of decane from microemulsion SM3 in 6%O_2 stream as a function of time at 313K.

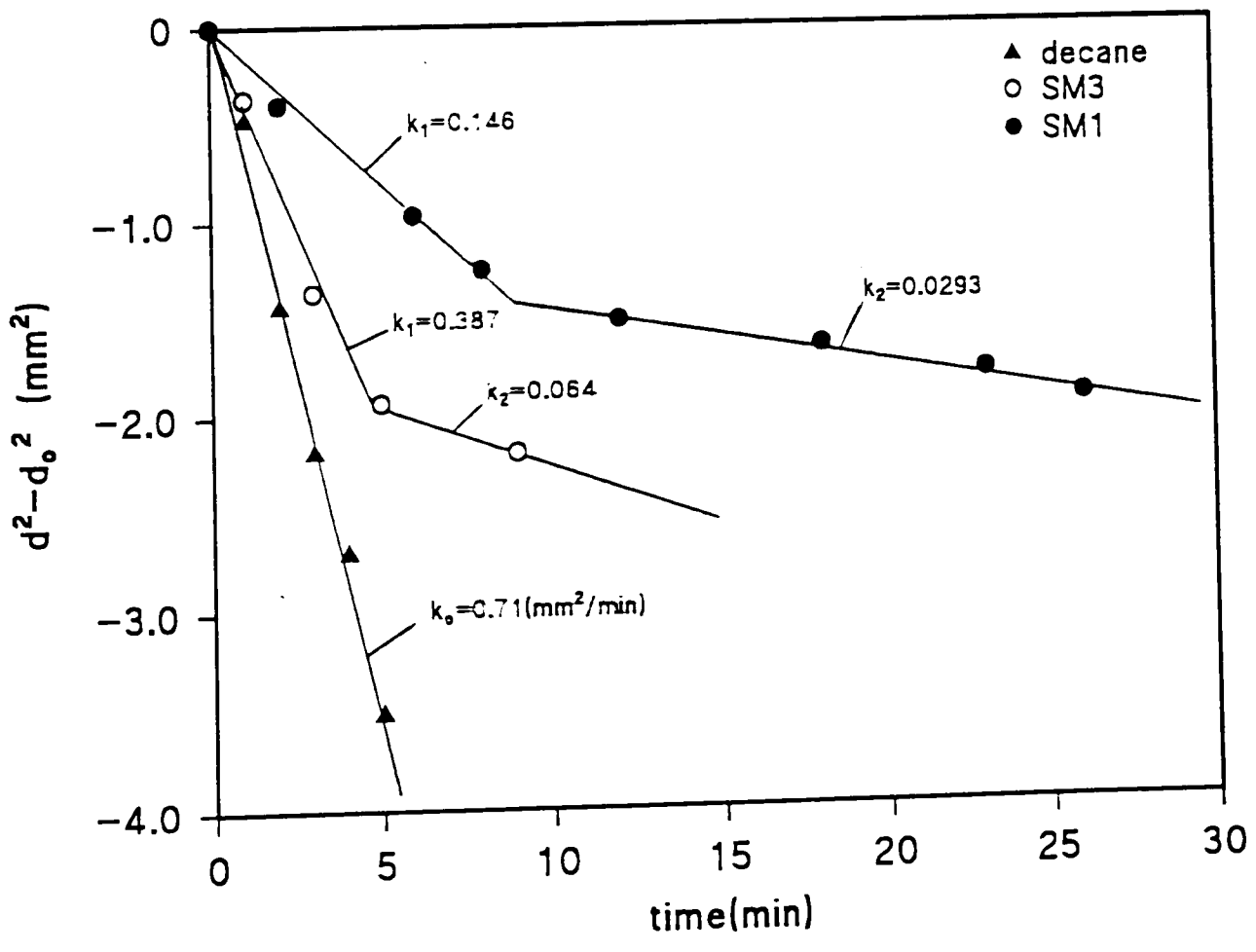

Figure 6.9 The change in droplet size in the He stream as a function of time at 313K.

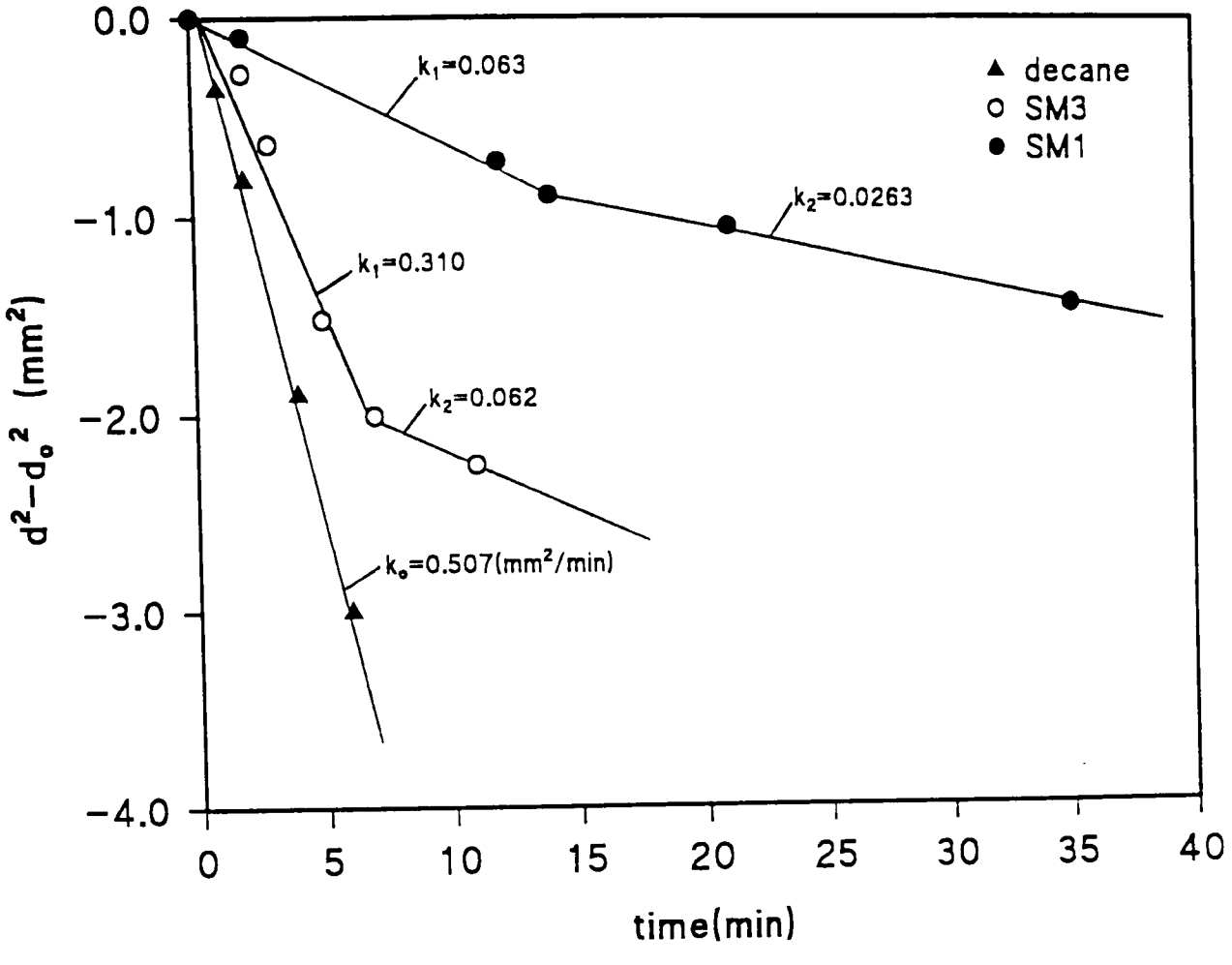

Figure 6.10 The change in droplet size in the 6%O_2 stream as a function of time at 313K.

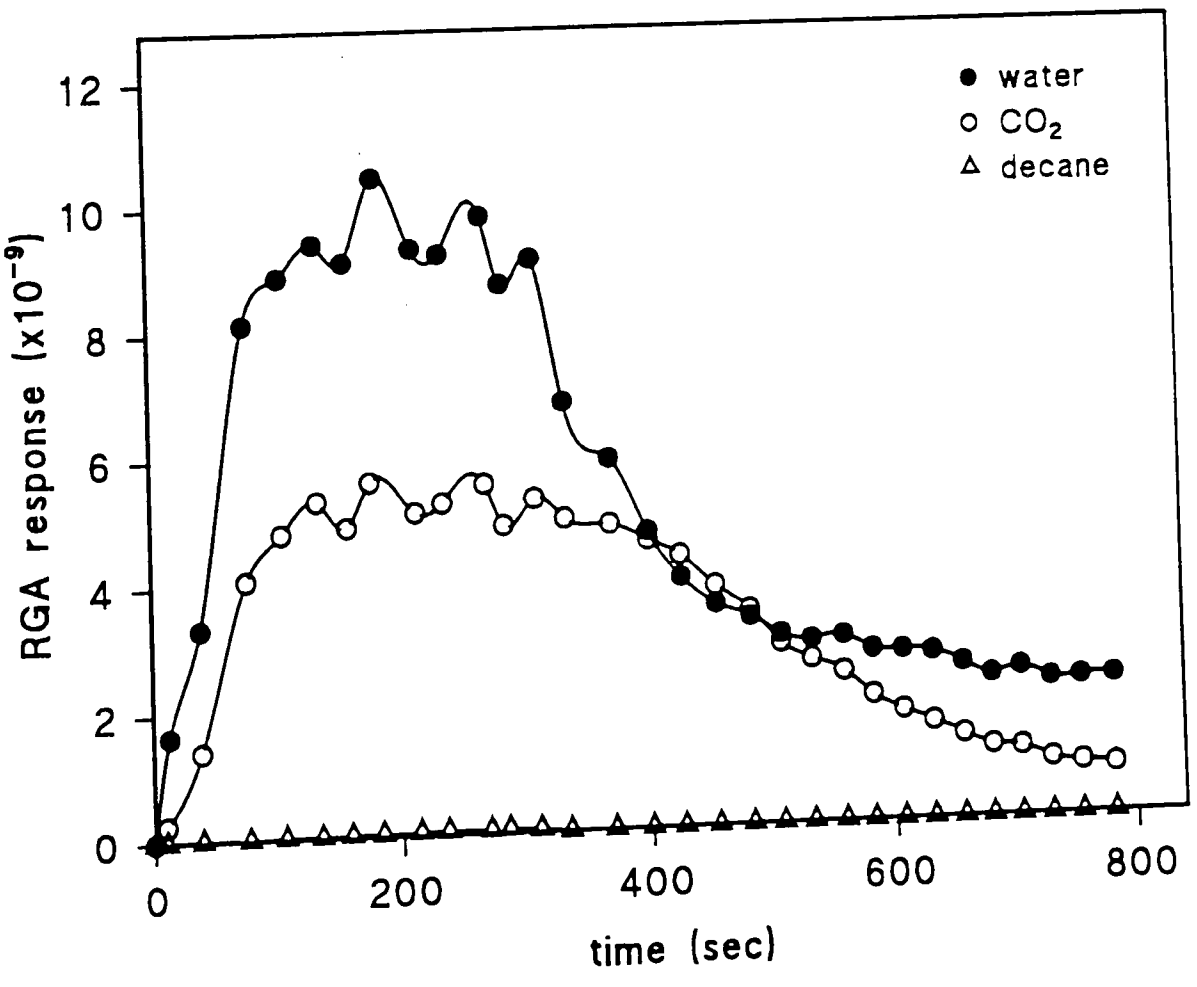

Figure 6.11 Combustion of decane on silica as a function of time at 423K

Table 6.3 Evaporation suppression factor for the initial and final rate constants.

Sample	Gas stream	Evaporation suppression factor	
		For initial rate (k_1/k_o)	For final rate (k_2/k_o)
SM1	He	0.205	0.041
SM3	He	0.545	0.090
SM1	6%O_2 in He	0.125	0.051
SM3	6%O_2 in He	0.602	0.122

The evaporation results show that evaporation rate increased with increasing the disperse phase (water content) of the microemulsions. Presumably, this is due to the interactions of the alkyl chain of the surfactant molecules with hydrocarbon which reduce the rate of evaporation of decane from the microemulsion SM1. At low water content the decane molecules have greater affinity for the surfactant therefore the rate of evaporation is slow. However, at high water content (6%) the surfactant molecules have greater interactions with the water and less affinity for decane, thus the evaporation rate was found to be fast for the microemulsion SM3.

The results for decane and microemulsions SM1 and SM3 on silica, oxidised Fecralloy and catalyst-coated Fecralloy at 423K are shown in Figures 6.11 to 6.17. Whilst the profiles for water, CO_2, CO and decane emission are similar in terms of amount produced, there are differences in water peaks for the microemulsions on oxidised Fecralloy and catalyst-coated Fecralloy in which the profile appears to have initial and later emissions. This is most enhanced for microemulsion SM1.The results for decane and microemulsions SM1 and SM3 on the same substrates at 573K are presented in Figures 6.18 to 6.26. At 573K again the profiles are similar for water, CO and CO_2 and decane but the most noticeable differences are in initial peaks appearing in the CO_2 mass value. This was also found to be the case for mass value 30 as shown in Figures 6.18 to 6.26. Since mass values of 30 and 44 can correspond to NO or formaldehyde or acetaldehyde then the initial peaks could be representative of formation of these components. Tests using a chemiluminescent NO_x detector (Rotork Analysis 441) proved that NO_x was not produced.

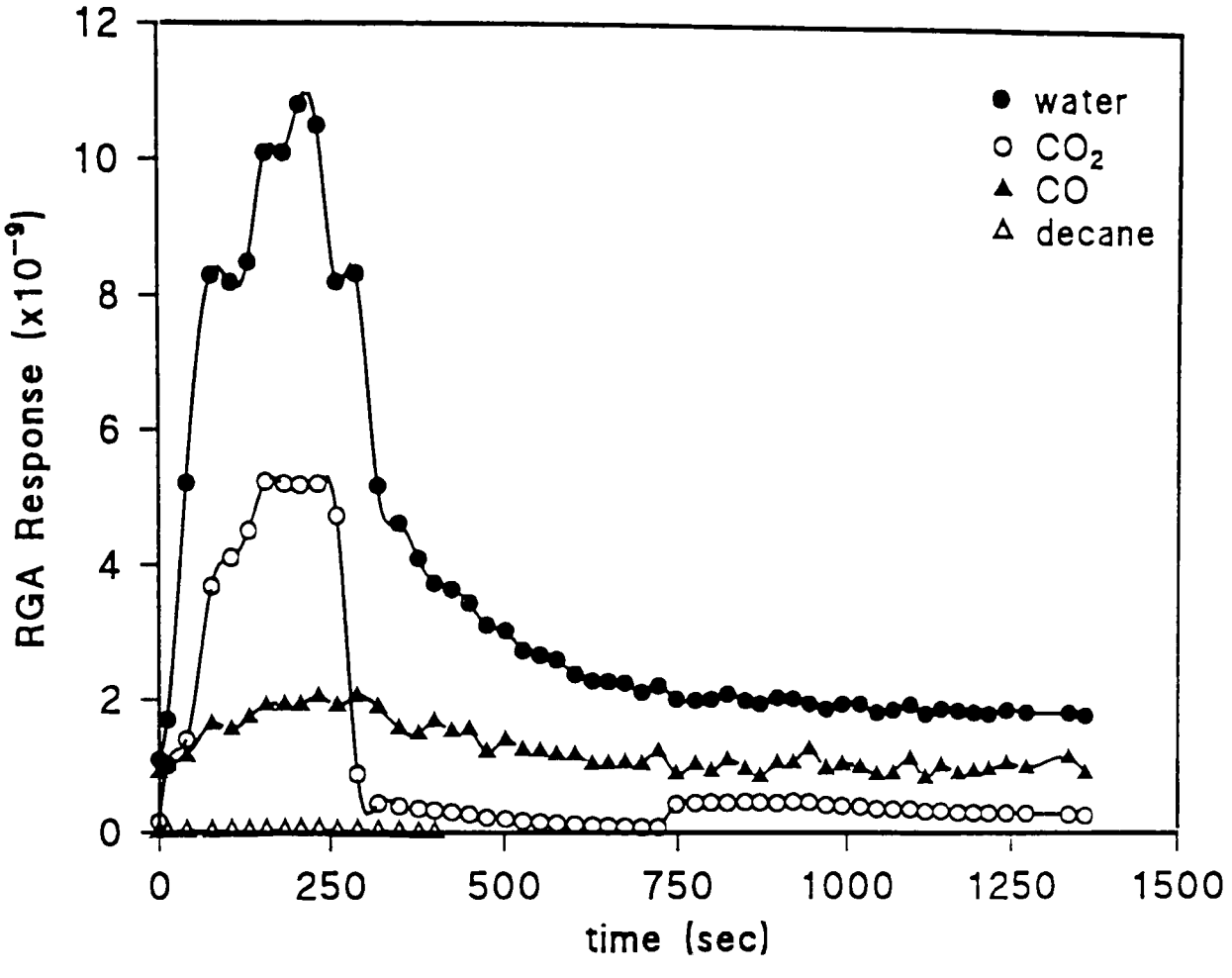

Figure 6.12 Combustion of microemulsion SM1 on silica as a function of time at 423K.

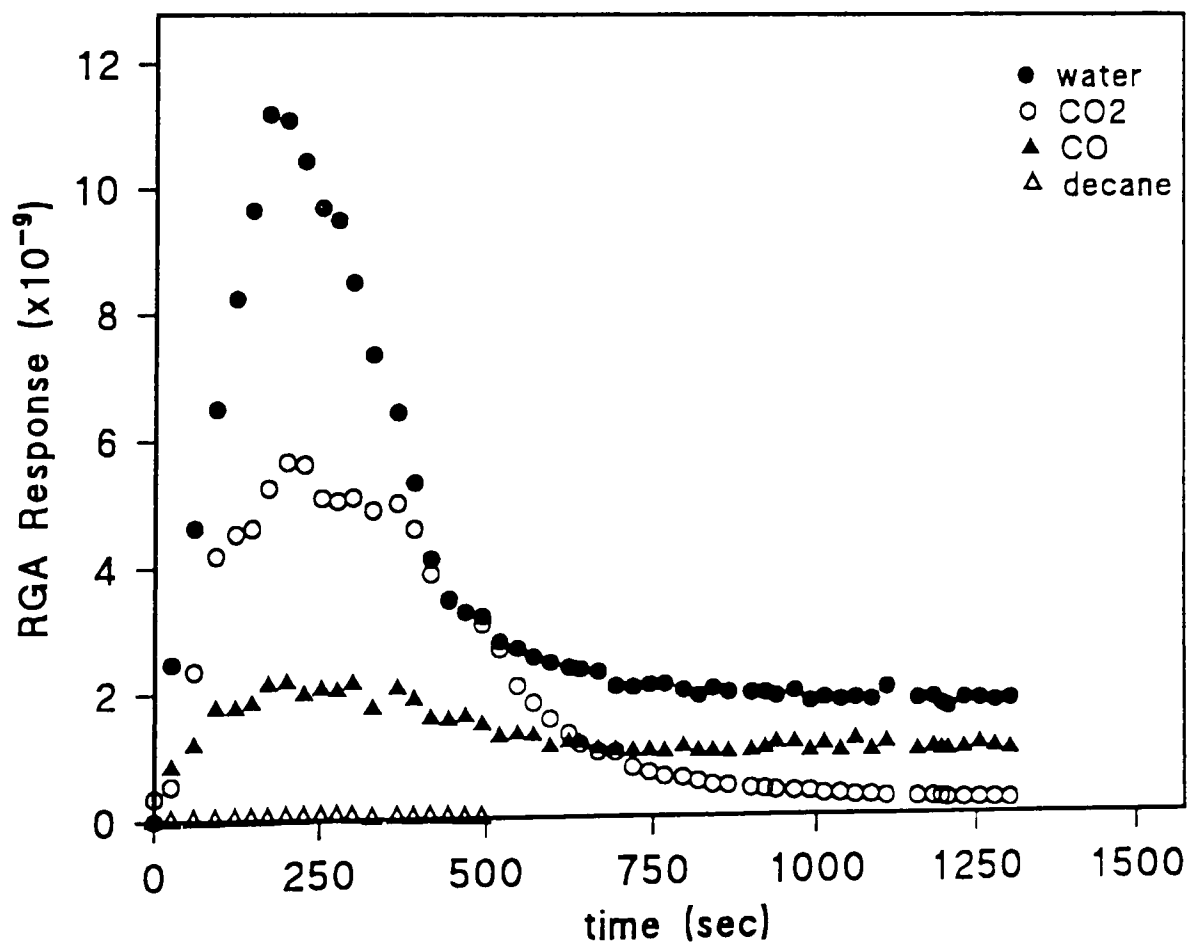

Figure 6.13 Combustion of decane on oxidised FeCralloy as a function of time at 423K

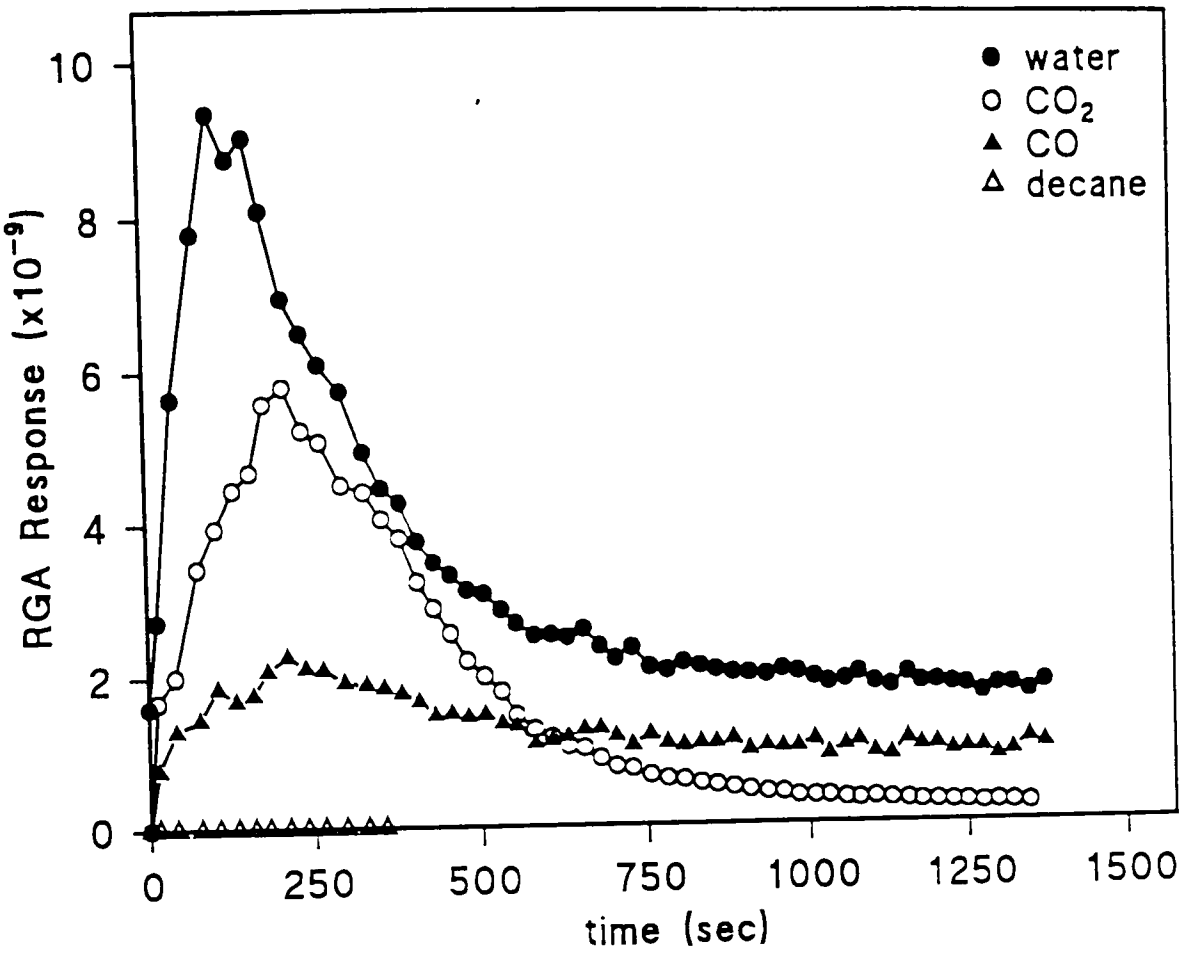

Figure 6.14 Combustion of microemulsion SM1 on oxidised Fecralloy as a function of time at 423K.

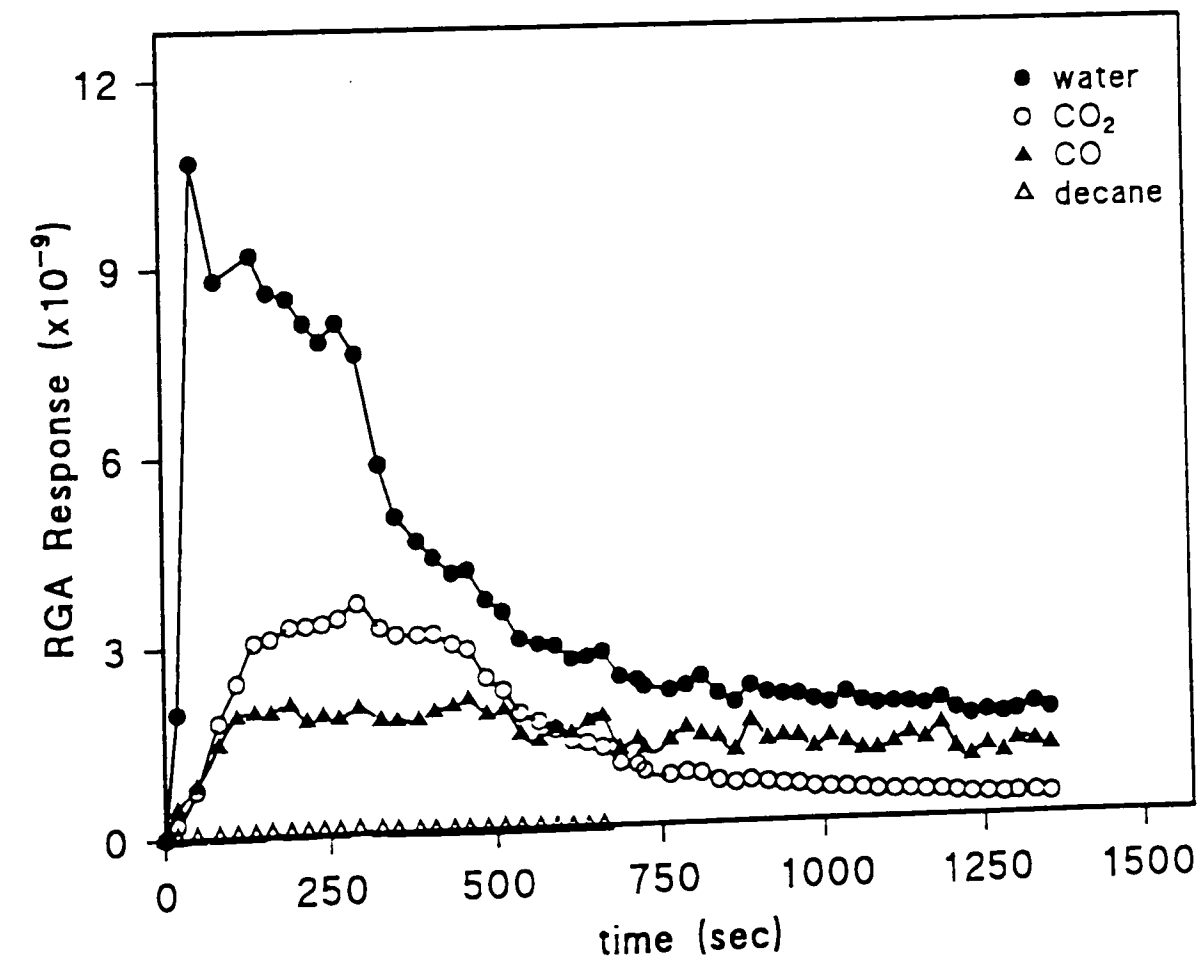

Figure 6.15 Combustion of microemulsion SM3 on oxidised Fecralloy as a function of time at 423K.

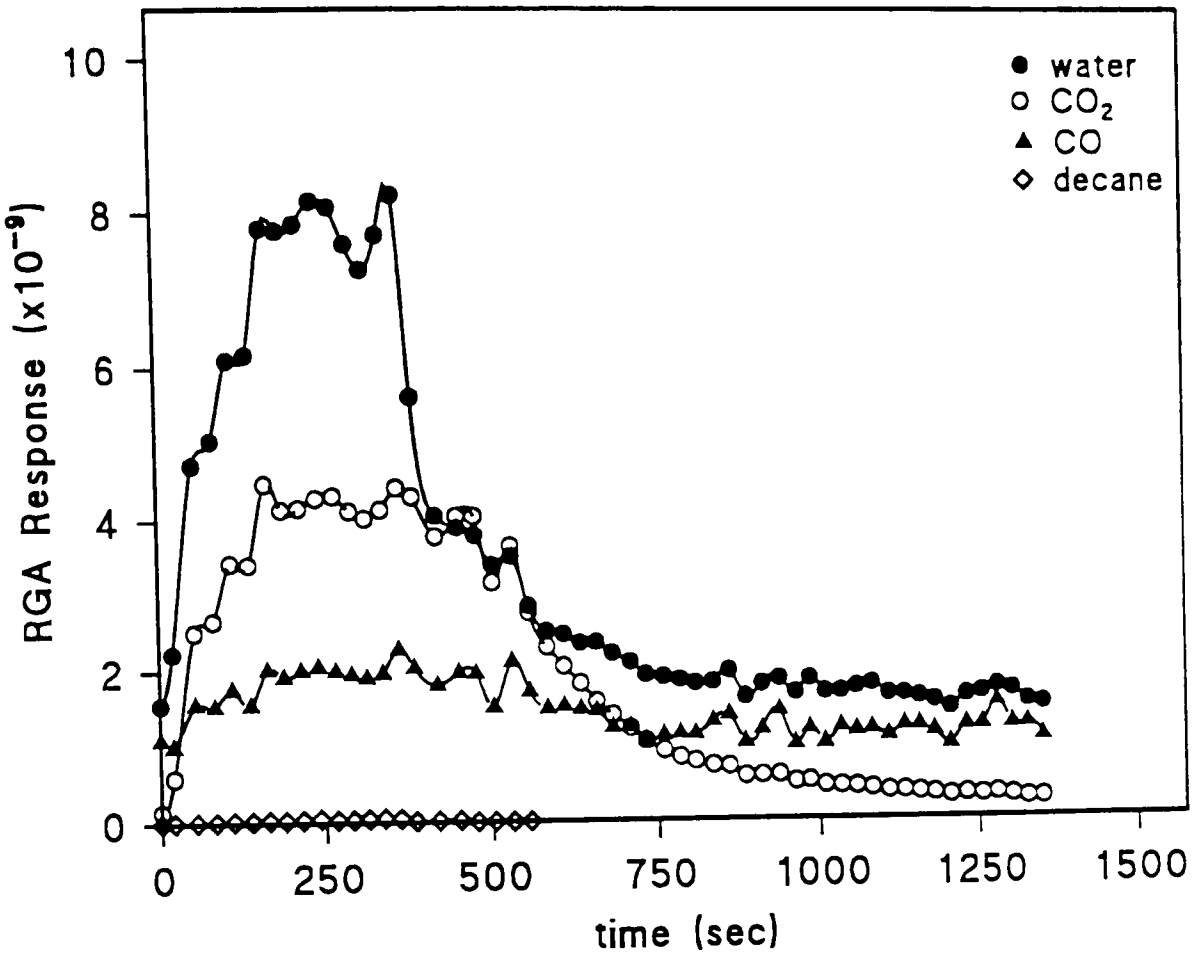

Figure 6.16 Combustion of decane on catalyst-coated Fecralloy as a function of time at 423K.

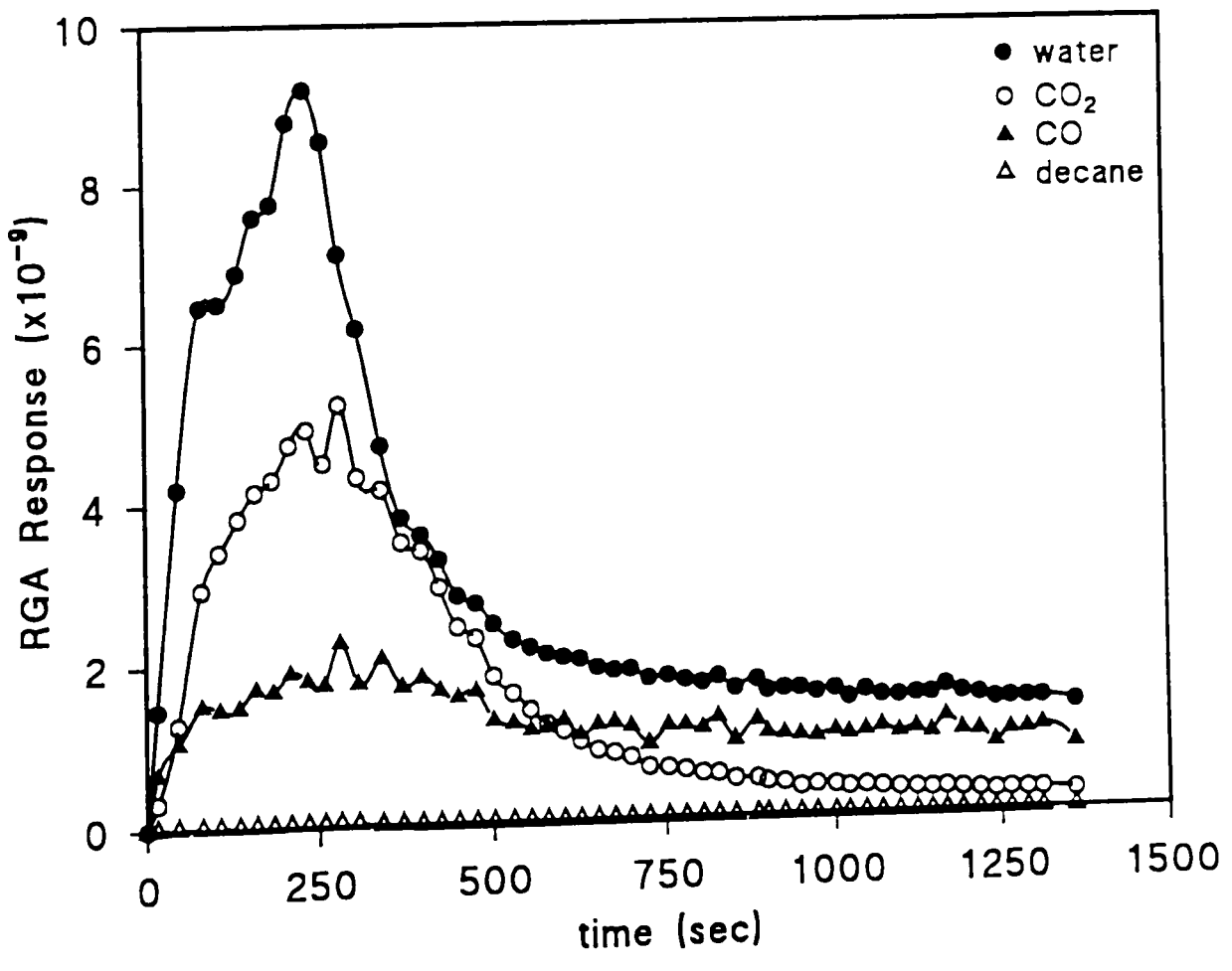

Figure 6.17 Combustion of microemulsion SM1 on catalyst-coated Fecralloy as a function of time at 423K

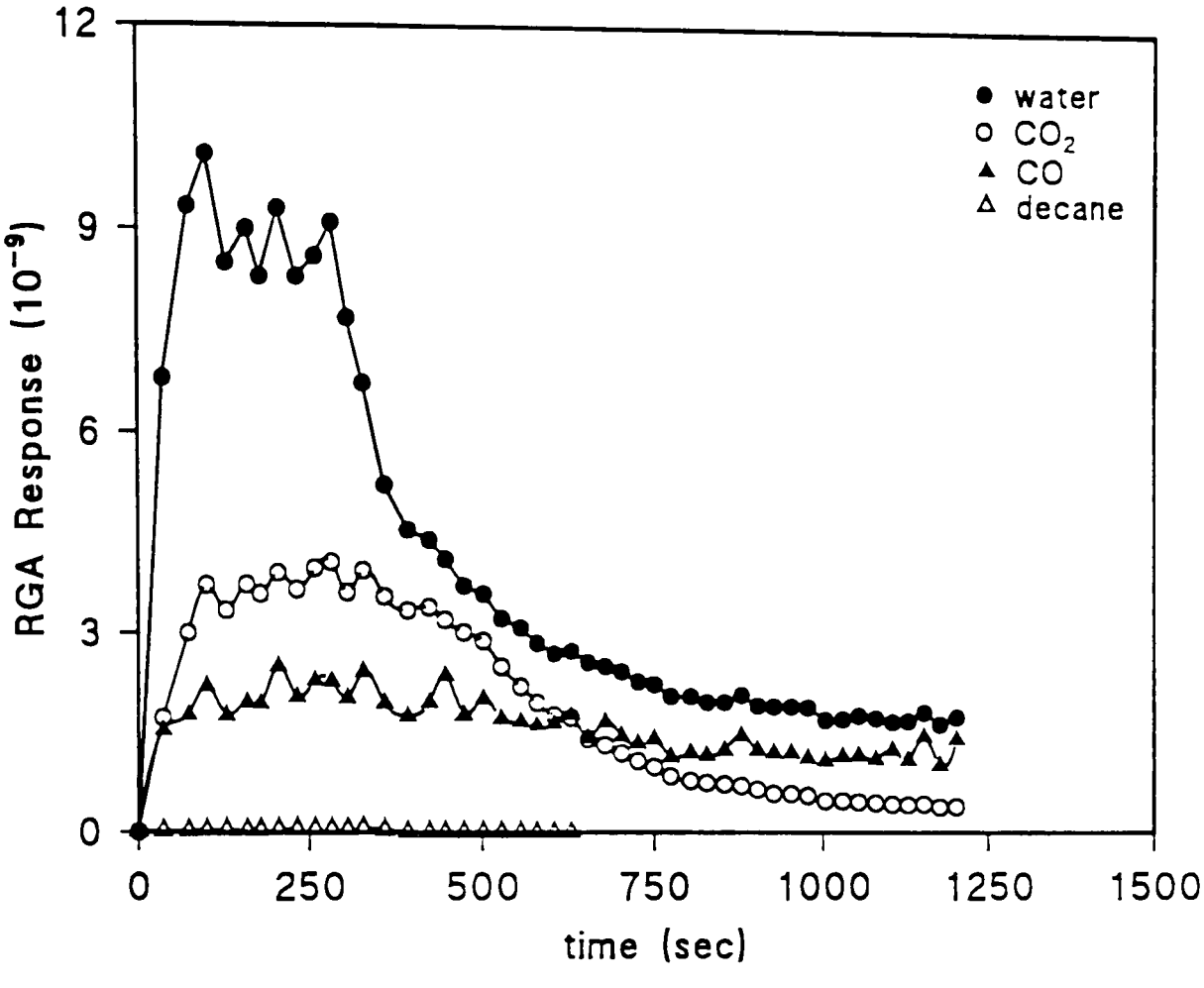

Figure 6.18 Combustion of decane on silica as a function of time 573K.

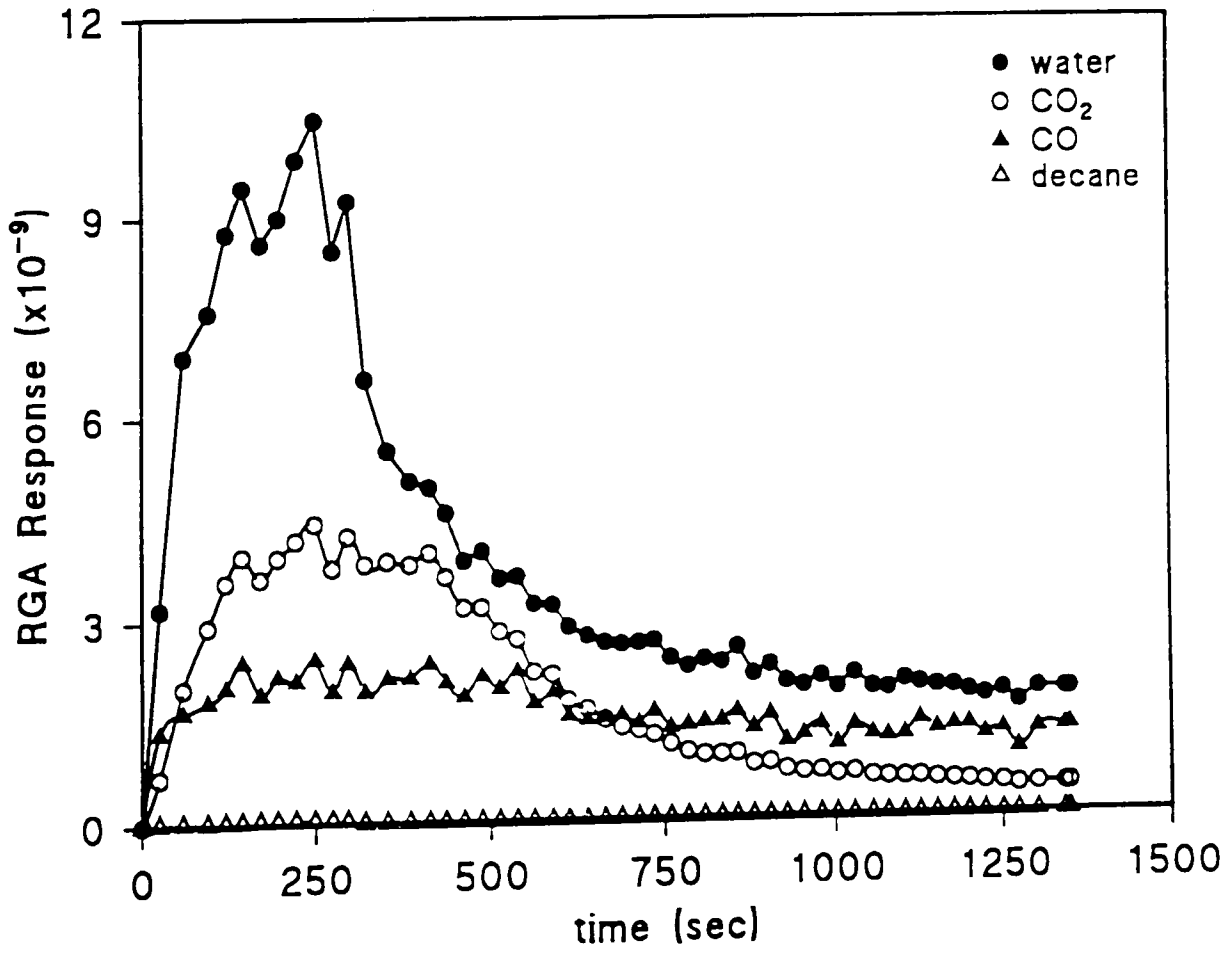

Figure 6.19 Combustion of microemulsion SM1 on silica as a function of time at 573K.

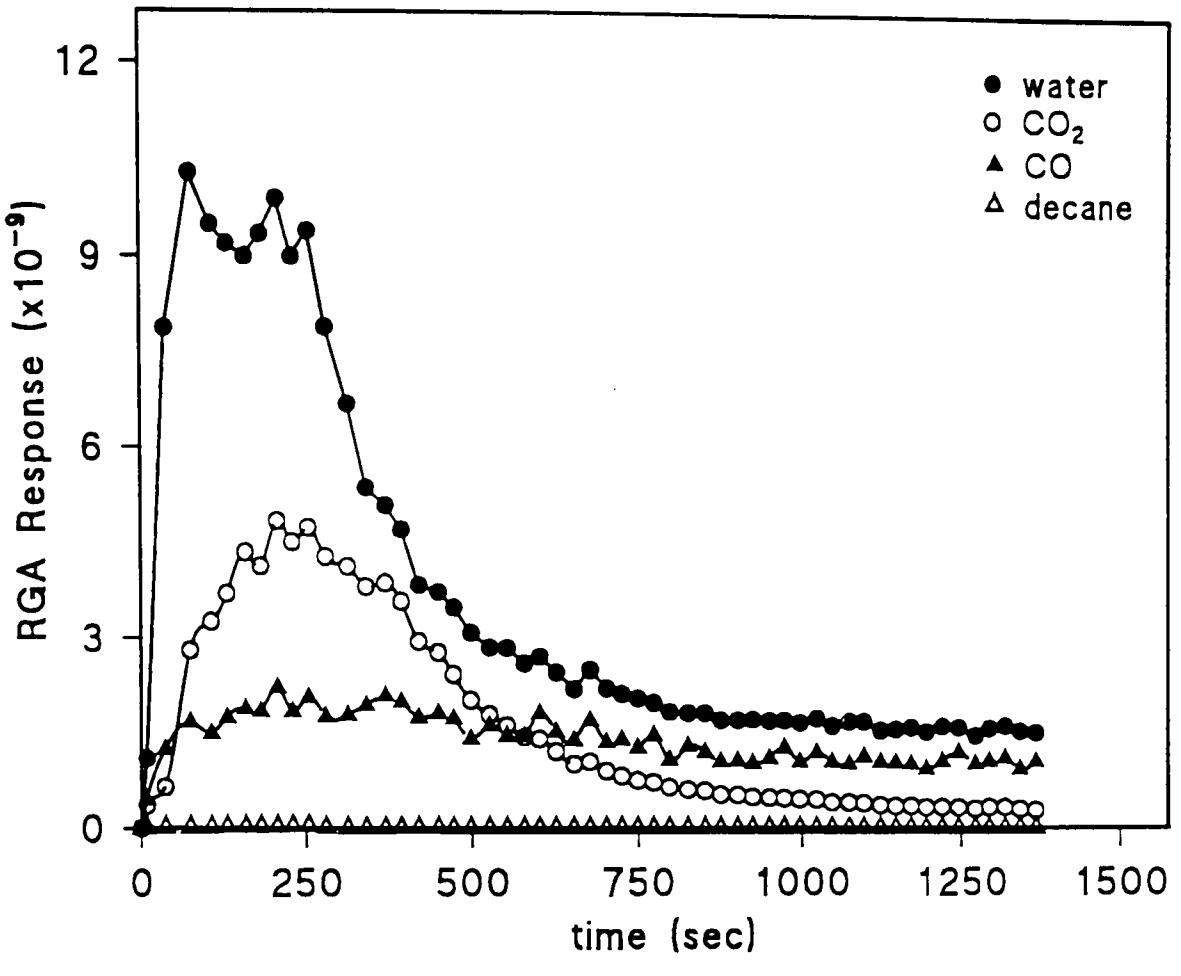

Figure 6.20 Combustion of microemulsion SM3 on silica at 573K

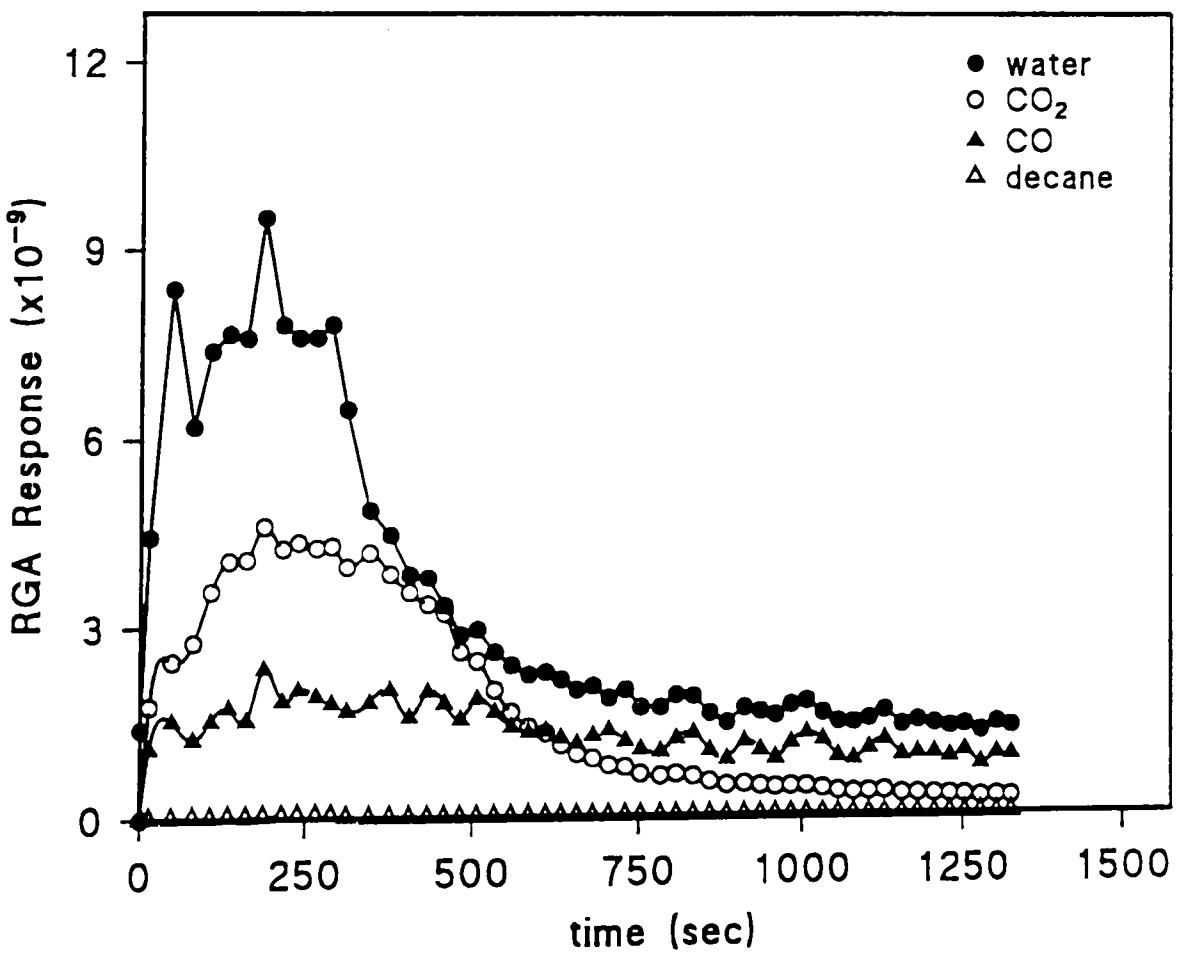

Figure 6.21 Combustion of decane on oxidised Fecralloy as a function of time at 573K

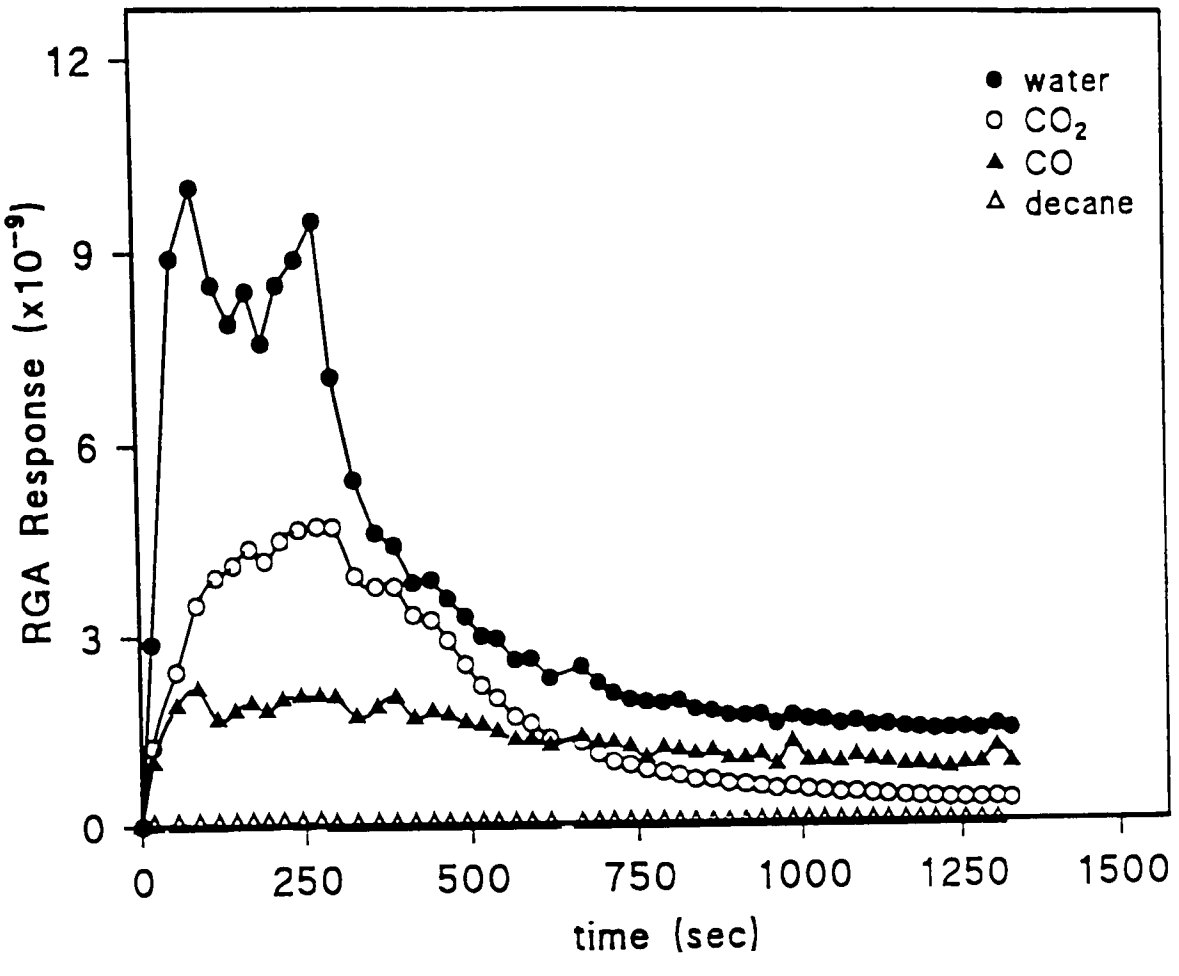

Figure 6.22 Combustion of microemulsion SM1 on oxidised Fecralloy as a function of time at 573K

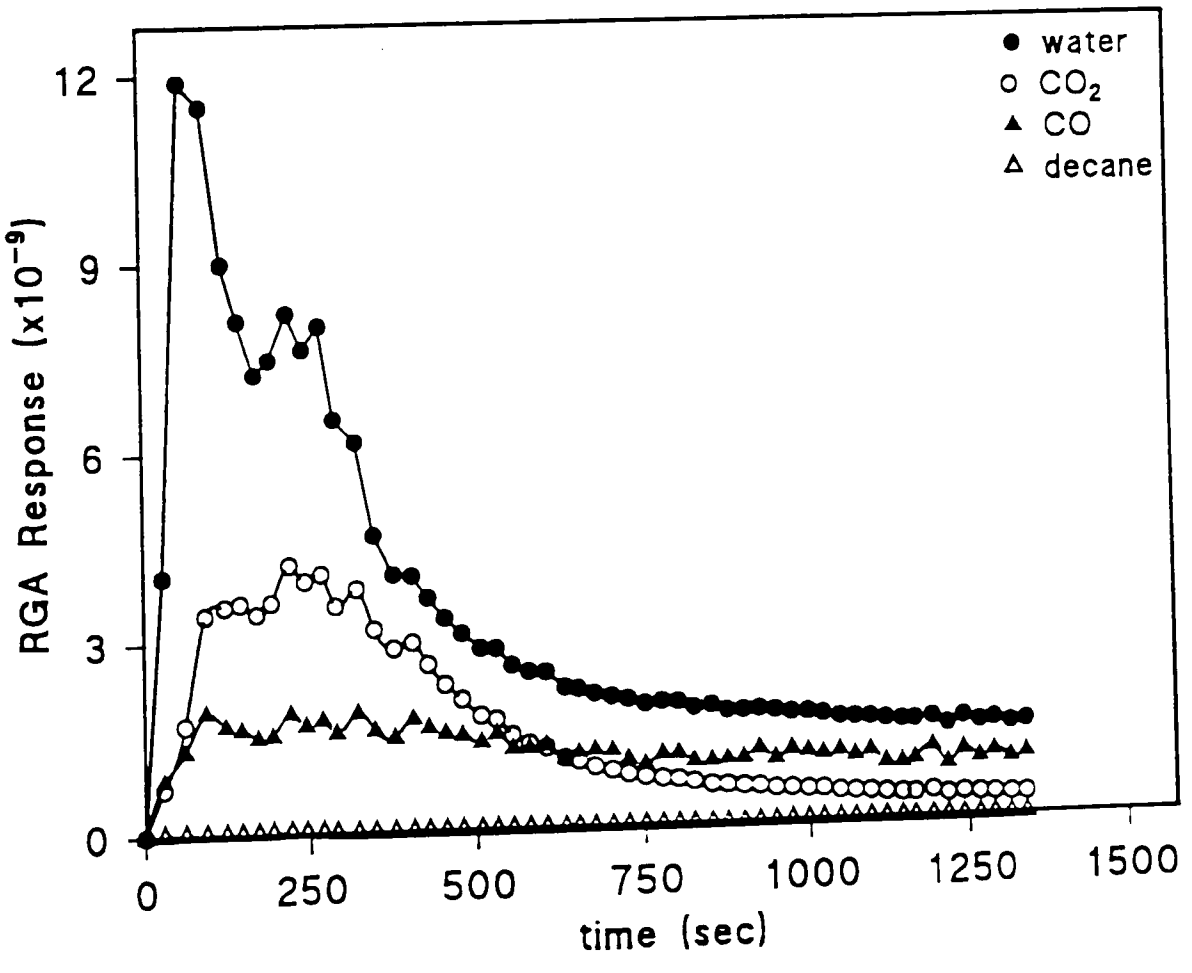

Figure 6.23 Combustion of microemulsion SM3 on oxidised Fecralloy as a function of time at 573K

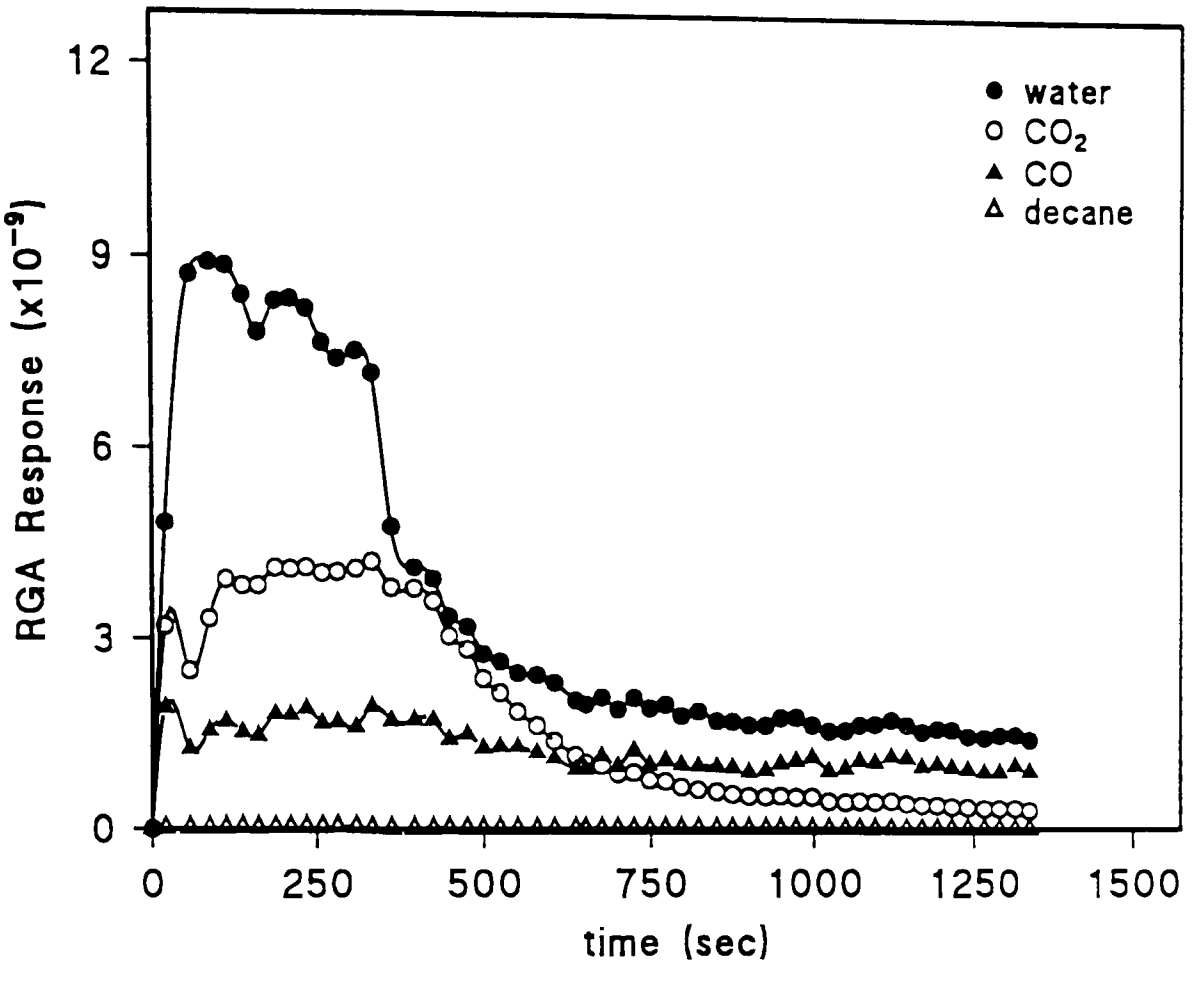

Figure 6.24 Combustion of decane on catalyst-coated Fecralloy as a function of time at 573K

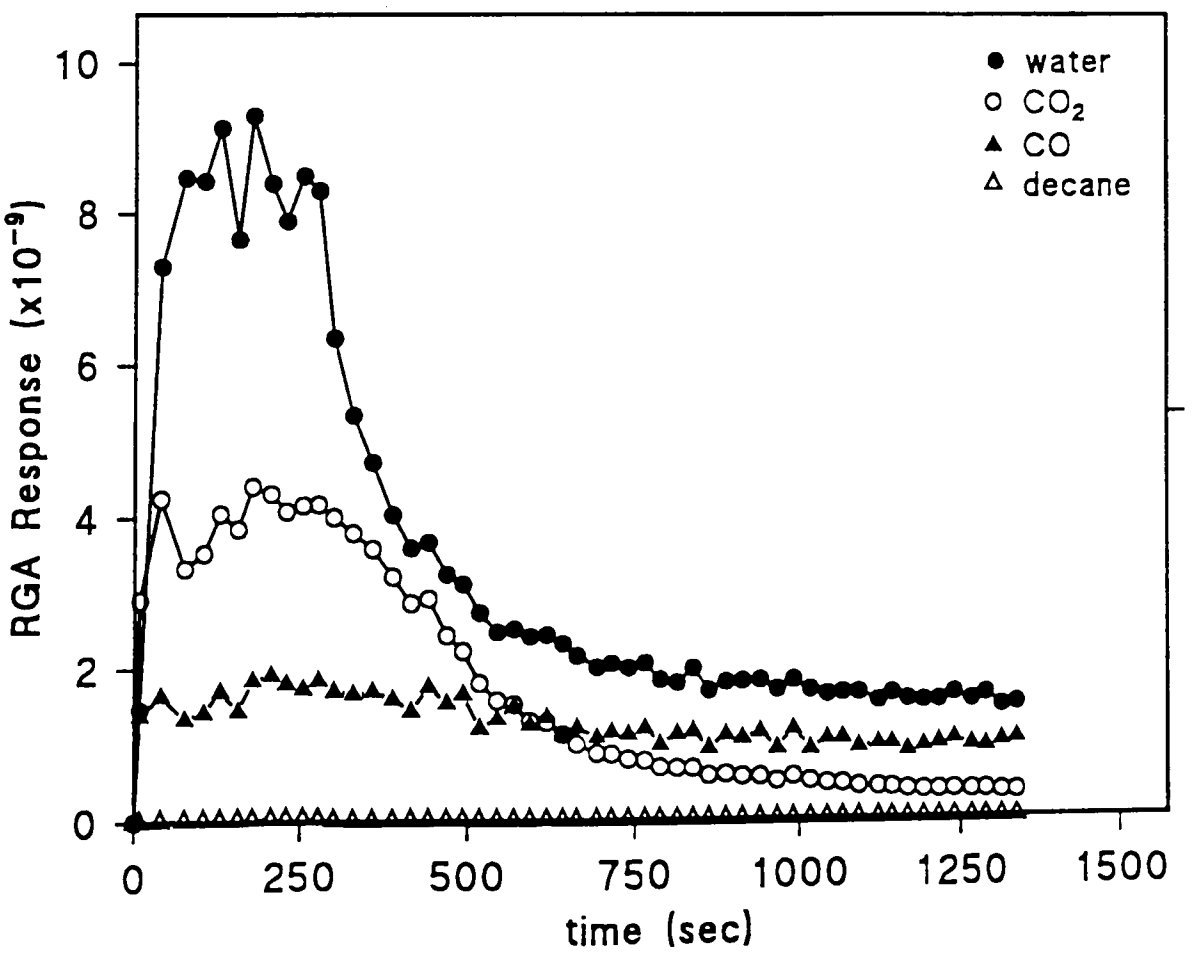

Figure 6.25 Combustion of microemulsion SM1 on catalyst-coated Fecralloy as a function of time at 573K

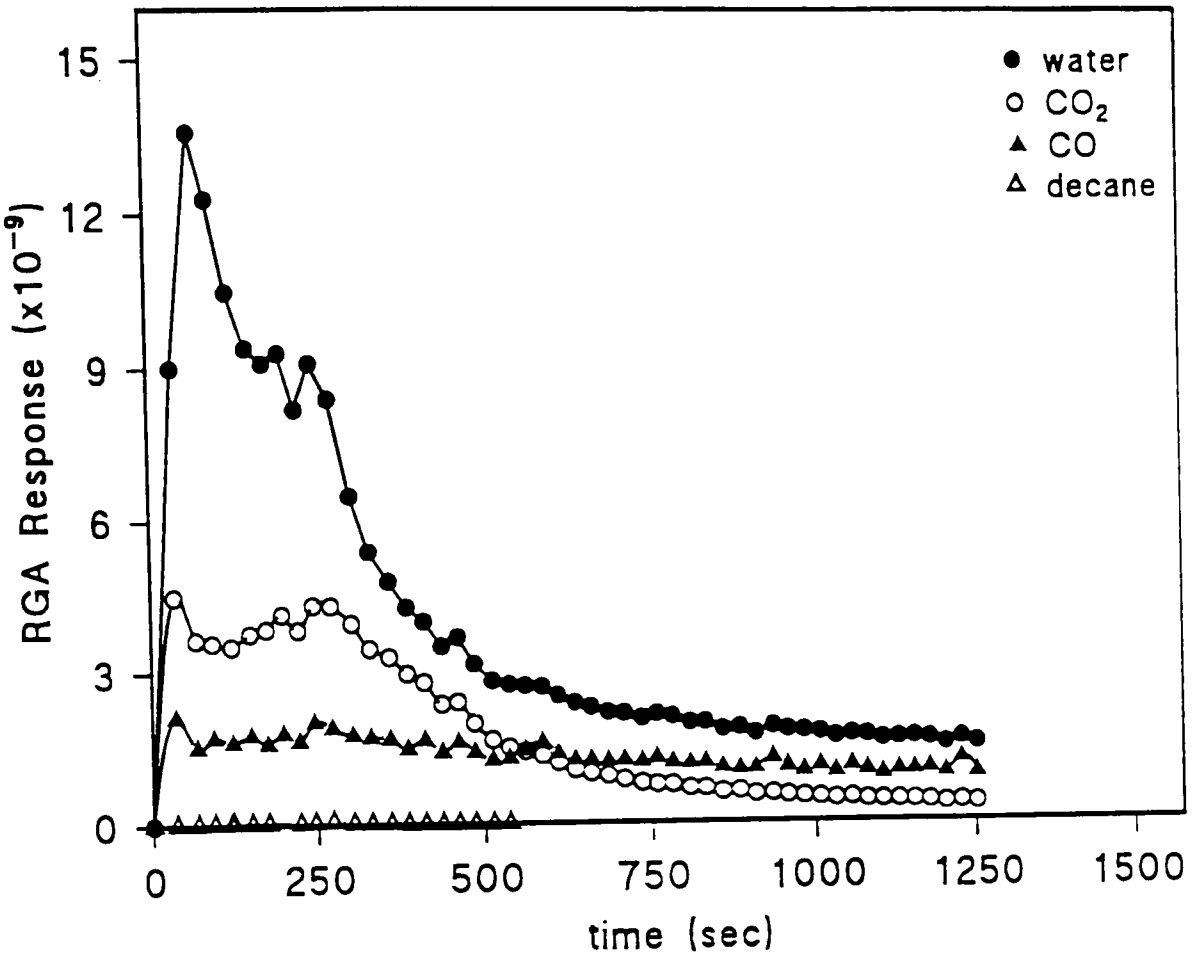

Figure 6.26 Combustion of microemuision SM3 on catalyst-coated Fecralloy as a function of time at 573K

In order to confirm the formation of formaldehyde and acetaldehyde during the combustion of microemulsion systems, HPLC analysis was carried out as described in the previous section 6.3. Initially, calibration curves were obtained for the pure derivatives as shown in Figures 6.27-6.28. The chromatographic results of the HPLC analysis for formaldehyde and acetaldehyde are presented in Figures 6.29 to 6.30 which suggested that these components were being produced to the extent of μmolar level (see Table 6.4).

This formation was not related to the concentration of pentan-1-ol present, although, the ratios

formaldehyde formed/pentan-1-ol injected = 0.0125

acetaldehyde formed/pentan-1-ol injected = 0.133

were low. This could be optimised for fuel/hydrocarbon utilisation. This microemulsion technology could therefore lead to a new Clean Technology route to aldehyde oxygenates and should be explored further. A mixture of bitumen oil, water and nonionic surfactant in the ratio 68:30:2 has produced an emulsion fuel known as "orimulsion" [70]. The present microemulsion combustion experiments could be related to such practical combustion problems.

Calculation

Percentage of pentan-1-ol in microemulsion = 12.5 % w/w

Percentage of pentan-1-ol in microemulsion = 11.935 % v/v

Volume of microemulsion injected = $5mm^3$

$5mm^3$ of microemulsion contains pentan-1-ol = $0.5965mm^3$

88.15g or $108.37cm^3$ of pentan-1-ol = 1 mole

$0.5965mm^3$ of pentan-1-ol = 5.504 µmol

Concentration of formaldehyde observed = 0.069 µmol

Concentration of aetaldehyde observed = 0.733 µmol

Ratio of formaldehyde formed/pentan-1-ol injected = 0.0125

Ratio of acetaldehyde formed/pentan-1-ol injected = 0.133

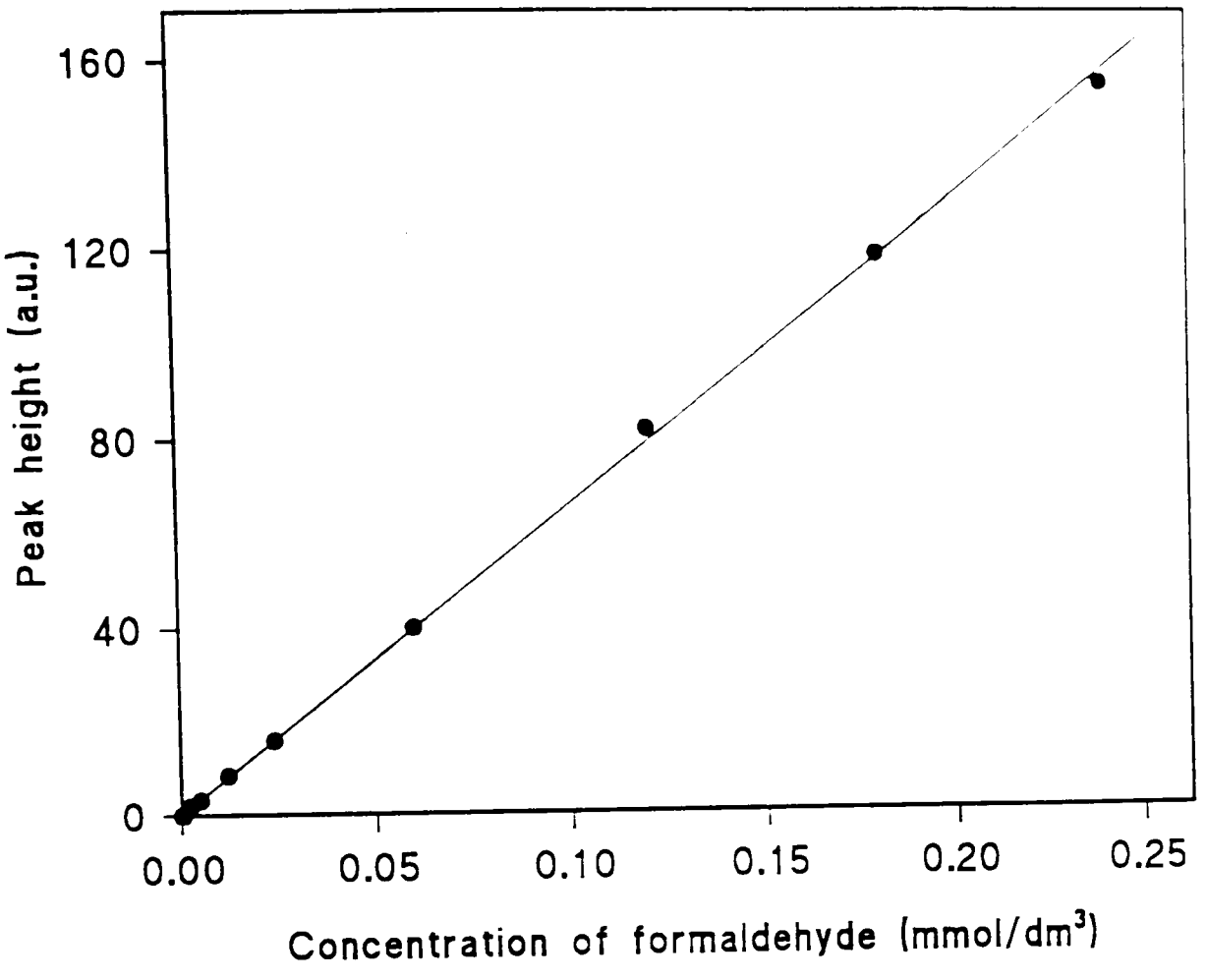

Figure 6.27 Calibration curve for formaldehyde giving a correlation coefficient 0.9996.

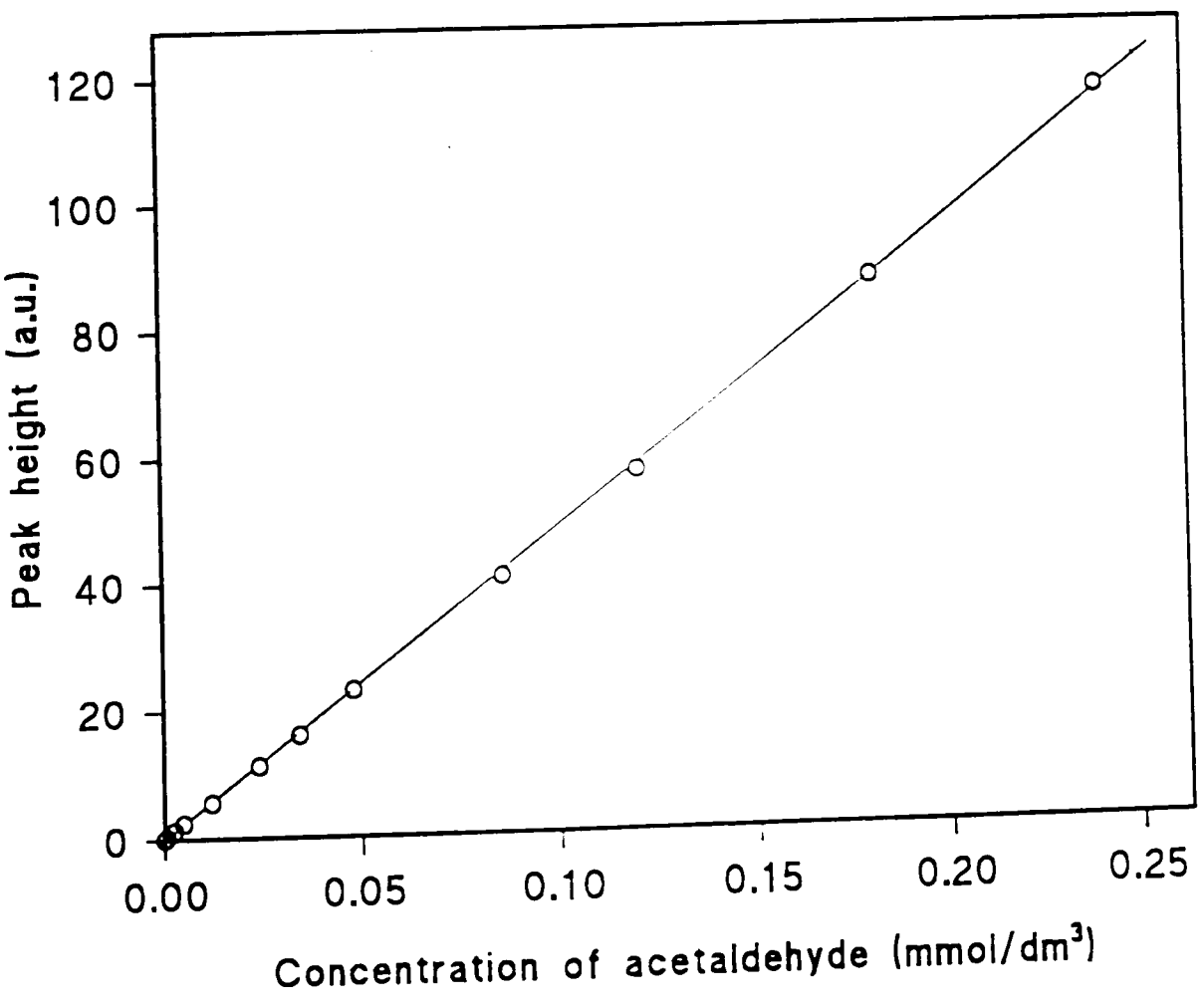

Figure 6.28 Calibration curve for acetaldehyde giving a correlation coefficient 0.9994.

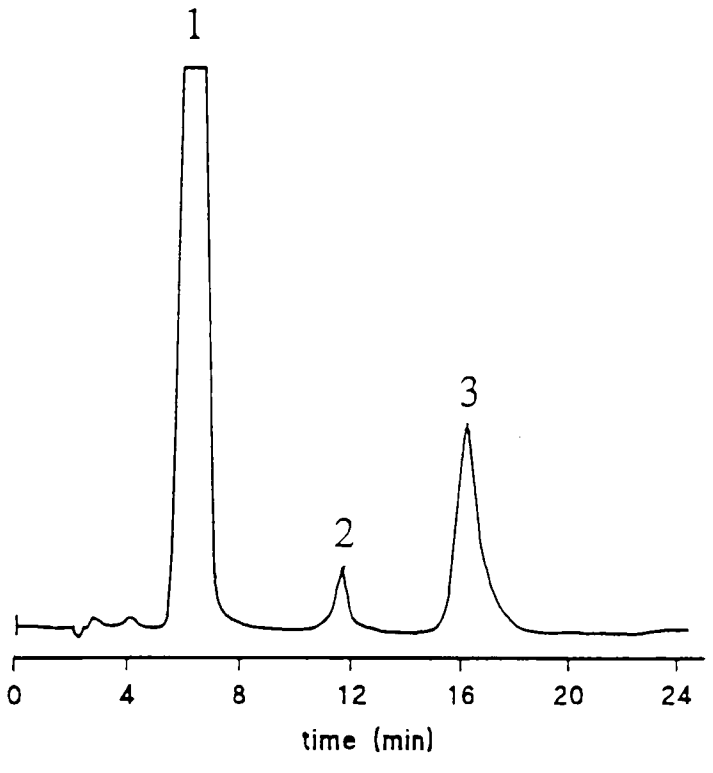

Figure 6.29 HPLC profiles for the microemulsion SM1 where peaks 1, 2 and 3 represent DNPH, formaldehyde and acetaldehyde respectively.

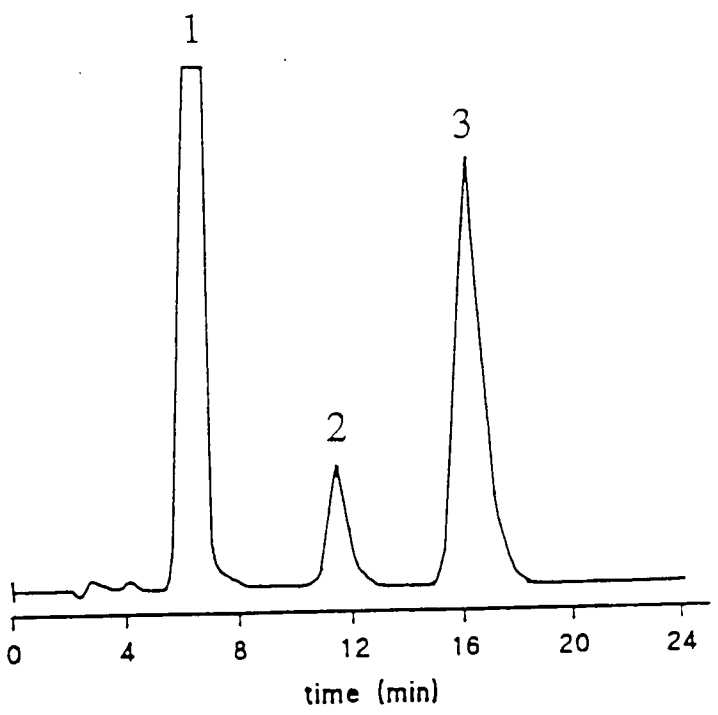

Figure 6.30 HPLC profiles for the microemulsion SM3 where peaks 1, 2 and 3 represent DNPH, formaldehyde and acetaldehyde respectively.

Table 6.4 Summary of the HPLC data

Microemulsion system	Percentage of pentan-1-ol (%v/v)	$5mm^3$ of microemulsion contains pentan-1-ol (µmol)	Concentration of formaldehyde produced (µmol)	Concentration of acetaldehyde produced (µmol)	Ratio of formaldehyde formed:pentan-1-ol injected	Ratio of acetaldehyde formed:pentan-1-ol injected
SM1	11.935	5.504	0.069	0.733	0.0125	0.133
SM3	12.079	5.557	0.261	0.966	0.0469	0.173

6.4.1 Summary of Results

In summary, the evaporation/combustion characteristics for the three microemulsions have been shown to vary with particle size and water content of the w/o microemulsion system. All microemulsions appear to produce similar amount of combustion products i.e. water, CO and CO_2 but variable extents of formaldehyde and acetaldehyde, dependent on the emulsion and catalyst used. Again importance of fact that formaldehyde/acetaldehyde can be produced in terms of fuel stock depletion.

6.5 SYNTHESIS OF COLLOIDAL SILICA BY MICROEMULSION METHOD

6.5.1 Introduction and Background

During the formation of a microemusion, the interfacial area increases enormously. The free energy of microemulsion formation should be negative to allow spontaneous formation to occur (see Chapter 2). This can only be achieved if the interfacial tension between oil and water ($\gamma_{o/w}$) is very small or even negative.

In most cases, the preparation of a microemulsion requires the presence of a primary surfactant and of a second surfactant, usually referred to as co-surfactant [36-40]. Surfactant and co-surfactant molecules adsorb at the oil/water interface and lower the interfacial tension.The preparation of colloidal sol by microemulsion method has been widely investigated in the last ten years. Colloidal silica particles are an interesting subject in colloid chemistry. Stober et al [41] suggested a method for preparing mono-disperse non-porous spherical particles of silica by the controlled hydrolysis of tetraethoxysilane $Si(OEt)_4$ (TEOS; where Et is an ethyl C_2H_5 group) in ethanol and ammonium hydroxide. Wang et al [42] synthesized submicron spherical particles of silica by the hydrolysis of sodium silicate in the w/o microemulsions. The average particle size was about 30 nm. Arriagada and Osseo-Asare [43-44] have investigated the synthesis of silica nanoparticle via the base-catalyzed controlled hydrolysis of TEOS in a nonionic reverse microemulsion. The overall reaction leading to the formation of silica may be represented as

$$Si(OEt)_4 + 2H_2O = SiO_2 + 4EtOH \qquad (6.1)$$

Regev [45] has made a dynamic study of the growth process of the hexagonal MCM41 mesoporous material in solution using cryo-TEM and X-ray scattering. It was found that clusters of elongated micelles are the precursors of the final product. A spherical-to-elongated micelle transition was detected upon addition of the silica source to the surfactant-base-water solution. Monodisperse colloidal silica-cadmium sulfide nanocomposite spheres have been synthesized by Chang and co-workers [46]. These spherical particles can be used in colloidal self-assembly processes for preparing crystalline colloidal arrays and also useful for fabricating optical devices [47-51]. They have also demonstrated a method to grow silica-CdS sphere nanocomposites which allows to produce colloidal particles with a variety of morphologies. Chang et al [52] described a method to further process these nanocomposite spheres in order to form complex voids within the silica colloids. These monodisperse silica spheres are porous and can be used for further modify the cavity surfaces. Many other research groups are also developing approaches to produce complex-nanostructure morphologies in various materials [53-55].

Polymerisation processes in microemulsions have recently been studied [56-59]. The inverse microemulsion polymerisation of water-soluble acrylamide monomers within an alkane continuous phase provides a potential route for production of polymers with novel physical properties and at high reaction rates [60].

Here, an attempt has been made to produce colloidal particle in the w/o microemulsions by adding TEOS at 298K. The size of the colloidal particles depended on the M-ratio which was the molar ratio of water to TEOS. The preparation and characterisation of the colloidal silica using TEM as well as their stability are discussed below.

6.5.2 EXPERIMENTAL

Colloidal silica particles have been synthesized in water-in-oil microemulsion microreactors. The w/o microemulsions were prepared by mixing water, surfactant, alcohol and hydrocarbon (as the composition shown in Table 6.5) at 298K and gently shaking. Tetraethoxysilane $Si(OEt)_4$ (TEOS) was added to the microemulsions to produce colloidal silica. Particle size of the colloidal silica depended on the M-ratio (i.e. the molar

ratio of water to TEOS). After 72 h, the microemulsions were appeared to be light blue indicating that the colloidal particles had been produced.

Table 6.5 Composition of w/o microemulsions including TEOS

Composition of w/o microemulsion (w/w%)					
Water	TX-114	Pentan-1-ol	Decane	TEOS added (g)	M-ratio
4.0	12.5	12.5	71.0	2.0	23.1
3.0	12.5	12.5	72.0	2.0	17.3
2.5	12.5	12.5	72.5	2.5	14.4
2.0	12.5	12.5	73.0	4.0	5.7

6.5.3 Transmission Electron Microscopy (TEM)

Electron microscopy is an extremely versatile technique capable of providing structural information over a wide range of magnification. At one extreme, scanning electron microscopy (SEM) complements optical microscopy for studying the texture, topography and surface features up to tens of micrometers in size can be seen and, because of the depth of focus of SEM instruments, the resulting pictures have a definite three-dimensional quality. At the other extreme, high resolution electron microscopy is capable, under favourable circumstances of giving information on an atomic scale by direct lattice imaging.

Electron microscopes are of either transmission or reflection in design. For examination in transmission (TEM), samples are usually thinner than 200nm. This is because electrons interact strongly with matter and are completely absorbed by thick particles. In order to minimise electron scattering a high vacuum is used. Electron microscopes contain several electromagnetic lenses. The condenser lenses are used to control the size and angular spread of the electron beam that is incident on the sample. Transmitted electrons then pass through a sequence of lenses and form a magnified image of the sample on a fluorescent viewing screen from which photograghs are then taken. A schematic representation of the transmission electron microscope is shown in Figure 6.31.

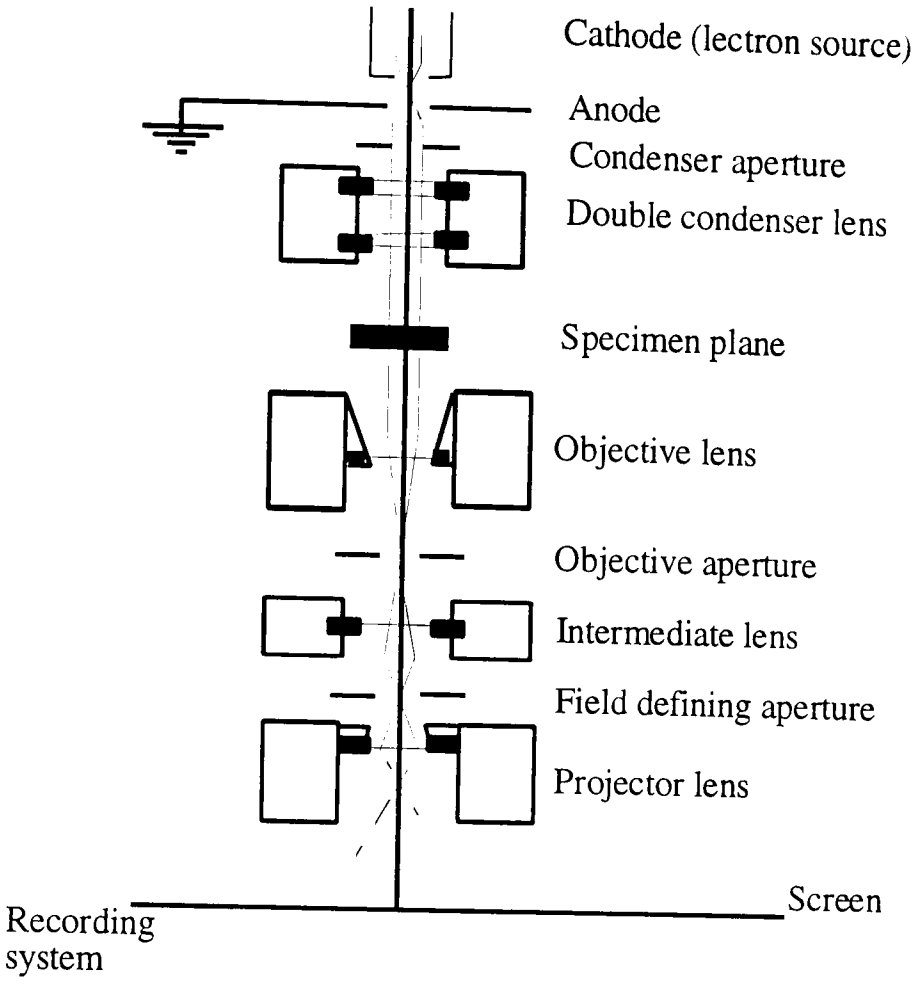

Figure 6.31 Schematic diagram of a typical transmission electron microscope

A transmission electron microscope has been used to obtain information concerning the external morphology, the size, shape of dispersion of small particles. A small drop of the colloidal dispersion was placed on a film coated copper grid using either a platinum loop or a fine capillary. After the solvents had evaporated the grids were inserted in the electron microscope for examination. The supporting films on the grids are normally nitrocellulose or polyvinyl formal.

6.5.4 RESULTS AND DISCUSSION

6.5.4.1 Particle Characteristics

The TEM results obtained in the experiments where the microemulsion phase remained stable even after particle formation are presented in the form of micrographs in Figures 6.32 and 6.33. These micrographs show that the silica particles are ultrafine (diameters in the range of 40-90 nm), fairly monodisperse and spherical in shape. In addition, the presence of the surfactant allows the formation of an ordered particle arrangement on the

(a)

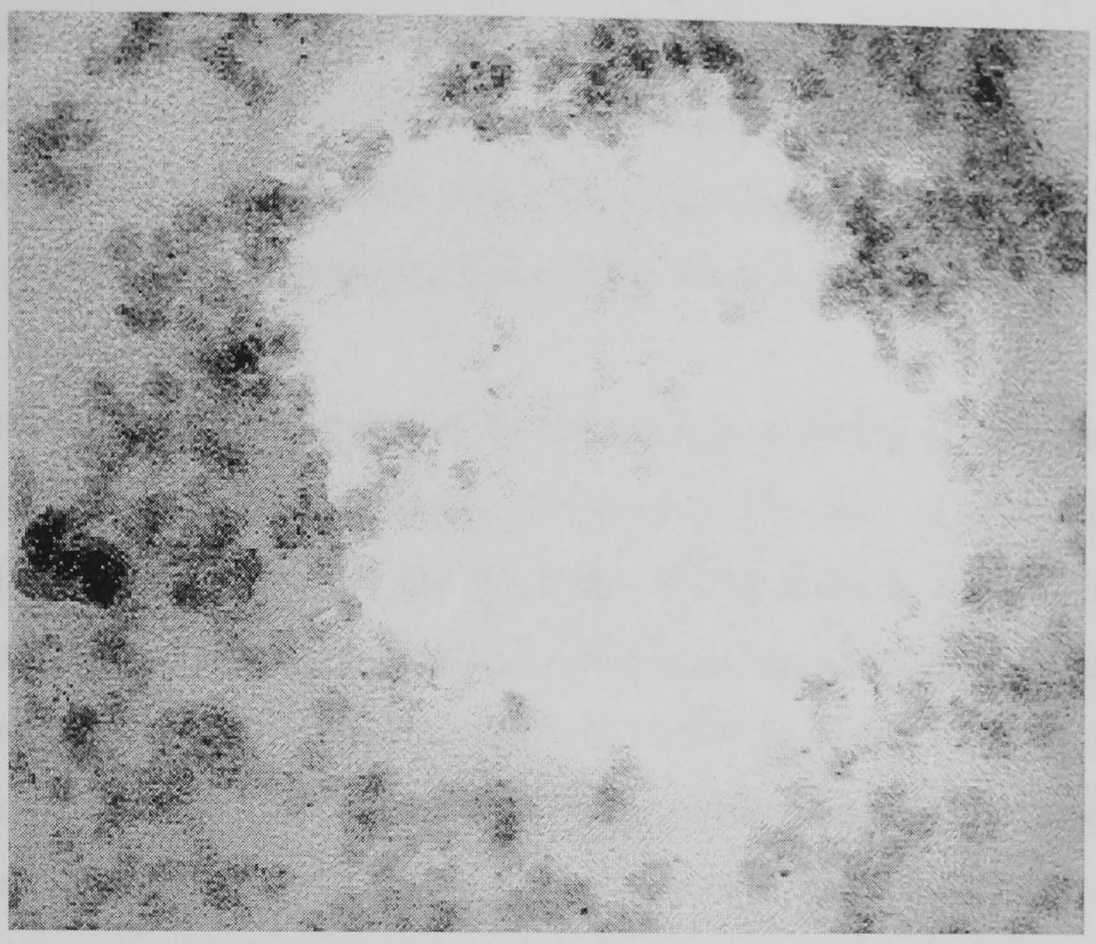

(b)

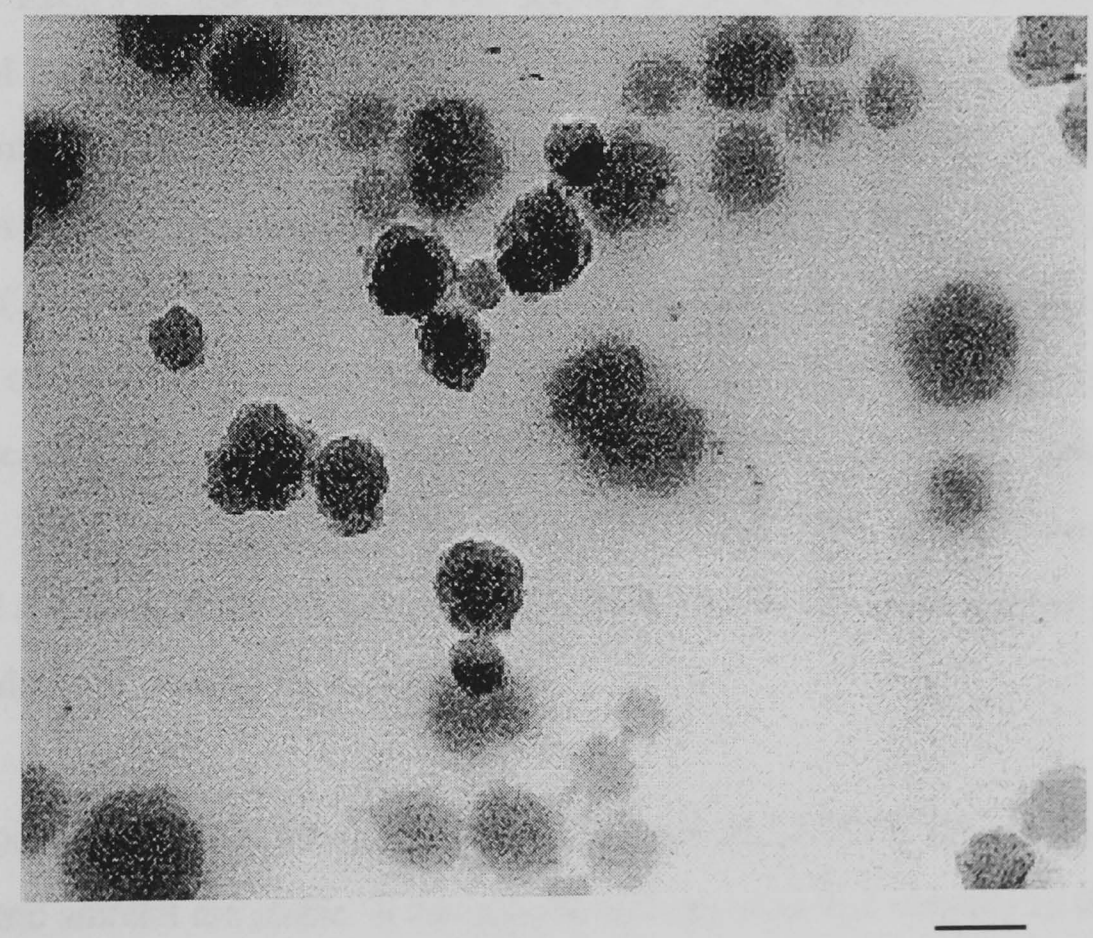

Figure 6.32 TEM micrographs of SiO_2 particles obtained by hydrolysis of TEOS in the w/o microemulsion ([water]/[TEOS] ratio M=14, water pH=10.5); (a) 48h (b) 160h at 298K.

TEM grid upon vaporisation of the solvents (i.e. pentan-1-ol and decane). The monodisperse particles produced in the reverse microemulsion system may be associated with a process of nuclei aggregation, which has been postulated [61] as the main mechanism of particle growth during the early stages of reaction.

The particle size distribution appeared to be as a function of time at a constant M-ratio (see Figures 6.32-6.33). The micrographs shown in Figure 6.32 (a) (b) correspond respectively to the samples taken 48 and 160 h after TEOS addition. It should be noted that here the synthesis experiment was initiated under conditions where the microemulsion occurred as a single phase. It has been postulated [62] that during the particle formation process there is a partial expulsion of water from the interior of the inverse micelles and this creates a second phase of bulk water which apparently induces the formation of new silica nuclei.

6.5.4.2 Effect of the Water/TEOS Molar Ratio (M-ratio)

The effect of M-ratio on dispersion stability has been investigated at a fixed surfactant/co-solvent concentration. All the dispersions with high M-ratio were stable for 3-4 months and over. However, the dispersions were not stable when water-to-TEOS ratios below the stoichiometric (2:1) required for complete TEOS conversion were used. The sample with M=2, settling of the solid product was observed after about 48h of reaction time. The particles produced at (M) values of 17.3 and 23.1 at 298K (720h after TEOS addition) are shown in the TEM micrographs of Figure 6.33 (a) (b). The particles were fairly monodispersed and no evidence of particle aggregation was observed in samples prepared at higher M values, as seen in Figures 6.32.

It has been reported [62] that the samples prepared with H_2O/TEOS molar ratios above the stoichiometric amount are stable. It has also been suggested that stability in the silica-containing NP-5 reverse micellar system is achieved through the presence of the surfactant and the availability of residual water molecules. The water molecules are envisaged as forming a thin polar film (water-shell) surrounding the hydrophilic silica surface. The oxyethylene groups of the surfactant molecules then adsorb at this aqueous film by

(a)

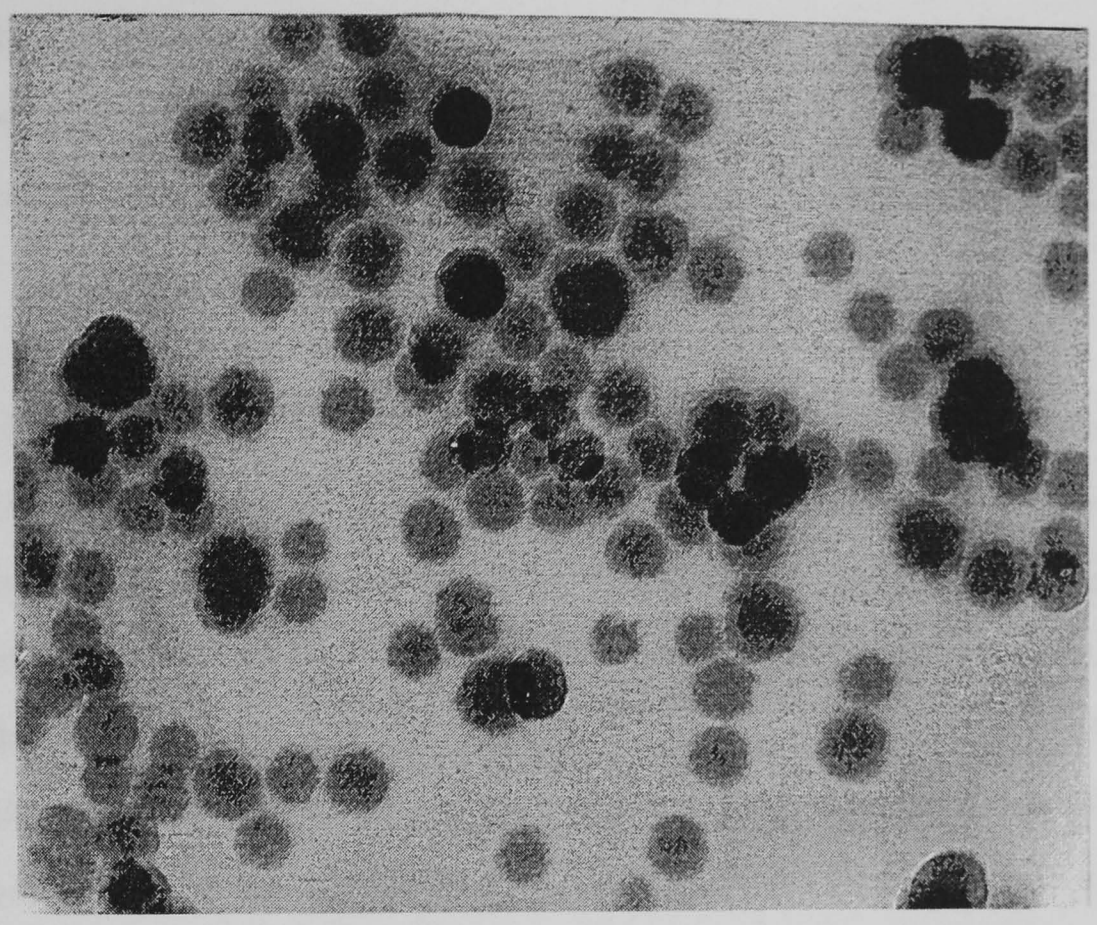

(b)

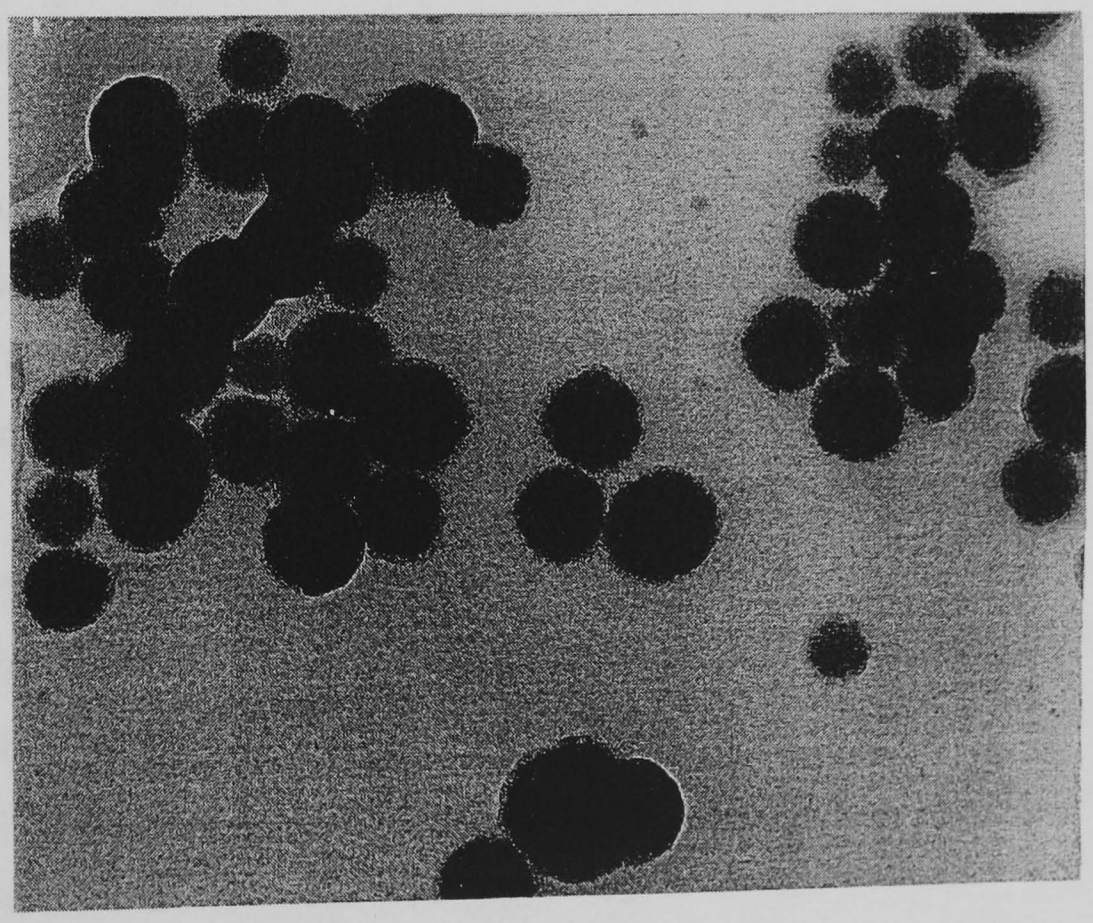

Figure 6.33 TEM micrographs showing the effect of M-ratio on the size distribution of SiO_2 particles after 720h; (a) M=17.3, (b) M=23.1 at 298K.

hydrogen bonding with the underlying water molecules. Under these conditions, stabilization of the surfactant-encapsulated solid particles against flocculation upon inter-particle collision may be the result of (a) electrostatic repulsion between the negatively charged surfaces (b) steric interaction between the tails of the adsorbed surfactant molecules.

Vincent et al [63] studied the flocculation of silica dispersions in ethanol-cyclohexane mixtures and examined the conditions for colloidal stability in a related system. It was observed that an increase in the volume fraction of cyclohexane decreased the magnitude of the zeta potential and resulted in greater instability of the silica dispersion. As M in the initial solution decreases, the ethanol/water ratio in the residual microemulsion (following particle formation) increases correspondingly (equation (6.1)). It has been observed [63] (in cyclohexane-ethanol mixrures) that by replacing water molecules in the water shell, the ethanol molecules should be able to provide a measure of colloidal stability. It must be recognized, however, that not all the ethanol molecules generated remain within the polar domain of the reverse micelles.

The ethanol reaction product can alter the microemulsion stability, transforming an initial single phase microemulsion into a two-phase reverse microemulsion-bulk water system. The creation of a second aqueous domain (i.e. bulk water, in addition to the water pools) provides another reaction site for particle nucleation and growth.

6.5.4.3 Summary of Results

The information obtained from the TEM results can be summarised as follows.The microemulsions with TX-100 as a surfactant can be used to produce monodisperse colloidal silica particles of desire size and morphology by changing the M-ratio. Higher M values enhance the colloidal stability. The product of the ethanol reaction can alter the microemulsion stability, transforming an initial single-phase microemulsion into a two-phase system.

References

[1] A. Williams and M. Pourkashanian, J. Institute of Energy, **December,** 209, (1987)

[2] E.G. Masdin and M.W. Thring, J. Institute of Fuel, 251, (1962)

[3] K.C. Adiga, Emerging Energy Technology Symposium, ASME, PD-**l41**, 9, (1992)

[4] Marketing Publication of BITOR EUROPE LTD. (1993)

[5] D.W. Naegeli and C.A. Moses, American Society of Mechanical Engineers. Paper 82-GT-33, (1982)

[6] S.C. Wong, A.C. Lin and H.Y. Chi, **23rd** Sympos. Int. on Combust., 1391, (1990)

[7] O.L. Gulder and J.K.S. Wong, **20th** Sympos. Int. on Combust., 1751, (1984)

[8] S.H. Chung and J.S. Kim, **23rd** Sympos. Int. on Combust., 1431, (1990)

[9] P. Cho, C.K. law and M. Mizamoto, Trans. ASME, J. Heat. Trans., **113,** 273, (1991)

[10] F.C. Zhuang, B. Ynag, J. Zhou and H. Yang, **23rd** Int. Sympos. Combust. 647, (1986)

[11] M.A. Cherian, M.T. Jacques and A. Williams, J. Inst. Energy, 70, (1990)

[12] I. Ahmad and S.R. Gollahalli, J. Propulsion and Power, **10,** 744, (1994)

[13] Y.Kitamura, Q. Huang, Y. Oka and T. Takahashi, J. Chem. Eng. Japan, **23,** 711, (1990)

[14] J.B. Jordan, A.N. Littler and A. Williams, J. of the Institute of Energy **December,** 222, (1986)

[15] A.T.S. Cunningham, B.J. Gliddon and R.T. Squires, Combustion in Engineering, Inst. Mech. Engineers Conference, (1983)

[16] E.M. Goodger, J. of the Institute of Fuel **September,** 132, (1977)

[17] R.M. Fristrom and A.A. Westenberg, "Flame Structure", New York, McGraw-Hill, 344 (1965)

[18] A. Feugier, in: J. Zung, Ed. "Evaporation-combustion of Fuels", Advances in Chemistry Series **166,** 178 (1978)

[19] P.A. Bonczyk, Fuel, **70**, 1403, (1991)

[20] V.M. Ivanov and P.I. Nefedov, NASA Tech. Trans. NASA TTF-258 (1965)

[21] M.T. Jacques, J.B. Jordan, A. Williams and L. Hadley-Coates, **16th**, Sympos. Int. on Combust., The Combustion Institute, 307 (1976)

[22] G. Greeves, I.M. Khan and G. Onion, **16th**, Sympos. Int. on Combust., The Combustion Institute, 321 (1976)

[23] M. Toussaint and M.P. Heap, Chemistry Commission of the International Flame Research Foundation Meeting, I Jmuiden, October (1974)

[24] R.E. Hall, Transaction of the ASME, J. Engineering Power, **98,** 425 (1976)

[25] V.M. Ivanov, B.V. Kantrorich, L.S. Rapiovets and L.L. Khotuntsev, J. Acad. Sci. USSR, **56**, (1957)

[26] C.T. Avedisian and R.P. Andres, J. Colloid Interface Sci. **64**, 438, (1978)

[27] J. Dooher, R. Genberg, R. Lippman, T. Morrone, S. Moon and D. Wright, Mech. Eng., **98**, 36, (1976)

[28] L.J. Spadaccini, and A. Palmask, J. Am. Chem. Soc., **16,** 232, (1977)

[29] J. B. Jordan and A. Williams, J. Inst. Energy Symp., (1981), Portsmouth, England.

[30] L.L. Baxter and Z.G. Habib, J. Combustion and Flame **90**, 199, (1992)

[31] Manufacturers Specification for Sensorlab VG Quadrupoles, Middlewich England, (1989)

[32] I. Howe, D.H. Williams, R.D. Bowen, Mass Spectrometry, Principles and Applications, 2nd Ed., McGraw Hill, USA, (1981)

[33] "Quadrupole Mass Spectrometry and its Applications", Ed. P.H. Dawson, Elsevier Scientific Publishing Company, Amsterdam, (1976)

[34] Manufacturers instruction manual for VG300D, VG Quadrupoles, Middlewich England, (1989)

[35] F.C. Zhuang, B. Ynag, J. Zhou and H. Yang, Twenty-first Symposium (International) on Combustion, The Combustion Institute, 647, (1986)

[36] P. Becher," Emulsions Theoery and Practice", Reinhold, New York, (1957)

[37] C. Kumar and H.N. Singh, Colloids and Surfaces **44,** (1990)

[38] S.I. Ahmad, K. Shinoda and S. Friberg, J. Colloid Interface Sci., **47,** 32, (1974)

[39] H. Saito and K. Shinoda, J. Colloid Interface Sci., **32,** 647 (1970)

[40] J. Lang, N. Lalem and R. Zana, J. Phys. Chem., **96,** 4667 (1992)

[41] W. Stober, A. Fink and E. Bohn, J. Colloid Interface Sci., **26,** 62, (1968)

[42] W. Wang, X. Fu, J. Tang and L. Jiang, J. Colloids and Surfaces A: Physicochemical and Engineering Aspects, **81,** 177, (1993)

[43] F. J. Arriagada and K. Osseo-Asare, Colloids and Surfaces, **69,** 105, (1992)

[44] K. Osseo-Asare and F. J. Arriagada, Colloids and Surfaces, **50,** 321, (1990)

[45] O. Regev, Langmuir, **12**, 4940, (1996)

[46] S. Chang, L. Liu, and S.A. Asher, J. Am. Chem. Soc., **116,** 6739, (1994)

[47] S. A. Asher, U.S. Patent 4,627,689, (1986);

[48] G. Haacke, H.P. Panzer, L.G. Magliocco and S.A. Asher, U.S. Patent 5,266,238, (1993)

[49] P.L. Flaugh, S.E.O. Donnell and S.A. Asher, J. Appl. Spectrosc. **38,** 847, (1984)

[50] S.A. Asher, P.L. Flaugh and G. Washinger, J. Appl. Spectrosc. **1,** 26, (1986)

[51] P.A. Rundquist, P. Photinos, S. Jagannathan and S.A. Asher, J. Chem. Phys. **95,** 1249, (1991)

[52] S. Chang, L. Liu, and S.A. Asher, J. Am. Chem. Soc., **116,** 6745, (1994)

[53] C. Roth, R. Kobrick, J. Aerosol Sci. **19,** 939, (1988)

[54] L. D. Keklikian and R.E. Partch, J. Aerosol Sci. **19,** 511, (1988)

[55] M. Ramamurti and K.J. Leong, J. Aerosol Sci. **18,** 175, (1987)

[56] F. Candau and Y.S. Leong, J. Polym. Sci. Polym. Chem. Ed. **23,** 193, (1985)

[57] F. Candau, Z. Zekhnini and J.P. Durand, J. Colloid Interface Sci. **114,** 398, (1986)

[58] C. Graillat, C. Pichot, A. Guyot and M.S. El Aasser, J. Polym. Sci. Polym. Chem. Ed. **24,** 427, (1986).

[59] V. Baade and K.H. Reichert, J. Eur. Polym. **20,** 505, (1984)

[60] E. Haque and S. Qutubuddin, J. Polym. Mater. Sci. Eng. **57,** 944, (1987)

[61] K. Osseo-Asare and F.J. Arriagada, Colloids and Surfaces, **50**, 321 (1990)

[62] F.J. Arriagada and K. Osseo-Asare, Colloids and Surfaces, **69**, 105 (1992)

[63] B. Vincent, Z. Kiraly, S. Emmett and A. Beaver, Colloids and Surfaces, **49**, 121 (1990)

CHAPTER SEVEN

CONCLUSIONS AND FURTHER RESEARCH

This research has produced basic and fundamental information about phase equilibria and interfacial characteristics in the microemulsion system. The major achievement of this work is the formulation of a model surfactant system for enhanced oil recovery. In addition, advances have been made in the studies of adsorption of surfactants onto rock surfaces, the formation of formaldehyde and acetaldehyde during the w/o microemulsion droplet combustion and synthesis of colloidal silica particles. Furthermore microemulsion characterisation carried out provides invaluable information in the selection of the best techniques to characterise the model surfactant system which leads to accurate and meaningful results.

It was decided that a great deal of importance lay in the understanding of the structure and properties of the surfactants (including the co-surfactants) used. The ability of the single surfactant or blends of two to form a stable microemulsion was to be given major attention.

However, a better understanding of the complex interaction between the injected fluids and the reservoir components (oil, brine and rock) is desirable for a successful application of various oil recovery processes. This can only come from a thorough understanding of the fundamental interfacial chemistry involved.

The more relevant details of the conclusions are presented here, under three main sections, as follows: phase equilibria in microemulsions and their characterisations, adsorption properties of the nonionic surfactants and microemulsion droplet combustion characteristics and synthesis of colloidal silica particles.

7.1 Phase Equilibria in Microemulsions

The phase equilibria of various oil/water/surfactant/co-surfactant systems have been investigated and characterised using several different analytical techniques. The results obtained maybe conveniently summarised as follows:

(i) Microemulsion microchemistry can be understood and fine-tuned in terms of phase equilibria and interfacial characteristics measured during salinity and temperature scans. Addition of alcohol enhances the solubilisation of the microemulsions.

(ii) The phase behaviour of nonionic surfactants can be improved by the addition of medium chain alcohols which act as co-surfactants and enhance the mutual solubility of a brine and oil.

(iii) Mixtures of surfactants (i.e. nonionic+anionic) together with a medium chain alcohol can be used as a model surfactant system in which the middle-phase microemulsions are produced that can be expected to meet the criteria for enhanced oil recovery; this is useful in view of the observations in accounting that enhanced oil recovery is becoming of growing commercial importance [1]. The system is stable at higher salinities and temperatures which are the requirements for enhanced oil recovery (EOR).

(iv) In systems containing oil, aqueous NaCl and surfactants (i.e. TX-100+SAS/SDS+ pentan-1-ol), ultra-low interfacial tensions (i.e. 0.1-0.01μN/m) can be attained. At a constant temperature and salt concentration, the surface tension falls as the TX-100 concentration increases and becomes constant at a concentration (CMC) corresponding to the onset of surfactant aggregation in either the aqueous or oil phase, depending on conditions. In the case of nonionic surfactants the CMC condition corresponds to a high concentration in the hydrocarbon phase and a low concentration in the aqueous phase.

(v) The interfacial tension at the CMC can be made to pass through a minimum value by varying salinity or temperature. At low salinity, TX-100 resides in the aqueous phase above the CMC, the associated surfactant is presumably in the form of aggregates swollen by the solubilisation of a hydrocarbon, i.e. an oil-in-water microemulsion exists. At high salinity, surfactant transfers to the oil phase and the solubilisation of water (w/o microemulsion) is favoured, leaving the monomers in the aqueous phase. When surfactant passes into a hydrocarbon phase it is accompanied by water in the form of reasonably monodisperse droplets packed with monolayer of surfactant. The curvature of the surface containing surfactant is opposite in aqueous and hydrocarbon phases. At intermediate values of salinity a middle-phase (a surfactant-rich phase) is formed. Surfactant transfer and phase inversion of the microemulsion systems are observed around conditions corresponding to minimum interfacial tensions.

(vi) Several analytical techniques have been used to characterise the middle-phase microemulsions as a function of salinity and temperature and are summarised as follows:

(a) It is possible with a modified spectrophotometer to perform the salinity and temperature scans of the microemulsion phases, and thus the equilibrium phase boundaries and optimum salinity can be determined accurately by using the computer programme presented in Appendix.

(b) The distribution of oligomers in the nonionic surfactants can be traced by HPLC analysis. The HPLC results also provide evidence of the shift in the distribution of oligomers in the microemulsion phases (see Figure 4.24 in Chapter 4).

(c) Solubilisation of water and oil in the microemulsion, and partitioning of alcohol in the aqueous and organic phases can be determined by gas chromatography. The solubilisation parameters can be used to obtain the optimum salinity (see Figure 4.31 in Chapter 4).

(d) Concentration of the surfactant in the middle-phase is measured by UV-

spectrophotometry.

(e) Dynamic light scattering can be used to obtain the mean droplet size and polydispersity index in the w/o microemulsions.

(f) Viscometry and electrical conductivity can be used to observe the phase transition in the microemulsion phases.

(g) The spinning drop method is used to measure the ultra-low interfacial tensions in the microemulsion phases.

(vii) Ultra-low interfacial tension can be achieved in the model surfactant system. On increasing the salinity, interfacial tensions between microemulsions and oil phases ($\gamma_{m/o}$), decrease whilst those between microemulsions and aqueous phases ($\gamma_{m/w}$) increase.

7.2 Adsorption of Surfactants on Surfaces

The adsorption of nonionic surfactants from aqueous and non-aqueous solutions has been studied at various temperatures and salinities from the view point that such adsorption is a major drawback in enhanced oil recovery processes; in the hope that a suitable set of temperature/salinity conditions could be found which result in a diminution or an elimination of undesirable adsorption [1]. From the present surfactant adsorption studies the following conclusions are drawn:

(a) The adsorption mechanism of non-ionic surfactants, and also of mixtures of non-ionic with anionic, includes a step of anchoring (of isolated molecules) followed by a step of aggregation (or "cooperative adsorption") comparable, in some respect, to an early micellization.

(c) For all nonionic surfactants studied here, the influence of chain-length, temperature and ionic strength is as follows:

(i) A higher number of ethoxy groups increases, at low concentration, the affinity for the surface but lowers, at higher concentration, the maximum

amount adsorbed.

(ii) Increasing the temperature or ionic strength favours the aggregation phenomena (through the hydrophobic effect) and therefore increases the amount adsorbed on the plateau of the adsorption isotherm.

(iii) At low coverages, a reverse influence of temperature and ionic strength is observed, because of the major part played by the surfactant/surface interactions (as compared with the surfactant/surfactant interactions).

(iv) Adsorption of TX-100 on quartz from the non-aqueous solution (decane) is more extensive than from water but can be reduced by the addition of alcohol. Short chain alcohols reduce the extent of adsorption to zero.

(d) Increasing the temperature close to the cloud point dramatically enhances adsorption of non ionic surfactants.

The nonionic surfactants are sensitive to temperature. However, the inclusion of a co-suractant (e.g. anionic surfactant, SDS or SAS) and/or co-solvent enhances the surfactant solubility and reduces the extent of adsorption (see Figures 4.14-4.16 and 5.14-5.15).

Considering the extensive studies on phase equilibria, interfacial characteristics and adsorption properties of the nonionic surfactants, it appears that the surfactant blend consisting of TX-100, SDS or SAS and pentan-1-ol is the most promising blend for enhanced oil recovery. The other blends also worked well and all could be improved upon.

7.3 Microemulsion Droplet Combustion and Synthesis of Colloidal Silica

The particle size and water content of the w/o microemulsion systems have an effect upon the evaporation/combustion characteristics for the three microemulsions studied. Similar amount of combustion products (i.e. water, CO and CO_2) but variable quantities of formaldehyde and acetaldehyde, dependent on the emulsion and catalyst used, are produced from the w/o microemulsions. The fact that formaldehyde/acetaldehyde can be

produced is important in terms of fuel stock depletion. Microemulsion combustion can lead to new oxygenated products.

Microemulsions stabilised with TX-100 can be used in a method to synthesize colloidal silica of desire particle size and morphology.

FURTHER RESEARCH

From studies made, it appears that work should continue on displacement studies of crude oil using the model surfactant system under the reservoir conditions. Anionic derivatives of the nonionic surfactant could be beneficial due to less adsorption on the rock surface and could be improved in terms of phase equilibria.

Adsorption of the surfactants could be carried out on various rock surfaces including sandstone, kaoline and dolomite. Complete characterisation of the rock formation is necessary to predict the adsorption properties of surfactants.

In droplet combustion, bitumen-in-water emulsions using the TX-100 as a stabiliser could be used to optimise the combustion products.

References

[1] D. Butler, J. Accountancy, **November**, 30, (1996)

Appendix Data Collecting Program

```
10 REM ** ABSORB V2.03 (C) PJS 23/09/94
20 REM ** Collects absorbance from a SP1800
30 MODE7:*DRIVE0
40 *ADC
50 ONERRORGOTO220
60 PROCinitialise:PROCtitle
70 *DRIVE0
80 MODE7:PROCmenu
90 ONI%GOTO100,130,140,120,150,160,170,180,190
100 PROCsetup
110 MODE4:PROCcollect:GOTO70
120 PROCload
130 MODE4:PROCdisplay:GOTO70
140 PROCsave
150 PROCfiles:GOTO70
160 CHAIN"ANALYSE"
170 CHAIN"TABLE"
180 CHAIN"MENU"
190 END
200 :
210 REM ERROR TRAP
220 VDU3,4:@%=2314:CLOSE#0:*DRIVE0
230 IFERR=17THEN70
240 REPORT
250 PRINT" at line ";ERL
260 PRINT$;:*FX21,0
270 REPEATUNTILGET=32
280 ONERRORGOTO220
290 GOTO70
300 :
310 DEFPROCinitialise
320 *FX16,1
330 *FX1,4
340 VDU3,4:CLOSE#0
350 S$="Press spacebar to continue"
360 dash$=STRING$(39,"-"):B$=STRING$(39," ")
370 A=1:B=1:C=1.2345:D=1:E=1:D=1
380 F%=0:N%=0:Q%=0
390 min%=1E8:max%=1E-8
400 DIMX%(402),Y%(402),A%(6),P%(5),T%(6),V%(3),A(3),B(3),C(3),P(3),W(6)
410 ENDPROC
420 :
430 DEFPROCtitle
440 CLS:PROCdouble(0,"** SP1800  ABSORBANCE **")
450 PROCdouble(2,"** Introduction **")
460 PRINT'dash$
470 PRINT'"Application : Absorbance measurement"
480 PRINT'"This program is used to collect and"
490 PRINT"record the absorbance of a surfactant"
500 PRINT"micro-emulsion for use in determining"
510 PRINT"the position of the phase boundaries"
520 PRINT"and the concentrations in the phases."
530 PRINT'dash$''S$
540 T=TIME+3000:*FX21,0
550 REPEAT:G$=INKEY$(5):UNTILTIME>T OR G$=" "
560 ENDPROC
570 :
580 DEFPROCmenu
590 CLS:PROCdouble(0,"** SP1800 ABSORBANCE **")
```

```
620 PRINT''"1. Collect an absorbance curve"
630 PRINT"2. Plot the absorbance curve"
640 PRINT"3. Save the data"
650 PRINT"4. Load a datafile"
660 PRINT"5. View the filenames"
670 PRINT"6. Load the analyser program"
680 PRINT"7. Load the data table program"
690 PRINT"8. Return to the 'Master Menu'"
700 PRINT"9. End this program"
710 PRINT''"Please enter your choice (1-9)"
720 PRINTdash$
730 PRINT"ABSORB V2 (C) P.Szadorski 1994"
740 PRINT"Note:Press ESCAPE at any time to"
750 PRINT"     return to this page":*FX21,0
760 REPEAT:I%=INSTR("123456789",GET$):UNTILI%
770 ONI%GOTO810,780,780,810,860,810,810,810,810
780 IFF%>0 THEN860
790 PRINT"First collect data"
800 PROCsbar:GOTO590
810 IFF%<>1THEN860
820 PRINT"You will lose data"
830 PRINT"Are you sure (Y/N)?":*FX21,0
840 REPEAT:B%=INSTR("yYnN",GET$):UNTILB%
850 IFB%<3THENF%=0:ELSE590
860 ENDPROC
870 :
880 DEFPROCdouble(I%,T$)
890 FORY%=I%TOI%+1
900   PRINTTAB(18-LEN(T$)/2,Y%)CHR$(141)T$
910   NEXT
920 ENDPROC
930 :
940 DEFPROCsbar
950 PRINTS$;:*FX21,0
960 REPEATUNTILGET=32
970 ENDPROC
980 :
990 DEFPROCsetup
1000 F%=FALSE
1010 CLS:PROCdouble(0,"** SIGNAL CHECK **")
1020 INPUT''"Date (DD/MM/YY)  : "D$
1030 IFLEN(D$)>8THEND$=LEFT$(D$,8)
1040 PRINT"Sample reference :"
1050 INPUT"(max 8 chrs)     : "N$
1060 IFLEN(N$)>8THENN$=LEFT$(N$,8)
1070 PRINT''"Check that there is a signal being"
1080 PRINT"received by the computer. The value"
1090 PRINT"should lie between 0 and 4095"
1100 PRINTTAB(0,23)"Press spacebar to collect data"
1110 VDU23;8202;0;0;0;
1120 *FX21,0
1130 PRINTTAB(0,20)"Absorbance signal"
1140 REPEAT
1150   REPEAT
1160     I%=ADVAL(0)DIV256
1170     UNTILI%=1
1180   PRINTTAB(23,20);ADVAL(1)DIV16" "
1190   UNTILINKEY-99
1200 F%=TRUE:N%=0
1210 ENDPROC
```

```
1240 V=20:X1=40:X2=1239:R=X2-X1:XG=R/40
1250 Y1=208:Y2=987:S=Y2-Y1:T=S-50
1260 VDU23;8202;0;0;0;
1270 MOVEX1,Y1:DRAWX1,Y2:DRAWX2,Y2:DRAWX2,Y1:DRAWX1,Y1
1280 PRINTTAB(9)"SP1800 ABSORBANCE PLOT"
1290 FORIZ=1TO10:PRINTTAB(0,8+IZ)MID$("Absorbance",IZ,1):NEXT
1300 FORIZ=5TO35STEP5
1310   MOVEIZ*XG+X1,Y1:PLOT1,0,V:PLOT0,0,(S-2*V):PLOT1,0,V
1320   NEXT
1330 VDU5:FORIZ=0TO40STEP5:I$=STR$(IZ)
1340   MOVEIZ*XG+X1-LEN(I$)*16,Y1-9:PRINTI$
1350   NEXT:VDU4
1360 PRINTTAB(16,27)"Time/sec"
1370 ENDPROC
1380 :
1390 DEFPROCcollect
1400 PROCbox
1410 minZ=1E9:maxZ=1E-9
1420 YG=T/4095
1430 T=TIME+300
1440 REPEAT UNTIL TIME>T
1450 VDU7:D=10:TIME=0:T=TIME
1460 AZ=ADVAL(1)DIV16
1470 MOVET/100*XG+X1,AZ*YS+Y1+25
1480 XZ(0)=T:YZ(0)=AZ
1490 FORNZ=1TO400
1500   REPEAT
1510     IZ=ADVAL(0)DIV255
1520     UNTILIZ=1ANDTIME>=D
1530   D=D+10
1540   AZ=ADVAL(1)DIV16:T=TIME
1550   DRAWT/100*XG+X1,AZ*YS+Y1+25
1560   XZ(NZ)=T:YZ(NZ)=AZ
1570   IFAZ<minZ THENminZ=AZ
1580   IFAZ>maxZ THENmaxZ=AZ
1590   NEXT:NZ=NZ-1
1600 REM XZ(0)=XZ(1):YZ(0)=YZ(1)
1610 XZ(NZ+1)=XZ(NZ):YZ(NZ+1)=YZ(NZ)
1620 XZ(NZ+2)=XZ(NZ):YZ(NZ+2)=YZ(NZ)
1630 :
1632 A=2/4095:B=0:C=0:D=0:E=0
1634 JZ=2:KZ=2:MZ=2
1640 REM set values for P(IZ)
1650 FORIZ=1TO3:PZ(IZ)=0:NEXT
1660 PZ(1)=1:PZ(2)=NZ-1:PZ(3)=(NZ):PZ(4)=NZ+1:PZ(5)=NZ+2
1670 REM set values for AZ(IZ)
1680 FORIZ=1TO3:AZ(IZ)=PZ(IZ):AZ(IZ+3)=PZ(IZ+1):NEXT
1690 REM set values for VZ(IZ)
1700 FORIZ=1TO3:VZ(IZ)=0:NEXT
1710 REM set values for TZ(IZ)
1720 FORIZ=1TO6:TZ(IZ)=0:NEXT
1730 REM set values for W(IZ)
1740 FORIZ=1TO6:W(IZ)=0:NEXT
1750 :
1760 REM set values for A(IZ)
1770 FORIZ=1TO3:A(IZ)=0:NEXT
1780 REM set values for B(IZ)
1790 FORIZ=1TO3:B(IZ)=0:NEXT
1800 REM set values for C(IZ)
1810 FORIZ=1TO3:C(IZ)=0:NEXT
```

```
1840 :
1850 DEFPROCdisplay
1860 PROCbox
1870 YG=T/(maxZ-minZ)
1880 MOVEXZ(0)/100*XG+X1,(YZ(0)-minZ)*YG+Y1+25
1890 FORIZ=1TONZ
1900   DRAWXZ(IZ)/100*XG+X1,(YZ(IZ)-minZ)*YG+Y1+25
1910   NEXT
1920 PRINTTAB(0,28)S$:*FX15,1
1930 REPEATUNTILGET=32
1940 ENDPROC
1950 :
1960 DEFPROCdrive
1970 IFEZ=0THEN*DRIVE0
1980 IFEZ=1THEN*DRIVE1
1990 IFEZ=2THEN*DRIVE2
2000 IFEZ=3THEN*DRIVE3
2010 CLS:*.
2020 FORIZ=0TO3:PRINTTAB(0,IZ)B$:NEXT
2030 PROCdouble(0,I$)
2040 ENDPROC
2050 :
2060 DEFPROCsave
2070 I$="** Save data to Drive "+STR$(EZ)+" **"
2080 PROCdrive
2090 REPEAT
2100   INPUTTAB(0,21)"Name for datafile "F$
2110   UNTILLEN(F$)>0ANDLEN(F$)<8
2120 DZ=OPENOUT(F$)
2130 PRINT#DZ,D$,N$,E,D,C,B,A,NZ,QZ
2140 PRINT#DZ,JZ,KZ,MZ
2150 FORIZ=1TO3:PRINT#DZ,P(IZ):NEXT
2160 FORIZ=0TO5:PRINT#DZ,PZ(IZ):NEXT
2170 FORIZ=1TO6:PRINT#DZ,AZ(IZ):NEXT
2180 FORIZ=1TO3:PRINT#DZ,VZ(IZ):NEXT
2190 FORIZ=1TO6:PRINT#DZ,TZ(IZ):NEXT
2200 FORIZ=1TO6:PRINT#DZ,W(IZ):NEXT
2210 FORIZ=1TO3:PRINT#DZ,A(IZ):NEXT
2220 FORIZ=1TO3:PRINT#DZ,B(IZ):NEXT
2230 FORIZ=1TO3:PRINT#DZ,C(IZ):NEXT
2240 PRINT#DZ,minZ,maxZ
2250 FORIZ=0TONZ+2
2260   PRINT#DZ,XZ(IZ),YZ(IZ)
2270   NEXT
2280 CLOSE#DZ:FZ=2
2290 *ACCESS *.* L
2300 ENDPROC
2310 :
2320 DEFPROCload
2330 FZ=0
2340 I$="** Load data from Drive "+STR$(EZ)+" **"
2350 PROCdrive
2360 REPEAT
2370   INPUTTAB(0,21)"Name for datafile "F$
2380   UNTILLEN(F$)>0ANDLEN(F$)<8
2390 DZ=OPENUP(F$)
2400 INPUT#DZ,D$,N$,E,D,C,B,A,NZ,QZ
2410 INPUT#DZ,JZ,KZ,MZ
2420 FORIZ=1TO3:INPUT#DZ,P(IZ):NEXT
2430 FORIZ=0TO5:INPUT#DZ,PZ(IZ):NEXT
```

```
2460 FORIZ=1TO6:INPUT#DZ,TZ(IZ):NEXT
2470 FORIZ=1TO6:INPUT#DZ,W(IZ):NEXT
2480 FORIZ=1TO3:INPUT#DZ,A(IZ):NEXT
2490 FORIZ=1TO3:INPUT#DZ,B(IZ):NEXT
2500 FORIZ=1TO3:INPUT#DZ,C(IZ):NEXT
2510 INPUT#DZ,minZ,maxZ
2520 FORIZ=0TONZ+2
2530   INPUT#DZ,XZ(IZ),YZ(IZ)
2540   NEXT
2550 CLOSE#DZ:FZ=2
2560 ENDPROC
2570 :
2580 DEFPROCfiles
2590 I$="** Files on Drive "+STR$(EZ)+" **"
2600 PROCdrive
2610 PRINTTAB(0,21);:PROCsbar
2620 ENDPROC
```

```
10 REM ** ANALYSE V2.06 (C) PJS 23/09/94
20 REM ** uses absorbance collected from
30 REM ** a SP1800 spectrophotometer set to xxx nm
40 MODE7:*DRIVE0
50 *LOAD ASSDMP
60 ONERRORGOTO200
70 PROCinitialise:PROCtitle
80 *DRIVE0
90 MODE7:PROCmenu
100 ON%GOTO110,120,130,140,150,160,170
110 PROCload
120 MODE4:PROCplot:GOTO80
130 PROCsave
140 PROCfiles:GOTO80
150 CHAIN"PLOTTER"
160 CHAIN"MENU"
170 END
180 :
190 REM ERROR TRAP
200 @%=&90A:*FX4,0
210 *DRIVE0
220 IFERR=17THEN80
230 ONERROROFF
240 REPORT
250 PRINT" at line ";ERL
260 PRINT$e$;:*FX21,0
270 REPEATUNTILGET=32
280 ONERRORGOTO200
290 GOTO80
300 :
310 DEFPROCinitialise
320 VDU3,4:e%=2314:F%=0:CLOSE#0
330 dash$=STRING$(39,"-"):B$=STRING$(39," ")
340 S$="Press spacebar to continue"
350 N%=0:F$="":$&800=F$
360 DIMX%(402),Y%(402),A%(6),P%(5),T%(6),V%(3),A(3),B(3),C(3),P(3),W(6)
370 ENDPROC
380 :
390 DEFFNA(X)=X*A+B
400 DEFFNX(X)=X*XG/100+X1
410 DEFFNY(Y)=(Y-minX)*YG+Y0
420 DEFFNZ(Y)=(Y-minX)*YG+Y0-25
430 :
440 DEFPROCtitle
450 CLS:PROCdouble(0,"** ANALYSER **")
460 PROCdouble(2,"** Introduction **")
470 PRINT'dash$
480 PRINT''"Application : Phase boundaries"
490 PRINT''"This program is used to determine the"
500 PRINT"position of phase boundaries, the % of"
510 PRINT"each phase and the concentrations of a"
520 PRINT"surfactant micro-emulsion from the"
530 PRINT"absorbance curve."
540 PRINT'dash$''S$
550 T=TIME+3000:*FX21,0
560 REPEAT:I$=INKEY$(5):UNTILTIME>T OR I$=" "
570 ENDPROC
```

```
580 :
590 DEFPROCmenu
600 CLS:PROCdouble(0,"** ANALYSER **")
610 PRINT'dash$
620 PRINT"   Do you want to:"
630 PRINT''"1. Load the data"
640 PRINT"2. Plot the absorbance curve"
650 PRINT"3. Save the data"
660 PRINT"4. View the filenames"
670 PRINT"5. Load PLOTTER program"
680 PRINT"6. Return to the 'Master Menu'"
690 PRINT"7. End this program"
700 PRINT''"Please enter your choice (1-7)"
710 PRINTdash$
720 PRINT"ANALYSE (C) P.Szadorski 1994"
730 PRINT"Note:Press ESCAPE at any time to"
740 PRINT"     return to this page":*FX21,0
750 REPEAT:I%=INSTR("1234567",GET$):UNTILI%
760 ONI%GOTO800,770,770,860,800,800,800
770 IFF%>0THEN860
780 PRINT"First load the data"
790 PROCsbar:GOTO800
800 IFF%=0THEN850
810 PRINT"You will quit current ":IFF%=1THENPRINT"data"ELSEPRINT"program"
820 IFF%=2THENPRINT"Data has been edited but not saved"
830 PRINT"Are you sure (Y/N)?":*FX21,0
840 REPEAT:B%=INSTR("yYnN",GET$):UNTILB%
850 IFB%<3THENF%=0:ELSE600
860 ENDPROC
870 :
880 DEFPROCdouble(I%,T$)
890 FORY%=I%TOI%+1
900   PRINTTAB(19-LEN(T$)/2,Y%)CHR$(141)T$
910   NEXT
920 ENDPROC
930 :
940 DEFPROCsbar
950 PRINTS$;:*FX21,0
960 REPEATUNTILGET=32
970 ENDPROC
980 :
990 DEFPROCplot
1000 *FX4,1
1010 REM draw box & labels
1020 V=20:X1=168:X2=1279:R=1239-X1:XG=R/40
1030 Y1=208:Y2=987:S=Y2-Y1:Y0=Y1+64:T=S-89:YG=T/(maxY-minY)
1040 VDU23;8202;0;0;0;
1050 MOVEX1,Y1:DRAWX1,Y2:DRAWX2,Y2:DRAWX2,Y1:DRAWX1,Y1
1060 PRINTTAB(12)"SP1800 ABSORBANCE PLOT"
1070 FORI%=1TO10:PRINTTAB(4,8+I%)MID$("Absorbance",I%,1):NEXT
1080 FORI%=5TO40STEP5
1090   MOVEI%*XG+X1,Y1:PLOT1,0,V:PLOT0,0,(S-2*V):PLOT1,0,V
1100   NEXT
1110 MOVEX1,Y0:PLOT1,-16,0
1120 MOVEX1,Y2-25:PLOT1,-16,0
1130 VDU5:FORI%=0TO40STEP5:I$=STR$(I%)
1140   MOVEI%*XG+X1-LEN(I$)*16,Y1-8:PRINTI$
```

```
1150   NEXT
1160 @%=&20204
1170 MOVE0,Y0+12:PRINT;FNA(min%)
1180 MOVE0,Y2-13:PRINT;FNA(max%)
1190 @%=2314:VDU4
1200 PRINTTAB(18,27)"Time/sec"
1210 REM plot curve
1220 MOVEFNX(XX(0)),FNY(YX(0))
1230 FORIX=1TONX
1240   DRAWFNX(XX(IX)),FNY(YX(IX))
1250   NEXT
1260 :
1270 REM show phase boundaries
1280 PRINTTAB(0,30)STRING$(39,"-")
1290 PRINTTAB(0,31)"  1:"TAB(11,31)":2:"TAB(20,31)":3:"TAB(29,31)":4:";
1300 @%=&20205
1310 FORIX=1TO4
1320   PX=PX(IX)
1330   IFPX>(NX-2)THENPX=NX:GOTO1370
1340   X=FNX(XX(PX))
1350   MOVEX,Y1:PLOT22,X,Y2
1360   PRINTTAB(IX*9-4,31)XX(PX)*C/100;
1370   NEXT
1380 :
1390 IFJX>1THEN1470
1400 PRINTTAB(0,28)"Phase boundaries 1)Use 2)Move 3)Reset"
1410 *FX15,1
1420 REPEAT:JX=INSTR("123",GET$):UNTILJX
1430 PRINTTAB(0,28)SPC:IFJX=1THEN2040
1440 FX=2:IFJX=3THENPROCresetp:GOTO1310
1450 :
1460 REM move boundaries
1470 PRINTTAB(0,28)"Set phase boundary  :"TAB(25,28)"Abs : "
1480 FORIX=1TO4
1490   @%=2314
1500   PRINTTAB(21,28);IX
1510   @%=&20205
1520   PX=PX(IX)
1530   LX=PX(IX-1)+1:HX=PX(IX+1)-1
1540   IFPX<LXTHENPX=LX
1550   IFPX>HXTHENPX=HX
1560   REPEAT
1570     X=FNX(XX(PX))
1580     MOVEX,Y1:PLOT22,X,Y2
1600     PX=PX-(PX>LX)*(INKEY-26)+(PX<HX)*INKEY-122
1610     PX=PX-(PX>(LX+25))*(INKEY-58)*25+(PX<(HX-25))*(INKEY-42)*25
1620     IF(PX<(LX+26))ANDINKEY-58THENPX=(PX+LX+1)DIV2
1630     IF(PX>(HX-26))ANDINKEY-42THENPX=(PX+HX+1)DIV2
1640     IFINKEY-90THENPX=LX
1650     IFINKEY-106THENPX=HX
1660     X=FNX(XX(PX))
1670     MOVEX,Y1:PLOT22,X,Y2
1680     PRINTTAB(23,28)FNA(YX(PX))"  "
1690     PRINTTAB(IX*9-4,31)XX(PX)*C/100;
1700     UNTILINKEY-74
1710   PX(IX)=PX
1720   REPEATUNTILNOTINKEY-74:*FX21,0
1730   NEXT
```

```
1740 PRINTTAB(0,28)B$
1750 :
1760 REM calc % of each phase
1770 IFP%(2)>NZ-2THEN3020
1780 IFP%(4)>=NXTHENQ%=2ELSEQ%=3
1790 percent=100/(XX(P%(Q%+1))-XX(P%(1)))
1800 FORI%=1TOQ%
1810   X=XX(P%(I%+1))-XX(P%(I%))
1820   P(I%)=percent*X
1830   NEXT
1840 :
1850 REM Set absorption boundaries at phase boundaries
1860 FORI%=1TOQ%
1870   AX(I%)=P%(I%):AX(I%+3)=P%(I%+1)
1880   NEXT
1890 :
1900 REM calc average absorbance for each phase
1910 FORI%=1TOQ%:RX=I%+3
1920   A%=0
1930   FORC%=AX(I%)TO AX(RX)
1940     A%=A%+Y%(C%)
1950     NEXT
1960   A%=A%/(AX(RX)-AX(I%)+1)+.5
1970   A(I%)=FNA(A%):B(I%)=A(I%):C(I%)=A(I%)
1980   V%(I%)=A%:T%(I%)=A%:W(I%)=A%
1990   T%(RX)=A%:W(RX)=A%
2000   NEXT
2010 J%=1:K%=2:M%=2
2020 :
2030 REM print phase %
2040 FORI%=1TOQ%:RX=I%+3
2050   MOVEFNX((XX(P%(I%))+XX(P%(I%+1)))/2)-16,Y1+57
2060   @%=&90A:VDU5:PRINTSTR$(I%)
2070   @%=&20104:VDU4:PRINTTAB((I%-1)*13,29)"Phase"STR$(I%)":";P(I%)"%";
2080   NEXT
2090 :
2100 REM move absorbance line up/down/tilt
2110 PRINTTAB(3,28)"Absorbance "
2120 PRINTTAB(0,30)B$:@%=&20204
2130 FORI%=1TOQ%
2140   PRINTTAB(0,28)"Phase "STR$(I%)
2150   LX=P%(I%):HX=P%(I%+1)
2160   XL=FNX(XX(LX)):XH=FNX(XX(HX))
2170   YLX=T%(I%):YHX=T%(RX)
2180   Y%=(YHX+YLX)DIV2:D%=(YHX-YLX)DIV2
2190   MINX=minX+ABS(DX):MAXX=maxX-ABS(DX)
2200   MOVEXL,FNY(YLX):PLOT22,XH,FNY(YHX)
2210   PRINTTAB((I%-1)*13,30)"ABS  "STR$(I%)":";FNA(Y%)
2220   IFJ%>1ORK%>1THENPRINTTAB(12,28)"Move"STRING$(16," "):GOTO2270
2230   PRINTTAB(19,28)"1)Use 2)Move 3)Reset":*FX15,1
2240   REPEAT:K%=INSTR("123",GET$):UNTILK%
2250   IFK%=1THEN2450
2260   F%=2:IFK%=3THENPROCreseta:GOTO2170
2270   REPEAT
2280     MOVEXL,FNY(YLX):PLOT22,XH,FNY(YHX)
2290     Y%=Y%+(Y%<MAXX)*INKEY-58-(Y%>MINX)*INKEY-42
2300     D%=D%+(Y%<MAXX)*INKEY-122-(Y%>MINX)*INKEY-26
2310     IFINKEY-106THEND%=0
2320     IFINKEY-90THENY%=(T%(RX)+T%(I%))DIV2:D%=(T%(RX)-T%(I%))DIV2
2330     YLX=Y%-D%:YHX=Y%+D%
```

```
2350    IFMAXZ)(YZ+ABS(DZ))THENMAXZ=maxZ-ABS(DZ)
2360    IFMINZ((YZ-ABS(DZ))THENMINZ=minZ+ABS(DZ)
2370    abs=FNA(YZ):PRINTTAB((IZ-1)*13+7,30);abs
2380    UNTILINKEY-74
2390  TZ(IZ)=YLZ:W(IZ)=YLZ
2400  TZ(RZ)=YHZ:W(RZ)=YHZ
2410  B(IZ)=abs
2420  REPEATUNTILNOTINKEY-74:*FX21,0
2430  :
2440  REM set absorbance limits
2450  IFTZ(IZ)=TZ(RZ)THEN3000
2460  TZ=TZ(IZ):L=W(IZ):H=W(RZ)
2470  Y=(TZ(RZ)-TZ(IZ))/(HZ-LZ)
2480  PRINTTAB(0,28)"Limit"
2490  :
2500  REM Position lower limit
2510  X=FNX(XZ(AZ(IZ))):W=FNZ(L)
2520  MOVEX,W:PLOT22,X,W+50
2530  :
2540  REM Position upper limit
2550  X=FNX(XZ(AZ(RZ))):W=FNZ(H)
2560  MOVEX,W:PLOT22,X,W+50
2570  PRINTTAB((IZ-1)*13+7,30);B(IZ)
2580  :
2590  IFKZ>1THEN2660
2600  PRINTTAB(19,28)"1)Use 2)Move 3)Reset":*FX15,1
2610  REPEAT:MZ=INSTR("123",GET$):UNTILMZ
2620  IFMZ=1THEN3000
2630  FX=2:IFMZ=3THENPROCreset1:GOTO2510
2640  :
2650  REM move lower absorbance limit
2660  PRINTTAB(19,28)"Move lower limit
2670  ZZ=AZ(RZ)-1:OZ=AZ(IZ)
2680  REPEAT
2690    X=FNX(XZ(OZ)):L=TZ+Y*(OZ-LZ):W=FNZ(L)
2700    MOVEX,W:PLOT22,X,W+50
2710    OZ=OZ-(OZ>LZ)*INKEY-26+(OZ<ZZ)*INKEY-122
2720    X=FNX(XZ(OZ)):L=TZ+Y*(OZ-LZ):W=FNZ(L)
2730    MOVEX,W:PLOT22,X,W+50
2740    UNTILINKEY-74
2750  abs=FNA((L+H)/2):PRINTTAB((IZ-1)*13+7,30);abs
2760  REPEATUNTILNOTINKEY-74:*FX21,0
2770  :
2780  REM move upper absorbance limit
2790  PRINTTAB(24,28)"upper"
2800  ZZ=AZ(IZ)+1:PZ=AZ(RZ)
2810  REPEAT
2820    X=FNX(XZ(PZ)):H=TZ+Y*(PZ-LZ):W=FNZ(H)
2830    MOVEX,W:PLOT22,X,W+50
2840    PZ=PZ-(PZ>ZZ)*INKEY-26+(PZ<HZ)*INKEY-122
2850    X=FNX(XZ(PZ)):H=TZ+Y*(PZ-LZ):W=FNZ(H)
2860    MOVEX,W:PLOT22,X,W+50
2870    abs=FNA((L+H)/2):PRINTTAB((IZ-1)*13+7,30);abs
2880    UNTILINKEY-74
2890  REPEATUNTILNOTINKEY-74:*FX21,0
2900  :
2910  AZ(IZ)=OZ:W(IZ)=L
2920  AZ(RZ)=PZ:W(RZ)=H
2930  B(IZ)=abs
```

```
2940   A%=0
2950   FORC%=0%TO P%
2960     A%=A%+Y%(C%)
2970     NEXT
2980   A%=A%/(P%-0%+1)+.5
2990   C(I%)=FNA(A%)
3000   NEXT
3010 J%=1:K%=1:M%=1
3020 @%=2314:*FX4,0
3030 :
3040 PRINTTAB(0,28)R$
3050 PRINTTAB(0,28)"File:"F$TAB(13,28)"Ref:"N$TAB(26,28)"Date:"D$
3060 REPEAT
3070   PRINTTAB(0,31)"Press 'P' to print,or Spacebar for menu":*FX15,1
3080   REPEAT:J$=CHR$(GET0R32):I%=INSTR("Pp ",J$):UNTILI%
3090   IFI%<3THENPRINTTAB(0,31)B$;:PROCdump
3100   UNTILI%=3
3110 ENDPROC
3120 :
3130 DEFPROCresetp
3140 FORI%=9%TO1STEP-1
3150   L%=P%(I%):H%=P%(I%+1)
3160   XL=FNX(X%(L%)):XH=FNX(X%(H%))
3170   YL%=T%(I%):YH%=T%(I%+3)
3180   PROCreseta
3190   NEXT
3200 FORI%=4TO1STEP-1
3210   P%=P%(I%)
3220   IFP%>N%THENP%=N%
3230   X=X(P%)+XG/100+X1
3240   MOVEX,Y1:PLOT22,X,Y2
3250   NEXT
3260 P%(1)=1:P%(2)=N%-1:P%(3)=N%:P%(4)=N%+1
3270 FORI%=1TO4
3280   PRINTTAB(I%*9-4,31)X%(P%)+C/100;
3290   NEXT
3300 J%=2:Q%=0
3310 ENDPROC
3320 :
3330 DEFPROCreseta
3340 PROCreset1
3350 MOVEXL,FNY(YL%)
3360 PLOT22,XH,FNY(YH%)
3370 A%=V(I%)
3380 T(I%)=A%:T(R%)=A%
3390 W(I%)=A%:W(R%)=A%
3400 A(I%)=FNA(A%):B(I%)=A(I%):C(I%)=A(I%)
3410 K%=2
3420 ENDPROC
3430 :
3440 DEFPROCreset1
3450 REM Erase lower limit
3460 X=FNX(X%(A%(I%))):W=FNZ(W(I%))
3470 MOVEX,W:PLOT22,X,W+50
3480 :
3490 REM Erase upper limit
3500 X=FNX(X%(A%(R%))):W=FNZ(W(R%))
3510 MOVEX,W:PLOT22,X,W+50
```

```
3520 .:
3530 REM reset
3540 AZ(IZ)=PZ(IZ):AZ(RZ)=PZ(IZ+1)
3550 W(IZ)=TZ(IZ):W(RZ)=TZ(RZ)
3560 B(IZ)=A(IZ)
3570 MZ=2:FZ=2
3580 ENDPROC
3590 :
3600 DEFPROCdump
3610 VDU2,1,27,1,64,3
3620 VDU2,1,27,1,108,1,7,3
3630 AZ=2:CALL&A00
3640 VDU2,1,13,1,10,1,10,1,10,3
3650 VDU2,1,27,1,64,3
3660 ENDPROC
3670 :
3680 DEFPROCdrive
3690 IFEZ=0THEN*DRIVE0
3700 IFEZ=1THEN*DRIVE1
3710 IFEZ=2THEN*DRIVE2
3720 IFEZ=2THEN*DRIVE3
3730 CLS:*.
3740 FORIZ=0TO3:PRINTTAB(0,IZ)B$:NEXT
3750 PROCdouble(0,I$)
3760 ENDPROC
3770 :
3780 DEFPROCload
3790 I$="** Load data from Drive "+STR$(EZ)+" **"
3800 PROCdrive
3810 REPEAT
3820   INPUTTAB(0,21)"Name for datafile "F$
3830   UNTILLEN(F$)>0ANDLEN(F$)<8
3840 FZ=0:QZ=0:$&B00=F$
3850 DZ=OPENIN(F$)
3860 INPUT#DZ,D$,N$,E,D,C,B,A,NZ,QZ
3870 INPUT#DZ:JZ,KZ,MZ
3880 FORIZ=1TO3:INPUT#DZ,P(IZ):NEXT
3890 FORIZ=0TO5:INPUT#DZ,PZ(IZ):NEXT
3900 FORIZ=1TO6:INPUT#DZ,AZ(IZ):NEXT
3910 FORIZ=1TO3:INPUT#DZ,VZ(IZ):NEXT
3920 FORIZ=1TO6:INPUT#DZ,TZ(IZ):NEXT
3930 FORIZ=1TO6:INPUT#DZ,W(IZ):NEXT
3940 FORIZ=1TO3:INPUT#DZ,A(IZ):NEXT
3950 FORIZ=1TO3:INPUT#DZ,B(IZ):NEXT
3960 FORIZ=1TO3:INPUT#DZ,C(IZ):NEXT
3970 INPUT#DZ,minZ,maxZ
3980 FORIZ=0TONZ+2
3990   INPUT#DZ,XZ(IZ),YZ(IZ)
4000   NEXT
4010 CLOSE#DZ
4020 FZ=1:IFQZ>1THENJZ=1:KZ=1:MZ=1
4030 ENDPROC.
4040 :
4050 DEFPROCsave
4060 I$="** Save data to Drive "+STR$(EZ)+" **"
4070 PROCdrive
4080 REPEAT
4090   INPUTTAB(0,21)"Name for datafile "F$
4100   UNTILLEN(F$)>0ANDLEN(F$)<8
```

```
4110 $&B00=F$
4120 DX=OPENOUT(F$)
4130 PRINT#DX,D$,N$,E,D,C,B,A,NZ,GZ
4140 PRINT#DX,JZ,KZ,MZ
4150 FORIX=1TO3:PRINT#DX,P(IX):NEXT
4160 FORIX=0TO5:PRINT#DX,PX(IX):NEXT
4170 FORIX=1TO6:PRINT#DX,AZ(IX):NEXT
4180 FORIX=1TO3:PRINT#DX,VX(IX):NEXT
4190 FORIX=1TO6:PRINT#DX,TX(IX):NEXT
4200 FORIX=1TO6:PRINT#DX,W(IX):NEXT
4210 FORIX=1TO3:PRINT#DX,A(IX):NEXT
4220 FORIX=1TO3:PRINT#DX,B(IX):NEXT
4230 FORIX=1TO3:PRINT#DX,C(IX):NEXT
4240 PRINT#DX,minX,maxX
4250 FORIX=0TONX+2
4260   PRINT#DX,XX(IX),YX(IX)
4270   NEXT
4280 CLOSE#DX:FX=3
4290 ENDPROC
4300 :
4310 DEFPROCfiles
4320 I$="** Files on Drive "+STR$(EX)+" **"
4330 PROCdrive
4340 PRINTTAB(0,21);:PROCsbar
4350 ENDPROC
```